PROCESSING AND CHARACTERIZATION OF BRICK-AND-MORTAR
STRUCTURED BULK BIO-INSPIRED COMPOSITES

A THESIS SUBMITTED TO
THE GRADUATE SCHOOL OF NATURAL AND APPLIED SCIENCES
OF
MIDDLE EAST TECHNICAL UNIVERSITY

BY

SELEN NİMET GÜRBÜZ

IN PARTIAL FULFILLMENT OF THE REQUIREMENTS FOR
THE DEGREE OF DOCTOR OF PHILOSOPHY

IN

METALLURGICAL AND MATERIALS ENGINEERING

AUGUST 2013

Approval of the thesis:

PROCESSING AND CHARACTERIZATION OF BRICK-AND-MORTAR STRUCTURED BULK BIO-INSPIRED COMPOSITES

submitted by **SELEN NİMET GÜRBÜZ** in partial fulfillment of the requirements for the degree of **Doctor of Philosophy in Metallurgical and Materials Engineering Department, Middle East Technical University** by,

Prof. Dr. Canan ÖZGEN   _____
Dean, Graduate School of **Natural and Applied Sciences**

Prof. Dr. Hakan GÜR   _____
Head of Department, **Metallurgical and Materials Engineering**

Assoc. Prof. Dr. Arcan Fehmi DERİCİOĞLU   _____
Supervisor, **Metallurgical and Materials Engineering Dept., METU**

Examining Committee Members:

Prof. Dr. Cevdet KAYNAK   _____
Metallurgical and Materials Engineering Dept., METU

Assoc. Prof. Dr. Arcan Fehmi DERİCİOĞLU   _____
Metallurgical and Materials Engineering Dept., METU

Prof. Dr. Göknur BAYRAM   _____
Chemical Engineering Dept., METU

Assoc. Prof. Dr. Caner DURUCAN   _____
Metallurgical and Materials Engineering Dept., METU

Assist. Prof. Dr. Kazım TUR   _____
Metallurgical and Materials Engineering Dept., Atılım University

Date: 29.08.2013

I hereby declare that all information in this document has been obtained and presented in accordance with academic rules and ethical conduct. I also declare that, as required by these rules and conduct, I have fully cited and referenced all material and results that are not original to this work.

Name, Last name : Selen Nimet GÜRBÜZ

Signature   :

ABSTRACT

PROCESSING AND CHARACTERIZATION OF BRICK-AND-MORTAR STRUCTURED BULK BIO-INSPIRED COMPOSITES

Gürbüz, Selen Nimet
Ph.D., Department of Metallurgical and Materials Engineering
Supervisor: Assoc. Prof. Dr. Arcan F. Dericioğlu

August 2013, 146 pages

The aim of this study was to fabricate inorganic-organic composites with an architecture resembling to natural nacre using a novel hybrid conventional method called Hot-Press Assisted Slip Casting (HASC). Alumina platelets, glass platelets and glass flakes with different aspect ratios were used as two-dimensional inorganic fillers to reinforce epoxy matrix. Correlation between processing parameters, inorganic content, orientation of the two-dimensional reinforcements and mechanical property enhancement of the fabricated composites was examined. In order to investigate the effect of interfacial compatibility and adhesion on the mechanical properties of the fabricated composites, reinforcement surfaces were modified with silane coupling agents. As received and functionalized reinforcement surfaces were studied by x-ray photoelectron spectroscopy to confirm the adsorption of silane molecules. Fabricated bio-inspired bulk lamellar composite materials were characterized in terms of their microstructural architecture and mechanical properties.

The results obtained indicated that HASC processing is an easy, fast and effective pathway to fabricate bulk inorganic-organic composites exhibiting nacre-like brick-and-mortar architecture. HASC processed composites reinforced by either alumina platelets or glass flakes exhibited enhanced mechanical performance as compared to neat epoxy and composites fabricated by simple mixing, as a result of their nacre-like architecture with well aligned reinforcements. Functionalization of the reinforcement surfaces by silane coupling agents improved the compatibility and adhesion between the reinforcements and the matrix resulting in further enhancement of mechanical properties of bulk lamellar composites fabricated by HASC process. Experimental investigations also revealed the fact that high aspect ratio reinforcements are more effective in reinforcing the epoxy matrix.

Keywords: Bio-inspired composites, Hot-press assisted slip casting, Artificial nacre, Silane coupling

ÖZ

BİYOLOJİK MALZEMELERDEN ESİNLENİLMİŞ TUĞLA-VE-HARÇ YAPILI HACİMLİ KOMPOZİTLERİN ÜRETİMİ VE KARAKTERİZASYONU

Gürbüz, Selen Nimet
Doktora, Metalurji ve Malzeme Mühendisliği Bölümü
Tez Yöneticisi: Doç. Dr. Arcan F. Dericioğlu

Ağustos 2013, 146 sayfa

Bu çalışma kapsamında, yeni geliştirilen ve "Sıcak-pres Destekli Slip Döküm (SDSD)" adı verilen hibrit konvansiyonel üretim yöntemi kullanılarak içyapı mimarisi itibariyle doğal sedefe benzeyen hacimli inorganik-organik kompozit malzemelerin üretimi amaçlanmıştır. Bu kapsamda, epoksi matris malzemesini destekleyici malzeme olarak iki boyutlu alumina plakalar ile farklı en-boy oranına sahip cam plakalar ve cam pullar kullanılmıştır. Proses parametreleri, inorganik miktarı, iki boyutlu inorganik destek malzemesinin dizilimi ile elde edilen nihai mekanik özellikler arasındaki bağıntı incelenmiştir. Arayüzey özelliklerinin nihai kompozit malzemenin mekanik özellikleri üzerindeki etkisinin incelenebilmesi için destek malzeme yüzeyleri silan bağlama ajanlarıyla modifiye edilmiştir. İşlem görmemiş ve modifiye edilmiş destek malzeme yüzeyleri X-Işınları Fotoelektron Spektroskopisi yöntemi ile karakterize edilerek silan ajan malzemesinin yüzeye tutunup tutunmadığı araştırılmıştır. Üretilen biyo-esinlenilmiş hacimli kompozit malzemelerin içyapı mimarileri ve mekanik özellikleri karakterize edilmiştir.

Elde edilen sonuçlar, yeni geliştirilen SDSD yönteminin sedef benzeri tuğla-ve-harç içyapı mimarisine sahip inorganik-organik hacimli kompozit malzemelerin üretiminde kullanılabilecek kolay, hızlı ve efektif bir üretim yöntemi olduğunu göstermiştir. SDSD yöntemi kullanılarak üretilen, alüminyum oksit plakalar ve cam pullar ile desteklenen kompozit malzemelerin sahip oldukları içyapı mimarileri itibariyle monolitik epoksi malzemesi ve basit karıştırma yöntemi ile üretilmiş kompozit malzemelere göre daha iyi mekanik performans gösterdiği saptanmıştır. Silan bağlama ajanları ile modifikasyon işleminin destek malzemesi ile matris arasındaki uyumluluğu ve bağlanmayı arttırdığı, buna bağlı olarak da SDSD yöntemi ile üretilen hacimli kompozit malzemelerin mekanik özelliklerinde iyileşme sağladığı görülmüştür. Ayrıca, deneysel araştırma sonuçları yüksek en-boy oranına sahip inorganik pulların epoksi matris malzemesini desteklemede daha efektif olduğunu göstermiştir.

Anahtar Kelimeler: Biyo-esinlenmiş kompozitler, Sıcak-pres destekli slip döküm, Yapay sedef, Silan bağlama

To my mother Semra F. Gürbüz
        To my husband Fatih Güner
                To my sister A. Ceren Gürbüz and my brother M. Özen Gürbüz
                &
                        To the loving memory of my father Ahmet Gürbüz

ACKNOWLEDGEMENTS

TABLE OF CONTENTS

LIST OF TABLES

TABLES

LIST OF FIGURES

FIGURES

xvi

xviii

LIST OF SYMBOLS

A	Fracture surface area of the specimens
α	Aspect ratio
α_c	Critical aspect ratio
b	Width of three-point bending and work of fracture test specimen
d	Depth (thickness) of three-point bending and work of fracture test specimen
D	Maximum deflection of the center of three-point bending and work of fracture test specimen
ε_f	Flexural strain
E	Area under the load-displacement curve
E_k	Kinetic energy of the ejected electron
E_l	Electron binding energy
ϕ	Work function of the specimen induced by the analyzer
P	Load at a given point on the load deflection curve
ρ	Density
ρ_R	Theoretical density of reinforcement
ρ_M	Density of epoxy
σ_f	Flexural stress
σ_p	Platelet strength
S	Support span
τ	Interface or matrix shear strength
$V_R\%$	Volume percentage of the reinforcement
$W_R\%$	Weight percentage of the reinforcement
W_{dry}	Dry weight
$W_{sat.}$	Saturated weight
$W_{susp.}$	Suspended weight

LIST OF ABBREVIATIONS

AP	Alumina Platelets
APS	Aminopropyltriethoxysilane
DGEBA	Bisphenol A-diglycidyl ether
FT-IR	Fourier Transform Infrared Spectroscopy
GO	Graphene oxide
GF	Glass Flakes
GF-ST	APS treated glass flakes
GP	Glass Platelets
GP-ST	APS treated glass platelets
GPS	Glycidoxypropyltrimethoxysilane
HASC	Hot-press Assisted Slip Casting
HASC-50	HASC processed composite under the applied load of 50 MPa
HASC-100	HASC processed composite under the applied load of 100 MPa
LBL	Layer-by-layer
LDH	Layered double hydroxide
MTM	Montmorillonite
PCDO	10,12-pentacosadiyn-1-ol
PMMA	Polymethyl methacrylate
PVA	Polyvinylalcohol
r-GO	Reduced graphene oxide
SAF	Surface Area of the Filler
SENB	Single Edge Notch Beam
SEM	Scanning Electron Microscopy
SM	Simple Mixed
SWS	Specific Wetting Surface or Surface Area Coverage of the Silane
S1	Alumina platelets GPS treated in ethanol-water mixture
S2	Alumina platelets GPS treated in distilled water
S3	Alumina platelets APS treated in toluene

S4	Alumina platelets APS treated in ethanol-water mixture
S5	Alumina platelets APS treated in distilled water
3PB	Three-Point Bending
ToF-SIMS	Time-of-Flight Secondary Ion Mass Spectroscopy
2D	Two-dimensional
XPS	X-ray Photoelectron Spectroscopy
WOF	Work of Fracture

CHAPTER 1

INTRODUCTION

The evolution of earth for billions of years has led to formation of numerous natural materials with complex structures. The properties of these materials are outstanding and, in many cases, they still surpass artificial materials in terms of their functional and mechanical characteristics. Spider silks, bone, nacre (the mother-of-pearl), sponge spicule, crab exoskeletons are some examples to such natural materials [1-5]. Dragline spider silk, for instance, exhibits unique combination of mechanical properties such as strength and toughness as well as wetting-induced supercontraction along with torsional shape memory, whereas spider capture silk possess high strength, elasticity and stickiness beside the ability of water collection from moist air [5, 6]. Sponge spicule is another example of natural materials. Besides revealing a unique combination of mechanical properties such as strength, stiffness, resilience and toughness, sponge spicules have remarkable fiber-optical properties similar to those of commercial telecommunication fibers. However, these fibers are tougher than artificial fiber materials [7, 8].

At this point arising question is how these magnificent natural materials possess outstanding mechanical performance along with the multifunctionality despite their weak building blocks. For decades, several research studies have been devoted to answer this question. Experimental investigations have revealed that the complex hierarchical structural arrangement extending from nano-, micro- to macro-scale is the main reason of this extraordinary combination of properties [1-5, 9].

It is clear that comprehensive understanding of the formation of these natural materials and exploration of the complexity, multifunctionality and multi-scale nature of structure-property relationship can to provide new insights for the design of next generation engineering materials. For this reason, there is still a considerable effort to fully interpret the design concepts which are optimized through the evolution of the earth and to adapt these intricate hierarchical structures to synthetic engineering materials [9-12]. In this context, designing and synthesizing materials taking inspiration from the architectures of natural materials has become a new and popular area of science usually referred as "bio-inspired materials science."

Nacre, the mother-of-pearl, being one of the most intriguing natural materials, is the source of inspiration of the current study. Nacre, consisting of 95 vol% inorganic platelets (aragonite) and 5 vol% organic biopolymer, is arranged in a so-called "brick-and-mortar" architecture. Despite its high brittle inorganic content, this fascinating natural material reveals enhanced mechanical characteristics including unique toughness and mechanical

strength combination [13-15]. This extraordinary combination of mechanical properties makes nacre the "bio-mimetic model" and the source of inspiration in many studies. Beside its extraordinary mechanical performance, due to its lamellar structure nacre appears iridescent exhibiting structural colors similar to opal and other natural photonic crystals such as peacock feathers and butterfly wings [5].

Many studies have been devoted to understand the structure-property relationship and to explore the underlying design principles found in nacre. Although, the main reason underlying this distinct combination of strength, stiffness and toughness is thought to be the micro-scale "brick-and-mortar" architecture spanning over several length scales, the experimental investigations also revealed that there exist nano- and micro-scale intriguing interfacial features each of which is suggested to undertake a task and operate synergistically leading to unique combination of mechanical properties [16-22].

Even though the investigations explicitly pointed out the multi-scale complex architecture of nacre as the reason of its outstanding mechanical performance, replication of this multi-scale hierarchical structure and all key features of nacre is a difficult task using the current technology [13]. For that reason, the bio-inspiration studies mainly focused on mimicking the micro-scale "brick-and-mortar" structure of nacre [23, 24].

Layer-by-layer assembly is the most widely used technique to fabricate composites with nacre-mimetic "brick-and-mortar" structure [12, 25-28]. Even though, nacre-like composites with brick-and-mortar structure are achieved successfully, this technique is a time consuming, multi-step and highly laborious methodogy as it requires repeating deposition, washing and drying cycles [29]. Furthermore, this technique can only be used to fabricate thin films with limited thicknesses [30]. Vacuum filtration-induced self-assembly (or paper-making process) [31-33] or water evaporation-induced self-assembly (or solution casting) [34-36] and tape casting (doctor-blading) [37-39] are alternative one-step, relatively simple, fast and scalable methodologies which can also be used to fabricate nacre-mimetic thin films. Electrophoretic deposition [40, 41], ion-beam sputtering [42], centrifugal deposition [43] etc. are other techniques employed to produce nacre-like bio-inspired free standing films and coatings. Although all of these processes are effective in fabricating strong and though bio-inspired self-standing films or coatings exhibiting hierarchical architectures, they cannot be used to fabricate nacre-like bulk composites that can be used in structural engineering applications.

In recent years, ice-templating or so-called freeze casting method [11, 44, 45], gel casting and hot-pressing [46, 47] as well as various flake powder metallurgy routes [48-50] and magnetic alignment [51] have been proposed to fabricate nacre-mimetic bulk composites. Although, all of these proposed techniques are relatively simple, most of them are multi-step and time-consuming processes. Consequently, there is still need for a simple, one-step, easily scalable, time and man-power efficient processing strategy which enables the fabrication of bulk composites reinforced by well-aligned 2D reinforcements in high volume fractions that can be used in large scale components.

2

Therefore, the aim of the current study was to fabricate bulk polymer matrix composites reinforced by aligned inorganic flakes that possess microstructural architectures inspired by the natural composite, nacre, using a newly proposed technique called "Hot-press Assisted Slip Casting (HASC)". This one-step novel technique combines two conventional processing methods; hot-pressing and slip-casting, to achieve hierarchical arrangement of the platelets in a polymer matrix and to enhance the volume fraction of the inorganic reinforcement in the resulting composite. In this technique applied pressure forces the liquid resin to flow out through a porous plaster, which functions as a filter, during which the alignment of two-dimensional (2D) inorganic reinforcements with their basal surfaces perpendicular to the hot-pressing direction is achieved.

As 2D inorganic reinforcements, alumina platelets along with glass platelets and flakes with different aspect ratios were used in order to investigate the effect of using different inorganic reinforcements and different aspect ratios on the mechanical properties of the hierarchically arranged composites with epoxy matrix. The effect of applied HASC processing pressures on the alignment of the reinforcements and total inorganic content were investigated.

To achieve interfacial compatibility along with improved adhesion and to reveal the effect of interfacial strength on the mechanical performance of the fabricated composites, the surfaces of the inorganic reinforcements were treated with organofunctional silanes having epoxy compatible functional groups to impart an optimized interfacial bonding between the matrix and the inorganic reinforcements. For the functionalization of the alumina platelet surfaces two different organofunctional silanes having epoxy- and amino-functionality, namely γ-glycidoxypropyltrimethoxysilane (GPS) and γ-aminopropyltriethoxysilane (APS), respectively, were used. On the basis of the experimental findings, organofunctional silane having amino-functionality, γ-aminopropyltriethoxysilane (APS), which gave the optimum result, was used to functionalize the glass reinforcements.

This thesis comprises six chapters. Brief information about natural materials, especially nacre which is the source of inspiration of this study, is mentioned in Chapter 2. Mechanical property-structure relationship and underlying design principles along with efforts made to fabricate nacre-like artificial composites are also discussed in this chapter. Chapter 3 includes the details of the HASC processing pathway used for the fabrication of inorganic-organic nacre-like bulk composites, surface functionalization procedures employed along with the characterization studies performed. Chapter 4 covers the experimental results achieved and discussions of the experimental findings such as the effect of processing parameters and the interfacial strength on the final mechanical performance of the fabricated bulk nacre-mimetic composites. In the following chapter, Chapter 5, the concluding remarks, obtained during the study, are summarized. Finally, in Chapter 6, recommendations for future work are discussed.

CHAPTER 2

LITERATURE REVIEW

Natural materials with their all amazing intriguing features and structural design along with the resultant mechanical performance attracts special interest and inspires the scientists and engineers for decades. Nacre is one of such extraordinary natural material and the source of inspiration of this study. In contravention of its weak constituents, this natural material exhibits high strength, stiffness, toughness together with the lightweight as a result of its multi-scale hierarchical architecture.

In this context, mechanical property-structure relationship and the design principles lying underneath along with efforts that have been made to fabricate nacre-like artificial composites will be discussed in this chapter. Furthermore, brief information about organofunctional silane coupling agents, used to achieve compatibility and interfacial adhesion by acting as chemical bridges at the interface between two dissimilar materials such as inorganic reinforcement and organic matrix, will also be given.

2.1 Natural Composites

With the emerging technology, the need for engineering materials, exhibiting high specific strength and stiffness along with high flaw tolerances, is continuously increasing. It is well known that the combination of these technology driven material properties can only be satisfied by composite materials with an appropriate structural design. However, selecting suitable constituents, deciding their size and morphology, optimizing the relative volume fractions of the constituents and anchoring these constituents by an appropriate architecture as well as tailoring the interface are not quite simple tasks [52, 53]. Despite its limited chemical resources, nature solve all these issues long time ago by optimizing its design concepts and organizing the structure in several length scales in a controlled manner [9].

Nacre, bone, sponge spicules, crab exoskeletons and spider silk are some examples of natural materials. Regardless of their weak and brittle constituents, these materials possess outstanding mechanical performance originated from their well-defined multi-scale hierarchical structural design [1-4]. In these materials, the intricate nano- and micro-scale structural arrangements, extending in several length scales, lead to multiple toughening and strengthening mechanisms acting together consistently resulting in macro-scale mechanical performance [4, 54].

The adaptation of these natural hierarchical structures to synthetic engineering materials requires the comprehensive understanding of the underlying design principles leading to extraordinary performance and multifunctionality [9]. For this reason, there has been an enormous effort to understand the formation of these natural materials, to explore the complexity, multifunctionality and multi-scale nature of structure-property relationship and to mimic their intricate structure to design lightweight, strong, stiff and tough synthetic materials for future engineering applications. Although significant advances have been achieved in exploring the mechanical response-structure relationship, mimicking the multilevel architecture of artificial composites still remains as a challenging goal since hierarchically complicated multi-scale structural organizations makes it difficult to replicate them synthetically [10-13].

Nacre, the mother-of-pearl, is one of the most inspiring natural materials. Despite its high brittle inorganic content, nacre is tough, strong and stiff [13]. The work of fracture of nacre is 3000 times higher than its inorganic constituent [15]. Its hierarchical arrangements in nano- and micro-scale enable high inelastic strains leading to elimination of stress concentrations and catastrophic failure making the nacre notch insensitive [16, 17].

This extraordinary combination of mechanical properties makes nacre "bio-mimetic model" and the source of inspiration in many studies and also in this study. In the following sub-sections, the multilevel structure-property relationship and the efforts to mimic the structure of this material will be mentioned briefly.

2.1.1 Nacre (Mother of Pearl)

2.1.1.1 Structure

Nacre is the inner lustrous layer of many mollusk seashells. Its structure consists of hierarchically organized polygonal aragonite ($CaCO_3$) platelets, separated and bonded by organic phase. The inorganic content of the nacre is 95 vol% which is higher than the organic content ever achieved by synthetic composites. The remaining 5 vol% consists of biomolecules (β-chitin, silk-like proteins and acidic glycoproteins) [14, 15, 55].

Nacre is formed through a very slow process, called biomineralization, involving the selective identification and absorption of mineral elements and organic matters from the local environment and their deposition into hierarchically ordered structure [43, 56]. During this process, nucleation and growth and hence, size, morphology and the distribution of the aragonite platelets is controlled by the constituents of thin organic layer in such a manner that the final structure resembles to brick-and-mortar structure in micro-scale [15, 55, 57]. This brick-and mortar structure (Figure 2.1.b), spanning multiple length scales, consists of highly oriented layer arrangement of aragonite platelets (bricks) separated and glued by 5-20 nm organic layer (mortar). The diameter and thickness of polygonal shaped aragonite platelets are 5-8 μm and 0.2-0.5 μm, respectively [14, 55, 57, 58].

6

Although this brick-and-mortar structure of nacre is thought to be the main reason of high mechanical performance; it is not only the fascinating structural aspect that nacre has. Detailed structural investigations reveal that there exist nano- and micro-scale intriguing features; surface waviness of aragonite platelets, platelet interlocks, mineral bridges and nano scale mineral islands called nanoasperities, each of which suggested to play a crucial role in the mechanical performance of nacre [16-22, 56].

An interesting feature of the nacre is the surface waviness of the aragonite platelets [22]. It has been reported that the amplitudes of surface roughness can reach significant values as compared with the thickness of the aragonite platelets [22]. Despite this noteworthy surface roughness, the platelets of adjacent layers integrate perfectly (Figure 2.1.d) [59].

In lower scale, there exist mineral bridges (Figure 2.1.e) and nanoasperities (Figure 2.1.f) on the surface of the aragonite platelets. Mineral bridges are extending through the holes in the organic layer and connecting the platelets at adjacent layers. These randomly arranged bridges are more or less circular in shape with a diameter of 36-54 nm and a thickness equal to the thickness of the organic layer between the platelets [20, 60]. It has been suggested that because of this mineral bridges, the organic layer separating the aragonite platelet layers should not be considered as monolithic instead should be considered as fiber reinforced composite, especially in modeling the fracture behavior of nacre [19]. The diameter and the height of the nanoasperities found on the surface of the platelets are 30-100 nm and 10 nm, respectively [16, 17].

Another remarkable fact is that each aragonite platelet is not monolithic but composed of cobble-like polygonal nanometer-sized grains separated by a very thin organic layer framework (Figure 2.1.g). The crystal orientation of these coherent nanograins, with an average size of 32 nm, is all same [59, 61].

Beside all these features, the organic constituent of nacre, itself, comprised of layered structure with β-chitin core layer sandwiched between two protein layers (Figure 2.2) [59, 62]. The outer protein layers controls the nucleation and growth of the inorganic constituent, aragonite platelets. The structure of the proteins in these outer layers, such as Lustrin A, is highly modular consisting of multidomains with folded modules connected in series [63, 64]. Core layer involves β-chitin fibers that impart mechanical and the chemical stability to the organic matrix of nacre [65].
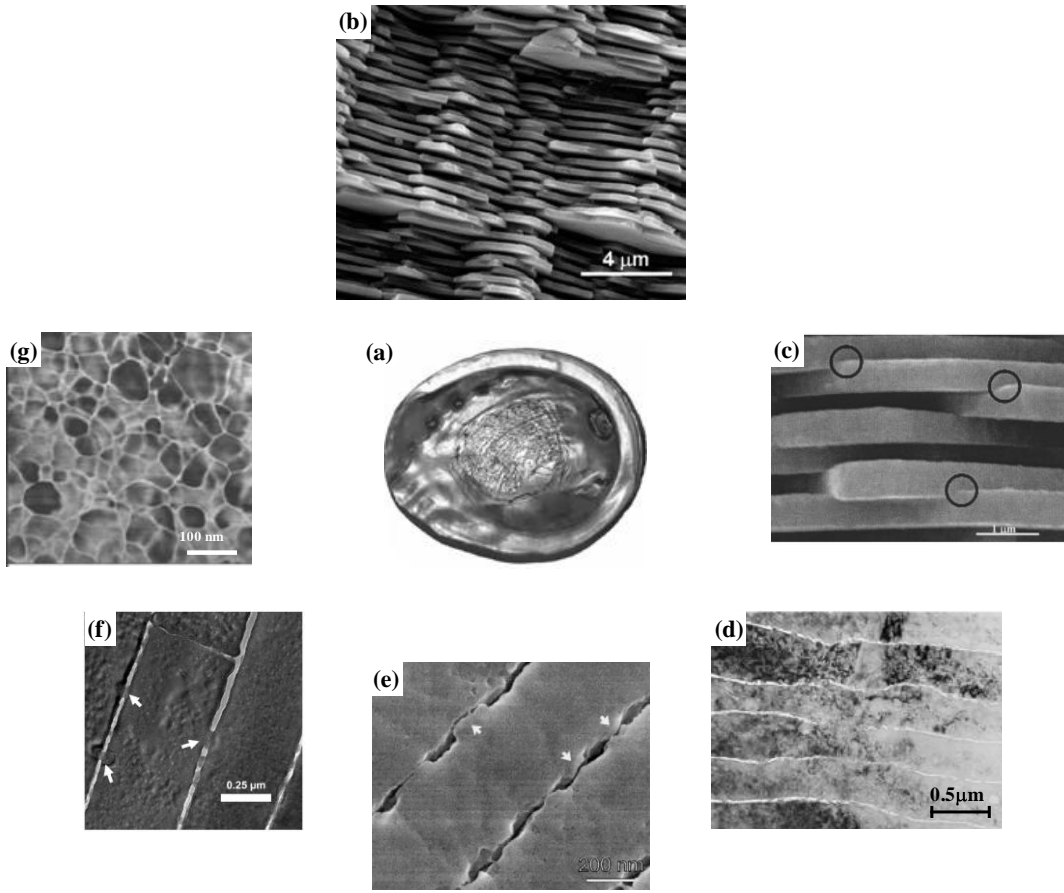
Figure 2.1 Multi-scale hierarchical structure of nacre (a) Inner nacreous layer of a red abalone shell [22], (b) SEM images showing (b) fracture surface of nacre, demonstrating a brick and mortar structure [58], (c) aragonite platelet interlocks [60], TEM images showing (d) tablet waviness [22], (e) nanoasperities [17], (f) tablet mineral bridges [56], and (g) AFM image showing the nanograins inside the aragonite platelet [66].
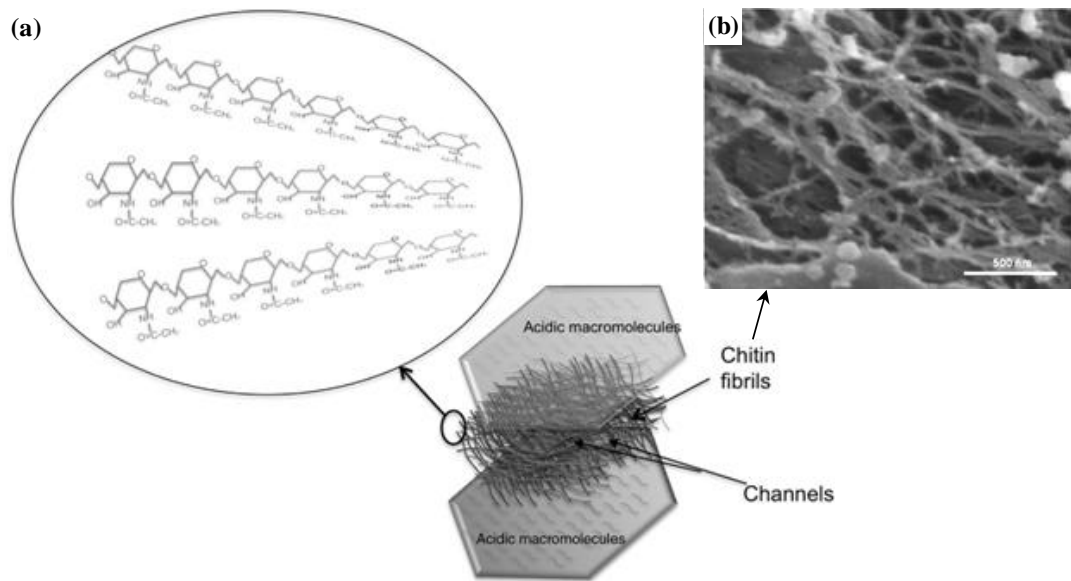
Figure 2.2 (a) Schematic representation of organic layer consisting of β-chitin core layer sandwiched between two protein layers [62], (b) demineralized shell revealing randomly oriented chitin fibrils from intertile layers [67].

2.1.1.2 Structure-Property Relationship

Up to date, an intensive research has been devoted to explore the mechanical properties and their relationships with multi-scale hierarchical arrangements found in nacre [15, 17, 20, 63, 68-73]. Jackson et al. [15] investigated the strength, stiffness and toughness of nacre from the bivalve mollusk, Pinctada and reported the tensile strength–flexural young modulus values of 170 MPa-70 GPa and 140 MPa-60 GPa, for dry and wet nacre, respectively. The work of fracture values of dry and wet nacre were 464 and 1240 J/m^2, respectively, for a span-to-depth ratio of 4. Sarıkaya et al. determined fracture strength and fracture toughness of abalone nacre as 185±20 MPa and 8 ± 3 MPa m$^{1/2}$, respectively [69]. Wang et al. investigated the flexural properties of abalone and pearl oyster nacre [17]. The reported values for flexural strength and modulus were 223 MPa - 69 GPa and 227 MPa - 77 GPa for abalone nacre and pearl oyster nacre, respectively. It is certainly clear that despite its high fraction of brittle inorganic content, nacre shows high toughness along with high strength and stiffness. The underlying reason for the unusual combination of these mechanical properties along with the lightweight is the nacre's multilevel structural design which was optimized with the evolution of the earth to a level that can not be tailored in artificial composites [14, 15, 58].

9

As a consequence of its design concepts, such as the strength and aspect ratio of the aragonite platelets, the interfacial strength along with the hierarchical arrangement of the constituents, the failure of nacre is governed by platelet pull-out mode (Figure 2.3.a) leading to both high toughness and strength [29]. During fracture, cracks extend through the relatively weak organic layer between the aragonite platelet layers and deflect around the highly oriented platelet edges resulting in a change in the stress state at the crack tip and hence, an increase in the resistance to crack growth [71, 74] . The crack deflection along with the platelet pull-out leads to a tortuous crack path and increase in the energy absorption resulting in high work of fracture. The interfacial adhesion between the organic layer and aragonite platelets also contributes to toughening by bridging the delaminating two adjacent aragonite platelet layers (Figure 2.3.a) preventing unstable crack growth [15, 70, 71, 75]. Therefore, in earlier studies, micro-scale brick-and-mortar structure driven toughening mechanisms such as crack deflection, platelet pull-out and organic matrix bridging (Figure 2.3.b) were reported as the main reasons for high toughness of nacre [15, 68, 70, 71, 73].

However, suggested brick-and-mortar architecture related toughening mechanisms are not adequate to explain the extraordinary toughness amplification in nacre [29, 63]. Further researches in this area reveal that several other toughening mechanisms, mostly driven by the interfacial architecture, are also operative contributing towards the toughness of nacre along with the above mentioned mechanisms. Some of these mechanisms are; interlocking of aragonite platelets, multiple cracking, viscoplastic deformation of the inorganic phase and unfolding of the domains in chain-molecules and breaking of cross-links, sliding of the platelets, breakage of the mineral bridges, plastic deformation of individual tile, organic bridging between the nano grains of the aragonite platelets etc. [29, 58, 76, 77].

(a)   **(b)**
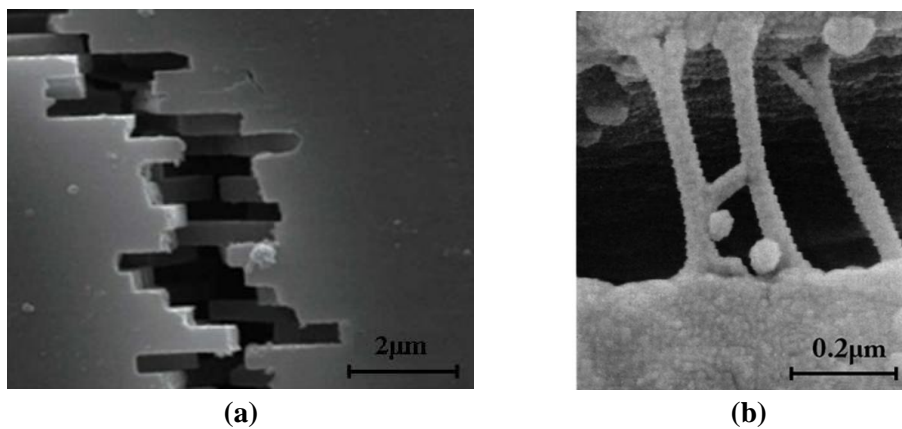
Figure 2.3 SEM images showing (a) tortuous crack path and platelet pull-out [78] and (b) fibrils of the organic matrix bridging a delamination crack. Note the large extension and 'splayed-out' anchorage points [15].

Figure 2.4 shows a typical stress-strain curve of nacre under tension indicating that dry nacre exhibits elastic deformation and fractures catastrophically whereas, the deformation behavior of the fresh nacre is associated with high inelastic strains [13]. The difference between the mechanical response of dry and wet nacre is arisen as a result of the hydration state of the organic phase. The organic phase between the aragonite platelets controls the shear stresses at the interface and hence, the behavior of the organic layer during sliding of the platelets. In dry nacre, dehydration of the organic phase lead to a stiff layer resulting in a strong but brittle material, similar to its constituent pure aragonite [14, 15, 22, 77]. Similar to wet nacre, fracture is governed by platelet pull-out in dry nacre, however, organic matrix bridging, one of the main toughening mechanisms in hydrated nacre, is not operative as a result of brittleness of the organic phase. This situation explains the lower toughness values of dry nacre and also the key function of the organic phase on the ductility and the toughness [15, 74].

(a)   **(b)**
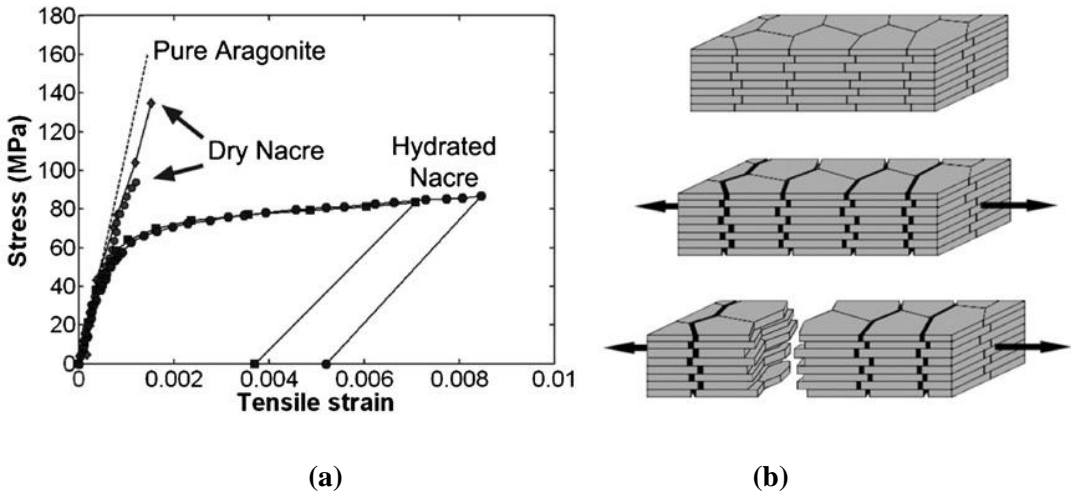
Figure 2.4 Stress–strain curves of pure aragonite along with dry and hydrated nacre from red abalone shell in tension (along the tablets), (b) Schematic view of the micro-scale mechanical behavior of nacre under tension (arrows indicate the loading direction) [13]

As mentioned before, in hydrated nacre, the micro- and nano-scale hierarchical structures enable large inelastic deformations after a linear elastic region [16, 17]. In elastic region, organic layer between aragonite platelet layers and mineral bridges withstand loads until they rupture. When the shear strength of the interfaces reached, aragonite platelets begin to slide on each other leading to local deformation [4, 59, 79]. At these locally deformed regions, the interfacial structural features resists for further sliding of the platelets leading strain hardening phenomena. At this stage, new platelet sliding regions that are energetically more favorable are activated and the deformation spans large volumes of structure [59]. The spreading of the sliding action and hence, inelastic deformation over

large volumes prevents localized deformations which can result in premature failure of the nacre [80]. The sliding of the platelets leads to separations at the platelet terminations and results in formation of dilatation bands (Figure 2.5.a and Figure 2.5.b) [16, 17]. The formation of these dilatation bands continues until all potential sites are saturated after which nacre fails under the mode of platelet pull-out [59].

(a)   (b)
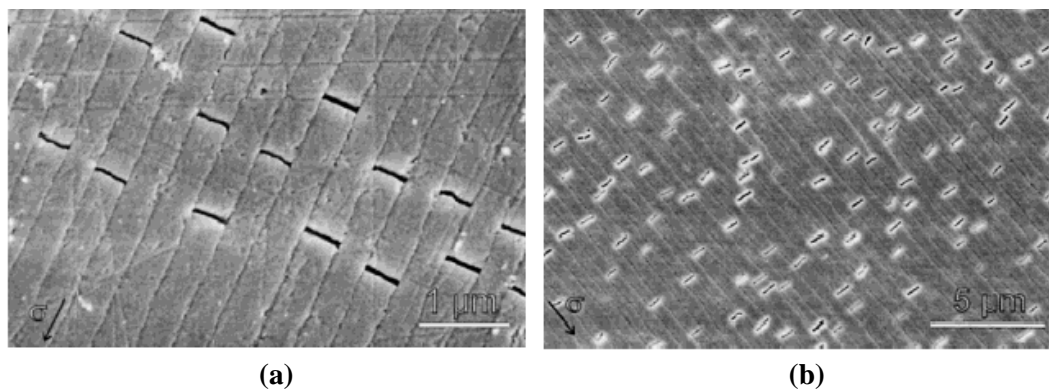
Figure 2.5 SEM images showing the dilatation bands for (a) abalone nacre and (b) pearl-oyster nacre. (Direction of tensile stress is indicated by black arrow) [17].

Several mechanisms have been proposed as the origin of the local strain hardening observed in nacre; biopolymer stretching [81], interlocking of the surface asperities [16, 17], relocking of the broken mineral bridges [21] and surface waviness of the aragonite platelets [22]. Schematic of these mechanisms can be seen in Figure 2.6. The interposing arrangements of the nanoasperities found on the surface of the platelets [16, 17] (Figure 2.6.a) and fractured mineral bridges [21] are supposed to resist the interfacial sliding of the platelets acting as a barrier leading to initial strain hardening. However, because of the large experimentally observed sliding distances and the increase in the sliding resistance with the progress of the sliding, none of these mechanisms along with the biopolymer stretching, strain hardening of which is limited, can be responsible for the whole strain hardening phenomena although they may contribute to hardening and impart shear strength [21, 22, 59, 77]. Barthelat et al. have addressed the local hardening phenomena to dovetail like micro-scale surface waviness of the aragonite platelets which can impose resistance to platelet sliding and pull-out over micrometer length scales [22]. Furthermore, dovetail geometry of the platelets can also lead to progressive locking resulting in an increase in the required load for pulling out the platelets [77, 80].
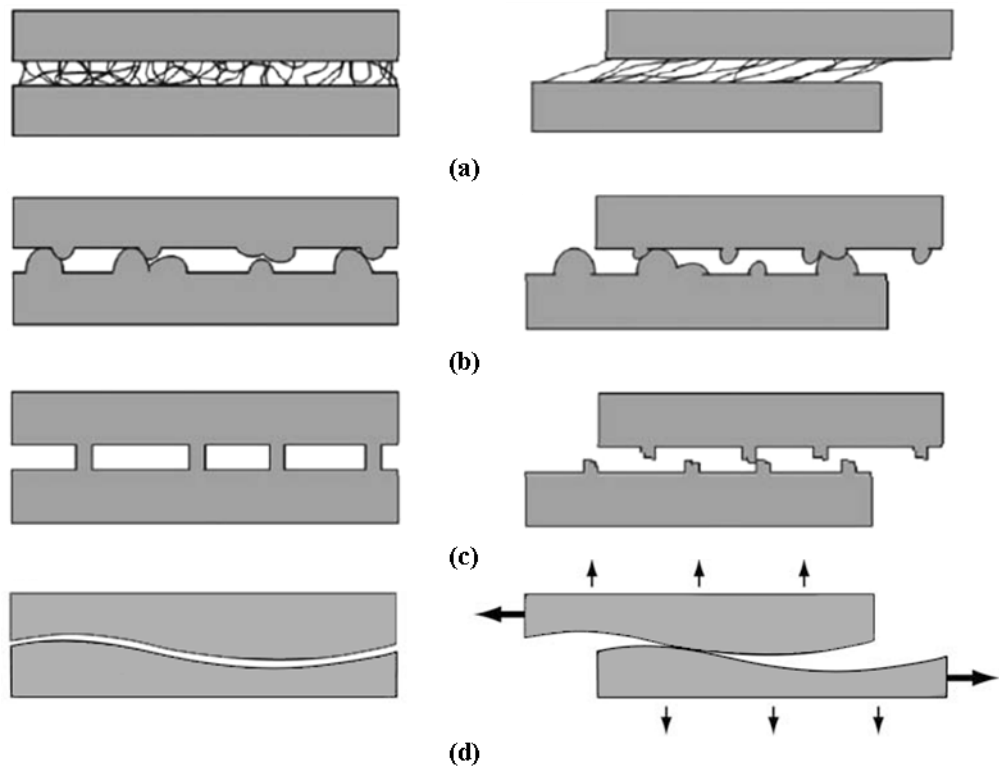
Figure 2.6 Schematics of the proposed nano-scale mechanisms controlling the shearing of the aragonite platelet interfaces: (a) biopolymer stretching, (b) interlocking of nanoasperities, (c) relocking of the fractured mineral bridges [21], (d) locking generated by surface waviness [22].

Platelet sliding induced large inelastic deformation has been also suggested a prominent toughening mechanism and the main reason for the robustness of nacre [17, 22, 59, 79]. Fracture experiments indicate the generation of white "process zone" associated with inelastic deformation in regions of high stress concentration, e.g. at crack tips [59, 75, 82]. The size of this process zone progressively increases with the increase in load until the crack starts to propagate (Figure 2.7) [4, 80, 82]. Generation of inelastic deformation at the crack tip leads to stress redistribution and energy dissipation required for crack propagation [17, 22, 59, 79].
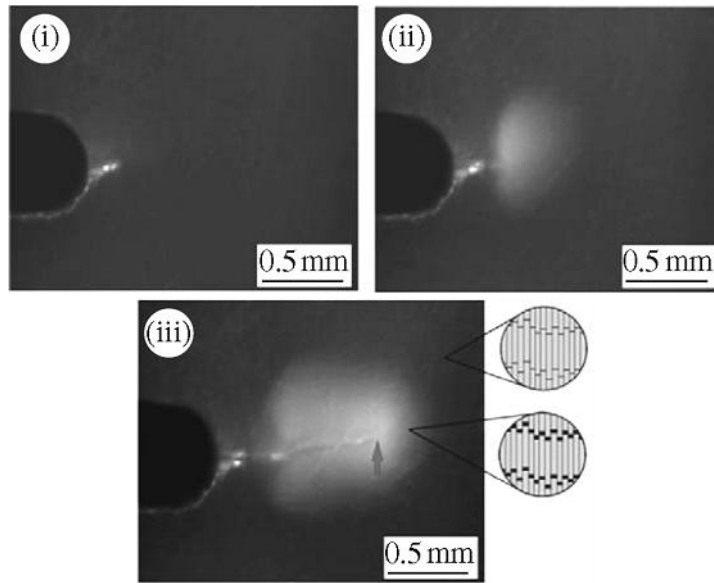
Figure 2.7 Polished notched sample under increasing load showing initial frame (zero load), stationary crack along with the increase in inelastic zone and propagation of the crack leaving a wake of inelastic deformations [4].

During sliding of the platelets, the ligaments of the organic layer preserve the integrity of the structure and allow the dilatation bands to evolve in steady state [16, 17, 81]. Sequential unfolding of the modular structure dissipates energy contributing toughness of the nacre [58, 76]. The required forces for unfolding and detachment of the proteins in the organic layer increase in the proximity of mineral bridges leading to an increase in the energy dissipation during pulling off the aragonite platelets [63, 72]. Beside, strengthening of the organic layer, these bridges aid two main toughening mechanisms; crack deflection and platelet pull-out by arresting the crack tip and avoiding its extensive growth and hence leading to crack deflection [19, 74].

Plastic deformation and rotation of the nanograins of the individual platelet contributes the toughening of nacre by redistributing the stress around strain concentration sites, and, consequently, blunting the crack tip [58, 83]. It has been reported that aragonite platelets are somewhat ductile in nature and along with the crack deflection, platelet sliding and the organic adhesive interlayer, the deformation of nanograins lead to 1000-fold increase in toughness with respect to that of its constituents [61]. Furthermore, progressive failure of interlocks is also suggested to be another feature that contributing to high toughness of nacre by guiding the fracture path and limiting the catastrophic failure [55, 60].

14

2.2 Bio-inspired Nacre-like Composites

As aforementioned, nacre is a complex material consisting of intricate nano- and micro-scale structural features, each of which undertake a task and operate synergistically leading to unique combination of mechanical properties such as high strength and stiffness along with the high toughness. As mentioned in the previous section, structural arrangement-mechanical performance relationship has been the focus of an intense research to explore the underlying design principles found in nacre. The advances achieved guide the bio-inspiration studies and provide new insights for the design of next generation composite materials. However, replication of the multi-scale hierarchical structure and key features of nacre is a difficult task using the current technology [13]. Therefore, up to date, the bio-inspiration studies mainly focused on mimicking the micro-scale "brick-and-mortar" structure of nacre [23, 24].

In the following sub-sections, the design principle lying underneath the micro-scale hierarchical architecture and the techniques used to fabricate composite materials with a brick-and-mortar structure will be mentioned briefly.

2.2.1. Design Concepts

The relationship between brick-and-mortar structure of nacre and the resultant mechanical properties is best described by the simple shear lag model [15]. According to this model, stress is transferred to discontinuous inorganic reinforcements via shear stresses developed at the reinforcement-matrix interface [15, 84]. For flake or platelet reinforcements, assuming that they are aligned parallel to their principal plane, this holds for all directions in the plane of the 2D reinforcements [84]. The tensile stress, being zero at the ends of the reinforcements, builds up until maximum is achieved at the center of the reinforcement [15, 85].

Based on this model, the aspect ratio of the platelets plays a crucial role in determining the fracture mode and the strength of nacre. If aspect ratio of a platelet is higher than a critical value ($\alpha>\alpha_c$), the stress transferred from matrix to reinforcements increases with the increase in the shear stress transfer lengths and exceeds the fracture strength of platelets leading to a failure mode of platelet fracture. On the other hand, if the aspect ratio of the platelets is lower than the critical aspect ratio, the failure mode is governed by platelet-pull out mode (either matrix failure or interface failure) [15, 84, 85]. To achieve effective stress transfer from matrix to reinforcements, aspect ratio should be as high as possible but lower than a critical value (α_c).

In the case of platelet fracture mode (Figure 2.8.a), failure is catastrophic leading to higher strengths but lower fracture energies. On the other hand, platelet pull-out mode (Figure 2.8.b) leads to lower strengths, as the strength potential of the incorporated reinforcement can not be fully utilized, but higher fracture energies due to the fact that the toughening

mechanisms such as platelet pull-out and matrix plastic flow can be operative before the complete failure of the composite [12, 84-86].

The critical aspect ratio of the 2D reinforcements, such as platelets or flakes, is defined as [84-86];

$$\alpha_c = \frac{\sigma_p}{\tau} \qquad \qquad (2.1)$$

where τ is either interface or matrix shear strength and σ_p is the platelet strength.
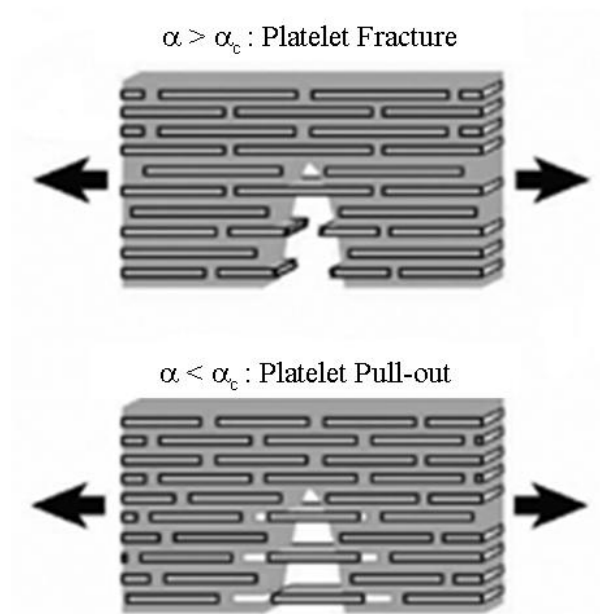
Figure 2.8 Fracture mechanisms for bio-inspired organic–inorganic composites with different platelet aspect ratio: (a) platelet fracture mode ($\alpha > \alpha_c$); (b) platelet pull-out mode ($\alpha < \alpha_c$) [12].

As mentioned in previous section, as a consequence of its design concepts, nacre exhibits unusual combination of mechanical properties such as high strength, stiffness and toughness. Experimental investigations and the theoretical modeling results indicate that the design aspects that are the thickness and the aspect ratio of the inorganic building blocks, hierarchical arrangement of the constituents along with the interfacial strength are optimized such that the failure is governed by platelet pull-out mode leading to both high

16

strength and toughness [15, 29]. The aspect ratio of the aragonite platelets ($\alpha \cong 8$-10) is found to be slightly below the critical aspect ratio (maximum allowable α_C=12) so that maximum strength is attained without causing catastrophic failure [12, 15, 87].

As compared to the resources that nature has, scientists and engineers have a wider opportunity in selection of constituents in the design of artificial composites. From Equation 2.1, it is clear that the use of high strength synthetic reinforcement enables higher critical aspect ratio values (α_C) and hence, allows the use of higher aspect ratio reinforcements (α). Therefore, by using high strength platelets it is possible to fabricate artificial composites reinforced by higher aspect ratio platelets that enable more efficient stress transfer without causing catastrophic failure [12]. The overlap between the platelets also increases with the increase in the aspect ratio which also leads to an increase in the stress transferred from the matrix to the platelets [22, 87].

In terms of toughness, the aspect ratio of platelets also plays a crucial role. Assuming that the composite failure is governed by platelet pull-out mode as in the case of nacre, reinforcing the composite with high aspect ratio platelets lead to an increase in toughness. The increase in the aspect ratio will lead to an increase in the work of fracture values by increasing the total pull-out work [15]. With the increase in the platelet aspect ratio, the extent of crack deflection also increases leading to a more tortuous crack path and hence, increase in the absorbed energy. Furthermore, Bekah et al. [87] have indicated that in nacre as the crack extends, the pulled-out platelets generates closure tractions on the crack faces as in the case of fiber bridging. Therefore, the increase in the aspect ratio leads to an increase in toughness. High aspect ratio, lower platelet thickness and high inorganic content have also positive effect on process zone toughening and hence, lead to an increase in the overall toughness [87].

To sum up, by taking into consideration the design aspects found in nacre that have been deduced from the mechanical response-structure relationship, the following design rules should be applied to achieve both high strength, stiffness and toughness [13, 15, 22, 29, 87, 88];

- The hierarchical brick-and-mortar structure should be achieved.

- To increase the overall stiffness, the composite should be reinforced by stiffer fillers. Furthermore, the stiffness of the interface between platelets and the matrix also contributes to the overall stiffness.

- The inorganic content should be as high as possible for high strength, stiffness and toughness.

- The thickness of the platelets should be low but aspect ratio of the platelets should be as high as possible but lower than the critical value to eliminate brittle fracture and favor the platelet pull-out failure mode.

– High interface adhesion and shear strength must be needed. However, the interface strength should be weaker than the strength of the platelets.

– The platelets should be wrapped with soft organic phase capable of withstanding large strains.

– In micro- or nano-scale, the strain hardening should occur to spread the platelet sliding throughout the material.

Beside the above mentioned design guidelines, there are also some other important factors that should be taken into consideration in fabrication of artificial nacre-like hierarchical composites. For instance, processing damages, such as fracture of the platelets, lead to a decrease in the strength and stiffness of the composite [84, 89, 90]. Especially, high aspect ratio platelets are more sensitive to fracture [90].

In addition to fracture of the platelets, voids and pores should also be avoided as they act as stress concentration and crack initiation sites [26, 47, 90]. Furthermore, platelet cluster in which platelets were stacked should also be avoided due to the fact that platelet clusters lead to decrease in strength either by leading to decrease in the effective stress transfer or by acting as potential sites for stress concentration [30, 31, 91-94].

Han et al. and Bonderer et al. designed a composite system based on shear lag model which is successfully applied to describe the strength of nacre [26, 86]. Han et al. [86] fabricated polyvinylalcohol (PVA) matrix composite films by using high strength layered double hydroxide (LDH) platelets with two different aspect ratios (α); smaller and larger than the calculated critical aspect ratio (α_c=40), to investigate the effect of aspect ratio on final mechanical properties. The results indicated that reinforcing the PVA with LDH nanoplatelets having an aspect ratio of $\alpha < \alpha_c$, lead to fracture mode of platelet pull-out, and hence, the fabricated composite film exhibited high strength, stiffness and toughness. On the other hand, nanocomposite films reinforced by LDH nanosheets with $\alpha >> \alpha_c$ resulted in relatively higher strength and stiffness but the fracture governed by platelet fracture mode leading to catastrophic failure.

Similarly, Bonderer et al. [26] have fabricated alumina platelet reinforced chitosan and polyimide composite films by applying design concepts which was based on shear lag model. To fabricate a tough and strong composite, ductile polymer matrix was reinforced by 200 nm thick surface modified high strength alumina platelets with an aspect ratio of ~ 40 which is lower than the critical aspect ratio (α_c=50). The results of this study indicated that although the tensile strength increased with incorporation of alumina platelets, beyond a certain value, further increase in the volume content of inorganic reinforcement lead to a decrease in strength (Figure 2.9.a). This decrease was attributed to the increase in the fraction of the pores along with the misalignment (Figure 2.9.b). Another important finding in this study is the effect of interfacial strength on both toughness and strength. Although the fracture was governed by platelet pull-out mode, strong interfacial adhesion between the

inorganic reinforcements and the matrix favored the matrix cracking rather than interface failure leading to an increase in mechanical performance in terms of both toughness and strength.

The experimental findings achieved in these studies have clearly demonstrated that by selecting appropriate constituents, optimizing the relative volume fractions of the constituents and anchoring these constituents by an appropriate architecture and by tailoring the interface to achieve strong interfacial interactions, it is possible to design a composite material the properties of which surpass the mechanical properties of nacre [26, 86].
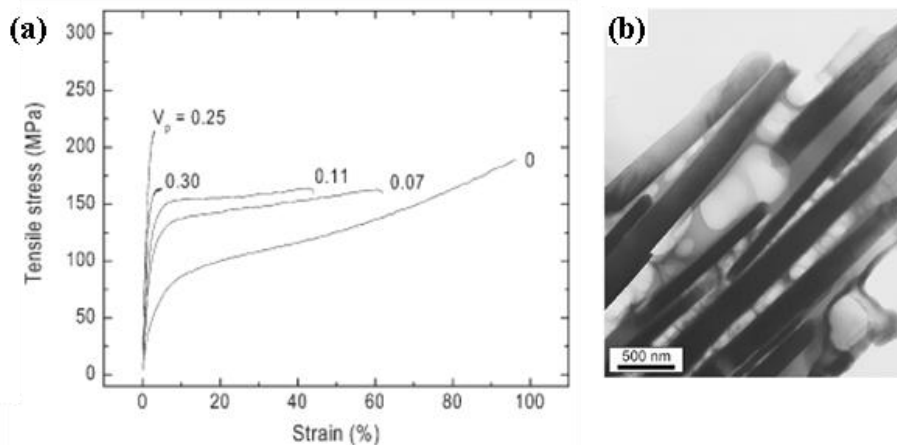
Figure 2.9 (a) Tensile stress vs. strain curve of polyimide matrix composite film and (b) TEM image of polyimide matrix composite films reinforced by TEM images of polyimide matrix composite films reinforced by 42 vol% surface modified alumina platelets [26].

2.2.2. Synthetic Pathways for the Fabrication of Nacre-like Structures

As mentioned before, up-to-date, bio-inspiration studies are mostly focused on the replication of micro scale brick-and-mortar structure of nacre. In this manner, the main effort was expended to find efficient, cost effective new pathways that control the structure in micro-scale in order to fabricate composite materials with hierarchically arranged structures [95].

Various methodologies have been employed to fabricate nacre-like bio-inspired composites. Figure 2.10 summarizes the techniques used to fabricate composites with a nacre-like hierarchical architecture.
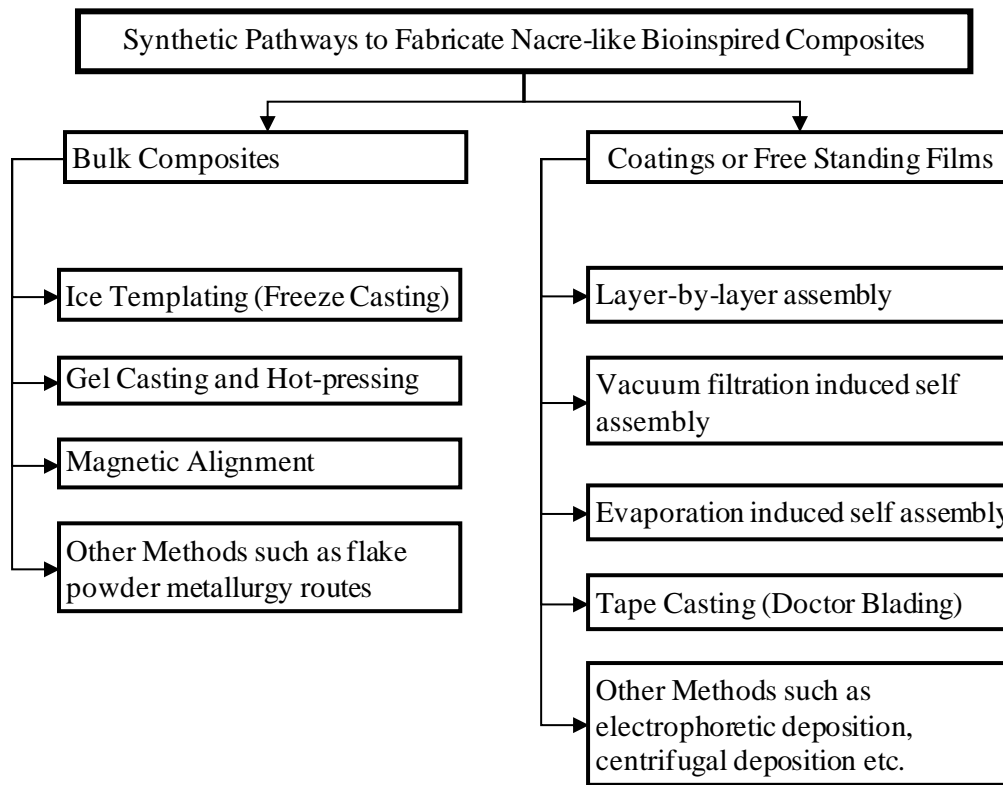
Figure 2.10 Synthetic pathways to fabricate nacre-like bulk composites, free-standing films and coatings.

Layer-by-layer assembly, being a convenient technique, is used to fabricate organic-organic or inorganic-organic composites either in the form of coating or free standing films. In this method, layered structure is achieved by sequential adsorption of building blocks by immersing the substrate into two dilute solutions (Figure 2.11.a) [96-99]. The driving forces for the deposition of individual layer can be electrostatic interaction, hydrogen bonding, charge transfer or hydrophobic interaction [29, 97]. Precise and nanometer-scale control over the structure makes this method suitable for the fabrication of hierarchically arranged structures [29, 96, 98, 99]. Along with these, its capability of incorporating high loading of inorganic fillers makes this method appropriate for the replication of brick-and-mortar structure of nacre [29].
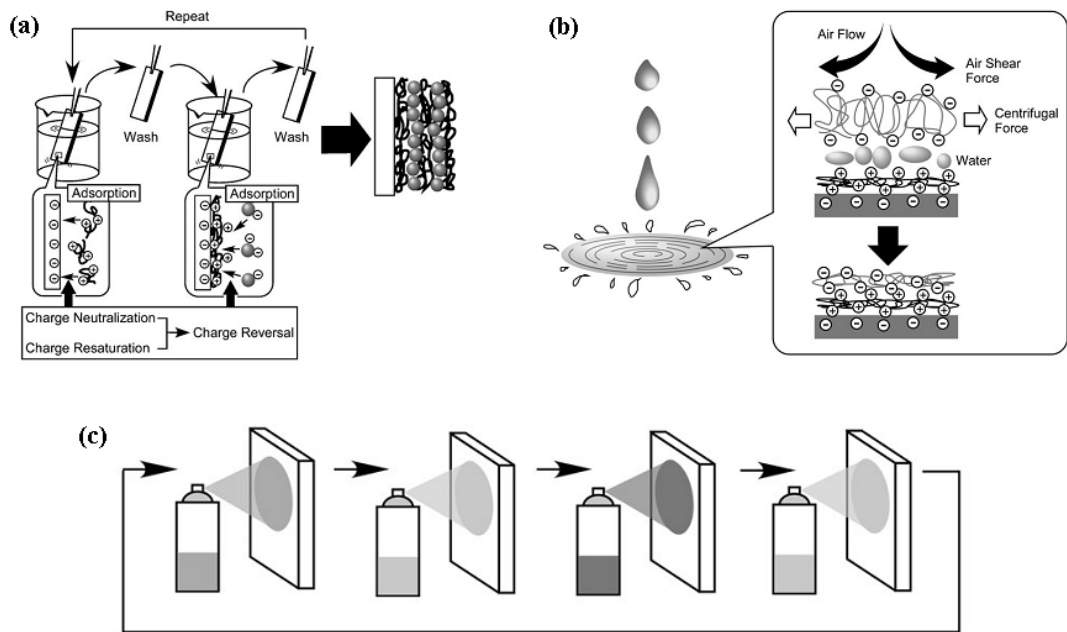
Figure 2.11 Layer-by-layer assembly via (a) dip coating, (b) spin coating and (c) spray deposition [100].

Beside all advantages, LBL assembly by dip coating is an inherently laborious and time-consuming method as it requires repeating dipping, washing and drying cycles to achieve practical film thickness [29]. Figure 2.12 shows SEM image indicating the thickness of MTM-PVA nanocomposite film after 300 bilayer deposition by dip coating [30].

Layer by layer assembly via spin coating (Figure 2.11.b) is a faster process as compared to dip coating [25]. It was reported that assembly of a 300 nm thick 100-bilayer Laponite clay-poly(diallyldimethylammonium)chloride film can be deposited in less than 1 h which is 20 times faster than conventional dip-coating process [25]. For this reason, in recent years, LBL assembly via spin coating method has also been used either with or without LBL assembly via dip coating method to fabricate inorganic-organic nacre-like composites [12, 26, 27]. Beside spin coating and dip coating, spray deposition method is also used to fabricate LBL assembled nacre-like composites (Figure 2.11.c) [28].
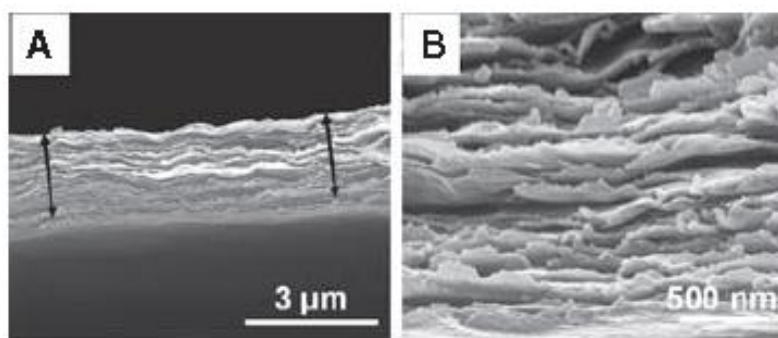
Figure 2.12 SEM images of a 300-bilayer, free-standing PVA/MTM nanocomposite; (a) cross section indicating the thickness of the film, (b) closer view showing the structure [30].

Alternative methodologies to LBL assembly for the replication of the brick-and-mortar structure of nacre are based on simple, fast and scalable one-step green pathways such as vacuum filtration-induced self-assembly (or paper-making process) [31-33, 101] or water evaporation-induced self-assembly (or solution casting) [34-36, 102-104] and tape casting (doctor -lading) [37-39, 105]. Although LBL assembly method provides precise control over the structure, these simple, relatively fast, scalable one – step techniques offer the advantage of processing thick and large-area composite films [106]. In evaporation induced self-assembly method, dispersion of inorganic filler and polymer are directly cast into a mould and the evaporation of the solvent give rise to hierarchical self-assembly of inorganic and organic constituents [34-36, 102] whereas in vacuum filtering-induced self-assembly, similar to traditional paper-making, alignment is directed by flow of the solvent during vacuum filtration [32, 101].

Tape casting or doctor-blading is another technique used to fabricate hierarchically ordered composite structures. In this technique, a viscous solution poured onto a substrate is spread with a blade having a predetermined slit height. Large area films or continuous coating with a uniform thickness can be produced with this method [107]. The orientation of micro- or nano-platelets is achieved by the shear forces acting and self-ordering of the high aspect ratio platelets [39, 107]. As compared to LBL method, this process is more efficient in fabrication of nacre-like composite films because of the fact that film thicknesses of 1-2 μm can be obtained in only one step [39]. At high inorganic platelet contents, in order to maintain the viscosity of the suspension in a desired level and to obtain a homogeneous dispersion, an additional solvent has to be added. In this case, the drying of the tape cast film is a critical step as too fast and uncontrolled drying can cause blisters, which act as defects and deteriorate the properties of the cast films [39].

For all these approaches, the most crucial point is to obtain homogeneous and stable dispersions. Otherwise, especially at high inorganic contents, premature aggregation, coagulation and phase separation may occur which leads to a decrease in the performance of the composite film [105].

In recent years, a new approach has been developed such that the surfaces of the 2D fillers were coated with organic layer. These core-shell hybrid building blocks then either by self-assembly techniques such as vacuum filtration and evaporation induced self-assembly techniques or by tape casting [104, 106-108]. Figure 2.13 shows the schematics of the strategy used for the fabrication of hierarchically arranged clay-polymer composite film.
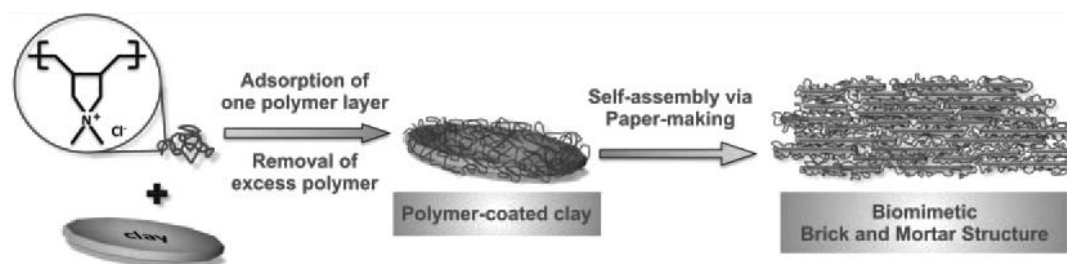
Figure 2.13 Multilevel self-assembly for the production of nacre-mimetic brick and mortar structure by core/shell hard/soft building blocks consisting of hard inorganic clay cores and soft polymer coatings [107, 108].

Well aligned nacre-like self-standing films of layered double hydroxides [109], montmorillonite [110-112] and graphene oxide [113, 114] can also be prepared either by vacuum or evaporation induced self-assembly techniques. These films have the potential of use in composite fabrication as layered reinforcement preforms [112]. In a recent study [114], highly aligned graphene oxide (GO) preforms (Figure 2.14.a), assembled by vacuum assisted filtration of aqueous exfoliated GO solution and subsequently dried. In order to fabricate composite film, produced preform was immersed in a 10,12-pentacosadiyn-1-ol (PCDO) solution and cross-linked under UV radiation (Figure 2.14.b and Figure 2.14.c). A reduction step was also carried out by immersing the GO and GO-PCDO films to hydroiodic acid (HI) solution in order to remove oxygen containing groups. Despite their low organic content, ~ 6.5 wt.%, the resultant nacre-like composite films exhibited high tensile strength along with outstanding toughness (Figure 2.14.d) superior than that of the nacre.
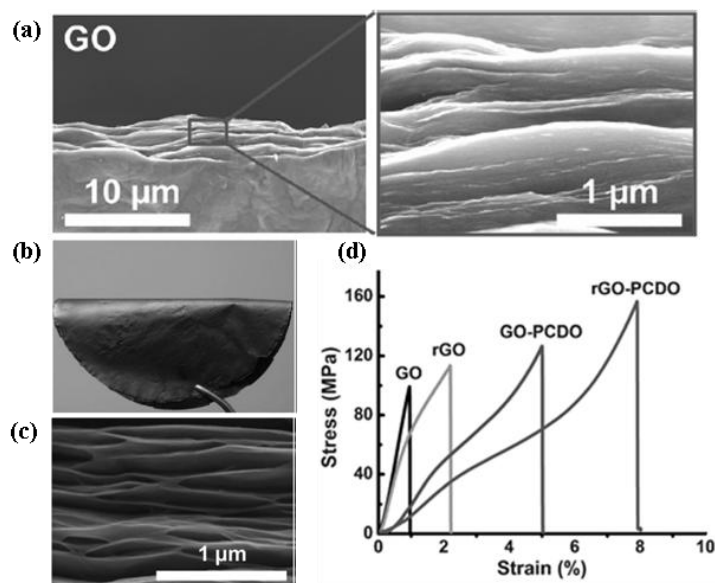
Figure 2.14 (a) and (c) SEM images of self-standing GO and GO-PCDO films, (b) image of GO-PCDO composite film (d) Stress-strain curves of GO and rGO films along with GO-PCDO and rGO-PCDO composites [114].

Although, the versatility of above mentioned method enables the fabrication of nacre-like polymer composites reinforced by various 2D building blocks, studies mainly focused on clay [25, 30, 101, 107, 115-117] [35, 102] [39, 105], layered double hydroxide (LDH) [27, 86, 118] and graphene oxide [31, 32, 36, 103] [104] reinforced composite films. Clay and LDH reinforced transparent and flexible composite films show enhanced mechanical properties with respect to their neat organic counterparts and further cross linking of these flexible free standing films with either glutaraldehyde (GA) or metal cations M^{n+} leads to considerable increase in strength to a level that even exceeds the strength of nacre [30, 86, 116]. These highly oriented films can be used in high performance flexible packaging of oxygen sensitive devices, lightweight transportation bodies and functional barrier coatings etc. [36, 39, 102, 105]. Whereas, high performance biocompatible composites reinforced by well-aligned graphene oxide (GP) or reduced graphene oxide (r-GO) platelets reinforced are potential candidates for biotechnology applications, such as drug delivery, cell culture, biosensors and electroactive substrates/scaffolds for tissue engineering [32, 103, 104].

Using LBL assembly and self-assembly methodologies, nacre-mimetic thin nanocomposite layered films were also successfully fabricated [119-122]. Figure 2.15 shows TEM images of titania (TiO_2)-polyelectrolyte and zirconia (ZrO_2)-organic layered nacre mimetic films. These LBL assembled films possessed better mechanical properties with respect to their bulk inorganic counterparts [121, 122].

24

Electrophoretic deposition [40, 41], ion-beam sputtering [42], centrifugal deposition [43] etc. are other techniques employed to produce nacre-like bio-inspired free standing films and coatings.
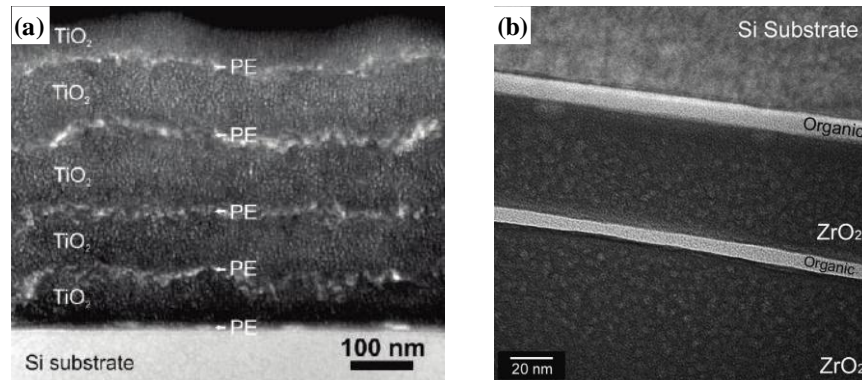
Figure 2.15 TEM images of (a) TiO_2-organic [121] and (b) ZrO_2 - organic [122] nacre-like layered film structure on silicon substrates.

Although all above mentioned methodologies are effective in fabrication of strong and though bio-inspired self-standing films or coatings exhibiting hierarchical architectures, they can not be used to fabricate nacre-like bulk composites that can be used in structural engineering applications. Ice-templating or so-called freeze casting method, first suggested by Deville et al. in 2006 [123], has been used to fabricate bulk porous ceramic scaffolds. These freeze cast ceramic scaffolds than infiltrated by a softer organic or inorganic constituent produce layered nacre-like bulk composites [11, 44, 123, 124].

The basic principle underlying this method is similar with the sea ice formation. The impurities in sea water are expelled from the forming ice during its formation and entrapped in the space between crystals. Using this principle, porous ceramic scaffolds are produced by controlled directional freezing of the prepared ceramic suspensions (Figure 2.16.a) and subsequently, sublimating the ice using a freeze drier [123]. The architecture of the produced scaffolds is templated by the ice crystals [11].

Ice templated ceramic scaffolds exhibit similar structural features as in the case of natural nacre such as well aligned inorganic layers along with dendritic surface roughness some of which spans between the neighboring layers as the mineral bridges in nacre (Figure 2.16.c). Figure 2.16.b and Figure 2.16.e indicate load-displacement curve for ice templated hydroxyapatite-epoxy and fracture surface of alumina-epoxy layered composites, respectively. These bio-inspired composites exhibit stable crack growth behavior and extensive crack deflection leading to both strong and tough composite [123].
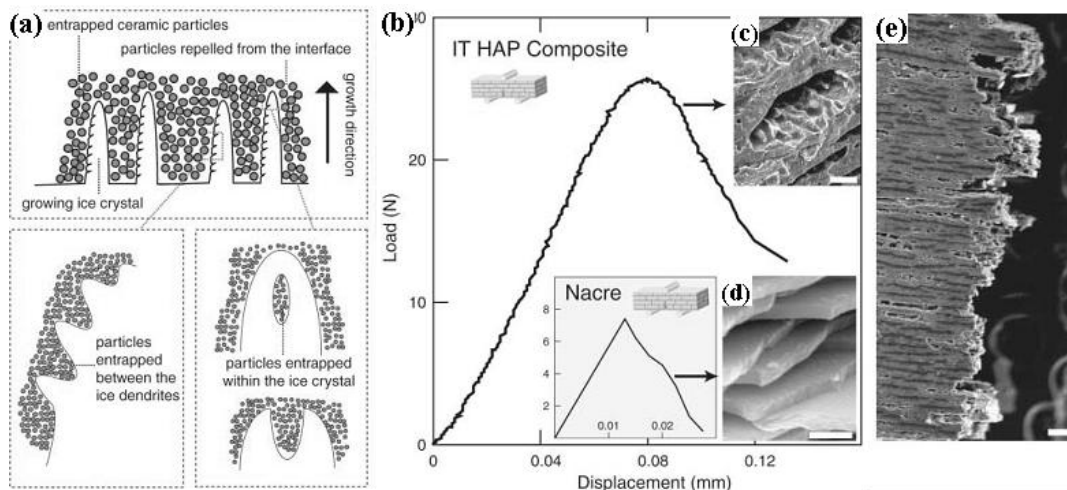
Figure 2.16 (a) Schematics of the processing principles, (b) three-point bending load-displacement data for ice templated HAP-epoxy composite and nacre (inset). Scanning electron micrographs of the (c) ice templated composites, (d) nacre of abalone shell, showing crack deflection at the lamellae and (e) ice templated alumina-epoxy composite showing the highly torturous crack path [123].

Using ice-templating methodology, it is also possible to fabricate composites with "brick and mortar structure" [11, 44, 45]. By transforming the ice templated layered structure to brick-and-mortar structure (Figure 2.17.a) through pressing, sintering and infiltrating with an organic phase, Munch et al. [11] fabricate nacre-like hierarchically arranged alumina-polymethyl methacrylate (PMMA) composite with an inorganic content of 80 vol% (Figure 2.17.b). Along with the sucrose addition to ceramic suspension which favored the surface roughness and ceramic bridge formation by changing the viscosity and phase diagram of the solvent, pressing and sintering further increased the density of the surface roughness and ceramic bridges (Figure 2.17.c). To promote adhesion at the interface, ceramic scaffold surfaces were grafted with γ-(trimethoxysilyl)propyl methacrylate (γ-MPS) before infiltration with PMMA. As a result of the brick-and-mortar architecture, interfacial features such as surface roughness and alumina bridges and interfacial strength along with the high inorganic content, fabricated composite showed higher strength, stiffness and toughness with respect to both its counterpart alumina-PMMA layered composite and natural nacre (Figure 2.17.d-Figure 2.17.f). Fracture surface analysis of alumina-PMMA composite with brick-and-mortar arrangement indicated that as a result of the governed fracture mode, which is pull-out, several toughening mechanisms acting at several length scales have contributed the overall mechanical performance as in the case of nacre [11].

26
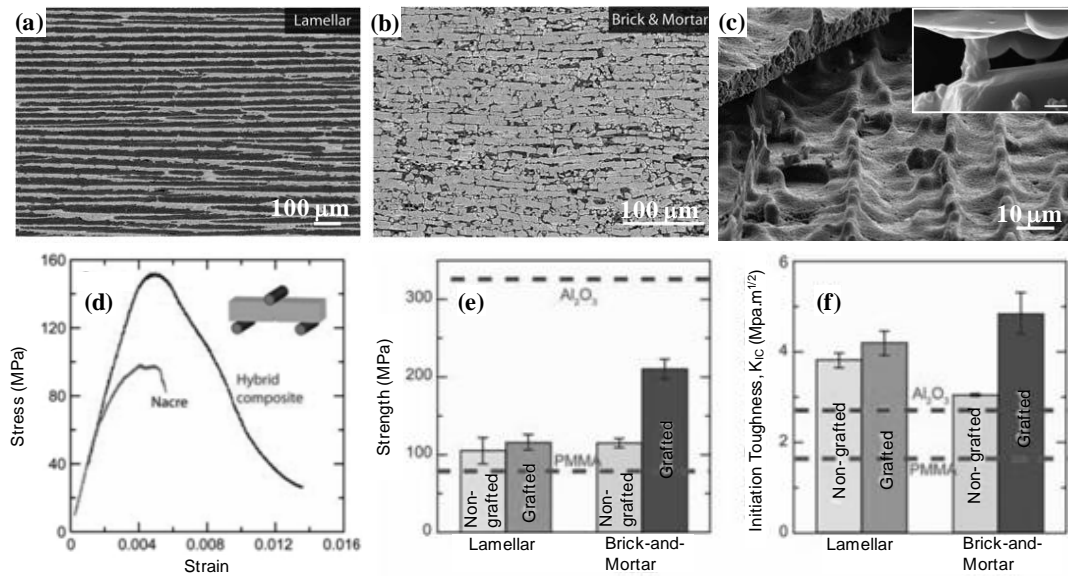
Figure 2.17 SEM images of (a) alumina/PMMA layered composites and (b) alumina/PMMA composite with brick-and-mortar architecture. SEM images showing (c) surface roughness of the layers or bricks (inset shows ceramic bridge (scale bar: 600 nm)). Mechanical response of synthetic nacre-mimetic composites (d) three point bending stress-strain curves, the influence of architecture and interfacial strength on (e) strength and (f) crack initiation fracture toughness [11].

"Gel casting and hot-pressing" is another technique proposed to fabricate bulk nacre-like inorganic-organic macroscopic composite films [46, 47]. In this two step technique, inorganic-organic mixture is prepared by dissolving the polymer in an organic solvent containing the inorganic platelets at high temperature and then, the cast mixture is cooled to enable the gelation of the polymer network and then dried. In the second step, to achieve bulk composite and improve alignment, cast composite was cut into pieces, superposed and subsequently hot-pressed. Using this method, alumina platelet-polypropylene [46] and alumina platelet-polyurethane matrix composites were fabricated [47]. The inorganic content of the fabricated composites was limited to 50 vol% due to the fact that with the increase in the inorganic content the increase in the platelet misalignment and void content along with the platelet stacking (Figure 2.18) leading to a decrease in both strength and modulus [46, 47].
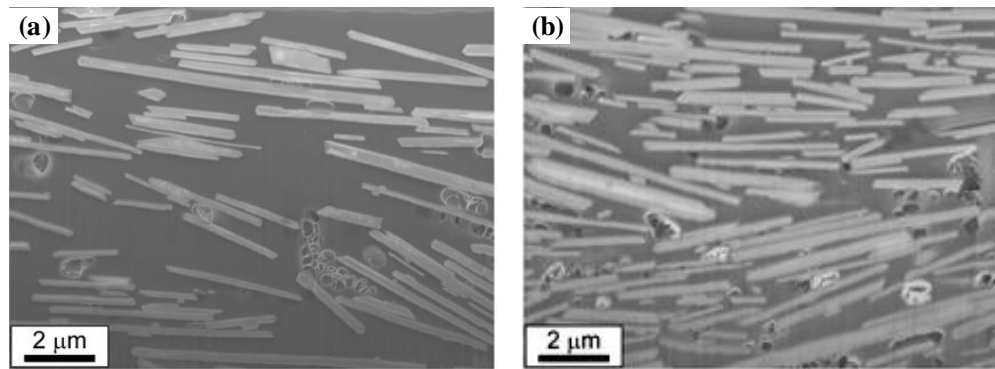
Figure 2.18 SEM images of the composites with a volume fraction (a) 30 vol% and (b) 50 vol % [46].

Various flake powder metallurgy routes are also used to fabricate nacre-mimetic bulk composites but in these techniques the building blocks were both inorganic [48-50]. Figure 2.19 shows the flake powder processing route used to fabricate glass flake-silver (Ag) matrix bulk composite with a nacre-like ordered structure. The fabricated composite with a glass flake content of 80 vol% exhibited two orders of magnitude larger work of fracture (WOF) value with respect to monolithic glass [49].

Although, all these proposed techniques are relatively simple, they are all multi-step and time-consuming processes. Recently, a single-step process is proposed for the fabrication of bulk nacre-mimetic composites [51]. This technique is based on the alignment of the inorganic platelets under the applied low magnetic fields [51].
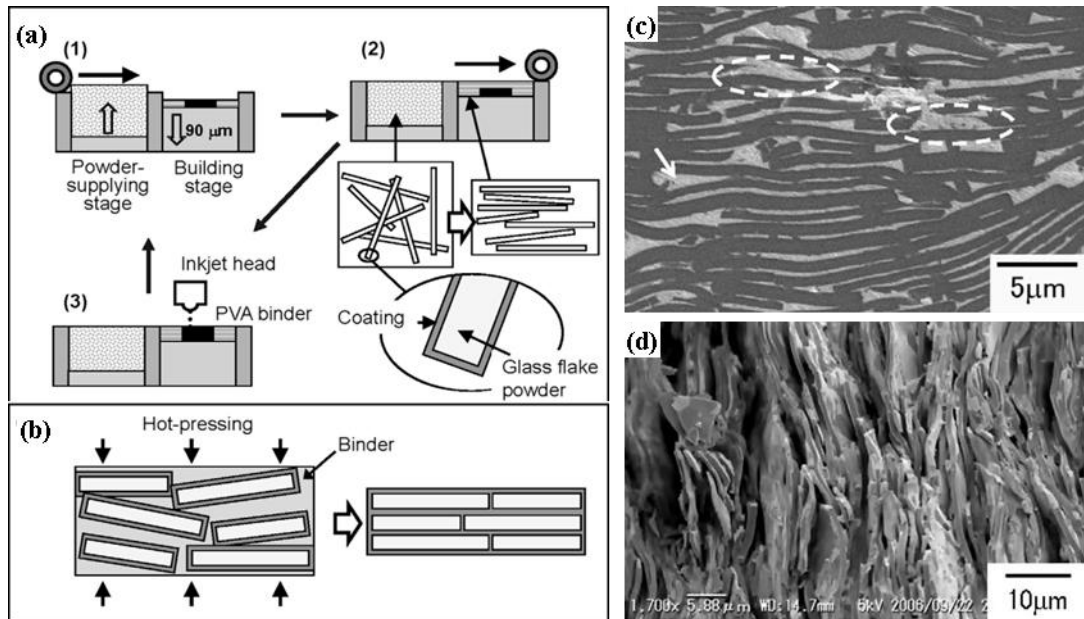
Figure 2.19 Schematic illustration of the two step processing procedure. (a) Fabrication of green samples with 3D printing machine (alignment is achieved by a roller, and polyvinyl alcohol (PVA) is used as a binder), (b) green samples are hot-pressed (flakes are consolidated and bonded by the coating which becomes the matrix layer. PVA is removed during heating), (c) microstructure of the fabricated composite, (d) fracture surface of the composite showing crack deflection at the powder/matrix interface [49].

Magnetic field induced alignment is a widely encountered concept in fabrication of textured crystalline materials [125-128] and composites reinforced by highly oriented 1D and 2D fillers [129-133]. The main drawback of this technique is the required high magnetic fields especially for the alignment of materials with low intrinsic anisotropic magnetic susceptibility [51, 134]. In most cases, this dilemma is overcome by tailoring the surface of the material with either magnetic nanoparticles [51, 133, 135, 136] or ferromagnetic coatings [137, 138] to enhance the magnetic response and to facilitate the control over the structural organization. Erb et al. used magnetic alignment technique and suggested that with the use of the right geometry along with the determination of appropriate size and aspect ratio of the reinforcing elements and decorating the surface with superparamagnetic nanoparticles, it is possible to fabricate composite structures with different three-dimensional hierarchical arrangements (Figure 2.20) under the applied low external magnetic fields [51]. The results achieved have been indicated that by changing the surface concentration of the magnetic nanoparticles decorated on the surface of the platelets and applying a combination of magnetic fields, it is possible to control the architecture which enables the tailoring of the properties in specific directions (Figure 2.20) [51].

29
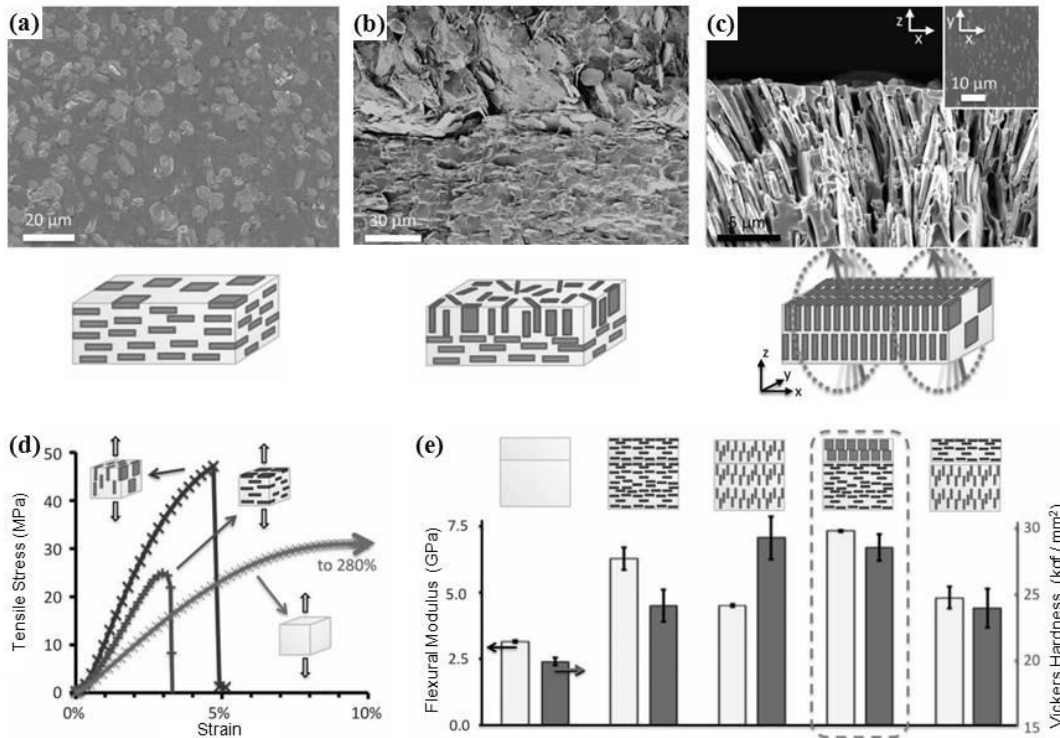
Figure 2.20 (a), (b) and (c) SEM images of the alumina platelet-polyurethane composites with different hierarchical arrangements, (d) tensile stress vs. strain curves of 20 vol% alumina platelets-polyurethane (PU) matrix composites having different hierarchical arrangements along with stress-strain curve of neat PU, (e) flexural modulus and out-of-plane hardness composites with different combinations of reinforcement orientation [51].

On the account of the above discussions, it is clear that up-to-date various processing routes have been proposed to replicate the hierarchical "brick-and-mortar" structure of nacre and its mechanical properties. Most of these studies have been focused on the fabricating nacre-like bio-inspired coatings and free standing films and, few studies have been dedicated to finding new pathways to fabricate nacre-like bulk composites. Although, significant advances and success achieved in production of strong, stiff and tough composites, there is still a need for a processing strategy which is;

- simple and one-step,
- time and man-power efficient,
- easily scalable,
- effective in alignment of the 2D reinforcing building blocks,
- effective in fabrication of bulk composites that can be used in large scale components and,
- enables the fabrication of nacre-like composites with high reinforcement contents.

2.3. Surface Functionalization with Organofunctional Silane Coupling Agents

Mechanical behavior of inorganic-organic composites is strongly affected by the properties of the interface between the reinforcement and matrix. Wettability and adhesion are important factors that control the effective load transfer from matrix to reinforcements, and hence play a crucial role in determining the overall performance of the material. Coupling agents are generally used to achieve compatibility and improve adhesion by acting as chemical bridges at the interface between two dissimilar materials such as inorganic reinforcement and organic matrix.

2.3.1. Organofunctional Silane Chemistry

Organofunctional silanes, with the general formula $X–(CH_2)_n-Si(OR)_3$, are the most widely used coupling agents. Silanes are monomeric silicon chemicals that exhibit dual nature of reactivity, both inorganic and organic, in the same molecule and hence, have the ability to bond inorganic material to organic material. The hydrolysable group, (OR), is generally alkoxy based such as methoxy, ethoxy, or acetoxy. This group can react and make strong chemical bonds with the hydroxyl groups of inorganic surfaces. The X group is a non hydrolysable organic moiety that possesses organic functionality such as epoxy, amino, methacryloxy, vinyl etc. This group provides the linkage to polymer and hence, should have organic compatibility [139-143]. Schematics of simplified chemical bridging mechanism of organofunctional silanes is shown in Figure 2.21.
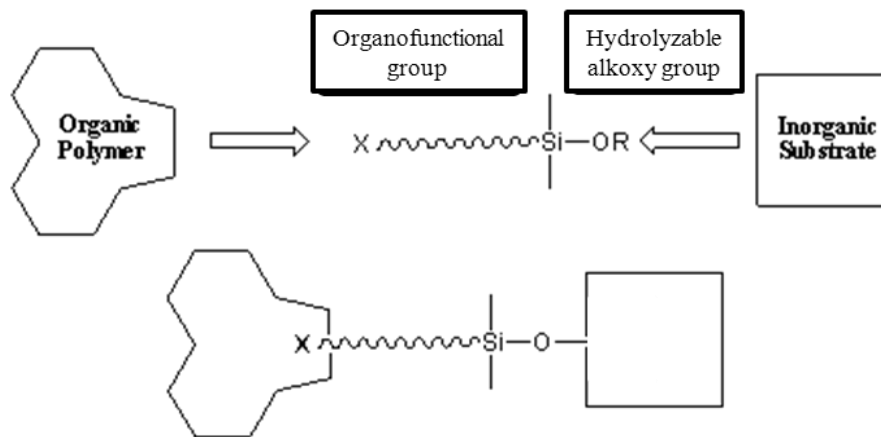
Figure 2.21 Organofunctional silanes acting as molecular bridges between inorganic substrate and organic matrix.

Silane molecule can link to polymer through chemical reactions and/or physiochemical interactions such as hydrogen bonding, interpenetrating network bonding mechanism (Figure 2.22) etc. [142, 143].
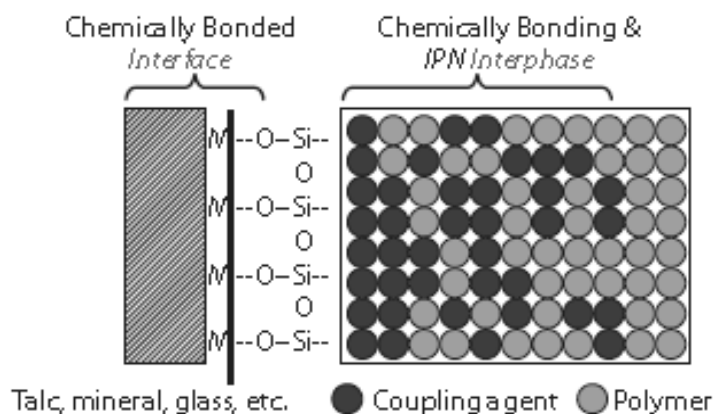
Figure 2.22 Interpenetrating bonding mechanism (IPN) [141].

Properties of the organic moiety of the silane molecule play a crucial role in selection of appropriate silane. For thermoset resins, chemical reaction between the organofunctional group and the resin is the main proposed mechanism for the interaction of the silane and polymer although interpenetrating network mechanism can also act to provide linkage. Therefore, the reactivity of the organofunctional group of the silane should match with the reactivity of the resin for copolymerization of silane with the resin [143, 144]. For instance, to achieve coupling between the inorganic substrate, such as inorganic fillers and reinforcements, and epoxy resin, silanes with epoxy and amino functional groups can be used. The interaction of the amino functional silane and the epoxy occurs through the chemical reaction between the reactive group and the epoxy moiety of the resin [145, 146]. For silanes with epoxy functionality, organofunctional group take part in the crosslinking of epoxy with the addition of hardener [147, 148]. Figure 2.23 illustrates the reaction between epoxy resin and two widely used silanes, namely, aminopropyltriethoxysilane and glycidoxypropyltrimethoxysilane.

For thermoplastics, interdiffusion and interpenetrating polymer network mechanism has been the suggested mechanism for the interaction between the silane and the thermoplastic polymer [149]. On this account, for thermoplastics, organofunctional group of the silane should be compatible with the thermoplastic [144]. Table 2.1 lists some thermoset and thermoplastic polymers and recommended silane coupling agent class.
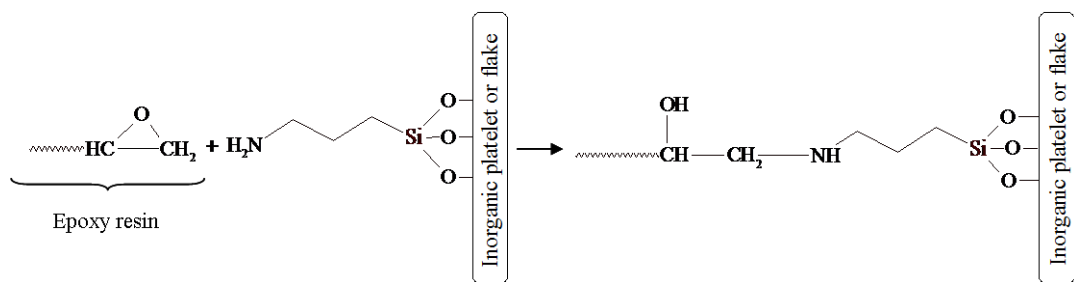
(a)
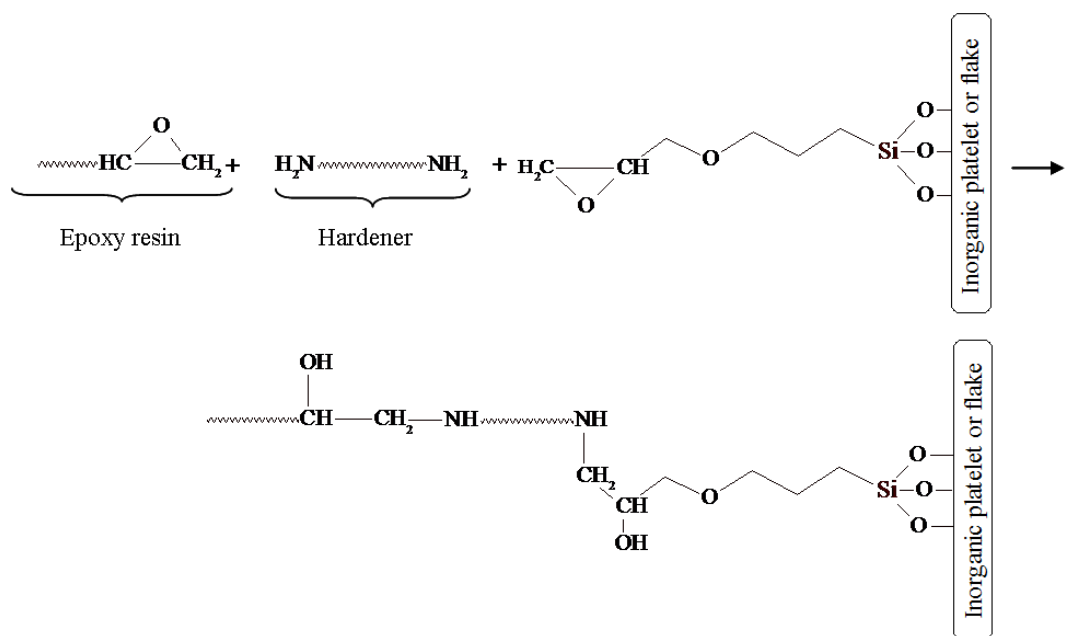
(b)

Figure 2.23 Coupling reaction between (a) aminopropyltriethoxysilane treated inorganic surface with epoxy resin (DGEBA) and (b) glycidoxypropyltrimethoxysilane with epoxy resin (DGEBA) through the interaction with curing agent.

Due to their dual nature and the ability of forming molecular bridges between organic polymers and inorganic materials, organofunctional silanes are mostly used as adhesion promoter, crosslinker and coupling agent [140, 141, 146].

Table 2.1 Silane coupling agents for some thermosets and thermoplastics.

Polymer	Organofunctionality of silane
Epoxy	Amino
	Epoxy
Polyacrylate	Amino
	Epoxy
	Methacrylic
	Vinyl
Polyester	Methacrylic
Polyolefin	Amino
	Vinyl
Polyurethane	Amino
	Epoxy
	Isocyanate
Polysulfide	Epoxy
	Vinyl

Surface modification of filler surfaces with silanes offers following advantages [140-142]:

- Improvement in the reinforcing effect of the filler and hence, in mechanical properties
- Modification of surface characteristics (water repellency or hydrophobicity)
- Enhancement in dispersion of fillers
- Improvement in wet-out between resin and filler
- Decrease the viscosity during compounding
- Improvement in dimensional stability
- Improvement in electrical properties, etc.

2.3.2. Functionalization of Inorganic Surfaces with Organofunctional Silanes

Reaction mechanism between silane and the inorganic surfaces is illustrated in Figure 2.24. In hydrolysis step, the alkoxy groups (OR) of the silane react with water or even with the moisture absorbed on the inorganic surface and hydrolyzes in a step-wise manner to form forming alkoxysilanol mono- and di-, and finally silane tri-ols ($RSi(OH)_3$) releasing alcohol (MeOH) [142, 143, 146, 150].

Condensation of silanols to form oligomers may start following the replacement of first and second OR units with hydroxyl units (OH). Hydroxyl groups of silanes interact with the hydroxyl groups of the inorganic surface and physisorbed via hydrogen bonding. Finally, this physisorbed silane layer is fixed by drying and curing via covalent bond formation [142, 143].

However, in real situation, functionalization of inorganic surfaces with silanes is not a simple task rather it is very complicated process. Hydrolysis and condensation reactions are influenced by many factors such as initial concentration of silane solution, pH, used solvent, the amount of water present, hydrolysis time, silane type etc [151-153]. As silanols formed upon the hydrolysis of silane molecules are very reactive, they have a tendency to self-condense with other silanols or alkoxysiloxanes and form siloxane networks. Silane molecules that are self-condensed and formed siloxane network may also crosslink or aggregate on the surface of inorganic substrate and form an inhomogeneous multilayer silane structure [154]. Therefore, in terms of effectiveness of the silane coupling agent, application of silanes as monomers is better than condensed siloxane oligomers [144].

The tendency of self-condensation can be controlled by taking various precautions such as using fresh solutions, low silane concentrations, alcoholic or organic solvents and by adjusting the pH of the used solvents [143, 154]. For instance, the condensation reaction of reactive silanol groups occurs very rapidly in water. However, the hydrolysis and condensation reactions in aqueous alcoholic or organic solutions proceed more homogeneously [155]. Furthermore, reaction of reactive silanol groups with other silanols and alkoxysiloxanes and hence, self-condensation can be retarded by adjusting the pH of the solvent to 4–5, as at this pH range condensation takes place very slowly whereas the hydrolysis reaction proceeds faster (Figure 2.25) [154, 156]. It has been also suggested that keeping the concentration of the silane in solution in the range of 0.01 wt. % – 2 wt. % is beneficial to avoid the condensation of oligomeric silanes [157].

The interaction of silanol moieties with inorganic surfaces, the orientation of the silane molecule at the inorganic surface along with the nature and the thickness of the silane layer are also strong function of processing parameters, such as pH, used solvent, drying temperature and time, properties of the inorganic substrate surface, etc [150, 154, 158].

(a)
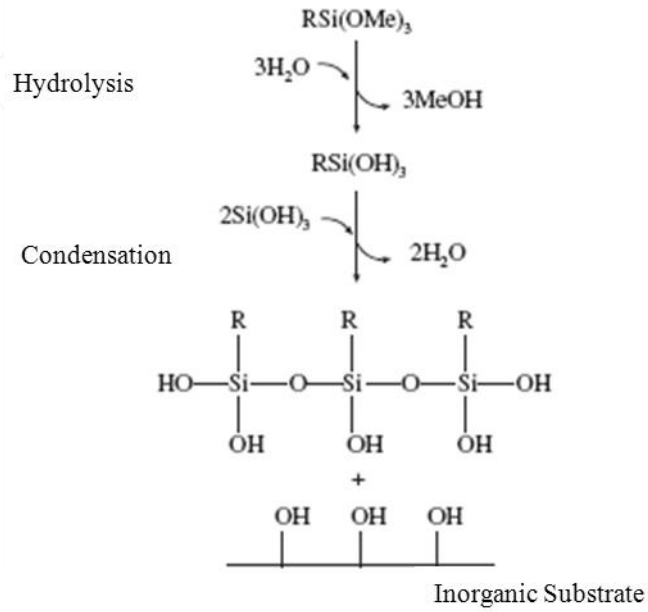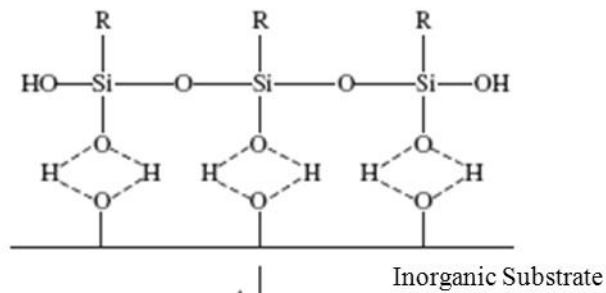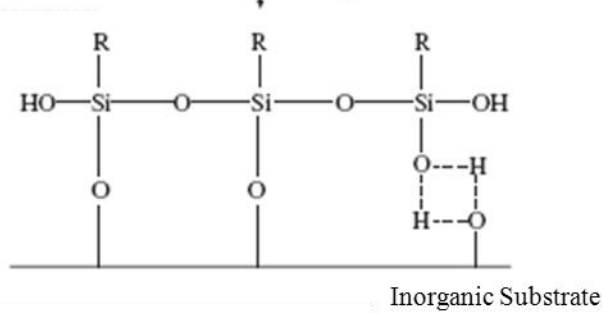
(b)

Figure 2.24 Reactions steps for surface functionalization of the filler. (a) Hydrolysis and condensation reactions of alkoxysilanes and (b) Bonding to inorganic substrate surface [141].
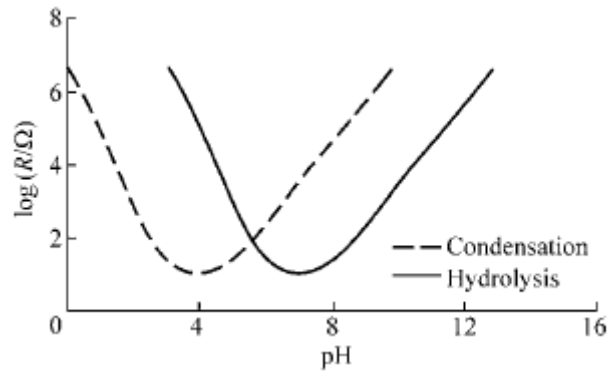
Figure 2.25 pH dependence of hydrolysis and condensation reaction of silanes [156].

Silane interphase consists of chemisorbed and physisorbed silanes [155, 159]. Thickness and the crosslink density of the silane layer and also the amount of the physisorbed silanes on the outermost layers effects the performance of the silane coupling agent and hence, interfacial strength [155, 159, 160]. Surface functionalization using a silane solution containing concentrated, condensed silane oligomer species may result in formation of thick silane layer [144]. In thick silane layers, weak outermost physisorbed layer may lead to a decrease in the interfacial strength [160]. Furthermore, if the thickness of this layer is on the order of hundred nanometers, the mechanical performance of this layer can affect and contribute to the overall performance of the composite [144].

Increase in crosslink density may also decrease the effectiveness of the silane layer [160]. Soto et al. [161] indicated that silane treatment of reinforcements led to a decrease in the mechanical performance of the composite due to the formed of dense highly-reticulated silane interlayer which limits the interaction between silane functional groups and organic matrix.

Kurt et al. [162] and Simon et al. [152] studied the effect of used solvent on the adsorption of 3-Aminopropyltriethoxysilane (APS) on inorganic surfaces and indicated that the adsorption from aqueous solutions results in formation of thick multilayer films [152, 162] whereas silane treatment in anhydrous solvent leads to more stable and homogeneous APS layer with limited aggregates as compared to silane treatment in acidic aqueous solution [152]. In another research, it has been found that elevated drying or curing temperatures, may lead to oxidation of epoxy ring [163] along with high crosslinking or deterioration of the γ-glycidoxypropyltrimethoxysilane films, deposited on oxidized aluminum substrate [158].

The performance of silane coupling at the interface is strongly influenced by the interaction of silane molecules with the inorganic surface and their orientation which also depends on the processing variables, as aforementioned. For instance, for silanes with epoxy- or amine-functionality, silane molecules can either interact with the platelet surface through silanol groups or through epoxide ring for epoxy-functional silane and protonated amino group for amino-functional silane [150, 155, 164, 165]. For an effective coupling, the interaction between the silane molecules and inorganic surface should occur via silanol groups and the organofunctional groups should orient upright with respect to the inorganic surface so that they can link to the organic polymer, for instance, they can take part in reaction with epoxy resin as shown in Figure 2.23.

To sum up, various factors characterize the silane layer and affect its performance such as interaction of silane molecules with the inorganic surface and their orientation, the fraction of available organofunctional groups for linkage with the organic polymer along with the homogenity of the adsorbed silane layer, silane up-take, the amount of physisorbed silanes on the outermost layers, etc. However, the influence of each variable is complicated [155].

For the characterization of the silane functionalized surface, most widely used techniques are X-ray photoelectron spectroscopy (XPS) [148, 158, 165-168], fourier transform infrared spectroscopy (FT-IR) [147, 168-170], time-of-flight secondary ion mass spectroscopy (ToF-SIMS) [148, 158], contact angle measurements [166, 167, 171] etc. Among these techniques, throughout this study, XPS technique was used in order to characterize the surfaces of the functionalized inorganic reinforcements. Therefore, in the following sub-section, brief information about X-ray photoelectron spectroscopy technique will be given.

2.3.3. Surface Characterization Technique: X-Ray Photoelectron Spectroscopy

X-ray photoelectron spectroscopy (XPS) is a qualitative and quantitative surface sensitive analytical technique that gives information about surface elemental composition as well as electronic and chemical state of the surface species [172, 173]. Using XPS technique, all elements other than H and He can be identified [172].

XPS uses photons to irradiate the material surfaces and hence, gives less damage to easily degraded materials as compared to Auger spectroscopy or Secondary ion mass spectrometry. Therefore it is much more preferred technique for the study of easily degraded materials such as polymers [174].

XPS technique is mainly used to identify and quantify the elemental composition as well as to study the chemical reactions which occur at the top few atom layers of materials [174]. The sampling depth of XPS technique is on the order of 5-10 nm [173]. In order to eliminate the contamination of the sample surfaces, XPS instruments operate at ultra high vacuum ($<10^{-6}$ Pa) [173, 174].

XPS is based on the photoelectric effect. Each surface atom has core electron with the characteristic binding energy that is generally equal to the ionization energy of that electron. When the specimen surface is irradiated with photons, an electron is ejected from either a valence electron shell or an inner core electron shell. Figure 2.26 shows the process of photoelectron emission [174].
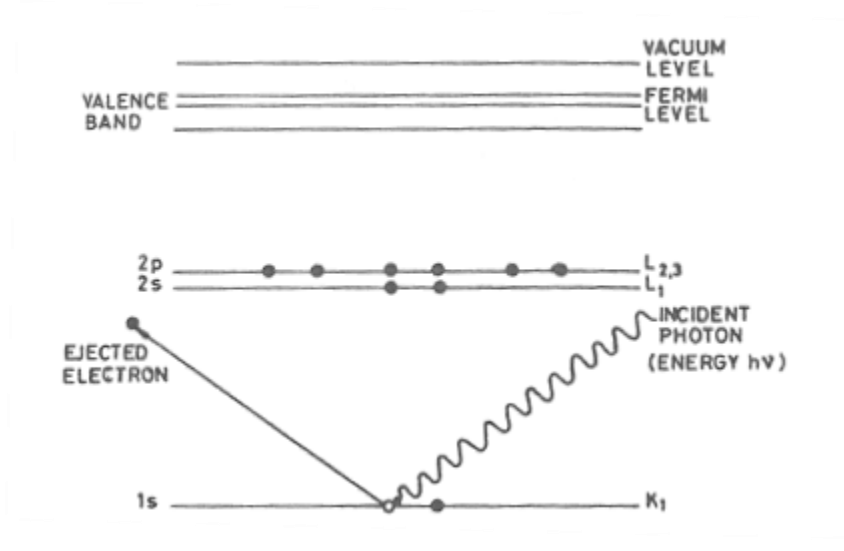
Figure 2.26 The process of photoelectron emission [174].

The kinetic energy of the ejected electron, E_k, is given by Equation 2.2;

$$E_k = h\nu - E_1 - \phi \qquad\qquad (2.2)$$

where $h\nu$ is the X-ray photon energy, E_1 is the electron binding energy and ϕ is the work function of the specimen induced by the analyzer. The energy of the ejected electron, E_k can be measured by energy analyzer. X-ray photon energy, $h\nu$ is specified from X-ray sources (for Al K_α, $h\nu$=1486.6eV, for Mg K_α, $h\nu$=1253.6 eV). Since the work function, ϕ, can be compensated artificially, electron binding energy can be calculated by using Equation 2.3 [174].

$$E_1 = h\nu - E_k \qquad\qquad (2.3)$$

XPS spectrum shows the photoelectron counts versus binding energy. Electronic core levels of the atoms in the close surface region appears as the characteristic peaks in this spectra and allows the identification of the atoms and quantify the relative surface composition [173, 174].

Beside photoelectrons, photoionization can also lead to emission of auger electrons. Therefore, XPS spectrum consists of photoelectron and Auger peaks superpositioned on background due to inelastic scattering in the sample. Before identification of the photoelectron peaks, these auger peaks should be specified [174].

Each element has its own photoelectron spectrum and this spectrum exhibits several features at different binding energies due to the fact that two elements can not have the same set of binding energies. Therefore, the position of the peaks along with their shapes can give information of the chemical state or chemical states of the elements [172]. For instance, when two atoms interact to form a compound, electron transfer occurs leading to change in the electron binding energies usually on the order of few eV [174]. This change in binding energy (changes in peak positions or chemical shifts in XPS spectra), allows the identification of chemical state of an atom [173, 174].

When photoelectron peaks are closely spaced and form a peak envelope with multiple photoelectron peak contributions, it is possible to apply peak fitting techniques to deconvolute the peak envelope to its contributors and identify the chemical states [172-174].

XPS surface characterization technique also allows the identification of surface elemental composition as a function of depth. To do this, surface of the sample is bombarded with argon ions to remove the atom layers while taking the XPS spectra [174]. However, the main drawback of depth profiling is that bombardment with argon ions may lead to a change in the chemical state of the surface and hence, chemical state identification cannot be performed accurately [174].

CHAPTER 3

EXPERIMENTAL PROCEDURE

In the scope of this dissertation, nacre-like bulk lamellar composites reinforced by aligned 2D inorganic fillers were fabricated using a hybrid conventional method called "Hot-Press Assisted Slip Casting (HASC)" process. High aspect ratio alumina platelets along with glass platelets and flakes were used as inorganic 2D fillers while low viscosity epoxy resin-hardener system was used as the matrix material. Micro-scale hierarchical arrangement and mechanical properties of the fabricated bio-inspired bulk lamellar composite materials were characterized.

In this chapter, the details of the novel technique HASC processing along with the physical properties of the materials used will be mentioned. Furthermore, the methods used to characterize the fabricated bio-inspired bulk composites with brick-and-mortar structure will be stated.

3.1 Materials

Inorganic–organic bulk lamellar composites were fabricated by reinforcing the epoxy resin with 2D alumina (Al_2O_3) and glass reinforcements. Generally, 2D reinforcements are characterized by their high aspect ratios, α, which can be defined as the ratio of diameter of reinforcement to its thickness. 2D reinforcements with an aspect ratio ranging between 4 and 30 are classified as platelets, whereas 2D reinforcements with an aspect ratio of 50-200 are classified as flakes [175].

Physical properties and the designation of the inorganic 2D platelets and flakes that were used in this study are summarized Table 3.1. Alumina platelets (AP) are polygonal in-shape with in-plane diameter (basal plane) of ~10 μm and thickness of ~0.30 μm (Serath YFA10030, Kinsei Matec, Okayama, Japan). Glass platelets (GP) are modified C-glass and highly corrosion resistant with an average diameter of <50 μm and thickness of 2.3-3.3 μm (ECR GF003, Glass Flake Ltd., Leeds, UK). Glass flakes (GF) are chemically resistant high aspect ratio C-glass flakes with an average diameter of 300 μm and a thickness of 2 μm (RCF2300, NSG Co. Ltd., UK). Chemical composition of GP glass platelets and GF glass flakes are shown in Table 3.2. Figure 3.1 demonstrates the SEM images of inorganic reinforcements used in this study.

Table 3.1 Properties of the inorganic reinforcements used in this study.

Designation	Type	Morphology	Density (g/cm3)	Aspect Ratio (α)
AP	α-Alumina	Platelet	3.98	~ 33
GP	Modified C-Glass	Platelet	2.6	~15-20
GF	C-Glass	Flake	2.5	~ 150
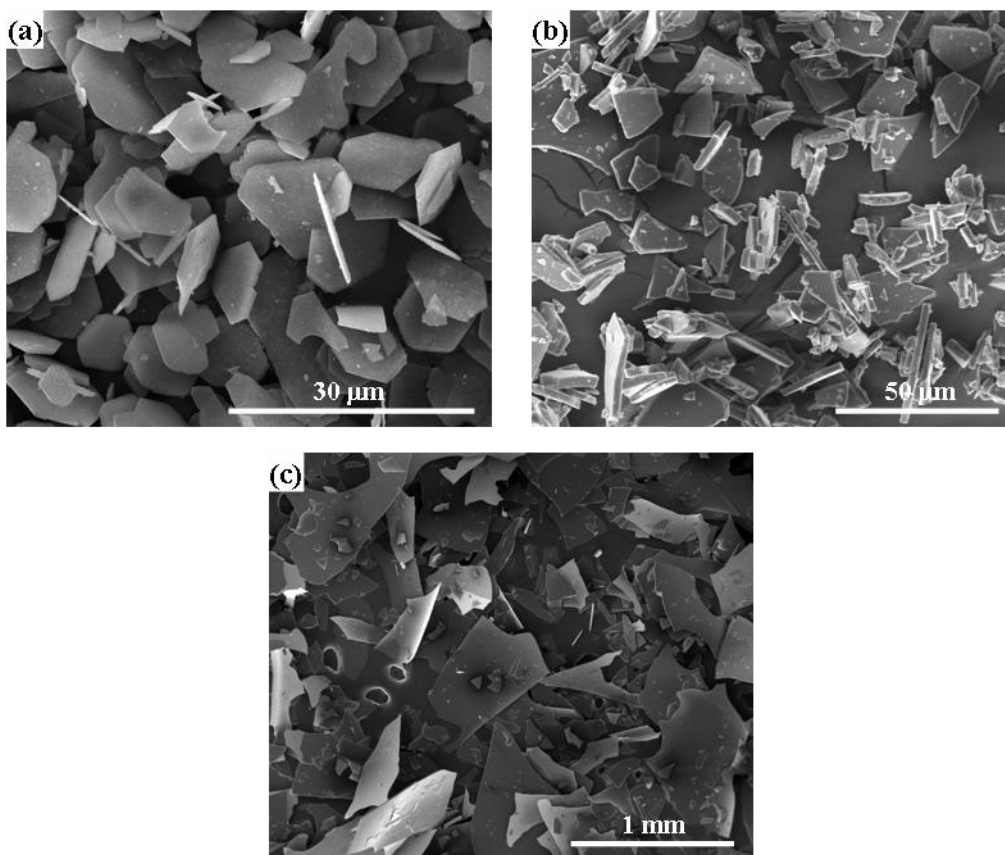
Figure 3.1 SEM images of (a) alumina platelets, (b) glass platelets and (c) glass flakes.

For the matrix, two different epoxy resins, namely Uni-Mount and Epo-Fix, were used. Uni-Mount resin is a low viscosity Bisphenol A-diglycidyl ether based epoxy resin and its hardener is 2,2'-dimethyl-4,4'-methylenebis(cyclo-hexylamine) (Electron Microscopy Sciences, Hatfield, UK). Density of UniMount resin and its hardener is 1.13 g/ml and 0.96 g/ml, respectively. Epo-Fix resin system is another low viscosity resin containing Bisphenol A-diglycidyl ether with hardener containing triethylenetetramine (Struers GmbH, Germany). Density of Epo-Fix resin and hardener is 1.1 g/ml and 0.98 g/ml, respectively.

The reason of using two different epoxy resin systems was the problems encountered in the supply of Uni-Mount resin and its hardener due to the stock problems. For that reason, the experimental studies began with the use of Uni-Mount epoxy resin, but continued with the use of another low viscosity epoxy resin, Epo-Fix. Figure 3.2 shows the chemical structure of Bisphenol A-diglycidyl ether based epoxy resins together with the hardeners used in this study.

Table 3.2 Chemical composition of modified C-glass platelets (GP) and C-glass flakes (GF).

	GP	GF
SiO_2	64-70%	65-72%
Al_2O_3	3-6%	1-7%
B_2O_3	2-5%	0-8%
ZnO	1-5%	0-6%
Na_2O+K_2O	8-16%	9-13%
MgO	1-4%	0-5%
CaO	3-7%	4-11%
TiO_2	0-3%	-
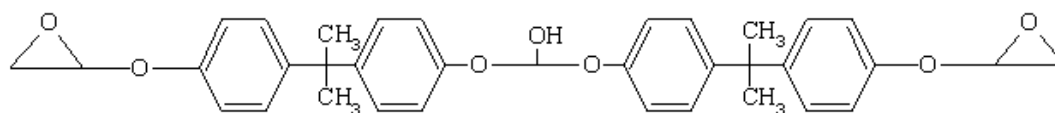
Bisphenol A-Diglycidyl Ether
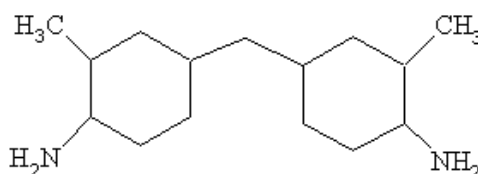
2, 2'-dimethyl-4, 4'-methylenebis(cyclo-hexylamine)

Triethylenetetramine

Figure 3.2 Chemical structure of Bisphenol A-diglycidyl ether, 2,2'-dimethyl-4,4'-methylenebis(cyclo-hexylamine) and triethylenetetramine.

For the surface treatment of the platelets, silanes having different functional groups; namely epoxy- and amino-functional were used. Epoxy- and amino-functional silane coupling agents used in this study were γ-glycidoxypropyltrimethoxysilane (GPS, Silquest A-187, Momentive Performance Materials Inc., Ohio, USA) and γ-aminopropyltriethoxysilane (APS, Silquest A-1100, Momentive Performance Materials Inc., Ohio, USA). Chemical structure of these organofunctional silane coupling agents is shown in Figure 3.3. During the surface treatments reagent grade glacial acetic acid, ethanol and toluene were used.
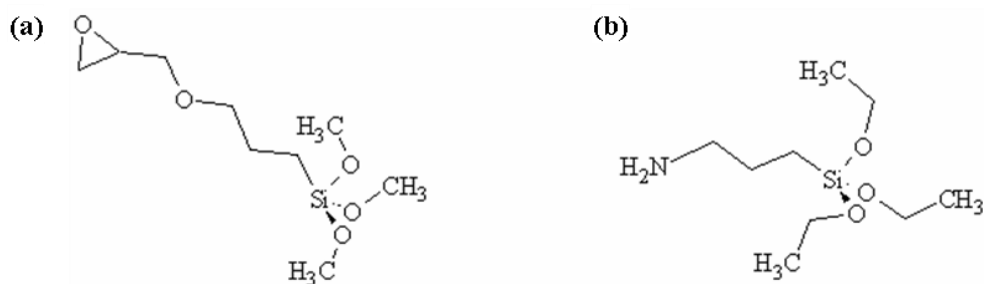
Figure 3.3 Chemical structure of silane coupling agents used in this study (a) GPS (epoxy-functional silane), (b) APS (amino-functional silane).

3.2 Fabrication of Inorganic–Organic Bulk Lamellar Composites with As-received Inorganic Platelets/Flakes

Throughout the study, epoxy matrix composites reinforced by inorganic platelets/flakes were fabricated using the hybrid conventional method called "Hot-press Assisted Slip Casting (HASC)." This novel technique combines two conventional processing methods; hot-pressing and slip-casting, to achieve hierarchical arrangement of the platelets/flakes in epoxy matrix and enhance volume fraction of the reinforcement. In this technique, a porous plaster, inside the rectangular cross-sectioned steel die, functions as a filter draining the excess resin and aids in increasing the reinforcement content together with the alignment of the platelets by the flow of the resin during the hot-pressing process.

Before each process, plaster of paris (pattern plaster), mixed with water at a ratio of 7:10 (plaster of paris:water) by weight, was cast into the steel die having an inner cavity of 20 by 27mm and allowed to dry at room temperature for ~1 day. Following this, the steel die, together with the disposable plaster cast into it, was placed and held in a drying oven at 40°C until composite processing to achieve further drying and to avoid absorption of humidity from air.

For the fabrication of the inorganic-organic composites, inorganic platelets were mixed with epoxy resin and hardener according to the ratios suggested by the manufacturer for the two component resin system at 2000 rpm using a planetary centrifugal homogenizing mixer (Thinky ARE-310, Tokyo, Japan), which provides uniform stirring during rotation and revolution. In the final mixture, volume fraction of inorganic reinforcements was ~22 vol% and ~20 vol% for alumina and glass platelets, respectively.

Prepared inorganic reinforcement-epoxy slurry was poured into the steel die. This die assembly was then placed in a conventional hydraulic hot-press, and initial pressure was applied until resin flow initiates through the porous plaster from underneath the steel die.

45

Following this, pressure was increased incrementally in a very gentle manner until the desired pressure level was reached. Temperature of the system was also increased simultaneously with the increase in pressure. Finally, the system was kept at 120°C for 20 min under the applied pressure to cure the epoxy matrix. Hot-press Assisted Slip Casting (HASC) method is schematically illustrated in Figure 3.4.

3.2.1 Alumina Platelets – Epoxy Matrix Bulk Lamellar Composites

For the fabrication of alumina platelet reinforced composites, low viscosity Bisphenol-A based Uni-Mount epoxy resin was used as the matrix material. Alumina platelets were mixed with epoxy resin and hardener, according to the ratio suggested by the manufacturer for the two component resin system (with a ratio of 6:20 by weight) at 2000 rpm using a planetary centrifugal homogenizing mixer. In the final mixture, volume fraction of platelets was ~22 vol%.

In order to investigate the effect of hot-pressing pressure on the platelet alignment and inorganic platelet content, six different pressures of 25, 50, 100, 150, 200 and 250 MPa were applied. To reveal the effect of platelet alignment and volume fraction on the improvement of the mechanical properties, neat epoxy as well as simple mixed (SM) samples (as-mixed and cured without applying pressure) were also prepared as control samples applying the same curing cycle.

3.2.2 Glass Platelets/Flakes – Epoxy Matrix Bulk Lamellar Composites

In order to investigate the effect of hot-pressing pressure on the alignment and volume fraction of the glass reinforcements and also to determine the optimum hot-pressing pressure, glass platelet reinforced composites were HASC processed under the applied hot-pressing pressures of 25, 50, 75, 100, 125 and 150 MPa. Optimization of process pressure and investigation of its effect on the composite microstructural architecture of the composites were performed in glass platelet-epoxy system due to the fact that glass platelets (GP) have lower in-plane dimension and thickness as compared to glass flakes (GF). To reveal the effect of platelet alignment and volume fraction on the improvement of the mechanical properties, neat epoxy as well as simple mixed (SM) samples (as-mixed and cured without applying pressure) were also processed as control samples applying the same curing cycle.

After the determination of the optimum hot-pressing pressures, glass flake reinforced composite samples were also fabricated. For the fabrication of glass platelet or glass flake reinforced epoxy matrix composites, low viscosity Bisphenol-A based Epo-Fix epoxy resin was used as the matrix material. Two component resin system was mixed according to the ratio suggested by the manufacturer (with a ratio of 6:20 by weight) before addition of the glass platelets or flakes into the mixture. For these composites, volume fraction of platelets/flakes was ~20 vol% in the final mixture.

"Hot-Press Assisted Slip Casting" Process

Inorganic Platelet
&
Epoxy Mixture

Porous Plaster
(Filter)

Casting of plaster into steel die
&
Drying

Preperation of platelet-epoxy mixture
&
Pouring the mixture into steel die

Heat   Pressure   Heat

Excess Resin

Hot-Pressing
&
Filtering the excess resin
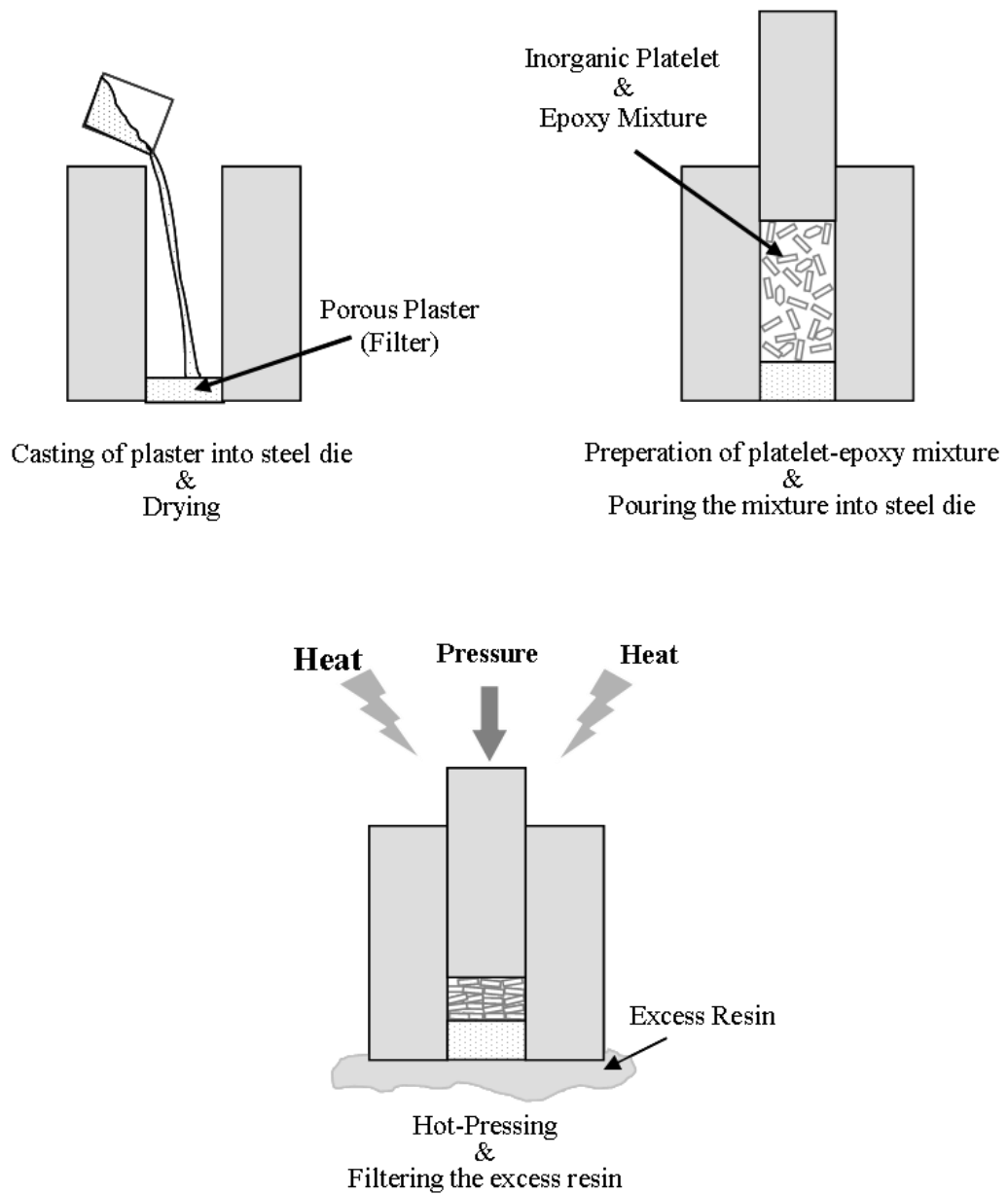
Figure 3.4 Schematic illustration of Hot-press Assisted Slip Casting Method (HASC).

3.2.3 Glass Flake-Epoxy Matrix Composites Fabricated by HASC at Low Processing Pressures

Glass flake-epoxy matrix composites with lower inorganic contents were also fabricated by HASC processing at low processing pressures. The applied processing pressures were kept lower than 10 MPa. For the fabrication of glass flake reinforced epoxy matrix composites, low viscosity Bisphenol-A based Epo-Fix epoxy resin was used as the matrix material. By taking into consideration the experimental findings that will be mentioned in Chapter 4, the glass flake content was kept lower than 20 vol% in the initial inorganic-organic mixture to decrease the viscosity of the initial mixture.

3.3 Surface Functionalization of Inorganic Platelets

3.3.1 Surface Treatment of Alumina Platelets

To achieve compatibility and interfacial bonding between inorganic reinforcement and organic matrix, surfaces of the alumina platelets were treated with two silane coupling agents having different organofunctionality; γ-glycidoxypropyltrimethoxysilane (GPS) and γ-aminopropyltriethoxysilane (APS). The amount of silane required for theoretical monomolecular layer coverage can be calculated using Equation 3.1 where SAF and SWS are the surface area of the filler and the specific wetting surface or surface area coverage of the silane in m^2/g, respectively [176].

$$\text{Weight \% of silane} = \frac{\text{SAF}}{\text{SWS}} \tag{3.1}$$

As long as the values of the SAF and SWS are known, the amount of silane required for monomolecular layer coverage can be determined. The surface area of the alumina platelets is given by the manufacturer as 2.38 m^2/g. The specific wetting surface values for the γ-glycidoxypropyltrimethoxysilane (GPS) and γ-aminopropyltriethoxysilane (APS) are stated by the manufacturer as 330 m^2/g and 353 m^2/g, respectively. Therefore, the required amount of silane for monomolecular layer coverage has been calculated as 0.72 wt.% and 0.67 wt.% for GPS and APS, respectively, in terms of the percentage of the reinforcement to be surface treated. However, to ensure the full treatment of the platelets excess amount of silane, ~2 wt.%, was used throughout the study.

3.3.1.1 Surface Treatment with GPS

Treatment of the alumina platelet surfaces with epoxy-functional silane was performed in two different solvents; 96vol% ethanol - 4vol% distilled water and distilled water. Used solvents and the designation of the treated platelets are given in Table 3.3.

Silane solution was prepared by addition of 1 vol% coupling agent drop by drop to prepared solvent under stirring. Before silane addition, pH of the solvent was adjusted to ~4.5 with diluted acetic acid to catalyze the hydrolysis process. Silane solution was stirred for 15 min and left for 1 h to allow complete hydrolysis of the silane. After complete hydrolysis and silanol formation, inorganic platelets were added to silane solution and sonicated in ultrasonic bath to achieve complete wetting of the platelets. The suspension was then filtered off to remove the solvent as well as unreacted silanol groups and dried at 120 °C for 1 h.

3.3.1.2 Surface Treatment with APS

Silanes with amino reactive end groups can be easily hydrolyzed in many solvents without the need to catalyze the solution. Consequently, for this silane type, silanization treatment were carried out in three different solutions; toluene, 96 vol% ethanol–4 vol% distilled water, distilled water. Designation of the surface functionalized platelets together with the solvent used in treatment is summarized in Table 3.3.

Silanization Treatment in Toluene and 96 vol% Ethanol–4 vol% Distilled Water Solutions:

1 vol% APS was added drop by drop to the solvent solution, at natural pH of the solution, while stirring. For hydrolysis of the coupling agent, silane solution was stirred for extra 15 min before adding the alumina platelets. To achieve complete wetting of the platelets, alumina platelet added mixture was further stirred before filtering off. Filtered cake was dried at 110 °C for 1 h under vacuum.

Silanization Treatment in Distilled Water (Suggested by Dow Corning):

1 vol% APS was added drop by drop to the distilled water while stirring. After addition of the silane, pH of the aqueous silane solution was adjusted to ~4 to retard the reaction between the silanols and the condensation of siloxanes with the addition of glacial acetic acid. For hydrolysis of the coupling agent, silane solution was stirred for extra 15 min and alumina platelets were added while the solution being stirred by high speed stirrer (Heidolph Silent Crusher M, Germany). To achieve complete wetting of the platelets, alumina platelet added mixture was stirred before filtering off. Filtered cake was dried at 110 °C for 1 h under vacuum.

Table 3.3 Designation of the surface treated platelets, type of silane and the solvent used in surface modification procedure.

Designation	Silane Type	Solvent
S1	GPS	96vol%Ethanol-4vol%Distilled water
S2	GPS	Distilled water
S3	APS	Toluene
S4	APS	96vol%Ethanol-4vol%Distilled water
S5	APS	Distilled water

3.3.2 Surface Treatment of Glass Platelets and Flakes

Surfaces of the glass platelets and flakes were treated with γ-aminopropyltriethoxysilane to achieve compatibility and interfacial interaction between the reinforcements and the epoxy matrix. The weight % of amino-functional silane required to achieve monomolecular layer coverage could not be calculated as the surface area of the glass platelets and flakes are unknown. Although, the required amount of silane would be lower as compared to the alumina platelets as a result of their larger dimensions, and hence lower surface area, the total amount of silane was kept at ~2 wt.% for both glass platelets and flakes due to the fact that unreacted excess silanol groups would be removed during the filtering step. Silane functionalization of the glass platelets and flakes were performed using toluene as solvent at natural pH of the solution.

For functionalization of the glass platelets, 1 vol% APS was added drop by drop to the solvent solution while stirring. For hydrolysis of the coupling agent, silane solution was stirred for extra 15 min before adding the glass platelets. After the addition of the glass platelets, to achieve complete wetting of the platelets, mixture was further stirred before filtering off. Filtered cake was dried at 110 °C for 1 h under vacuum.

For glass flakes, silane treatment procedure was exactly same as the treatment of glass platelets with an exception that treatment of flakes was performed with 0.25 vol% silane solution. This situation arose from the fact that the addition of flakes to 1 vol% silane solution had increased the viscosity of the mixture to a level that mixing became almost impossible. For that reason, silane solution was diluted with the addition of extra toluene and optimum amount of solvent was determined.

3.4 Fabrication of Inorganic–Organic Bulk Lamellar Composites with Surface Treated Platelets

Surface functionalized inorganic platelet/flake reinforced epoxy matrix bulk lamellar composites were fabricated in the same way as described in Section 3.2.

3.4.1. Bulk Lamellar Epoxy Matrix Composites Reinforced by Surface Treated Alumina Platelets

For the fabrication of composites reinforced by surface functionalized alumina platelets, Epo-Fix resin was used as the matrix material. Composites were fabricated under the applied hot-pressing pressure of 100 MPa. In order to investigate the effect of platelet alignment and surface functionalization on the resulting mechanical properties, in addition to the composites fabricated by HASC under the applied hot-pressing pressure of 100 MPa (HASC-100MPa), simple mixed (as-mixed and cured without applying pressure) samples with as-received and surface treated platelets were also prepared.

3.4.2. Bulk Lamellar Epoxy Matrix Composites Reinforced by Surface Treated Glass Platelets and Flakes

Surface treated glass platelet and flake reinforced epoxy matrix composites were fabricated by HASC process under the applied pressure of 50 MPa and 100 MPa. For the fabrication of the composites, Epo-Fix resin was used as the matrix material. To investigate the effect of platelet/flake alignment and surface functionalization on the resulting mechanical properties, simple mixed samples reinforced by surface treated platelets were also prepared.

Furthermore, composites reinforced by mixed glass reinforcements were also fabricated by HASC under the applied pressure of 50 MPa and 100 MPa. The designation of the fabricated composites and the relative volume fractions of glass platelets and the glass flakes in the glass reinforcement mixture are presented in Table 3.4.

3.4.3. Bulk Lamellar Epoxy Matrix Composites Reinforced by Surface Treated Glass Flakes Fabricated by HASC at Low Processing Pressures

Surface functionalized glass flake-epoxy matrix composites with lower inorganic contents were also fabricated by HASC processing at low processing pressures. The applied processing pressures along with glass flake content in the initial inorganic-organic mixture were same with those of the composite samples reinforced by as-received glass flakes mentioned in Section 3.2.3.

Table 3.4 Designation of the fabricated composite, relative volume fraction of glass platelets and glass flakes.

Designation	Volume Fraction of Glass Platelets (GP) (%)	Volume Fraction of Glass Flakes (GF) (%)
100GP:0GF	100	0
90GP:10GF	90	10
70GP:30GF	70	30
50GP:50GF	50	50
30GP:70GF	30	70
10GP:90GF	10	90
0GP:100GF	0	100

3.5 Characterization

3.5.1 Determination of Inorganic Reinforcement Content

In order to determine the inorganic reinforcement content of composite samples (by weight percent), thermogravimetric analysis were carried out using thermogravimetric analyzer (TA Instruments SDT Q600). At least three specimens from each sample were analyzed from room temperature to 700°C with a heating rate of 10°C/min under air atmosphere. The weight percentage of the epoxy, which was removed physically by combustion, and that of the residue (inorganic platelets or flakes) were determined for each analysis. The volume percentage of the reinforcement ($V_R\%$) was calculated using Equation 3.2.

$$V_R\% = \frac{W_R \rho_M}{\rho_R (1 - W_R) + \rho_M W_R} \times 100 \qquad (3.2)$$

W_R is the determined weight percentage of the reinforcement, where ρ_R and ρ_M are the theoretical density of reinforcement and density of epoxy, respectively.

Densities (ρ) of the neat epoxy samples were determined by Archimedes' principle (Equation 3.3) using water as an immersion medium. Dry weight (W_{dry}), saturated ($W_{sat.}$) and suspended ($W_{susp.}$) weights of the samples were measured using a precision balance.

$$\rho = \frac{W_{dry}}{W_{sat.} - W_{susp.}} \qquad\qquad (3.3)$$

3.5.2 Microstructural Characterization

Specimens, cut from each composite with diamond precision saw (Buehler IsoMet 5000), were mounted in cold mounting epoxy resin. In order to remove the surface roughness and to obtain a flat surface, specimens were ground by a standard metallographic process using silicon carbide emery papers. For the microstructural characterization, surfaces of the specimens were polished with 1 μm and 0.5 μm diamond suspensions. Microstructural characterization of the as-processed composites was conducted using scanning electron microscope (SEM) (FEI Nova Nano SEM 430). Fracture surfaces of the three-point bending specimens were also examined using SEM (JEOL JSM-6400 and FEI Nova Nano SEM 430).

3.5.3 Mechanical Characterization

Mechanical characterization of the fabricated composites was conducted through hardness, three-point bending and work of fracture tests (WOF). For all these tests, applied loading direction was parallel to hot-pressing direction (perpendicular to reinforcement basal surfaces). For all mechanical tests, specimens from each composite were cut with diamond precision saw (Buehler IsoMet 5000).

3.5.3.1 Hardness Measurement

Vickers hardness measurements of the composites reinforced by as-received alumina and glass platelets were carried out using microhardness tester (Shimadzu HMV 2 E) with an applied maximum load of 0.5 kg for 10 seconds.

3.5.3.2 Three-Point Bending Tests

Flexural strength, strain and modulus of the composites were measured by three-point bending tests. Length (l), width (b) and thickness (d) of the three-point bending specimens were 20, 5 and 1 mm, respectively. Tests were conducted using a using a screw-driven type testing machine (Instron 5565A) with a span length of 16 mm and cross-head speed of 0.4 mm/min. From the load vs. deflection data, flexural strength (σ_f) and strain values (ε_f) were calculated using Equation 3.4 and Equation 3.5, respectively.

$$\sigma_f = \frac{3PS}{2bd^2} \qquad\qquad (3.4)$$

$$\varepsilon_f = \frac{6Dd}{S^2} \qquad\qquad (3.5)$$

where;

P = load at a given point on the load deflection curve, N,
D = maximum deflection of the center of the specimen, mm,
S = support span, mm,
b = width of the specimen tested, mm,
d = depth (thickness) of the specimen tested, mm

3.5.3.3 Work of Fracture Tests

In addition to the three-point bending tests, to investigate the effect of interfacial bonding on the crack growth behavior and energy required for fracture, work of fracture tests were also conducted for composites reinforced by as-received and silane treated reinforcements. The specimens with single edge notch beam (SENB) geometry were tested with a span of 16 mm and cross-head speed of 0.05 mm/min using the afore mentioned screw-driven type testing machine. Length (l), width (b) and thickness (d) of the work of fracture test specimens were 20, 3 and 4 mm, respectively. The span (S)/thickness (d) ratio was kept as 4 to facilitate stable fracture [15]. The notch, with a size of 0.45d-0.55d, was machined with diamond saw and a sharp pre-crack at the root of the machined notch was introduced by sliding a fresh razor blade across the notch. After the tests, area under the load-displacement curves (E) were computed, and fracture surface areas of the specimens were measured (A). Using these values in Equation 3.6, work of fracture (WOF) values for each specimen was calculated.

$$WOF = \frac{E}{2A} \qquad\qquad (3.6)$$

3.5.4 X-Ray Photoelectron Spectroscopy (XPS)

Surface functionalization of the inorganic reinforcements with silane coupling agents was characterized by X-ray photoelectron spectroscopy (XPS) (PHI 5000 Versa Probe). XPS analyses of both as-received and silane-treated alumina and glass reinforcements were

carried out using monochromatic Al Kα radiation source. XPS survey spectra were collected with pass energy of 187.85 eV at a photoelectron take-off angle of 45°. High resolution XPS spectra of Si2p and N1s core levels were acquired with pass energy of 58.70 eV. Peak deconvolution of N1s core levels for amino-functional silane was performed using mixed Gaussian-Lorentzian function after the subtraction of Shirley background.

3.5.5 Particle Size Analysis

During silane treatment of the inorganic reinforcements, some of the reinforcement-silane solution mixtures were stirred at high speeds. In order to investigate whether high stirring speeds had damaged the reinforcements or not, especially high aspect ratio glass flakes, particle size analyses were performed before and after silane treatment using Malvern Mastersizer 2000 particle size analyzer. During analyses, water was used as dispersant.

CHAPTER 4

RESULTS AND DISCUSSION

In this study, epoxy matrix composites reinforced by high aspect ratio α-alumina platelets and C-glass platelets/flakes were fabricated using a newly developed process "Hot-press Assisted Slip Casting" (HASC). In this chapter, results obtained from the studies accomplished will be summarized. The effect of process parameters including applied hot-pressing pressure on the alignment of the inorganic reinforcements together with their volume contents will be mentioned. Correlation between the structural architecture of the fabricated composites and the mechanical performance along with the impact of interfacial adhesion will also be discussed.

4.1 Inorganic–Organic Bulk Lamellar Composites Reinforced by Alumina Platelets

4.1.1 Epoxy Matrix Composites Reinforced by As-received Alumina Platelets

"Hot-press Assisted Slip Casting" (HASC) is a novel technique offering the advantages of increasing the inorganic content and favoring aligned platelet orientation. In this process, the porous plaster which is cast into the steel die acts as a filter and enables the drainage of the low viscosity resin under the action of hot-pressing pressure and hence, leading to an increase in the inorganic reinforcement content.

In this study, to reveal the effect of applied HASC processing pressures on the alignment of the high aspect ratio reinforcements and their volume fraction, composites were fabricated under the applied pressures of 25, 50, 100, 150, 200 and 250 MPa. The inorganic content of the fabricated composite samples were determined using thermogravimetric analysis (TGA). At least three analyses were conducted for each specimen and at each analyses 20-30 mg sample, which were taken from different location of the fabricated composites, were analyzed. The standard deviation in calculated volume fraction values was ranging between 0.4-1.5 vol% for all composite samples.

Figure 4.1 demonstrates the variation in the alumina platelet content as a function of applied hot-pressing pressure. Volume fraction of the alumina platelets increases with the applied hot-pressing pressure ranging between 46-68 vol%, where the maximum platelet content was achieved at 250 MPa applied pressure. Increase in inorganic content is continuous up to the hot-pressing pressure of 100MPa, above which the inorganic platelet content almost levels off ranging between 65-68 vol%.

In HASC process, flow of the resin through the randomly oriented platelets under the action of the applied pressure forces them to align with their basal surfaces perpendicular to hot pressing direction. Even at low processing pressures, HASC processing provides considerable alignment of reinforcing platelets compared to simple mixing (SM, mixing the platelets with the resin and curing without applying pressure) process. Increase in the hot-pressing pressure further improves the alignment of platelets leading to a structure resembling to "brick-and-mortar" structure together with the reduction of the matrix (epoxy) content as the draining efficiency of the excess resin through the filter increases. Figure 4.2 shows the SEM images of polished cross-sections of the composites which were fabricated by simple mixing and by HASC under the action of 25 MPa, 100 MPa and 200 MPa.
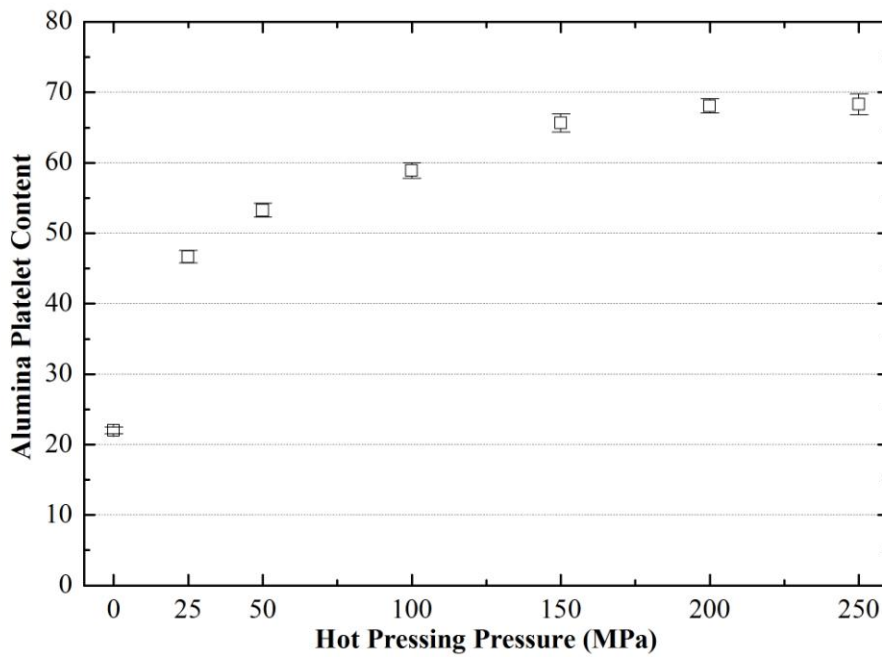
Figure 4.1 Change in alumina platelet content with applied hot-pressing pressure.
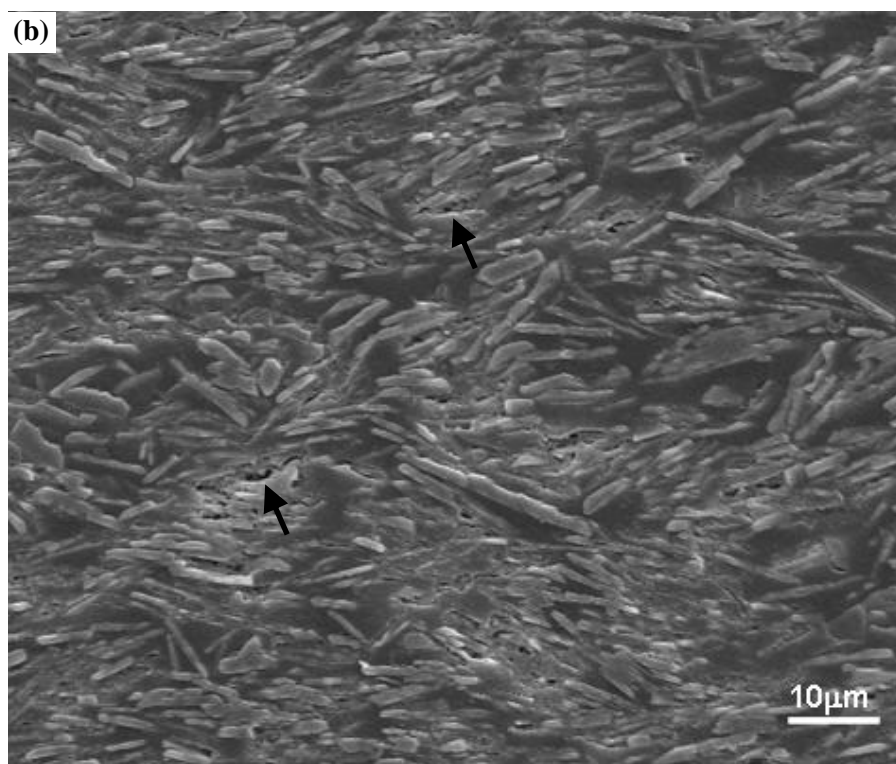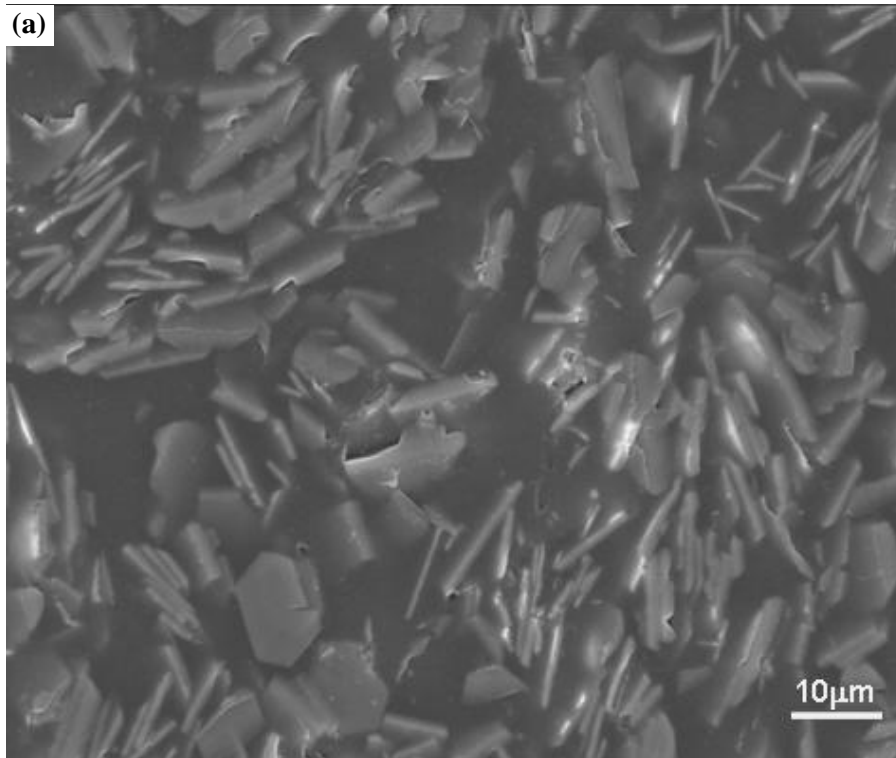
Figure 4.2 Cross-sectional microstructure of (a) simple mixed and HASC processed composites for the applied pressures of (b) 25 MPa, (c) 100 MPa and (d) 200 MPa.

(c)

(d)
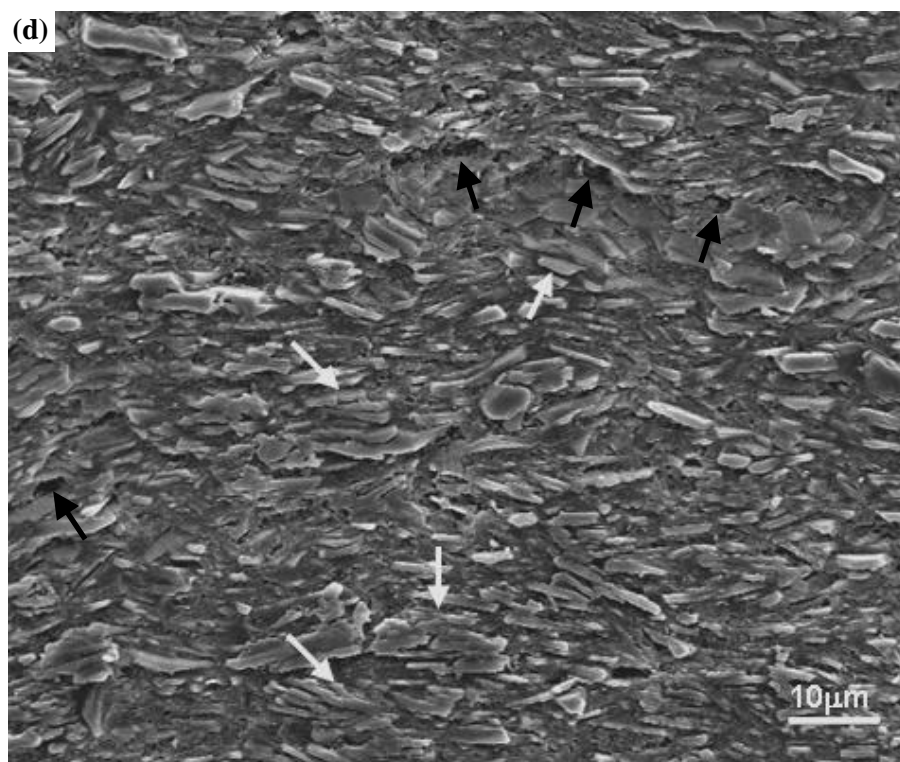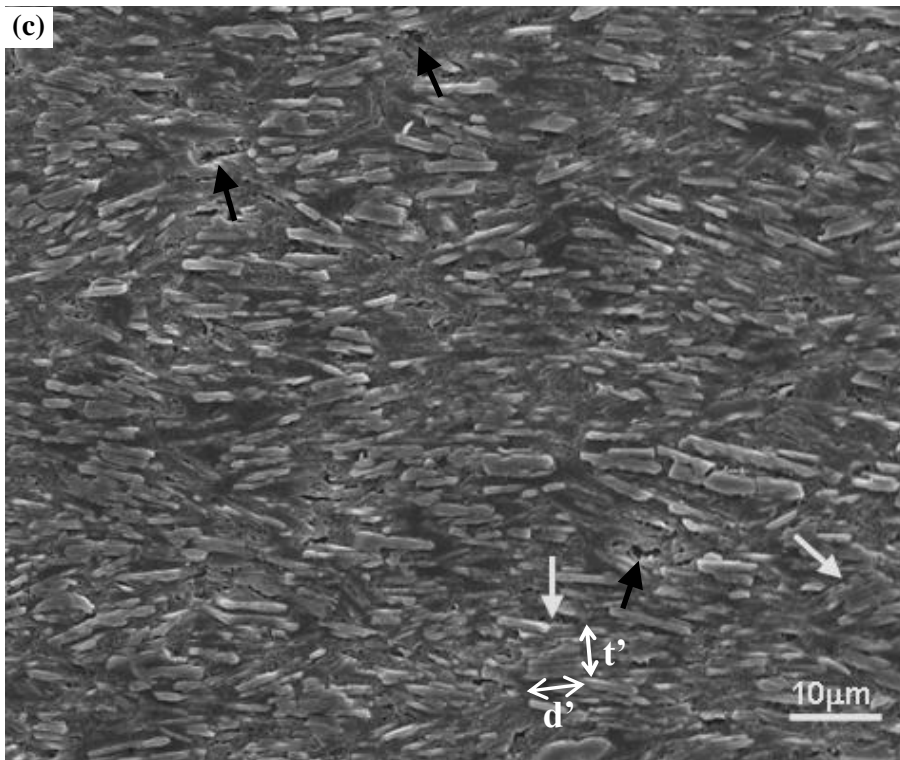
Figure 4.2 (continued).

In order to reveal the effect of platelet alignment and content on mechanical properties of the composites three-point bending tests and hardness measurements were conducted. Figure 4.3 shows the flexural strength vs. flexural strain curves of the HASC processed composites together with those of the simple mixed and the neat epoxy samples (inset in Figure 4.3). Three-point bending test results of the fabricated composites indicated that incorporation of alumina platelets, even in the case of simple mixed composites, leads to an increase in the flexural strength compared to that of the neat epoxy.

For HASC processed composites, increase in the platelet content and enhancement in platelet orientation gives rise to a further improvement in the flexural strength leading to ~2 fold increase at ~59 vol% platelet content (Figure 4.4). For platelet volume fraction of ~66 vol%, flexural strength decrease back to ~94 MPa being still ~54% higher than that of the neat epoxy. For composites HASC processed at pressures above 100 MPa having platelet contents higher than ~66%, flexural strengths are almost leveled-off with large scatter in the measured values, showing a similar trend as in the case of inorganic reinforcement content (Figure 4.1).
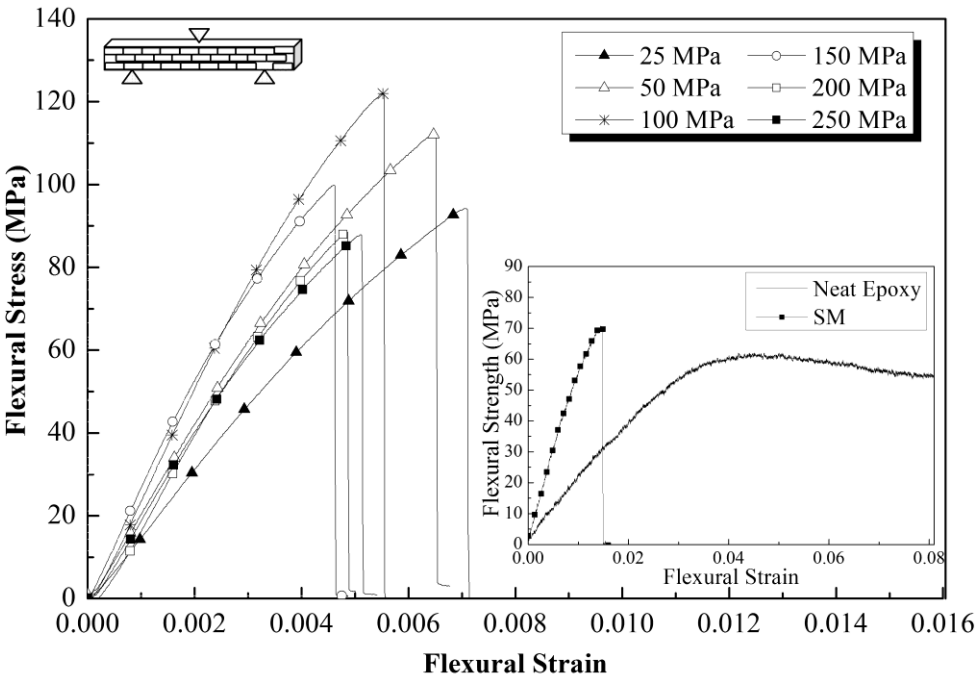
Figure 4.3 Flexural stress-strain curves of HASC processed composites together with simple mixed composite and neat epoxy.

The increase in the flexural strength values with the incorporation of rigid as-received platelets into epoxy matrix points out that the load could be transferred to the platelets. This can be a sign of at least partial wetting of the alumina platelet surfaces with low viscosity and low surface tension epoxy resin and also existence of weak interaction at the interface between the platelets and the epoxy. This finding is expected as the wetting of the reinforcement surfaces mainly depends on the surface tension of the filler and the matrix together with the viscosity of the liquid resin.

The decrease in the flexural strengths beyond 100 MPa of HASC processing pressure can be attributed to excessive drainage of the resin from the composite leading to considerable decrease in the epoxy content and enlargement of platelet clusters, in which platelets are stacked together with insufficient epoxy between adjacent platelets (white arrows in Figure 4.2). These complications inhibit proper wet-out of the individual platelets, and consequently effective load transfer at the interface. Improper wetting of the platelet surfaces also leads to the formation of voids, fraction of which also increases along with the platelet content (black arrows in Figure 4.2). Along with the voids and critically sized platelet clusters, which are thought to act as stress concentration sites, reduction in the load transfer efficiency results in a decrease in mechanical performance of the composites.
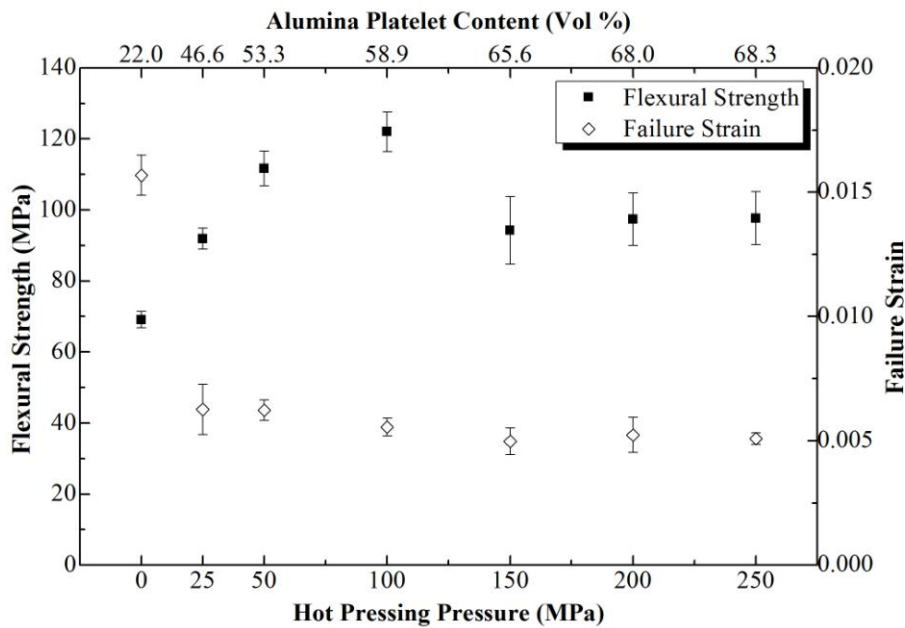
Figure 4.4 Variation in flexural strength and failure strain as a function of applied hot pressing pressure, and hence platelet content.

Figure 4.5 shows the fracture surfaces of HASC processed composites under the applied processing pressures of 25 MPa and 200 MPa. From this figure it is evident that fracture occurs through platelet/matrix interface debonding. The platelet surfaces are relatively smooth indicating the presence of weak interfacial bonding pointing out to the lack of adhesion between platelets and the matrix.

It is known that stiffness of composites containing rigid discontinuous fillers such as ribbons, platelets and short fibers is dependent on various factors such as filler content, size and aspect ratio (α) along with filler/matrix modulus ratio and alignment of the fillers [85]. In the current study, incorporation of rigid fillers with an aspect ratio (α) > 30 into epoxy matrix results in an increase in the flexural modulus compared to that of the neat epoxy. With the increase in the platelet volume fraction and enhancement of the platelet alignment, flexural modulus values of HASC processed composites show an increase by ~8 to 13 fold and ~3 to 4 fold with respect to those of neat epoxy and simple mixed composites, respectively (Figure 4.6). Enhancement in flexural modulus of the composites can be attributed to the fact that incorporated high aspect ratio rigid reinforcements constrict the deformation of the matrix especially in the vicinity of the platelets. For composites HASC processed with an applied pressure of 150 MPa and higher, slight decrease in flexural moduli is thought to be caused by the increase in the size of the platelet clusters leading to a decrease in effective reinforcement aspect ratio. Aspect ratio of platelets or flakes is defined as the ratio of diameter to thickness (d/t). For well-defined platelet clusters, effective aspect ratio can be defined as the ratio of the average diameter to the average thickness of the platelet cluster (d'/t') as shown in Figure 4.2.c.

As in the case of flexural strength and modulus, HASC process leads to a substantial enhancement in the hardness values of the composites as compared to neat epoxy and simple mixed composites (Figure 4.7).
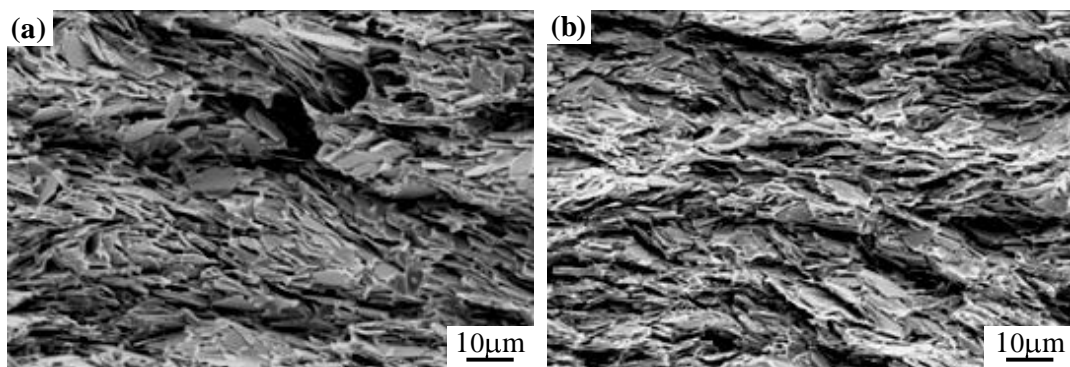
Figure 4.5 Fracture surface of HASC processed composites for the applied pressures of (a) 25 MPa and (b) 200 MPa.
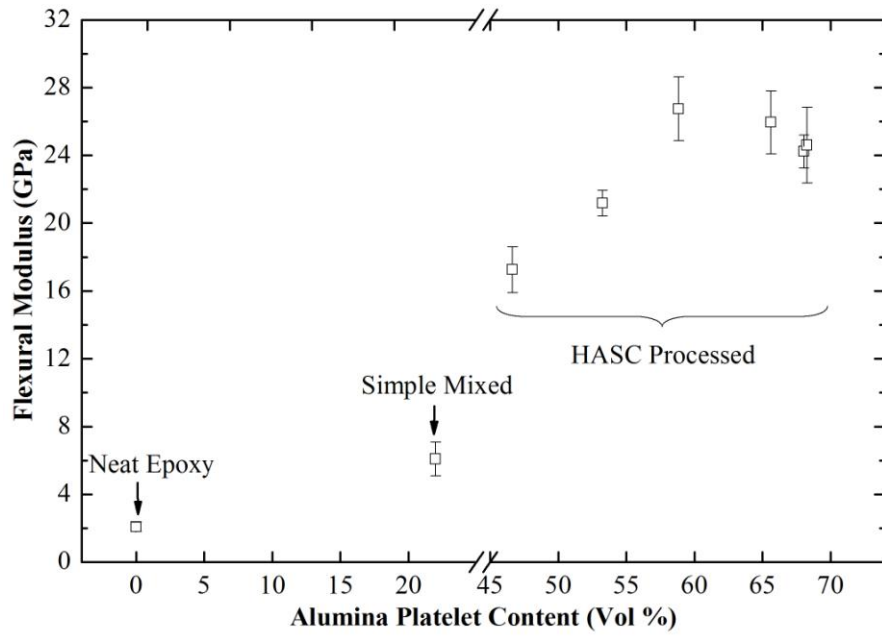
Figure 4.6 Variation in flexural modulus as a function of alumina platelet content.
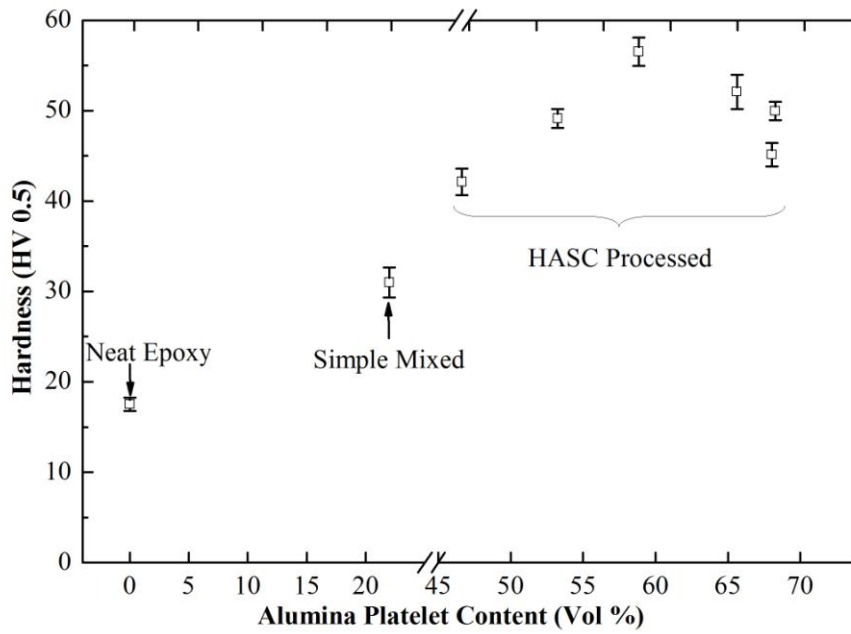
Figure 4.7 Variation in hardness values as a function of alumina platelet content.

4.1.2 Surface Functionalization of Alumina Platelets

Mechanical properties of the composites, especially toughness, are mainly governed by the interfacial strength between the reinforcements and the matrix. Therefore, to achieve compatibility and to enhance wettability and interfacial strength, the surfaces of the platelets were treated with two different silane coupling agents having different functional groups. Surfaces of the as-received and silane treated platelets were characterized using X-ray photoelectron spectroscopy (XPS) technique.

Figure 4.8 presents XPS survey spectra of GPS and APS treated platelets together with the survey spectrum of as-received alumina platelets for comparison. Peaks at 23 eV, 75 eV, 120 eV and 530 eV are O2s, Al2p, Al1s and O1s peaks, respectively, where peaks at 978 eV and 999 eV correspond to OKL1 and OKL2 Auger peaks. For GPS treated platelets either in ethanol-distilled water solution (S1) and distilled water (S2), survey spectra (Figure 4.8.a and Figure 4.8.b) show additional peaks corresponding to Si2p and Si1s, whereas for APS treated platelets treated in toluene (S3), ethanol-water mixture (S4) and in distilled water (S5) survey spectra indicate N1s peak in addition to Si2p and Si1s peaks (Figure 4.8.c, Figure 4.8.d and Figure 4.8.e).

In addition to survey spectra, high resolution XPS spectra (insets in Figure 4.8) of Si2p and Si2p, N1s core levels also prove the adsorption of GPS and APS silanes, respectively. For all silane treated platelets, presence of intense Al2p and Al2s peaks in XPS spectra indicate the adsorption of thin silane film on the surfaces of the platelets. Table 4.1 summarizes the elemental composition of as-received and silane treated platelets determined from XPS survey spectra.

For GPS treatment, the surface elemental composition of Al is lower in the case of platelets treated in distilled water (S2) pointing out that the thickness of the adsorbed silane layer is thicker as compared to the platelets treated in ethanol-distilled water mixture (S1).

For both type of silanes, silane molecule can either interact with the platelet surface through silanol groups or through epoxide ring for epoxy-functional silane and protonated amino group for amino-functional silane [155, 165, 177]. Figure 4.9 illustrates possible interaction mechanisms of GPS and APS silanes with the platelet surfaces.
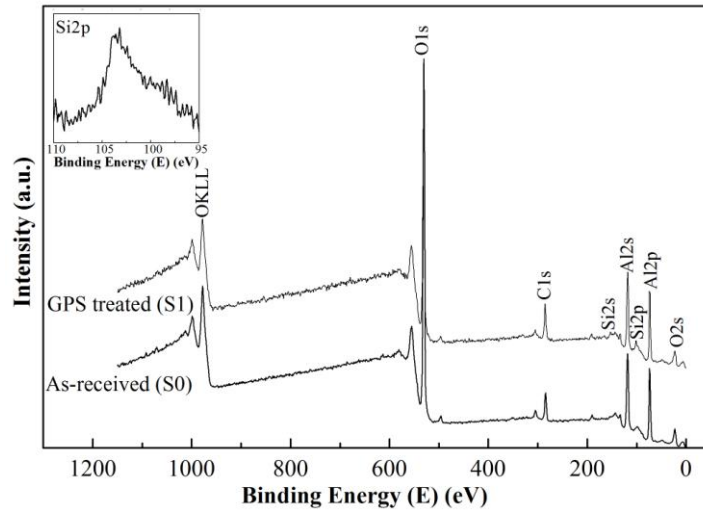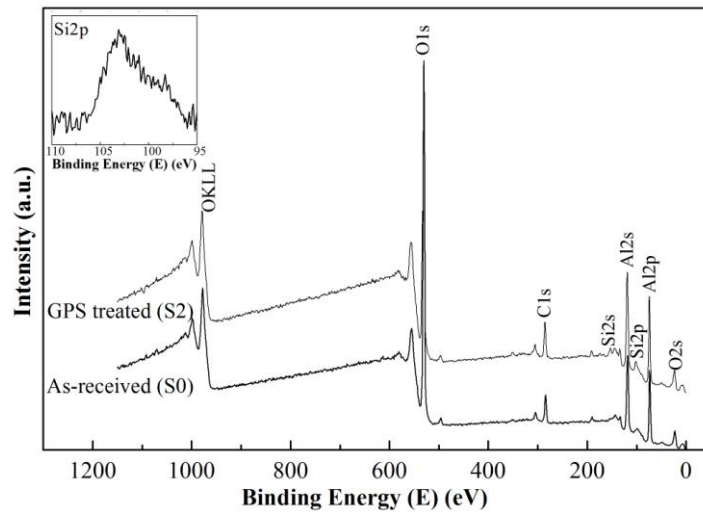
Figure 4.8 XPS spectra of (a) GPS treated platelets in ethanol-distilled water solution (S1), (b) GPS treated platelets in distilled water solution (S2), (c) APS treated platelets in toluene (S3), (d) APS treated platelets in ethanol-distilled water solution (S4) and (e) APS treated platelets in distilled water (S5) together with the XPS spectra of as-received platelets (S0). Insets show high resolution XPS spectra of Si2p and Si2p, N1s core levels for GPS and APS treated platelets, respectively.
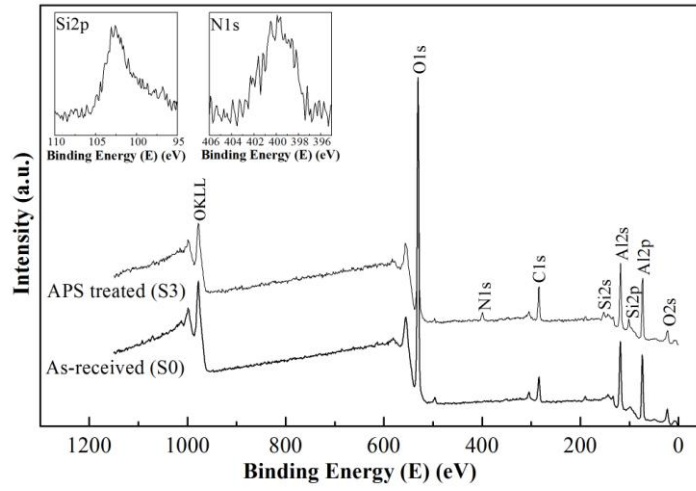
(c)
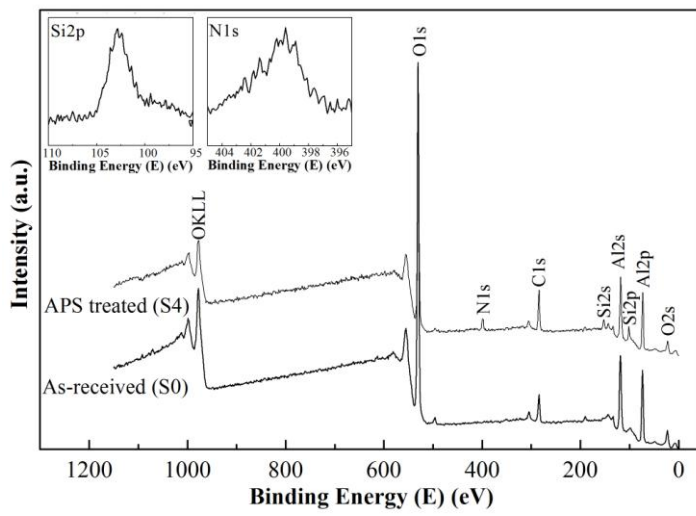
(d)
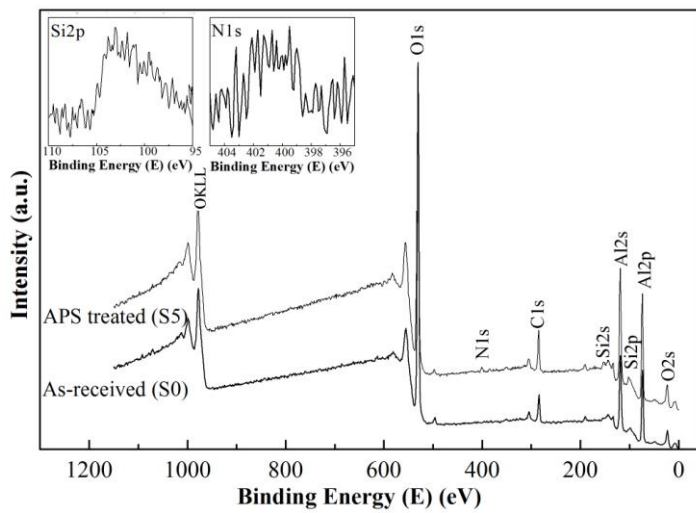
(e)

Figure 4.8 (continued)**.**

Table 4.1 Elemental surface composition (at%) of as-received and silane treated platelets.

Designation	Al	O	C	Si	N
S0	39.9	51.9	8.2	-	-
S1	21.8	61.7	15.5	1.0	-
S2	21.1	62.4	12.1	1.4	-
S3	21.7	59	15.4	1.2	2.7
S4	20.3	55.7	19.4	1.1	3.5
S5	25.0	62.3	11.1	0.6	1

(a)

(b)
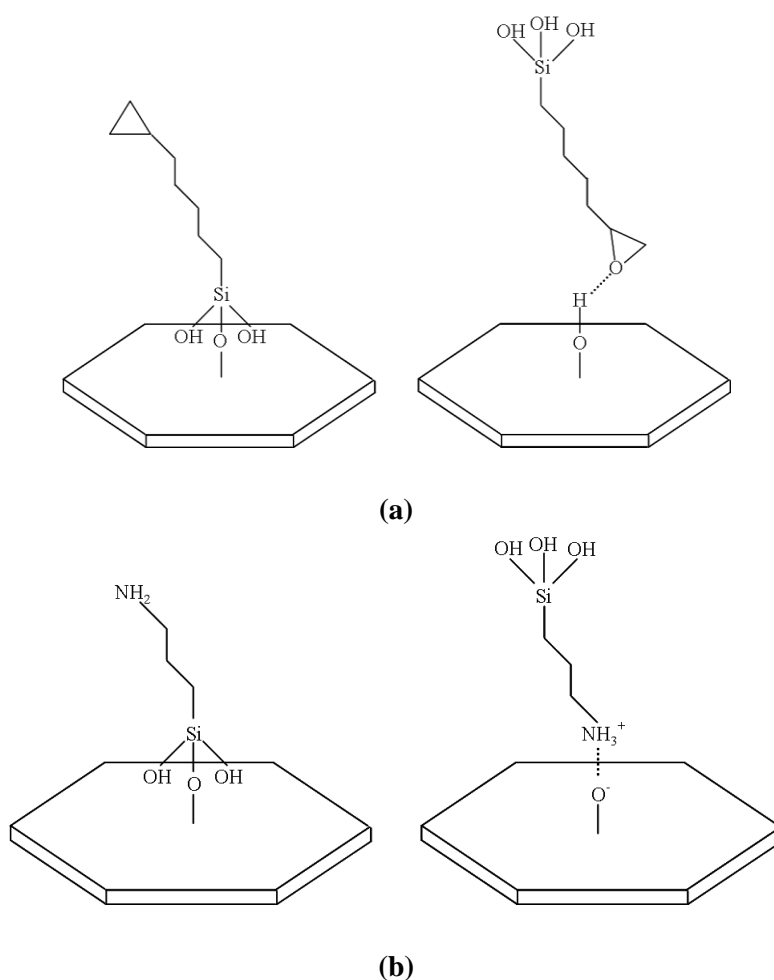
Figure 4.9 Possible interaction mechanisms for (a) GPS and (b) APS with the inorganic surface with the inorganic surface.

As mentioned in Section 2.3, silane coupling agents provide chemical linkage at the interface between two dissimilar materials such as inorganic reinforcement and organic matrix. For effective coupling at the interface, hydrolysable group of the silane molecule should react and make strong chemical bonds with the hydroxyl groups at the inorganic surfaces, whereas its organofunctional group should provide linkage with the organic phase. The linkage of the APS and the epoxy matrix is suggested to occur through the chemical reaction between the reactive group (amino functionality) and the epoxy moiety of the resin [145, 146] as shown in Figure 2.23.a. On the other hand, for silanes with epoxy functionality such as GPS, organofunctional group is suggested to take part in the crosslinking of epoxy with the addition of the hardener [147, 148] (Figure 2.23.b). Therefore, the orientation of silanol molecules on the inorganic surfaces is crucial for the effectiveness of the silane treatment.

In a previous study, it has been suggested that surface atomic ratio of N/Si can provide information about the orientation of APS molecule on the substrate surface [165]. It has been stated that ideal N/Si ratio would be different for each type of adsorption conformation (Figure 4.10) such that N/Si <1 for type (a), N/Si =1 for type (b) and N/Si > 1 for type (c) if every adsorbed molecule had identical orientation. If all three type surface adsorption conformations exist on the surface simultaneously, determined absolute N/Si ratio can provide information about which type is most prevalent.
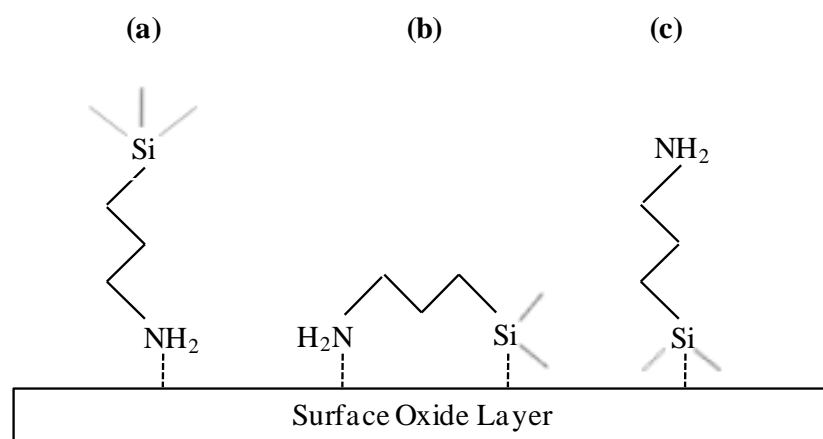
Figure 4.10 Model of possible adsorption conformations of APS on an oxide surface. Interaction via (a) protonated amine group, (b) protonated amine group and condensed silanol adsorption, (c) silanol groups [165].

69

In the current study, N/Si atomic ratio for APS treated platelets are ~2 and ~3 for the surface functionalization applied in toluene and ethanol-water mixture, respectively, and ~1.6 in the case of APS treated platelets in distilled water. This indicates that APS molecule is adsorbed mainly through silanol groups rather than protonated amino group.

Al surface concentrations for the platelets treated with amino-functional silane in different solvents indicate that the deposited silane layer is thinnest for platelets treated in distilled water (S5). Among the platelets treated either in toluene or in ethanol-distilled water solvent, deposited silane layer is thinner for platelets treated in toluene (S3) than those treated in ethanol-water mixture (S4) as it can be deduced from the elemental surface Al concentrations.

Figure 4.11 illustrates deconvoluted high resolution XPS spectra of N1s core levels for S3, S4 and S5. The peak centered at 399.8 eV in Figure 4.11.a is attributed to free NH_2 groups indicating that the interaction between amino silane and platelet surface occurs merely through silanol groups for platelets functionalized with APS in toluene [178, 179].

For platelets functionalized with amino silane in ethanol-water mixture, N1s core level was deconvoluted into two components which are centered at 399.6 and 401.5 eV with relative percentages of 81% and 19%, respectively (Figure 4.11.b). The peak at lower binding energy can be assigned to free amine groups, and the peak at higher binding energy can be attributed to protonated amino groups [179, 180] indicating that although interaction was mainly via silanol groups, some of the silane molecules also adsorbed through protonated amino groups on platelet surfaces. This result points out that only 81% of the adsorbed silane molecules have free NH_2 groups, oriented towards the matrix side, to link with the epoxy matrix by participating in chemical reaction with the resin.

Similar to APS treated platelets in ethanol-distilled water solution, deconvolution of N1s core level indicates presence of two peaks for amino silane treated platelets in distilled water (Figure 4.9.c) separated from each other by a binding energy of 1.6 eV. These two peaks centered at 399.6 eV and 401.2 eV can be attributed to free amine and protonated amino groups, respectively [179, 180]. The relative percentages of deconvoluted peaks pointed out that 54% of the silane molecules adsorbed through silanol groups and the remaining 46% of the silane molecules adsorbed through protonated amino groups in distilled water and hence, only 54% of the silane molecules can react with the epoxy resin. Since the applied deconvolution procedure involves various assumptions which may vary according to the mathematical treatment used, reported relative percentages are not absolute, yet they better represent a qualitative manner describing the variety in the chemical interaction between the silane molecule and the inorganic surface.
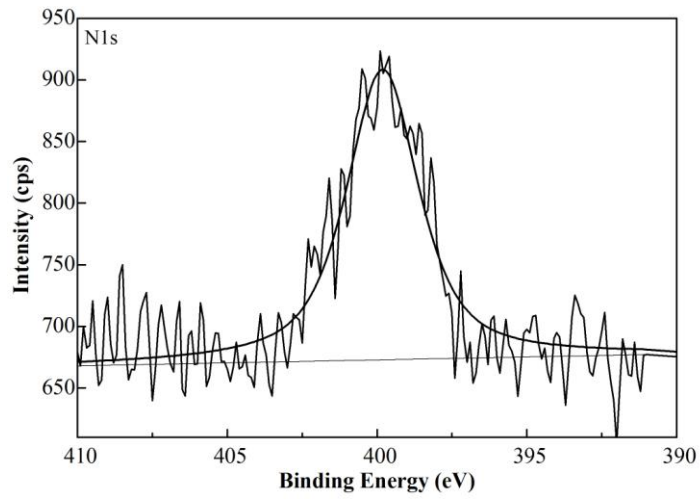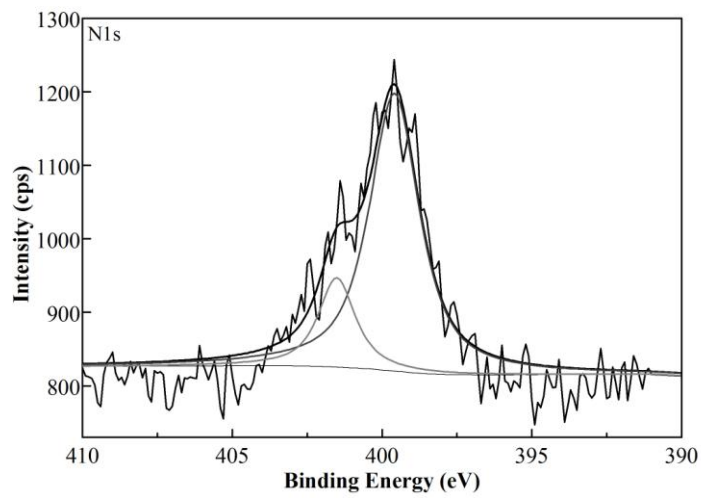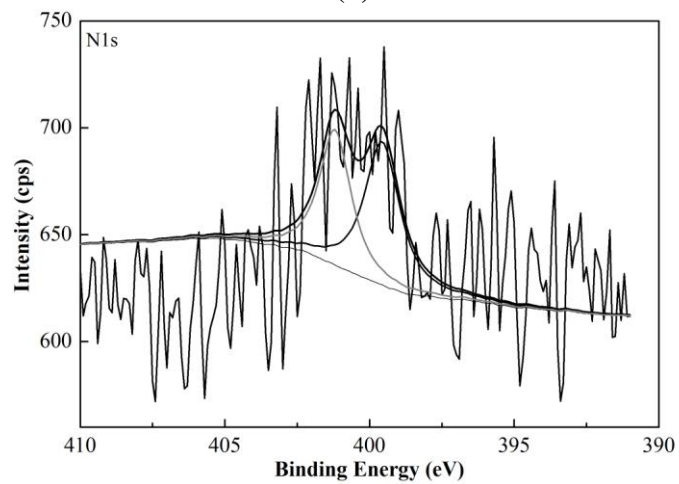
Figure 4.11 High resolution XPS spectra of N1s core level for (a) APS treated platelets in toluene (S3), (b) APS treated platelets in ethanol-water mixture (S4) and (c) APS treated platelets in distilled water (S5).

4.1.3 Epoxy Matrix Composites Reinforced by Surface Treated Alumina Platelets

Mechanical behavior of inorganic-organic composites is strongly affected by the properties of the reinforcement and matrix interface. Wettability and adhesion are important factors that control the effective load transfer from matrix to reinforcements. For this reason, to improve wettability and interface adhesion between the platelets and the epoxy matrix, surfaces of the platelets were functionalized with two different types of silanes; epoxy- and amino- functional silanes. To reveal the effect of surface treatment on mechanical properties, both simple mixed (SM) and HASC processed composites reinforced by as-received and silane treated alumina platelets were fabricated. HASC processed composites were fabricated under the applied pressure of 100 MPa due to the fact that the composites processed at this pressure offered the optimum result in terms of both platelet alignment and the mechanical performance as mentioned in Section 4.1.

Figure 4.12.a shows the flexural stress-strain curves for simple mixed and HASC processed composites reinforced by both as-received and GPS treated platelets. Even in the case of composites fabricated by simple mixing, reinforcing the epoxy matrix by platelets treated with GPS in ethanol-water mixture (S1) have led to ~16% and ~30% enhancements in flexural strength and flexural strain values, respectively, as compared to composite reinforced by as-received platelets (Figure 4.12.b).

The improvement in flexural strength is more pronounced in the case of HASC processed composite leading to an increase of ~35% in flexural strength accompanied by ~13% enhancement in flexural strain value with respect to HASC processed composite reinforced by as-received platelets. For the composites reinforced by platelets treated with GPS in distilled water (S2), situation is completely different. Incorporation of S2 platelets has led to a decrease in flexural strength value for both simple mixed and HASC processed composites along with a decrease in failure strain in the case of composite fabricated by HASC processing.

For S2 platelets, XPS result showed that the surface Si concentration is 40% higher than the platelets treated in ethanol-water mixture indicating that the deposited silane layer was thicker. It is known that the silanol groups are highly reactive and condensation of these reactive silanols occurs rapidly in water [155]. Although, pH of the water was adjusted to 4.5 to catalyze hydrolysis and retard the condensation processes, highly reactive silanol groups might have self-condensed and formed siloxane oligomers and network structures. These oligomeric species might have crosslinked or aggregated on the surface of the inorganic platelets and formed an inhomogeneous multilayer silane structure [154]. This weak physisorbed partially polymerized outermost layer might have led to a decrease in the effectiveness of silane coupling and hence, in the mechanical performance of the composite.
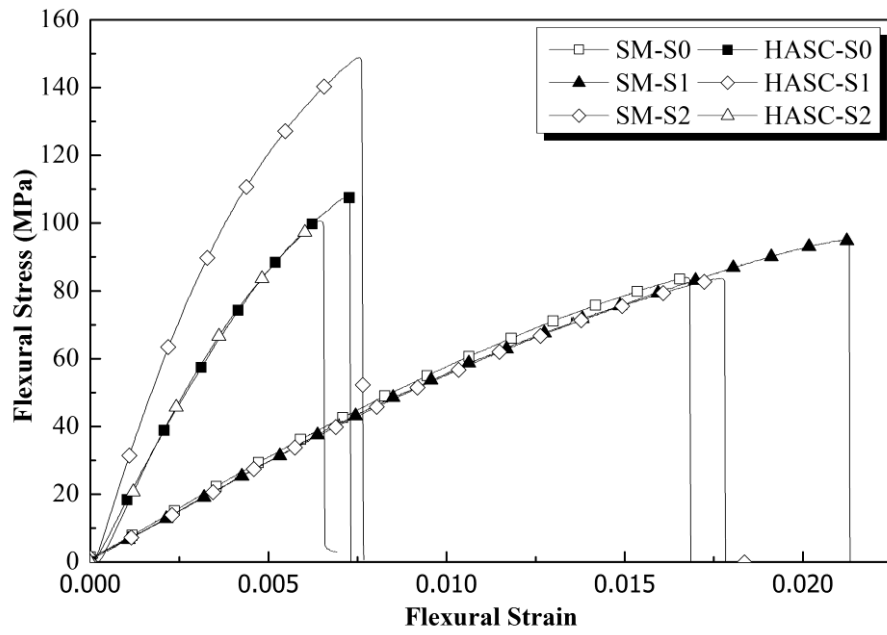
(a)

(b)

Figure 4.12 Flexural Stress-Strain curves (a) and variation in flexural strength and failure strain (b) for simple mixed and HASC processed composites reinforced by as-received and GPS treated platelets.

Figure 4.13 presents the variation of flexural modulus for composites reinforced by as-received and GPS treated platelets. For simple mixed composites, reinforcing the epoxy with surface functionalized platelets does not impart extra stiffness when compared to simple mixed composite reinforced by as-received platelets. The situation is also similar in the case of HASC processed composite reinforced by S2 platelets. However, for HASC processed composite reinforced by the GPS treated S1 platelets, high reinforcement volume fraction reveals the effect of surface treatment leading to ~27% enhancement in stiffness with respect to the composite reinforced by as-received platelets.

Figure 4.14 and Figure 4.15 shows fracture surfaces of three-point bending (3PB) tested composites reinforced by either as-received or GPS treated platelets. Fractographs of either simple mixed or HASC processed composites reinforced by as-received platelets (Figure 4.14) clearly demonstrate the presence of clean platelet surfaces indicating weak interfacial bonding between the platelets and the matrix. Arrows in Figure 4.14.a and Figure 4.14.b illustrate platelet debonding and smooth platelet pull-out sites revealing that the fracture mechanism is mainly governed by platelet debonding and pull-out for these composites.
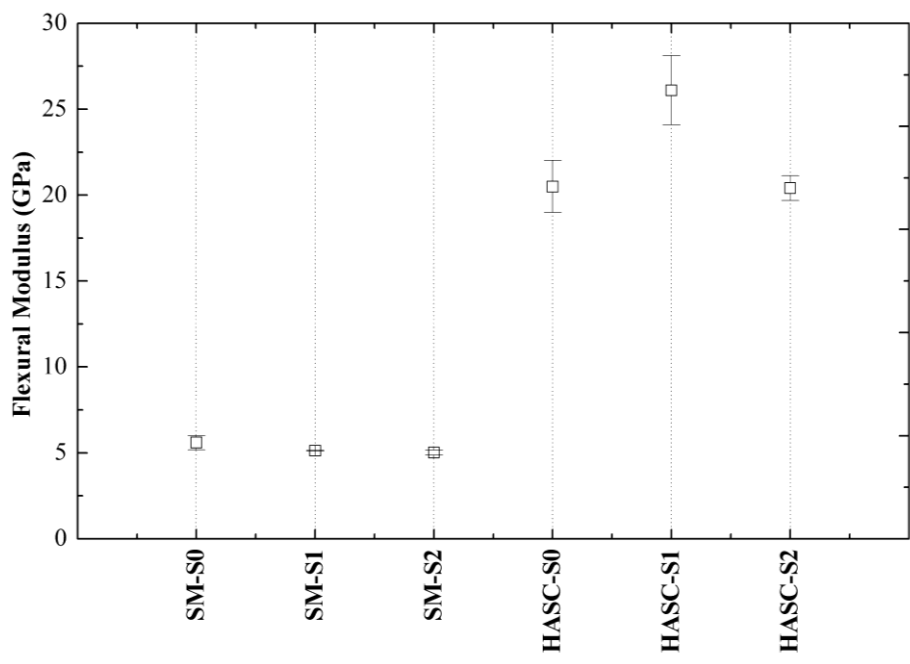
Figure 4.13 Effect of alumina platelet surface functionalization with GPS on flexural modulus of simple mixed composites and HASC processed composites under the applied pressure of 100 MPa.
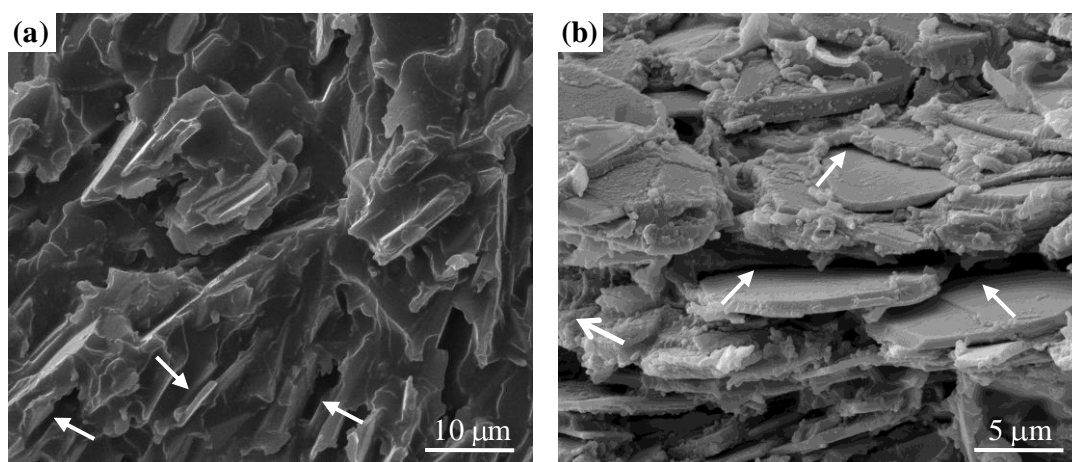
Figure 4.14 Fracture surfaces of 3PB specimens of composites reinforced by as-received platelets; (a) simple mixed, (b) HASC processed under the applied load of 100 MPa.

For simple mixed composite reinforced by platelets GPS treated in ethanol-water mixture (Figure 4.15.a), it is hard to distinguish individual platelets in the structure. This can be attributed to the random orientation of platelets and coverage of the platelet surfaces with epoxy. In addition to this, it can be stated that fracture did not occur through the platelet-matrix interface, but rather through the matrix caused by the proper wetting of the platelets and relatively strong chemical bonding between the platelets and the matrix. On the other hand, for composite reinforced by platelets GPS treated in distilled water (Figure 4.15.b), presence of clean platelet surfaces (black arrow) and platelet pull-out sites (white arrows) explicitly indicates that effective coupling between the inorganic surfaces and the epoxy matrix could not be achieved.

Fracture surface of HASC processed composite reinforced by GPS treated S1 platelets (Figure 4.15.c) emphasizes the effect of surface functionalization on interfacial adhesion. In this micrograph, rough platelet surfaces indicate effective adhesion of the platelet surfaces to epoxy, and hence, presence of a relatively strong chemical bonding between the platelets and the matrix. It is again clear that for these composites main fracture mechanism is not platelet-matrix debonding, yet rather via the propagation of crack through the matrix deflecting near the platelets leaving the surfaces of platelets covered with epoxy.
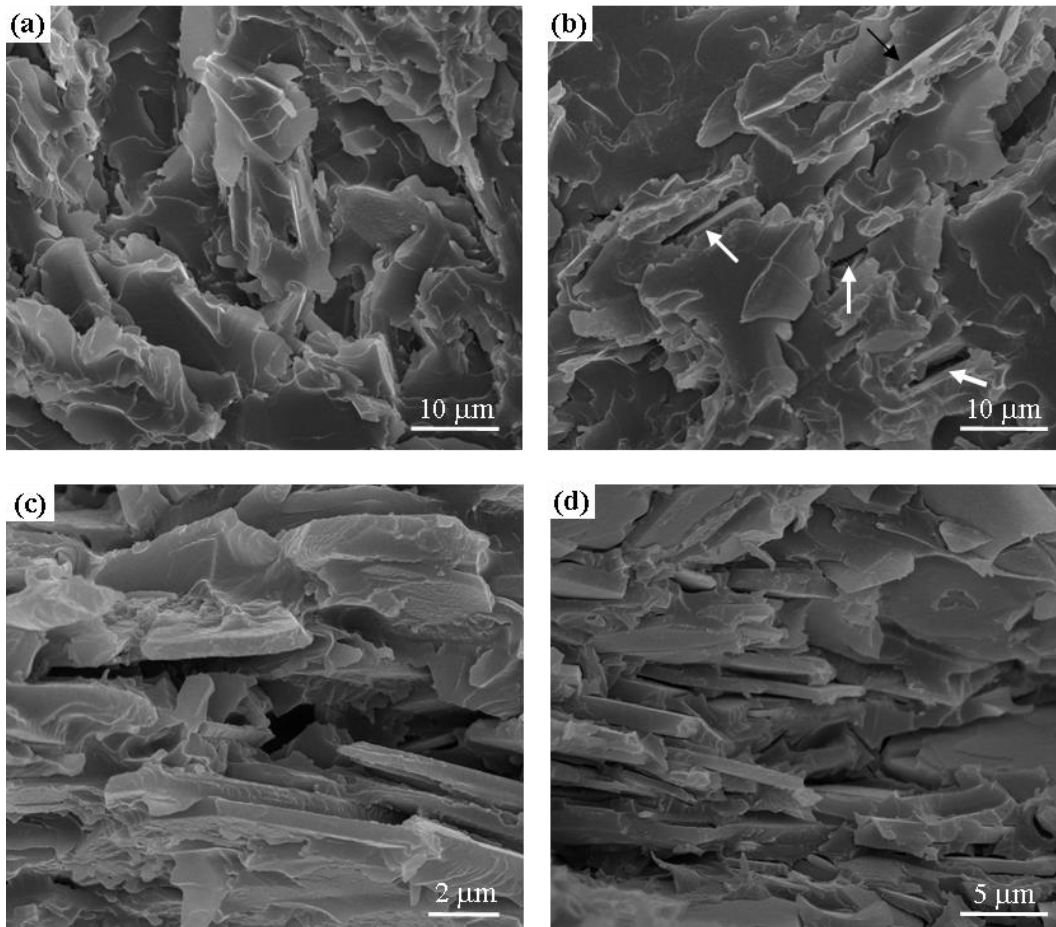
Figure 4.15 Fracture surfaces of 3PB specimens of composites reinforced by GPS treated platelets; (a) SM-S1, (b) SM-S2, (c) HASC-S1 and (d) HASC-S2.

Figure 4.15.d demonstrates the fracture surface of the HASC processed composite reinforced by the GPS treated platelets S2. Based on the clean platelet surfaces, it can be stated that although the governed fracture mode is platelet pull-out, fracture seems to have occurred along the platelet-matrix interface leaving the platelet surfaces almost smooth. Along with the mechanical test results, this fact explicitly reveals the fact that coupling and chemical bridging could not be achieved at the interface between inorganic platelets and the epoxy matrix.

This result is in good agreement with the already discussed decrease in flexural strength for the HASC processed composite reinforced by the platelets treated with GPS in distilled water (S2) (Figure 4.12.b) confirming the ineffective silane layer formation on the platelet surfaces leading to their weaker interaction with the epoxy matrix.
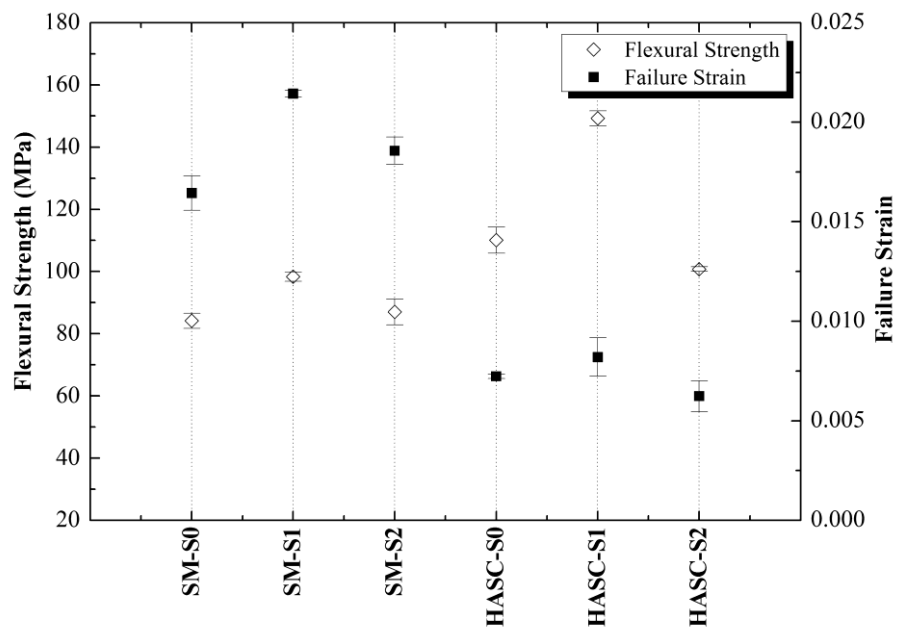
Figure 4.16 shows the flexural stress-strain curves of simple mixed and HASC processed composites reinforced by both as-received and APS treated platelets. This figure demonstrates explicitly the effect of surface treatment of platelets, in terms of the enhancement of flexural strength and strain for both simple mixed composites and HASC processed composites under the applied hot pressing pressure of 100 MPa. Together with the increase in the inorganic content (available interfacial area) and preferential alignment of high aspect ratio reinforcements (Figure 4.17), the effect of coupling at the reinforcement-matrix interface is more pronounced for HASC processed composites compared to simple mixed ones (Figure 4.18).
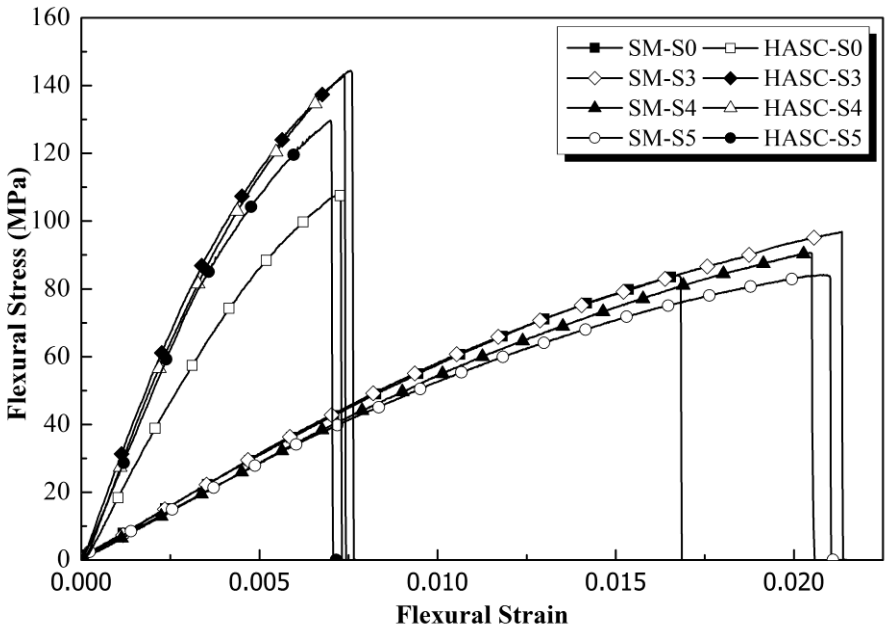
Figure 4.16 Flexural Stress-Strain curves for simple mixed composites and HASC processed composites reinforced by both as-received and APS treated platelets.

For simple mixed composites, incorporation of APS treated S3 and S4 platelets have led to ~7-16% improvement in flexural strength as compared to simple mixed composite reinforced by as-received platelets. This improvement in flexural strength for platelets S3 and S4 is not accompanied by a decrease in failure strain, instead followed by ~23-33% increase indicating existence of chemical bonding, and hence effective load transfer at the interface (Figure 4.18.a). For HASC processed composites, as mentioned earlier, increase in inorganic platelet content together with their hierarchical arrangement, makes the effect of surface functionalization more remarkable leading to ~27-33% and ~1-14% increase in flexural strength and failure strain values, respectively, when compared to HASC processed composites reinforced by as-received platelets.

77
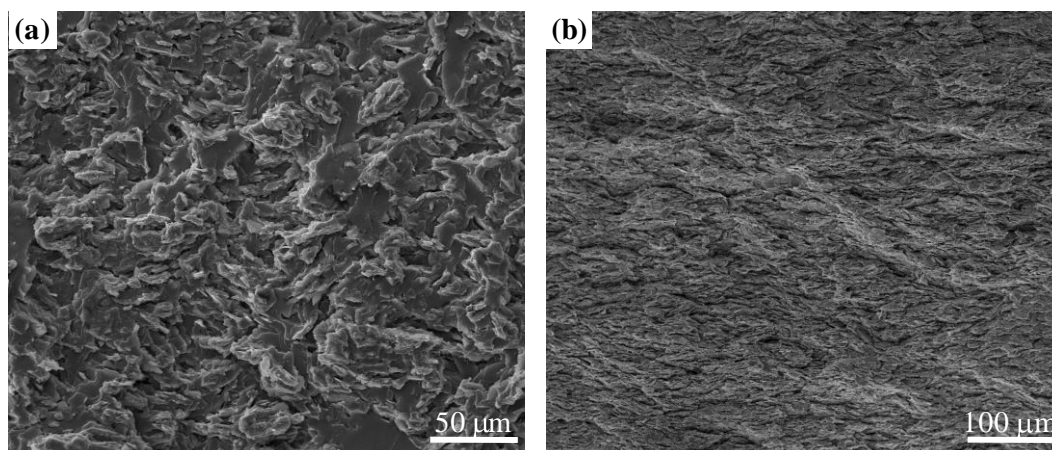
Figure 4.17 Fracture surfaces of composite samples reinforced by surface treated alumina platelets surface treated with APS in ethanol-water mixture; (a) SM-S4 and (b) HASC-S4.

For simple mixed composites reinforced by the platelets treated in distilled water (S5), although the incorporation of the surface treated platelets did not impart any improvement in flexural strength value, failure strain value increased by a factor of ~27% as compared to simple mixed composite reinforced by as-received platelets. For the HASC processed composite, incorporation of surface treated platelets have led to a ~15% enhancement in flexural strength value which is also accompanied by a ~2% improvement in failure strain as compared to HASC processed composite reinforced by as-received platelets.

Silane treatment of the platelets with APS does not seem to have a significant effect on the stiffness of the simple mixed composites (Figure 4.18.b). However, for HASC processed composites, surface treatment of the platelets have led to 14-26% enhancement in flexural modulus of the composites imparting extra stiffness. Among all APS surface treatments applied, APS treatment in distilled water seems to be the least effective in improving the mechanical properties of alumina platelet reinforced composites.

Results obtained from the three point bending tests bring about the fact that although surface treatment of the platelets with amino-functional silane leads to an improvement in mechanical properties independent of the solvent used for silanization, reinforcing the composite with platelets APS functionalized in toluene is the most effective way to improve the mechanical properties. Furthermore, obtained mechanical results along with the presented XPS data also imply that as the decrease in the fraction of adsorbed silane molecules which can take part in the reaction with the epoxy resin leads to a decrease in the effectiveness of the silane treatment as in the case of APS functionalized platelets S4 and S5. This decrease becomes more pronounced for the composite reinforced by APS functionalized S5 platelets due to the fact that only 54% of the deposited silane molecules can take part in chemical reaction with epoxy.

78
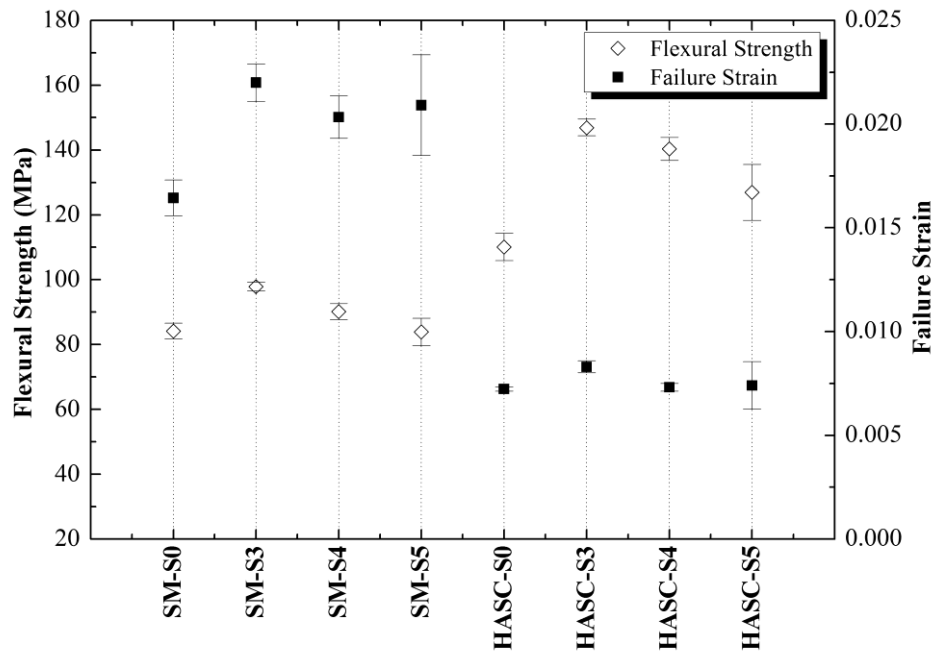
(a)
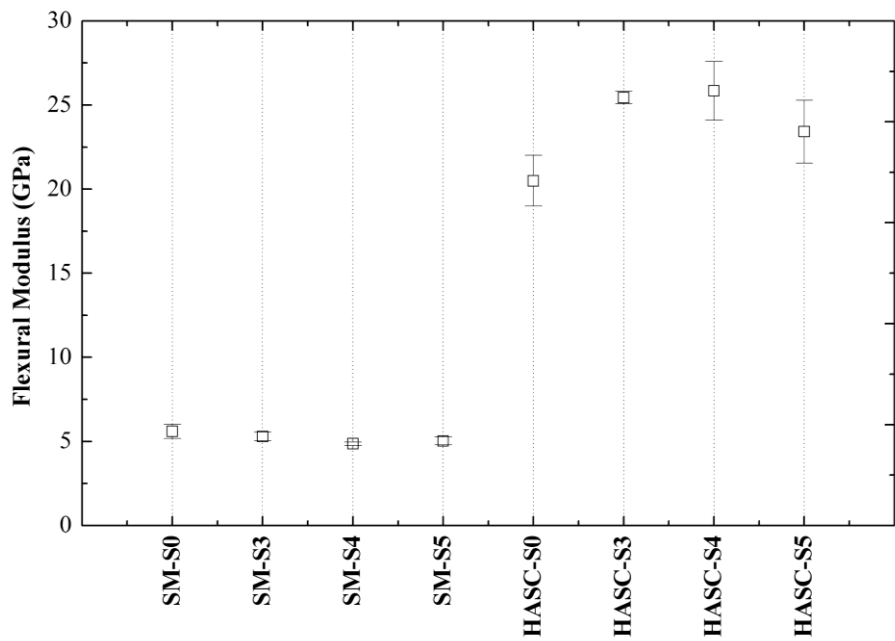
(b)

Figure 4.18 Effect of alumina platelet surface functionalization with APS on mechanical properties of simple mixed and HASC processed composites; (a) flexural strength and failure strain and (b) flexural modulus.

Micrographs of simple mixed composite reinforced by platelets treated with APS in distilled water (S5) are shown in Figure 4.19. Similar to GPS treated platelets; it is hard to distinguish individual platelets in the fractographs for simple mixed composite samples reinforced by APS treated platelets. Fracture surfaces of HASC processed composites reinforced by platelets treated with amino-functional silane (Figure 4.19.c–f) illustrates the effect of surface functionalization on interfacial bonding. In these micrographs, rough platelet surfaces indicate effective adhesion of the platelet surfaces to epoxy, and hence presence of an effective chemical bonding between the platelets and the matrix. It is again clear that for these composites main fracture mechanism is not platelet-matrix debonding, yet rather it is via the propagation of crack through the matrix deflecting near the platelets leaving the surfaces of the platelets covered with epoxy.

On the account of the three-point bending tests results, work of fracture tests (WOF) were conducted only for composites reinforced by as-received platelets along with the composites reinforced by silane treated platelets incorporation of which has led to considerable improvement in mechanical performance; namely, platelets GPS treated in ethanol-water mixture (S1) and platelets APS treated either in toluene (S3) or ethanol-water mixture (S4).

Figure 4.20 shows the load-displacement curves of simple mixed and HASC processed composites with SENB specimen geometry along with the load-displacement curve of neat epoxy. Average WOF value, expressing the energy absorbed by a notched specimen until fracture, was calculated as 350 J/m^2 for neat epoxy. For simple mixed and HASC processed composites reinforced by as-received alumina platelets, average WOF values were calculated as 129 J/m^2 and 135 J/m^2, respectively, which are considerably lower as compared to the WOF value of neat epoxy.

When WOF test results of simple mixed and HASC processed composites are compared, it can be deduced that although there is no considerable difference between the WOF values, fracture behavior of the composites completely differs from each other. Load-displacement curve of the simple mixed composite showing an abrupt decrease from the maximum point demonstrates that crack propagation is unstable leading to catastrophic failure.

For HASC processed composite with an architecture resembling to brick-and-mortar structure, crack propagation is stable as indicated by the tail behavior following the maximum in load-displacement curve. This tail behavior clearly indicates that main fracture, and hence energy absorption mechanism is platelet debonding and pull-out for the HASC processed composite.
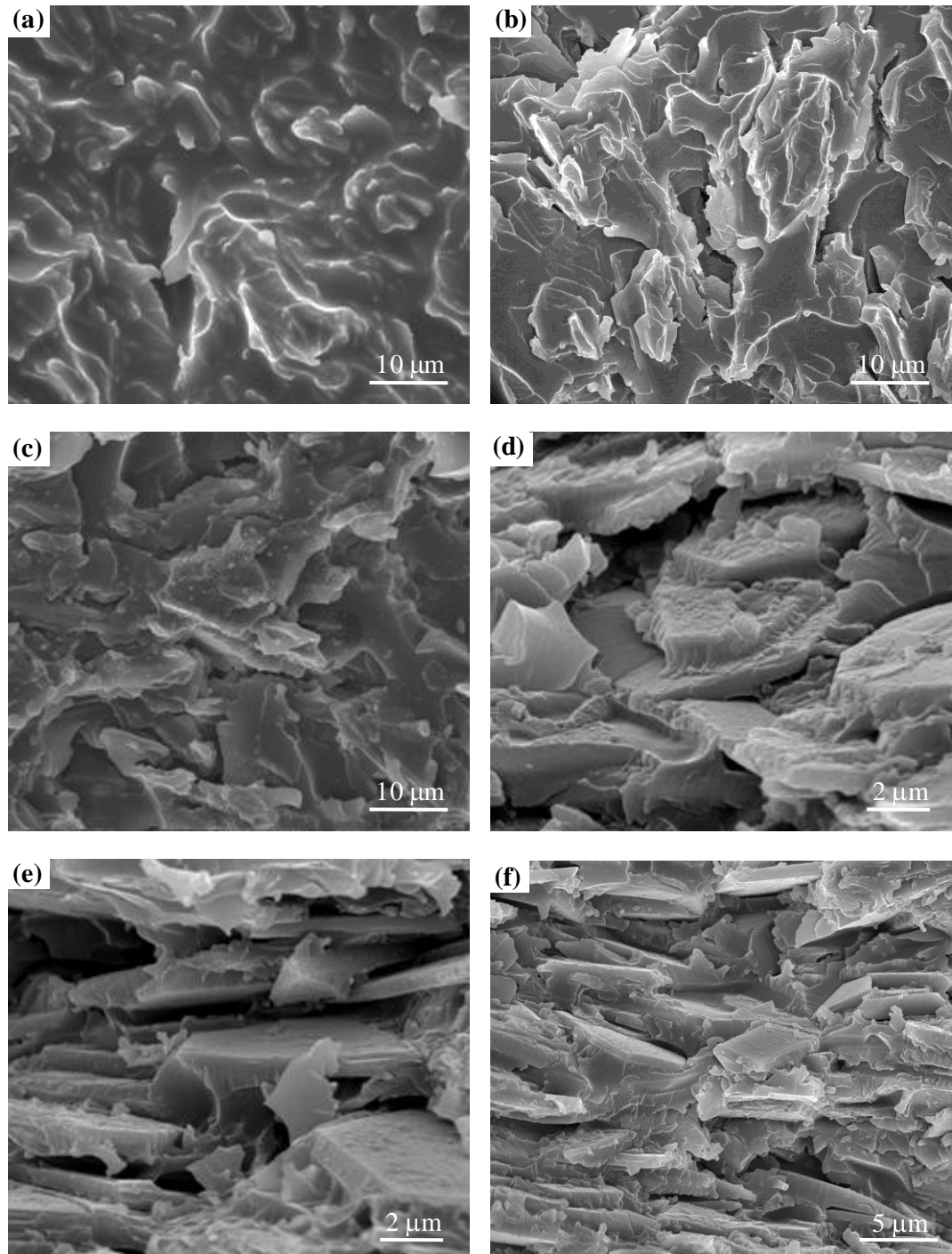
Figure 4.19 Fracture surfaces of 3PB specimens; (a) SM-S3, (b) SM-S4, (c) SM-S5, (d) HASC-S3, (e) HASC-S4 and (f) HASC-S5.
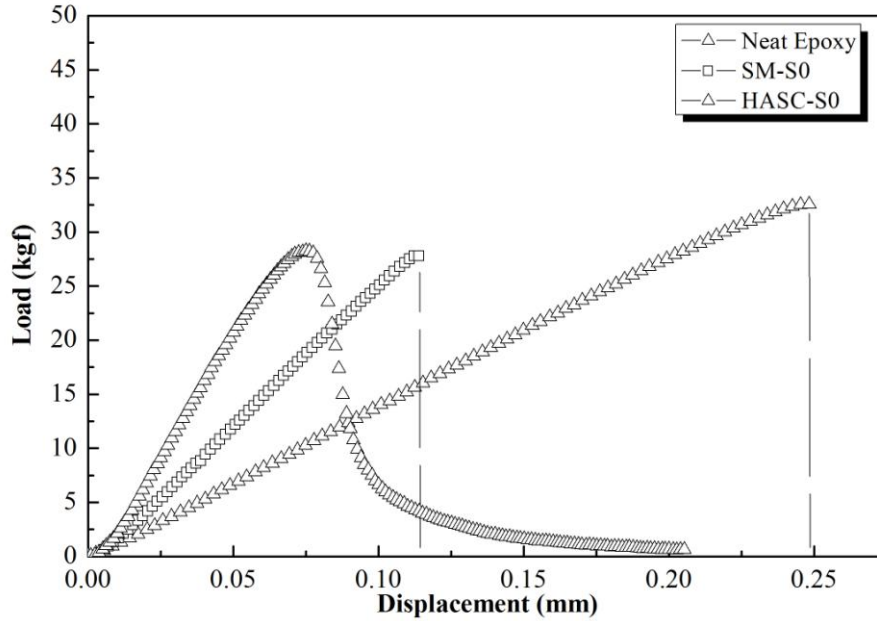
Figure 4.20 Load-displacement curves for SENB specimens of simple mixed and HASC composites reinforced by as-received alumina platelets along with the load-displacement curve of neat epoxy.

Load-displacement curves of simple mixed and HASC processed composites reinforced by surface functionalized platelets are shown in Figure 4.21 and Figure 4.22 together with the load-displacement curves of composites reinforced by as-received platelets for comparison. Average WOF values of simple mixed composites reinforced by silane treated platelets are ranging between 137-159 J/m^2 where the lowest value was obtained for composite reinforced by platelets treated with APS in ethanol-water mixture (Figure 4.21). Although silane treatment does not seem to lead to a change in the failure mechanism of the simple mixed composites, which is catastrophic, energy absorbed until fracture increases by ~6-23% when compared to simple mixed composite reinforced by as-received platelets.

The improvement in WOF values is more outstanding in the case of HASC processed composites reinforced by silane treated platelets ranging from 160-178 J/m^2 being ~19-32% higher than those of HASC processed composites reinforced by as-received platelets. This improvement is comparable for platelets treated with GPS in ethanol-distilled water (S1) and APS in toluene (S3) while it is lower for platelets treated with APS in ethanol-water mixture (S4). The results of three-point bending and WOF tests of both simple mixed and HASC processed composites reinforced by surface treated platelets indicate the impact of interfacial adhesion between reinforcement and the matrix on the mechanical properties of inorganic reinforced composites.

82
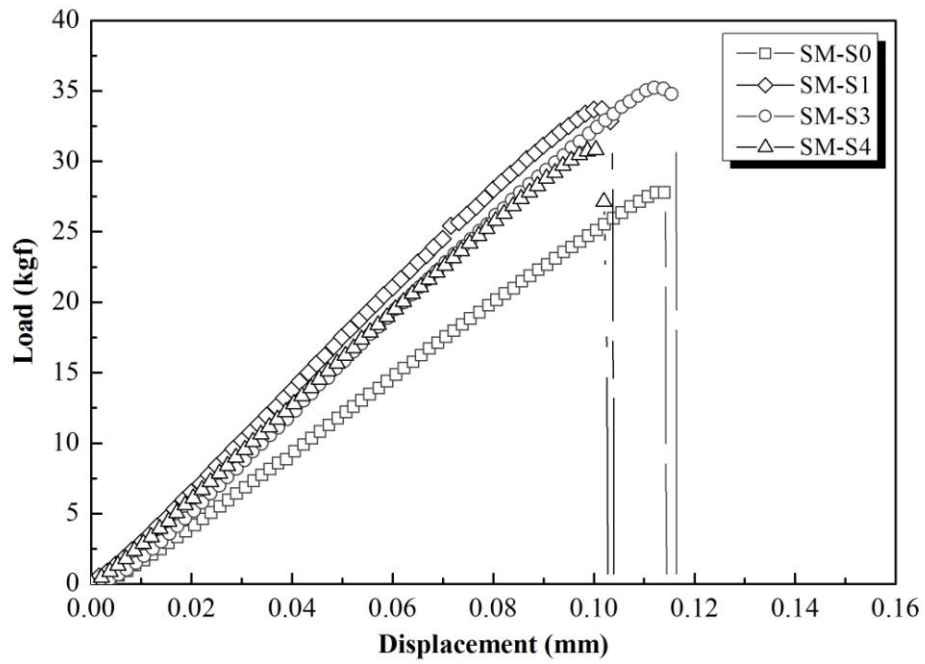
Figure 4.21 Load-displacement curves for SENB specimens of simple mixed composites reinforced by as-received and silane treated alumina platelets.
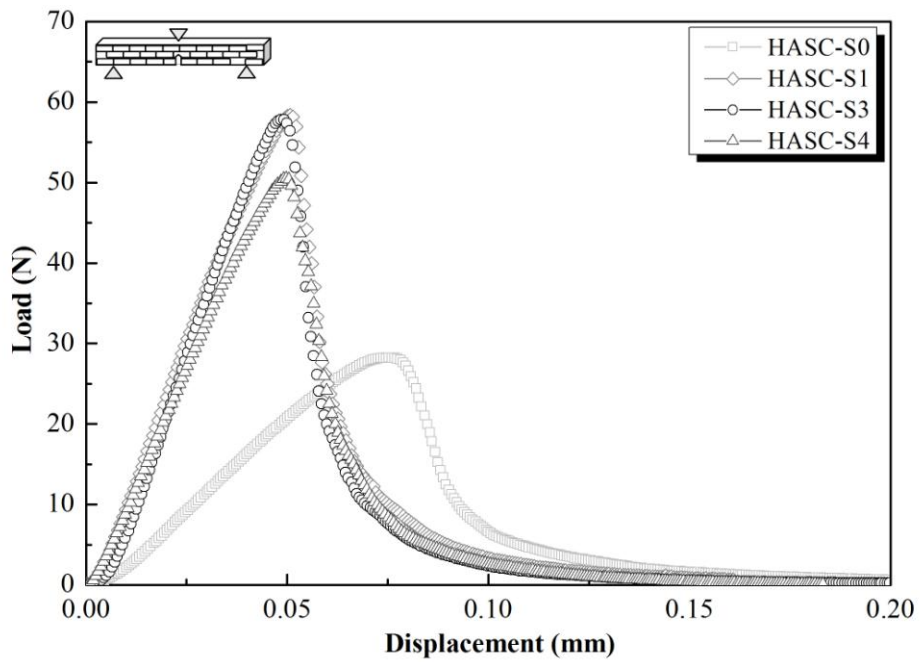
Figure 4.22 Load-displacement curves for SENB specimens of HASC processed composites reinforced by as-received and silane treated alumina platelets.

4.2 Inorganic–Organic Bulk Lamellar Composites Reinforced by Glass Platelets and Flakes

4.2.1 Epoxy Matrix Composites Reinforced by As-received Platelets and Flakes

In the scope of the study, glass platelet-epoxy matrix composites were also fabricated using the HASC process under the action of different applied pressures. Incorporated glass platelets are thicker and their aspect ratio is lower than those of the alumina platelets. The inorganic content of the initial reinforcement-epoxy mixture was 20 vol% before processing. HASC processing led to considerable increase in the inorganic content which is 2.5 fold in the case of the applied pressure of 25 MPa (Figure 4.23). Further increase in the applied processing pressure resulted in further increase in the inorganic content of the composite samples with a maximum inorganic content of ~ 63 vol% achieved at the applied pressure of 150 MPa. As in the case of alumina platelet-reinforced composites, the increase in the inorganic content almost levels-off but in this case for the processing pressures exceeding 75 MPa.
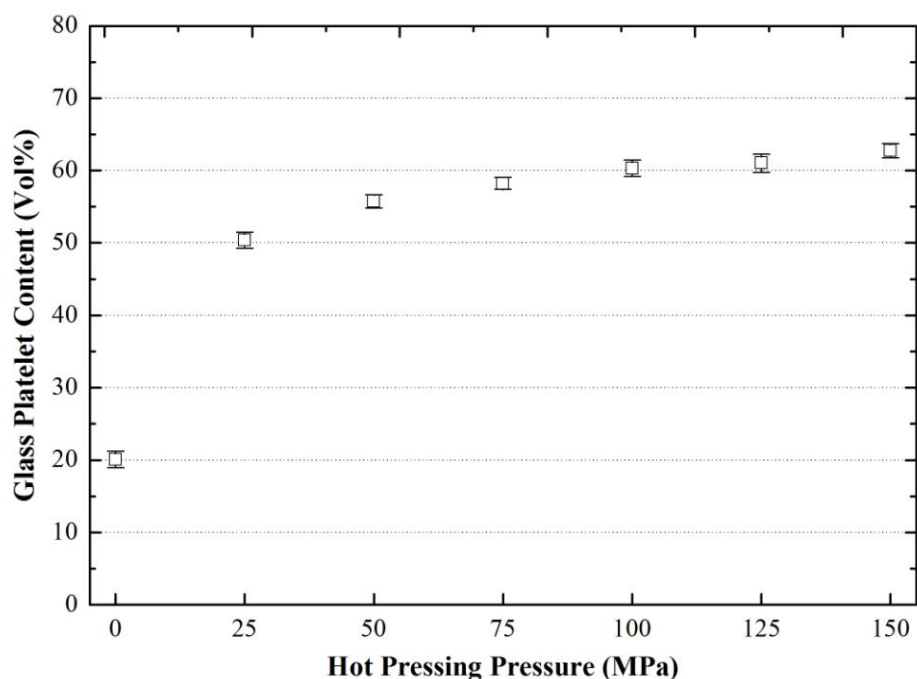
Figure 4.23 Glass platelet content of the composites fabricated under the action of different HASC processing pressures.

84

Figure 4.24 illustrates the SEM images of the polished cross-sectional microstructure of simple mixed and HASC processed composites for the applied pressures of 50 MPa, 100 MPa and 200 MPa. It is clear from these images that although alignment of the platelets is favored by the drainage of the epoxy resin, misalignment sites also exist for all HASC processed composites. Beside the platelet clusters which exist in all HASC processes composites, elongated voids at the platelet – matrix interface (shown with black arrows in Figure 4.24) can be explicitly seen indicating decoupling at the interface. Another interesting finding is the fact that in some regions, glass platelets were broken into two or more pieces, with a concomitant reduction in aspect ratio, probably during HASC processing. It is also explicit from the SEM images that platelet clusters, elongated voids at the interfaces and breakage of the platelets are becoming more pronounced with the increase in the applied processing pressure for the HASC processed composites, especially at applied pressures exceeding 50 MPa.

On the contrary to alumina reinforced composites, incorporation of glass platelets leads to a decrease in both flexural strength and strain values of the neat epoxy (Figure 4.25). For the simple mixed sample, incorporation of 20 vol% glass platelet with random orientation into epoxy matrix results in ~22% reduction in flexural strength. Reinforcing the epoxy with ~56 vol% aligned glass platelets through HASC processing, which is 2.7 fold higher than the inorganic content of the simple mixed composite, through HASC processing has led to a decrease of only ~4% in flexural strength with respect simple mixed composite. However, further increase in the inorganic content resulted in a more dramatic decrease in the flexural strength ranging between 44-57% and 28-45% with respect to neat epoxy and simple mixed composite, respectively. The decrease in the flexural strength with the incorporation of glass platelets even for the low inorganic containing simple mixed composite can be attributed to the lack of coupling between platelets and the epoxy matrix along with the presence of voids at the interface leading to a decrease in the stress transfer from matrix to the reinforcement. Beside these, the dramatic decrease in flexural strength for the composites HASC processed with an applied pressure of 75 MPa and higher is thought to be arisen from the increase in the number of fractured platelets along with the increase in the size of the platelet clusters leading to further decrease in effective load transfer.

Figure 4.26 shows the fracture surfaces of the three-point bending (3PB) tested simple mixed and HASC processed composites under the applied processing pressure of 50 MPa. From this figure it is evident that fracture occurs through platelet/matrix interface leaving the platelet surfaces clean indicating the lack of adhesion between the platelets and the matrix. Platelet debonding (shown with black arrows) and the smooth platelet pull-out sites (shown with white arrows) reveals that the fracture mechanism is mainly governed by platelet debonding and platelet pull-out for these composites, not by platelet fracture.
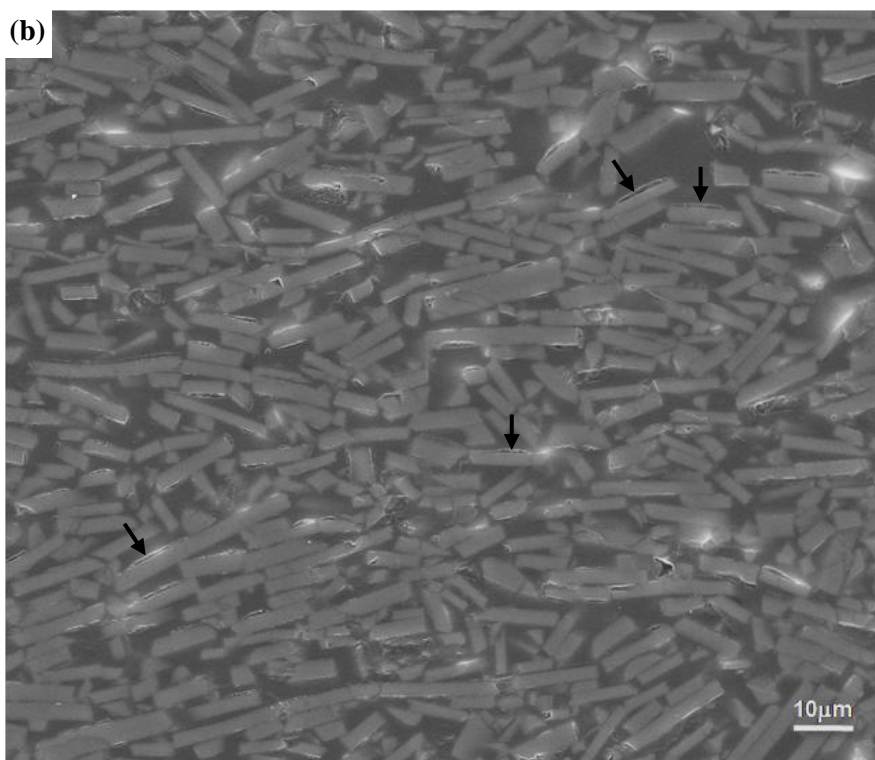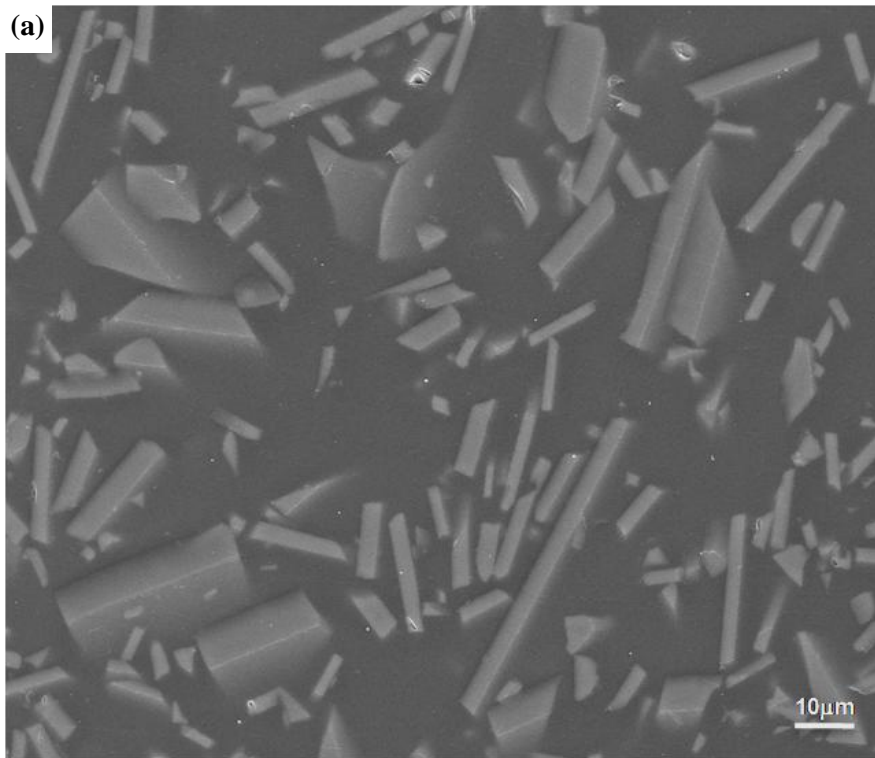
Figure 4.24 Cross-sectional microstructure of (a) simple mixed and HASC processed composites for the applied pressures of (b) 50 MPa, (c) 100 MPa and (d) 150 MPa.

(c)

(d)
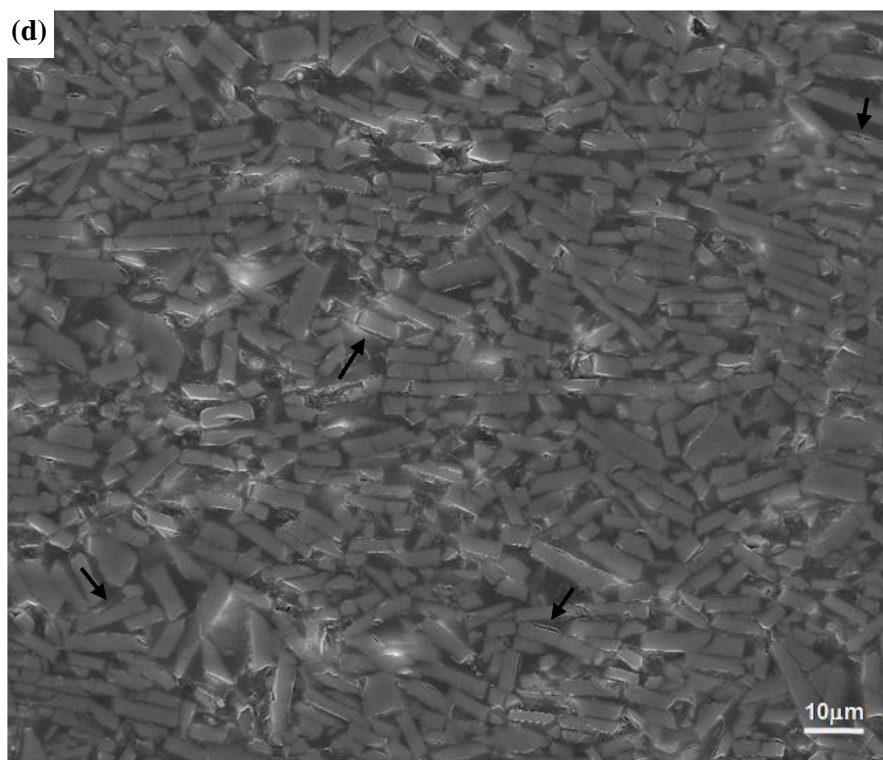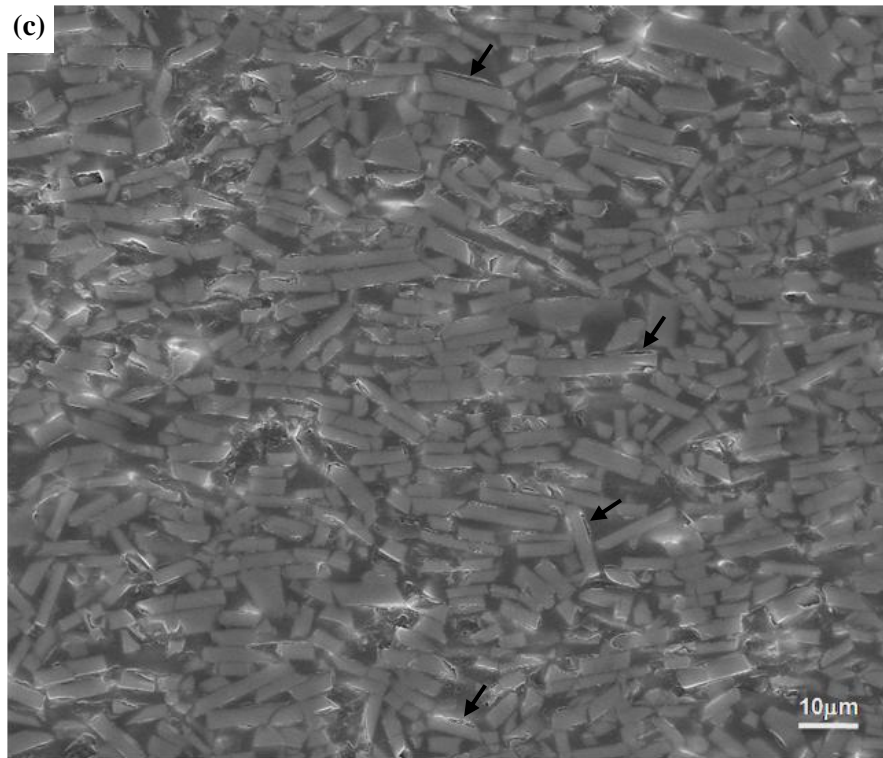
Figure 4.24 (continued).
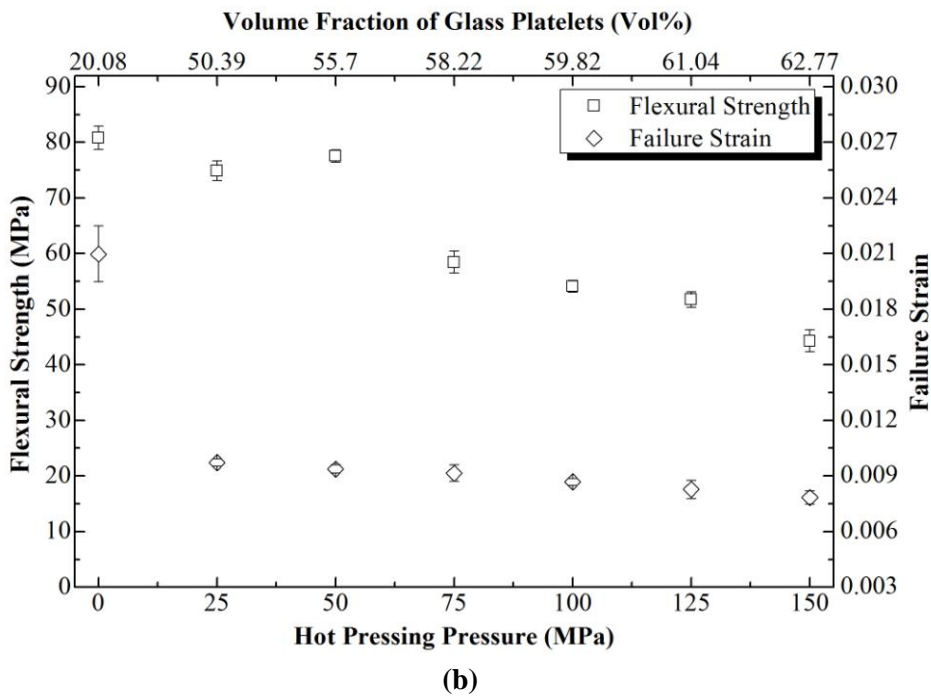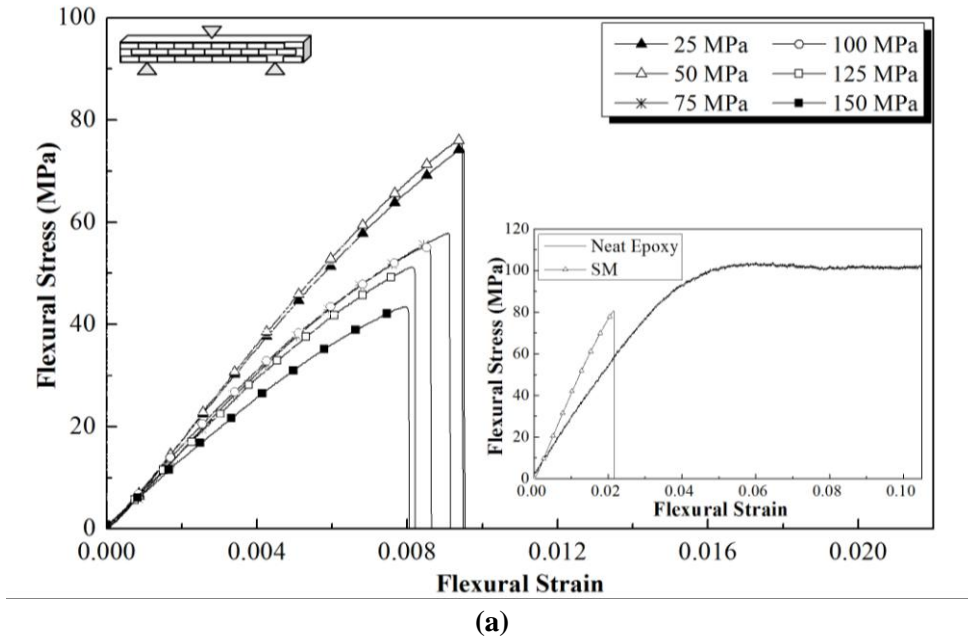
Figure 4.25 (a) Flexural stress-strain curves for glass platelet reinforced epoxy matrix composites along with neat epoxy, (b) variation in flexural strength and failure strain as a function of applied hot pressing pressure, and hence glass platelet content.
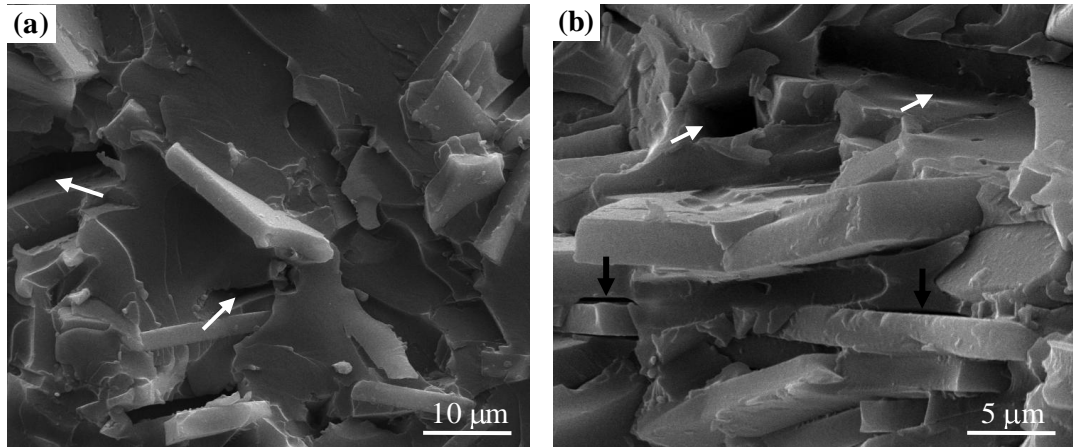
Figure 4.26 SEM images showing the fracture surfaces of (a) simple mixed and (b) HASC processed composite under the applied pressure of 50 MPa.

On the other hand, incorporation of rigid glass platelets into epoxy matrix has led to an increase in both flexural modulus and hardness with respect to neat epoxy (Figure 4.27 and Figure 4.28). In the case of simple mixed composite, incorporation of 20 vol% glass platelets resulted ∼2 and ∼1.3 fold enhancements in flexural modulus and hardness, respectively. For the HASC processed composites, the increase in inorganic content along with the alignment of the platelets has led to further increase in flexural modulus and hardness values up to a glass content of ∼56 vol%, above which further increase in platelet content have caused a decrease in both values. The decrease in the flexural modulus through HASC processing after ∼4 and ∼2.3 fold increases with respect to neat epoxy and simple mixed composite, respectively, can be attributed to the decrease in the effective aspect ratio. This is caused by the rupture of the platelets and increase in the size of the platelet clusters leading to a decrease in the efficiency of rigid 2D fillers in restricting the deformation of the matrix.
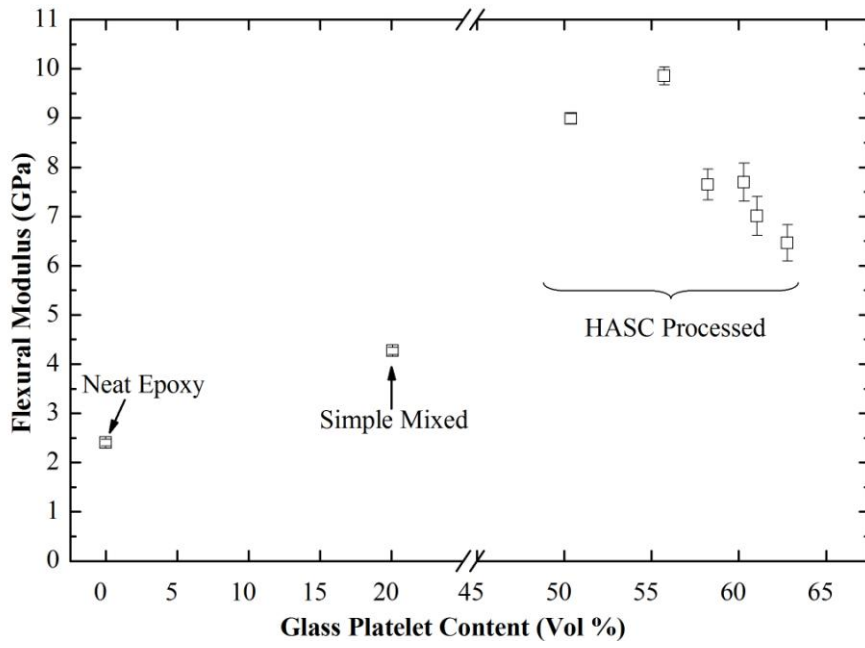
Figure 4.27 Variation in flexural modulus as a function of glass platelet content.
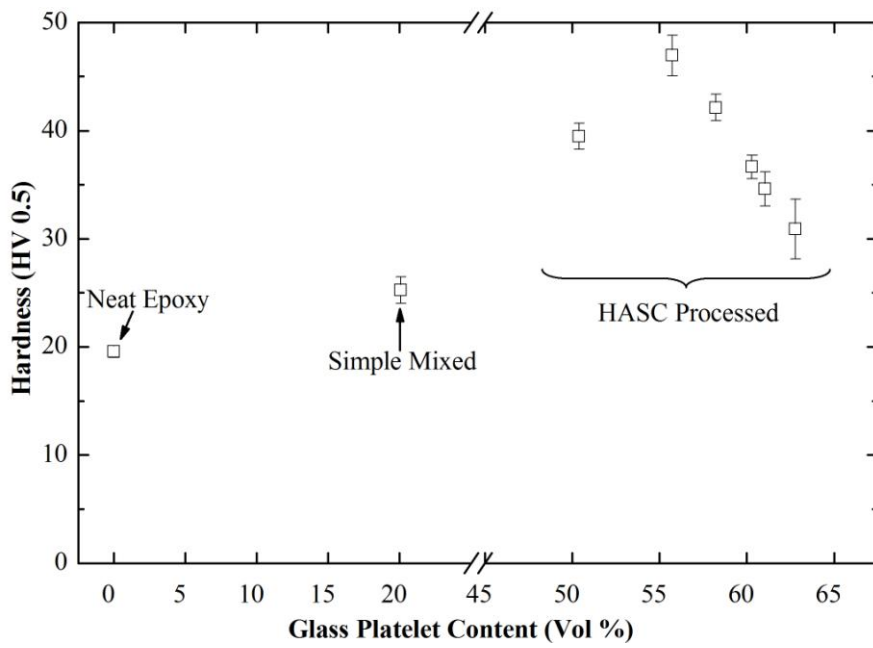
Figure 4.28 Variation in hardness as a function of glass platelet content.

It is known that in the case of discontinuous reinforcements, such as platelets, flakes and short fibers, reinforcing efficiency increases with the increase in the aspect ratio of the filler. Therefore, the aspect ratio of the platelets or flakes should be as high as possible, yet lower than the critical value so that the fracture is governed by platelet pull-out mode, which maximizes the energy absorbed during fracture, not by the platelet fracture leading to catastrophic failure of the material [15, 29, 85]. On this account, high aspect ratio glass flakes were also used to reinforce the epoxy matrix. The thickness and the aspect ratio (α) of the chemically resistant C-glass flakes are 2 μm and 150, respectively. To compare the results with those of the composites reinforced by C-glass platelets with a thickness of 2.3-3.3 and an aspect ratio in the range of 15-20, the volume fraction of the flakes were kept as ~20% in the initial mixture. The glass flake reinforced composites were fabricated by HASC processing under the applied pressure of 50 MPa, at which condition optimum results were achieved for glass platelet reinforced composites. In addition to this, 100 MPa was also applied to reveal the effect of higher processing pressures. For the simple mixed composite, incorporation of 20 vol% high aspect ratio glass flakes made the mixture so viscous that the elimination of air bubbles became impossible as hot-pressing was not applied to this sample. Although all tests were also performed for the glass flake reinforced simple mixed composite, the results will not be presented here as they are not reliable because of the very large bubbles that were entrapped in the cured sample.

For the HASC processed glass flake reinforced composites, applied pressures of 50 MPa and 100 MPa have led to excessive drainage of the epoxy resin through the porous filter leading to composites reinforced by ~76 and ~78 vol% high aspect ratio glass flakes, respectively. It is interesting to note that although the processing pressures were the same, there is a 20 vol% difference in the inorganic content of the composites reinforced by glass platelets and glass flakes under the identical applied pressure.

It is evident from the cross sectional view of the HASC processed composite under the applied load of 50 MPa (Figure 4.29) that high viscosity of the initial epoxy-flake mixture made the elimination of entrapped air voids difficult during HASC processing. It is also clear that although flow of the resin through the randomly oriented flakes forced them to align during processing, applied pressure and the interaction between the adjacent flakes resulted in bending and fracture of the flakes.

Although, fracture surface analysis of the three-point bending test specimens (Figure 4.30) along with the Figure 4.29 explicitly demonstrates that HASC processing is an efficient process for the alignment of the high aspect ratio 2D reinforcements, high aspect ratio reinforcements have more tendency to form large clusters with insufficient epoxy between the adjacent flakes detrimental for the efficient load transfer.
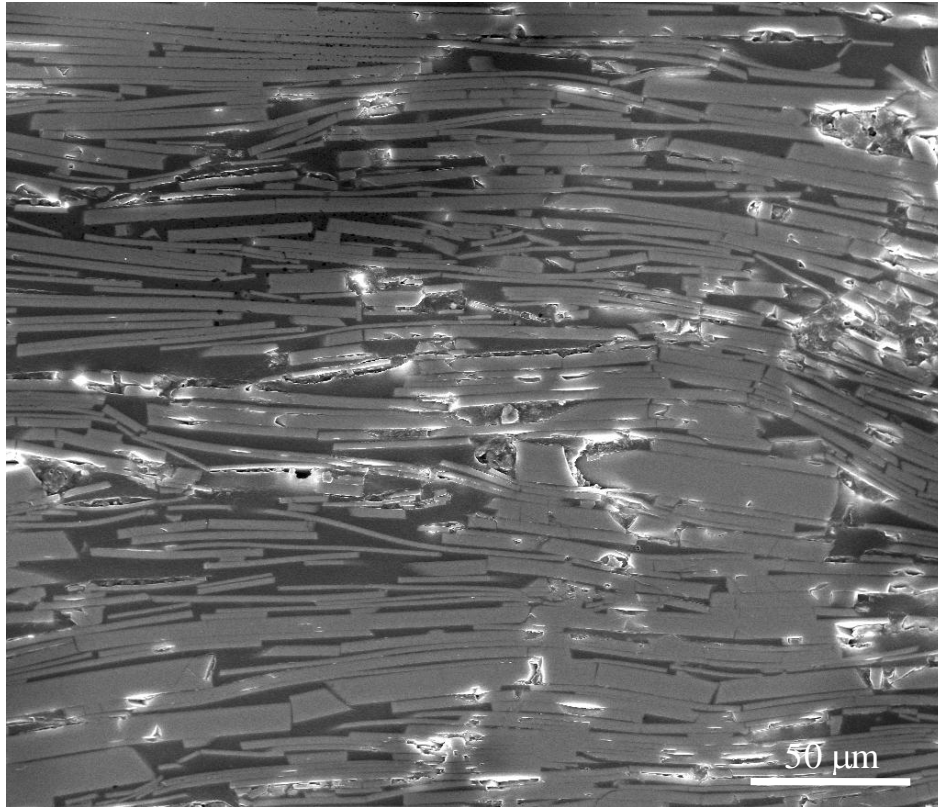
Figure 4.29 Cross-sectional microstructure of the glass flake reinforced composite HASC processed at 50 MPa.

As mentioned earlier, high aspect ratio reinforcements are more effective in carrying loads as compared to low aspect ratio reinforcements. However, three-point bending test results indicated that incorporation of the high aspect ratio glass flakes results in a drastic decrease in the flexural strength leading to ~2.4 fold and ~3.5 fold reduction with respect to neat epoxy for the flake contents of 76 vol% and 78 vol%, respectively. On the other hand, flexural modulus of the HASC processed composites, determined as 10±0.5 GPa and 6.9±0.9 GPa for the flake contents of 76 vol% and 78 vol%, respectively, is higher than the flexural modulus of the neat epoxy which is 2.4±0.1 GPa. However, despite the higher content of high aspect ratio reinforcing flakes, they are on the same order as the flexural modulus of glass platelet reinforced composites processed under the applied loads of 50 MPa and 100 MPa. The unexpected decline in the mechanical properties of the composites reinforced by highly aligned high aspect ratio glass flakes is thought to be arisen from the combined effect of microstructural features such as platelet clusters, voids and fractured platelets, along with the lack of bonding between the flakes and the epoxy matrix, all of which leads to formation of stress concentration sites or decrease the effective stress transfer from the matrix to the flakes.
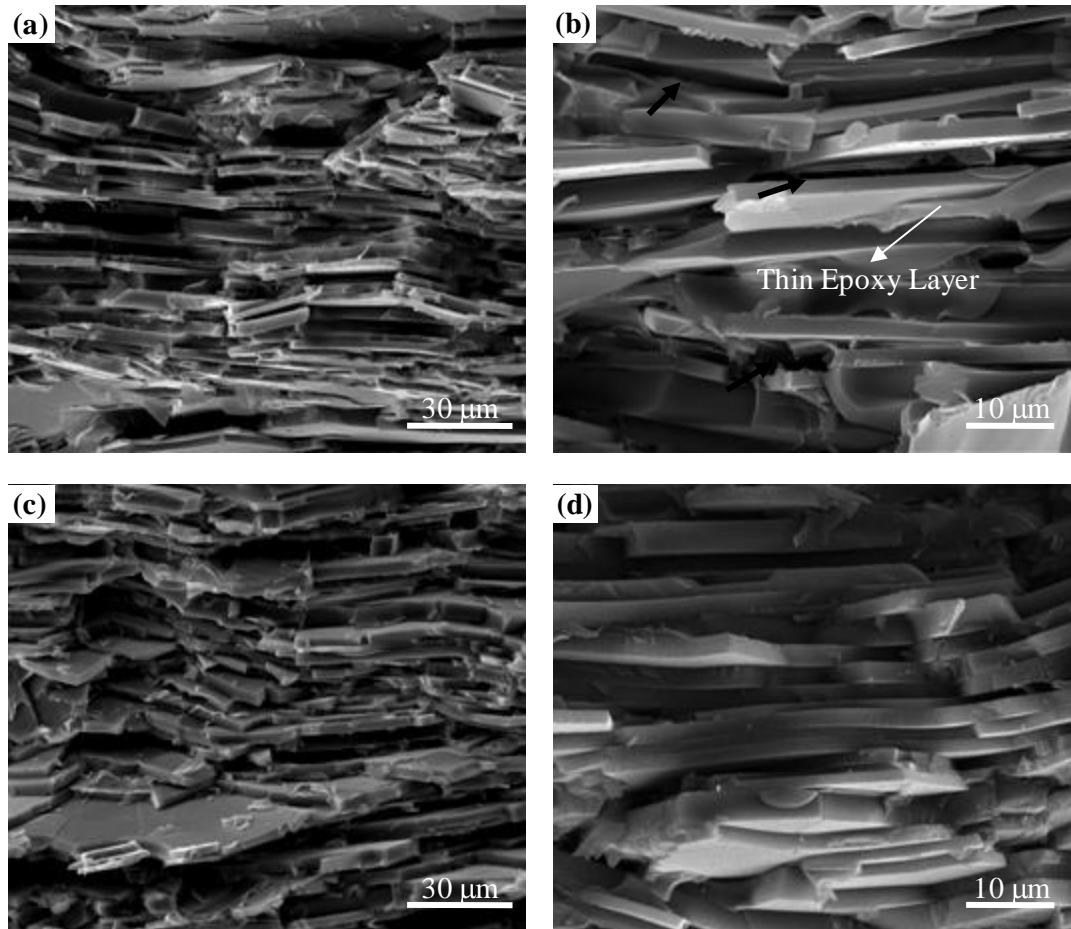
Figure 4.30 Fracture surfaces of 3PB specimens of HASC processed composites for the applied pressures of (a)-(b) 50 MPa and (c)-(d) 100 MPa.

Fractographs of the three-point bending test specimens demonstrate that the fracture occurs through the weak interface between glass flakes and the epoxy matrix leaving the flake surfaces clean and smooth. This reveals the fact that fracture is mainly governed by the flake pull-out rather than flake fracture which points out that the aspect ratio of the flakes is lower than the critical aspect ratio of the glass flake reinforcement – Epo-Fix epoxy system. Another important fact is the stress-strain behavior of these composites under flexural stresses (Figure 4.30). Unlike to alumina and glass platelet reinforced composites, for which after maximum stress failure occurs suddenly, for glass flake reinforced composites, following an increase up to the maximum, the stress decreases abruptly to some extent and then begins to decrease gradually. The distinction between these mechanical behaviors can be attributed to the higher aspect ratio of the glass flakes such that flakes continued to carry load until their embedded parts were completely pulled-out off the matrix leading to a slowly descending curve called the tail behavior.
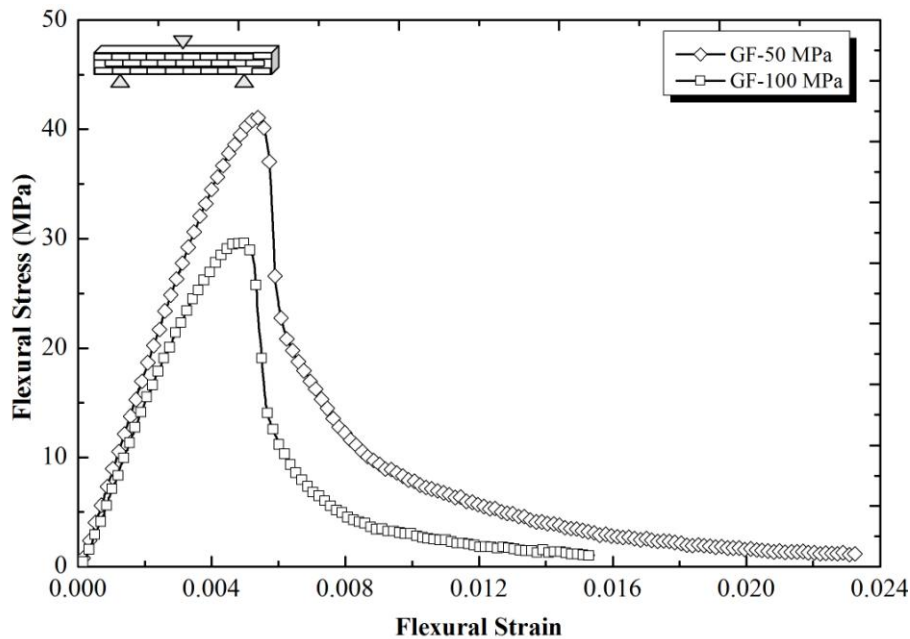
Figure 4.31 Flexural stress-strain curves of 3PB tested glass flake reinforced composites.

4.2.2 Surface Functionalization of Glass Platelets and Flakes

In order to achieve coupling at the interface between glass reinforcements and the epoxy matrix and to enhance wettability and interfacial strength, the surfaces of the glass platelets and flakes were treated with amino functional silane coupling agent, γ-aminopropyltriethoxysilane (APS). To examine the success of silane treatment and to investigate the interaction between glass reinforcement surfaces and the APS, surfaces of the as-received and silane treated reinforcements were characterized by X-ray photoelectron spectroscopy (XPS) technique.

The silane coupling agent, APS, was chosen for the surface functionalization of glass reinforcements because of three reasons; firstly, surface functionalization with APS in toluene has resulted in optimum mechanical performance in the case of composites reinforced by surface functionalized alumina platelets, secondly, treatment procedure for the surface functionalization with APS in toluene is easier as it does not require pH adjustment to catalyze the hydrolysis process, and finally, for this coupling agent more information can be deduced from XPS characterization studies as compared to GPS coupling agent.

94

Figure 4.32 presents XPS survey spectra of APS treated and as-received glass platelets and flakes. Peaks at 25 eV, 63 eV, 89 eV, 103 eV, 154 eV, 285 eV, 293 eV, 347 eV, 532 eV, 1021 eV and 1072 eV are O2s, Na2s, Mg2s, Si2p, Si2s, C1s, K2p, Ca2p, O1s, Zn2p and Na1s peaks, respectively, where peaks at 306 eV, 498 eV and 978 eV correspond to MgKLL, NaKLL - ZnLMM and OKLL Auger peaks. For APS treated platelets or flakes, XPS survey spectrum shows additional peak corresponding to N1s. In addition to survey spectra, high resolution XPS spectra (insets in Figure 4.32) of N1s core level also prove the adsorption of APS silane on the glass surface.

Table 4.2 summarizes the elemental composition of as-received and silane treated glass platelet and flake surfaces determined from the XPS survey spectra. For silane treated flakes and platelets, presence of peaks other than Si, N, C and O peaks in the XPS spectra indicate that the thickness of the adsorbed silane layer is less than the analysis depth of XPS. On this account, C, O and Si signals can be attributed to both silane layer adsorbed on the surfaces of the glass reinforcements and also to the glass reinforcement itself.

For the APS treated glass flakes (GF-ST), the surface elemental composition of N is 3.5 % which is higher than the value of 2.7 at% in the case of silane treated glass platelets (GP-ST) pointing out that the thickness of the adsorbed silane layer is thicker for the APS treated glass flakes. An interesting point here is that after silane treatment there is a slight decrease in the Si surface composition for glass flakes. This situation may have arisen depending on the thickness of the deposited silane layer due to the fact that silane layer has a lower Si concentration than the bare glass flake surface. However, in the case of glass platelets, the Si surface concentration of the GP-ST is higher with respect to as-received glass platelets (GP). This may also be an indication of thicker silane layer in the case of GF-ST as compared to GP-ST.

As mentioned previously, amino functional silane APS can either interact with the platelet or flake surface through silanol groups or through protonated amino group (Figure 4.9). In order to explore the interaction between the glass platelet and flake surface and the APS, high resolution XPS spectra of N1s core levels were deconvoluted (Figure 4.33). The peaks centered at 399.6 eV and 399.5 eV in Figure 4.33.a and Figure 4.33.b, respectively, are attributed to free NH_2 groups indicating that the interaction between amino silane and glass surface occurs merely through silanol groups for functionalized glass platelets and flakes [179, 181, 182].
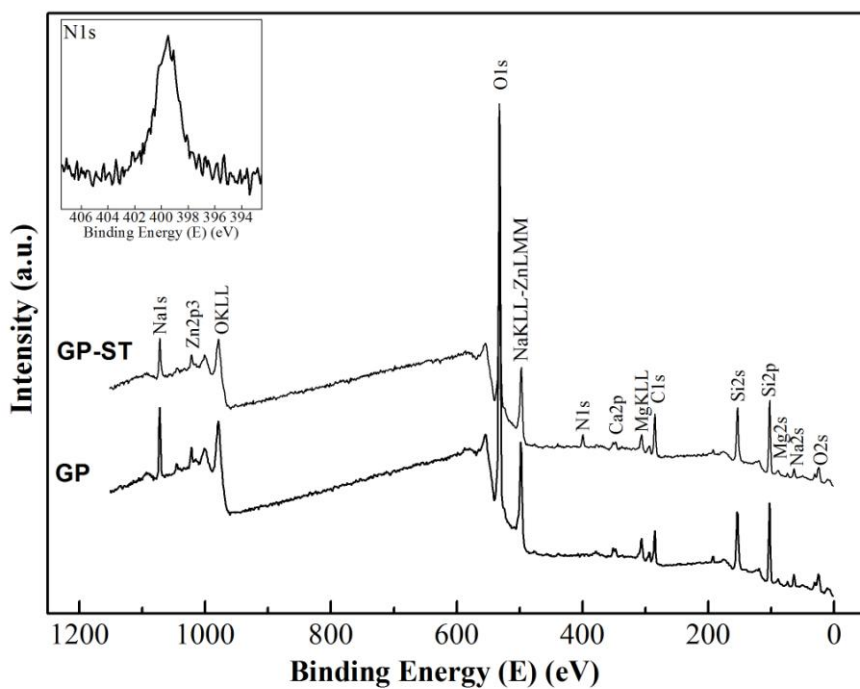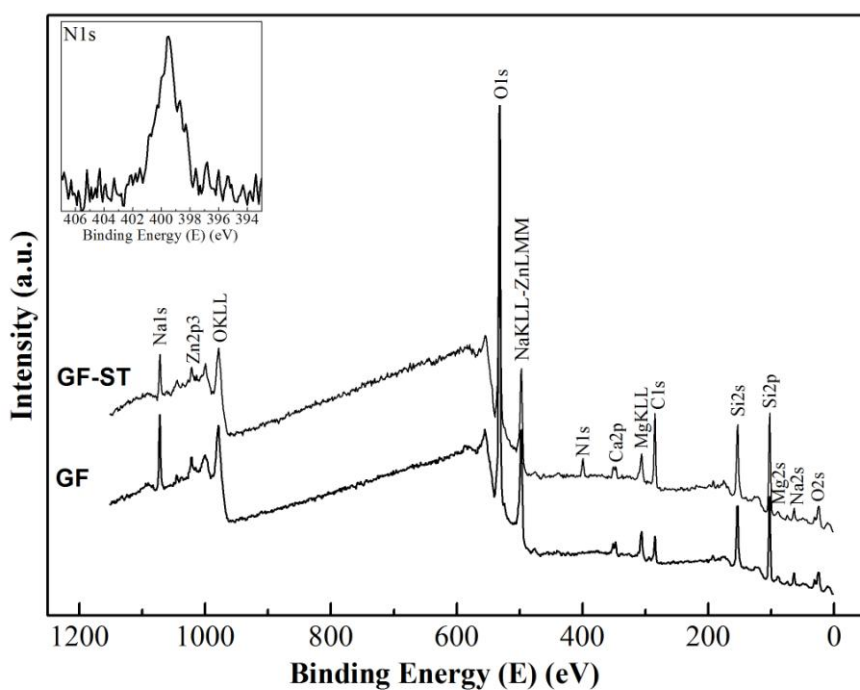
Figure 4.32 XPS spectra of APS treated (a) glass platelets (GP-ST) and (b) glass flakes (GF-ST) together with the XPS spectra of as-received platelets (GP) and flakes (GF). Insets show high resolution XPS spectra of N1s core levels for APS treated platelets and flakes.

Table 4.2 Elemental surface composition (at %) of as-received and silane treated glass platelets and flakes.

Elements	Designation			
	GP	GP-ST	GF	GF-ST
O	51.5	46.4	52.1	42.8
Si	16.1	16.9	17.2	17.0
C	12.7	17.4	10	18.9
Na	4.8	2.5	4.7	2.1
Ca	0.8	0.7	1.2	0.9
Zn	0.4	0.2	0.1	0.1
Mg	13.7	13.5	14.7	14.6
N	-	2.4	-	3.6

As discussed in the previous chapter, in order to investigate whether high stirring rates lead to damaging of the reinforcements, especially for high aspect ratio glass flakes, or not, particle size analyses were performed before and after silane treatment. The result of these analyses is presented in Appendix A. Silane treatment of the reinforcements has led to a shift in particle size distribution curves to higher values as compared to as-received platelets. This finding clearly indicates that glass reinforcements were not damaged during silane treatment. Slight shift in particle size distribution to higher values can be attributed to increase in the size of the reinforcements as a result of the silane layer adsorbed on the surfaces of the glass platelets and flakes.
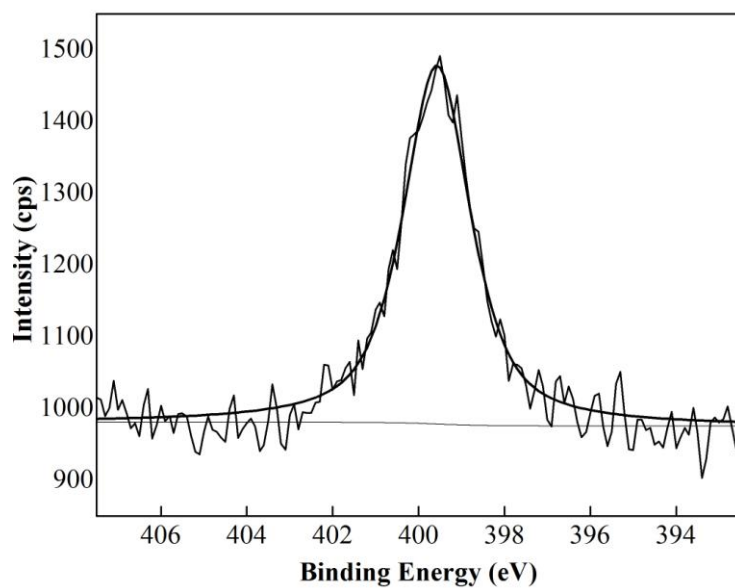
(a)
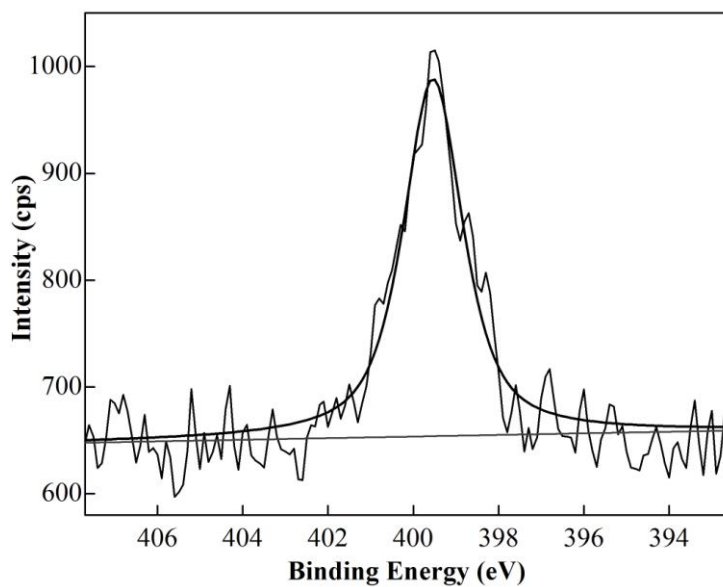
(b)

Figure 4.33 High resolution XPS spectra of N1s core level for APS treated (a) platelets (GP-ST) and (b) flakes (GF-ST).

4.2.3 Epoxy Matrix Composites Reinforced by Surface Treated Glass Platelets and Flakes

As mentioned previously, in order to achieve interface compatibility, and hence effective load transfer from matrix to reinforcements, the surfaces of the glass reinforcements were treated with APS. To reveal the effect of interface adhesion on the mechanical properties, composites reinforced by surface treated glass platelets and flakes were fabricated by HASC processing under the applied pressure of 50 MPa and 100 MPa. Figure 4.34 illustrates the flexural stress-strain curves of composites reinforced by both as-received and surface treated glass platelets and flakes.

It is interesting to note that even in the case of composite fabricated by simple mixing, reinforcing the epoxy matrix with APS treated glass platelets (GP-ST-SM) has led to significant improvement in mechanical properties resulting in ~38% and ~69% increase in flexural strength and flexural strain values, respectively, as compared to composite reinforced by as-received platelets (GP-SM). For the composites HASC processed under the applied pressures of 50 MPa (GP-ST-HASC 50) and 100 MPa (GP-ST-HASC 100), more remarkable enhancement is achieved reaching to ~63% and ~100% increase in flexural strength values accompanied by ~52% and ~44% enhancement in flexural strain values, respectively, with respect to HASC processed composite reinforced by as-received platelets (GP-HASC 50 and GP-HASC 100) (Figure 4.35.a). Furthermore, unlike to composites reinforced by as-received platelets, incorporation of surface treated glass platelets has led to an increase in flexural strength of the neat epoxy. This increase is ~7% in the case of simple mixed composite. With the increase in the glass platelet content and the improvement in the orientation of the glass platelets, enhancement in flexural strength increases to ~21% for composite GP-ST-HASC 50. Nevertheless, further increase in the HASC processing pressure has not led to further improvement in flexural strength values instead led to an improvement of only ~5%, which is lower than the improvement achieved in the case of the simple mixed composite as expected based on the discussions in Section 4.2.1.

For glass flake reinforced composites, the situation is similar to composites reinforced by silane treated glass platelets such that reinforcing the epoxy with surface treated high aspect ratio glass flakes has led to ~60% and ~85% improvement in flexural strength values accompanied by a little improvement in failure strain for HASC processed composites fabricated under the applied pressures of 50 MPa (GF-ST-HASC 50) and 100 MPa (GF-ST-HASC 100), respectively, as compared to composites reinforced by as-received flakes (GF-HASC 50 and GF-HASC100). However, it is clear that although silane treatment has led to significant improvement in flexural strength by increasing the effective load transfer between the matrix and the reinforcements, flexural strength values are still lower than the flexural strength of the neat epoxy. This result indicates that microstructural features such as platelet clusters, voids and fractured platelets also play a crucial role in determining the final mechanical properties of the composites.
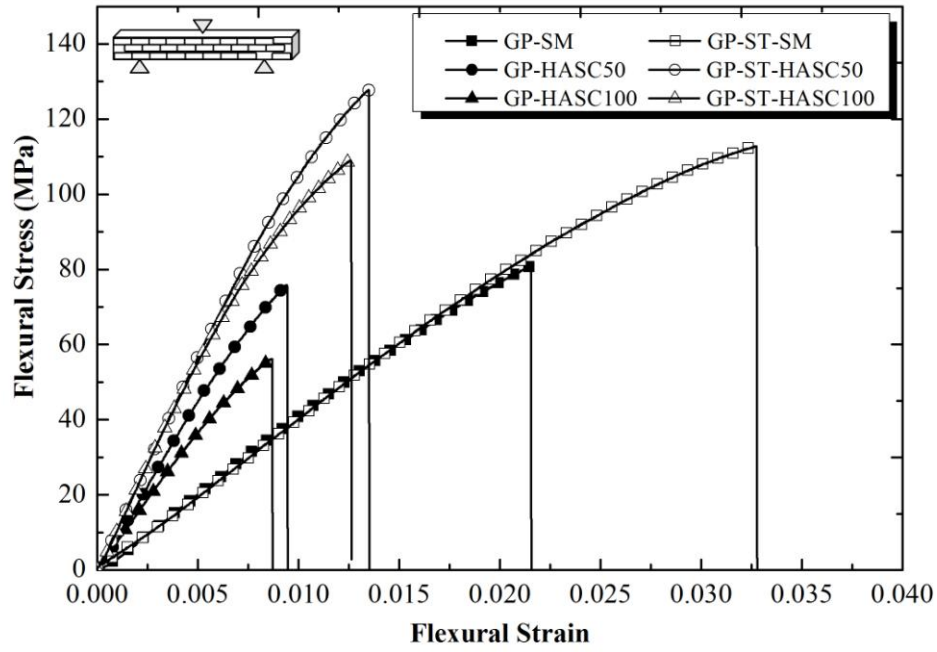
(a)
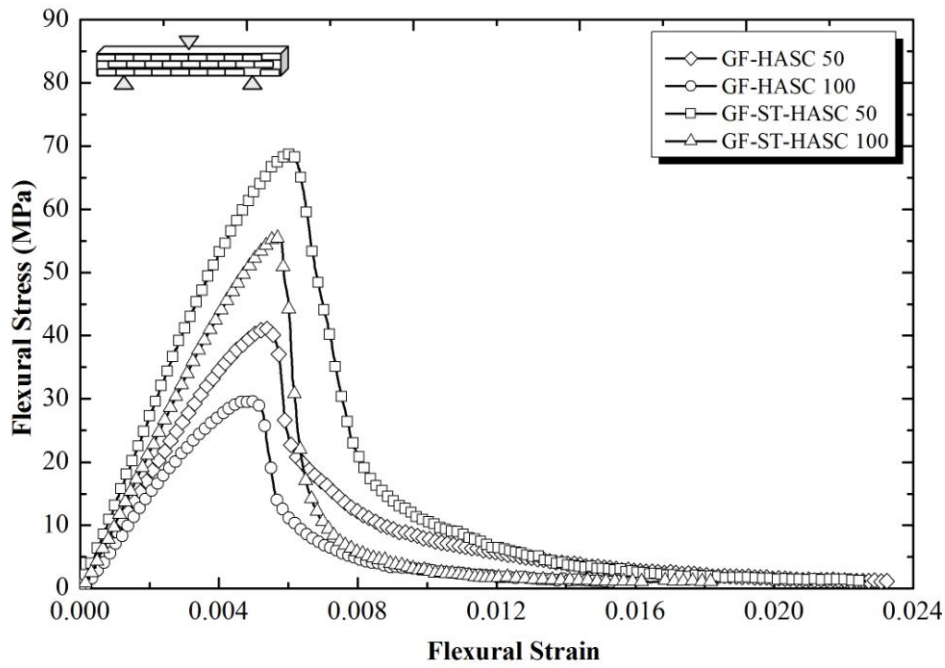
(b)

Figure 4.34 Flexural stress-strain curves of the composites reinforced by (a) as-received and silane treated glass platelets (b) as-received and silane treated glass flakes.

100

For simple mixed composite, reinforcing the epoxy with surface functionalized glass platelets does not impart extra stiffness when compared to simple mixed composite reinforced by as-received glass platelets (Figure 4.34.a). On the other hand, the increase in the glass platelet content along with the improvement in the alignment of these glass platelets via HASC processing reveals the effect of surface treatment leading to ~18% and ~52% enhancement in stiffness for GP-ST-HASC 50 and GP-ST-HASC 100, respectively, with respect to the composite reinforced by as-received platelets.

The effect of silane treatment is more pronounced in the case of composites reinforced by high aspect ratio glass flakes (Figure 4.35). The improvement in flexural modulus values are ~45% and ~78% for GF-ST-HASC 50 and GF-ST-HASC 100, respectively, as compared to the composites reinforced by as-received flakes (Figure 4.35.b). Another interesting finding is that although stiffness of a composite is dependent on filler content, size and aspect ratio (α) beside the alignment of the fillers and the filler/matrix modulus ratio [85], the flexural modulus values for composites reinforced by either as-received glass platelets or flakes are on the same order. However, the composite reinforced by silane treated flakes has ~24% higher modulus value than the composite reinforced by silane treated glass platelets under the applied processing pressure of 50 MPa. This finding clearly illustrates that coupling at the interface between the filler and the matrix also plays an important role in revealing the effect of aspect ratio on the stiffness of composite.

Figure 4.36 shows fracture surfaces of three-point bending (3PB) tested composites reinforced by either as-received or APS treated platelets and flakes. Unlike to fractographs presented in Figure 4.26 and Figure 4.30 which demonstrate the presence of clean platelet surfaces indicating weak interfacial bonding between the platelets or the flakes and the matrix, Figure 4.36 illustrates rough platelet and flake surfaces pointing out the effective adhesion of the inorganic surfaces to epoxy, and hence, presence of an effective chemical bonding between the glass reinforcements and the matrix. These micrographs also clearly indicate that for these composites main fracture mechanism is pull-out as in the case of composites reinforced by as-received reinforcements, but in this case crack propagates through the matrix deflecting near the reinforcements not through the platelet-matrix interface leaving their surfaces covered with epoxy.
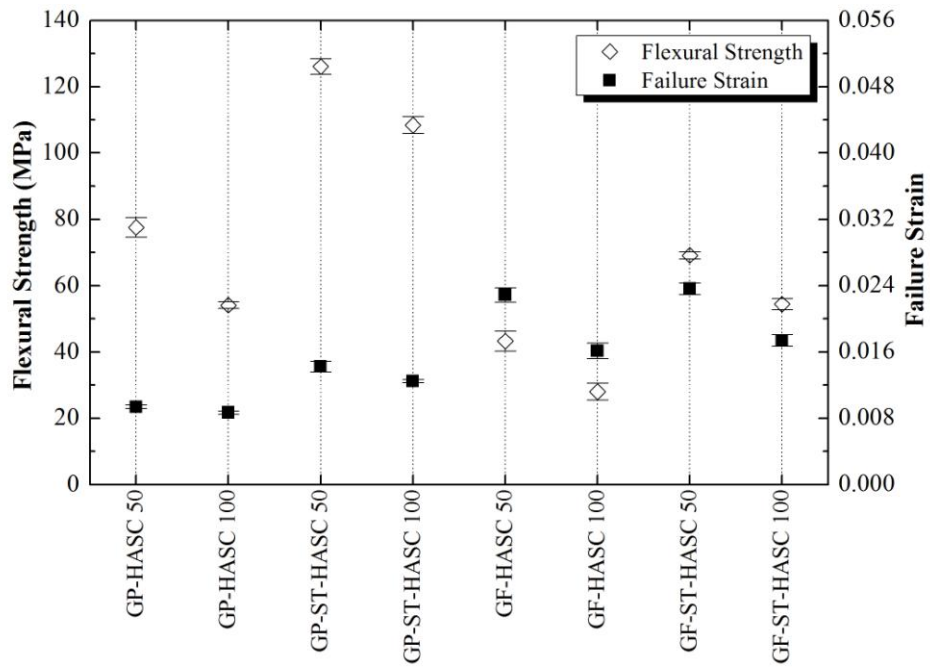
(a)
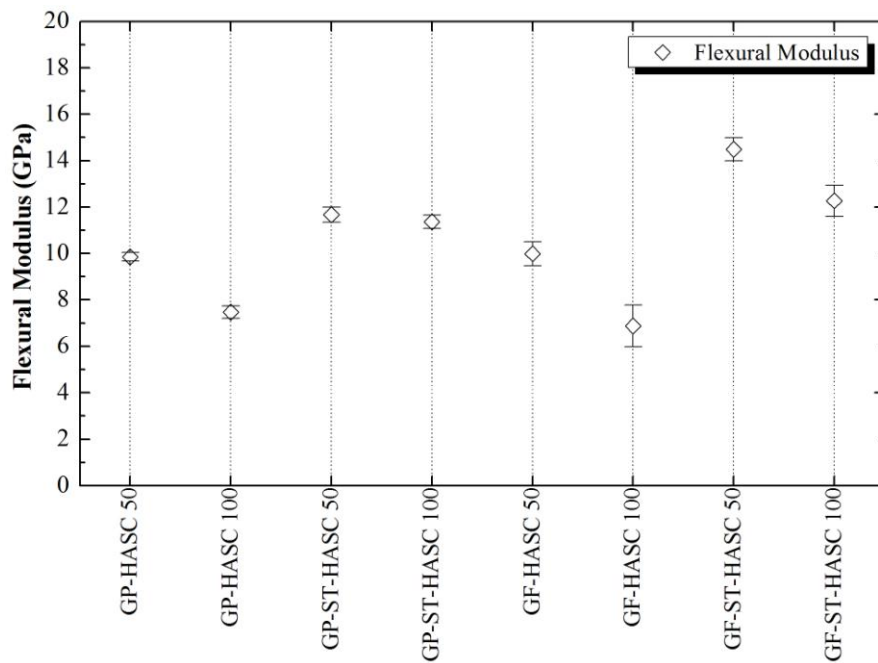
(b)

Figure 4.35 Effect of glass reinforcement surface functionalization on the mechanical properties of HASC processed composites; (a) flexural strength and failure strain and (b) flexural modulus.
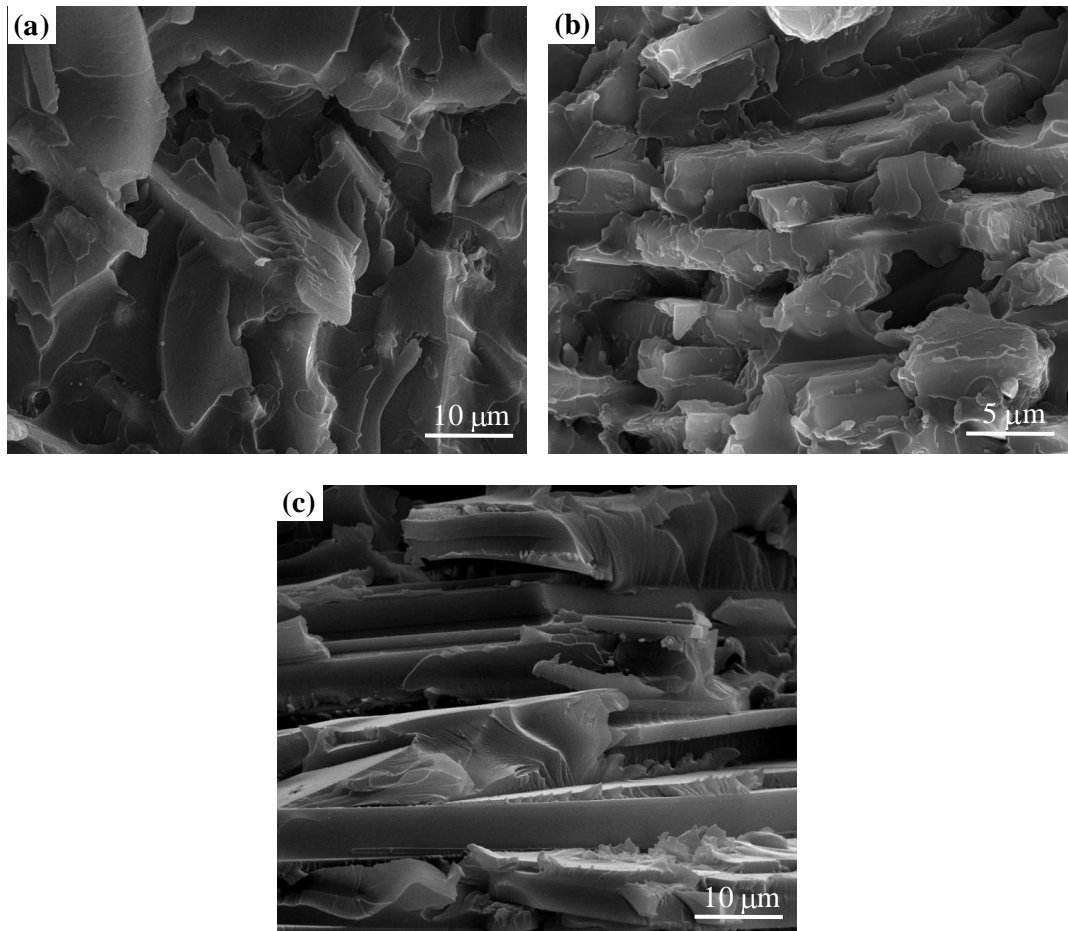
Figure 4.36 Fracture surfaces of 3PB tested specimens (a) GP-ST-SM, (b) GP-ST-HASC-50 and (c) GF-ST-HASC-50.

Composites reinforced by silane treated mixed glass platelets (GP) and flakes (GF) were also fabricated using HASC processing technique. Glass platelets and flakes were mixed during silane treatment at different relative volume fractions. Figure 4.37 illustrates the flexural stress-strain curves of these composites. It is clear from these curves that up to 50% volume fraction of GF, after peak value, the strength decrease to zero abruptly as in the case of composites reinforced by 100 vol% GP. However, for composites with a relative volume fraction of GF $\geq$ 50%, the fracture behavior changes such that after a peak value, the stress decreases suddenly to some extent, yet begins to decrease slowly.

(a)

(b)
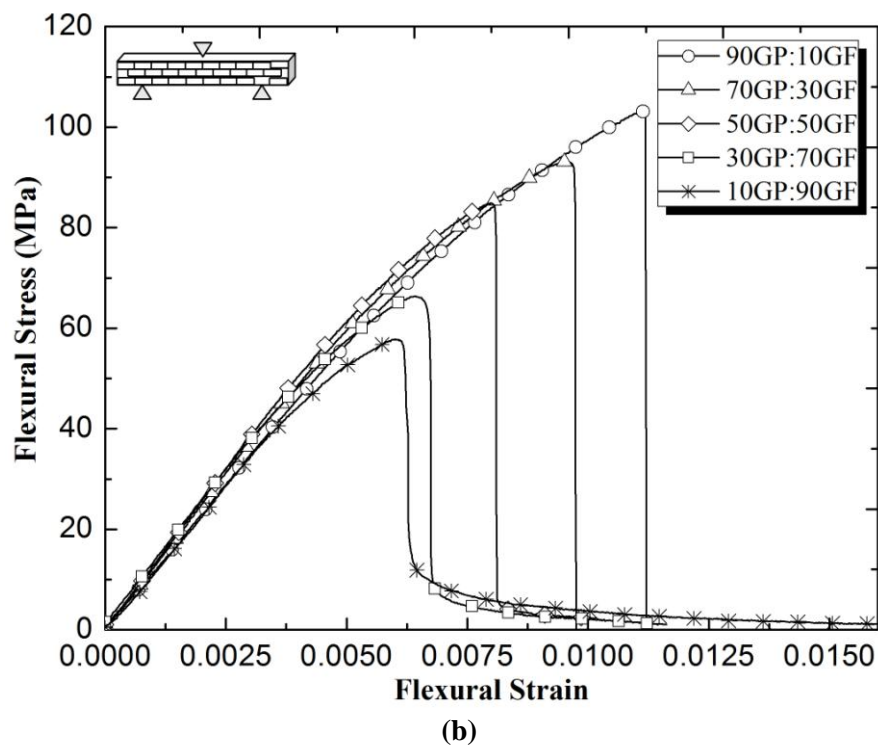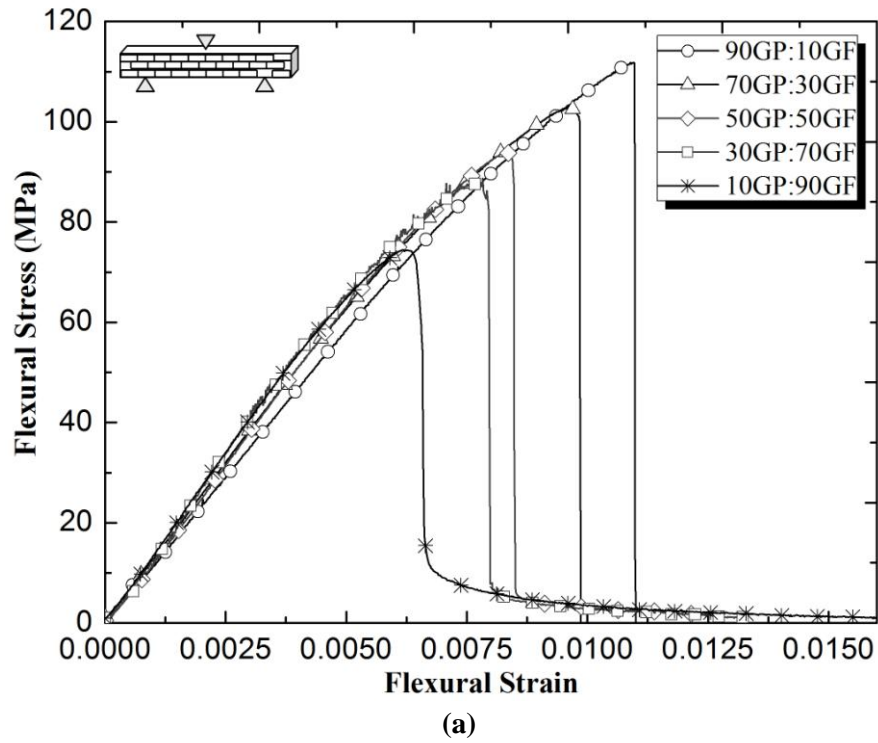
Figure 4.37 Flexural stress-strain curves for composites reinforced by mixture of glass platelets and flakes HASC processed under the applied pressure of (a) 50 MPa and (b) 100 MPa.

The increase in the volume fraction of GF has also led to an increase in the total inorganic content, but resulting in lower flexural strength values for both HASC processed composites under the applied pressures of 50 MPa and 100 MPa (Figure 4.38). The increase in the relative volume fraction of GF has led to a decrease in the failure strain values up to GP:GF ratio of 70:30, followed by an increase with further increasing GF volume fraction caused by the observed tail behavior.

Figure 4.39 shows variation in flexural modulus as a function of relative volume fractions of glass platelets and flakes. For HASC processed composites under the applied pressure of 50 MPa, the increase in the relative volume fraction of high aspect ratio flakes results in an increase in the flexural modulus values as expected (Figure 4.39.a). However, this is not the case for the composites HASC processed under the applied pressure of 100 MPa. Up to relative GP:GF volume fraction ratio of 30:70, the increase in the GF fraction leads to an increase in the stiffness of the composites. However, beyond this ratio, flexural modulus values are almost leveled-off following a slight decrease. As mentioned earlier on, slight decrease in flexural modulus values can be attributed to the increase in the size of the flake clusters leading to a decrease in effective reinforcement aspect ratio.

On the account of all these findings, it can be stated that with the increase in the volume fraction of GF, the reinforcing effect of higher aspect ratio flakes becomes more dominated over lower aspect ratio glass platelets.

Besides 3PB tests, work of fracture tests were also conducted, yet only for simple mixed and GP-HASC 50 and GP-ST-HASC 50 composites in the case of glass platelet reinforced composites and GF-HASC 50 and GF-ST-HASC 50 in the case of glass flake reinforced composites. Figure 4.40 shows the load-displacement curves of simple mixed and HASC processed composites with SENB specimen geometry. Average WOF values, expressing the energy absorbed by a notched specimen until fracture, were calculated as 115 J/m^2 and 110 J/m^2 for simple mixed and HASC processed composites, respectively, both of which were reinforced by as-received platelets. These WOF values explicitly indicate that incorporation of glass platelets into epoxy matrix has led to considerable reduction in the WOF value of the neat epoxy which was calculated as 350 J/m^2 as mentioned before.

Fracture behavior of the simple mixed and HASC processed composites completely differs from each other in the case of alumina platelet reinforced composites demonstrating the fact that crack propagation is unstable leading to catastrophic failure for the simple mixed composite, whereas for HASC processed composite crack propagation is stable as indicated by the tail behavior following the maximum in load-displacement curve. This tail behavior clearly indicates that main fracture, and hence energy absorption, mechanism is platelet debonding and pull-out for the HASC processed composite.
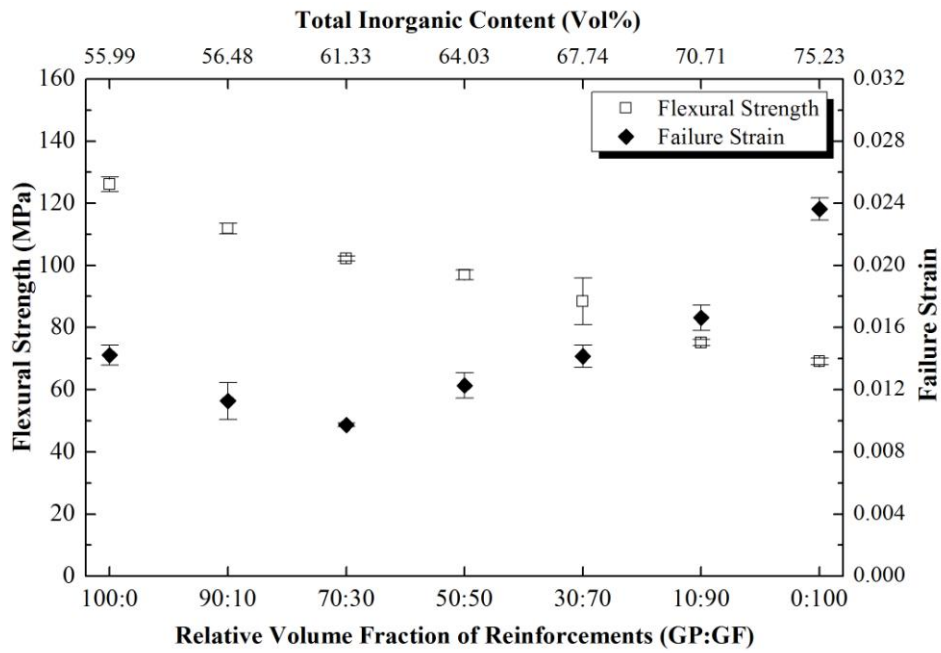
(a)
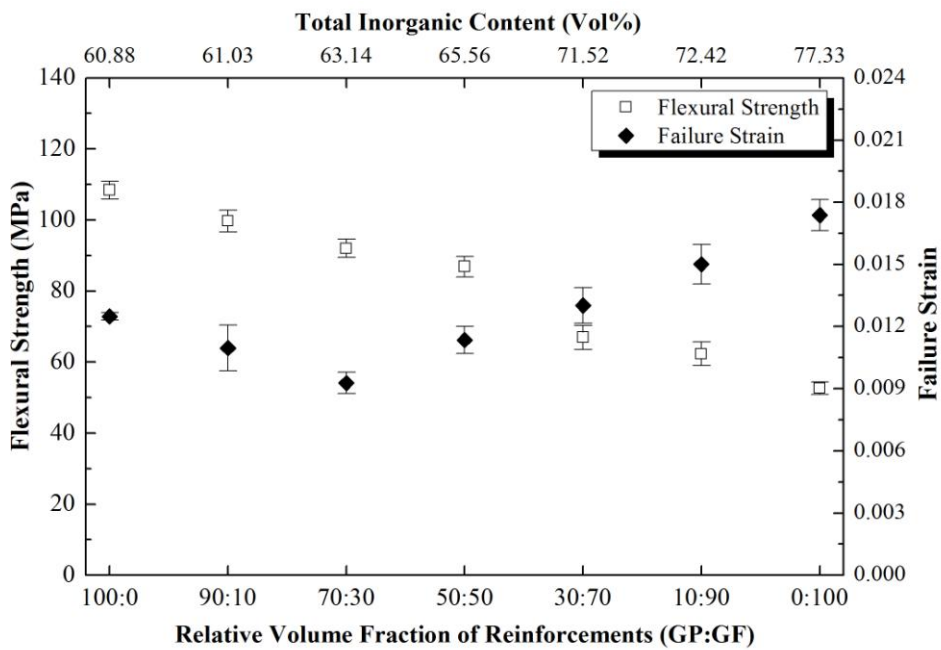
(b)

Figure 4.38 Variation in flexural strength and failure strain as a function of relative volume fractions of glass platelets and flakes for composites HASC processed under the applied pressures of (a) 50 MPa and (b) 100 MPa.
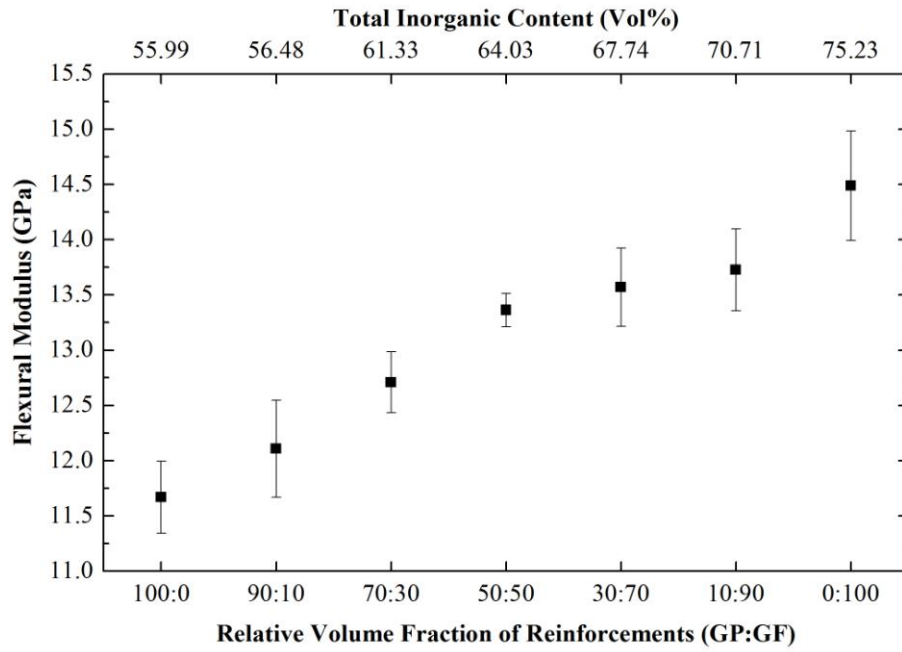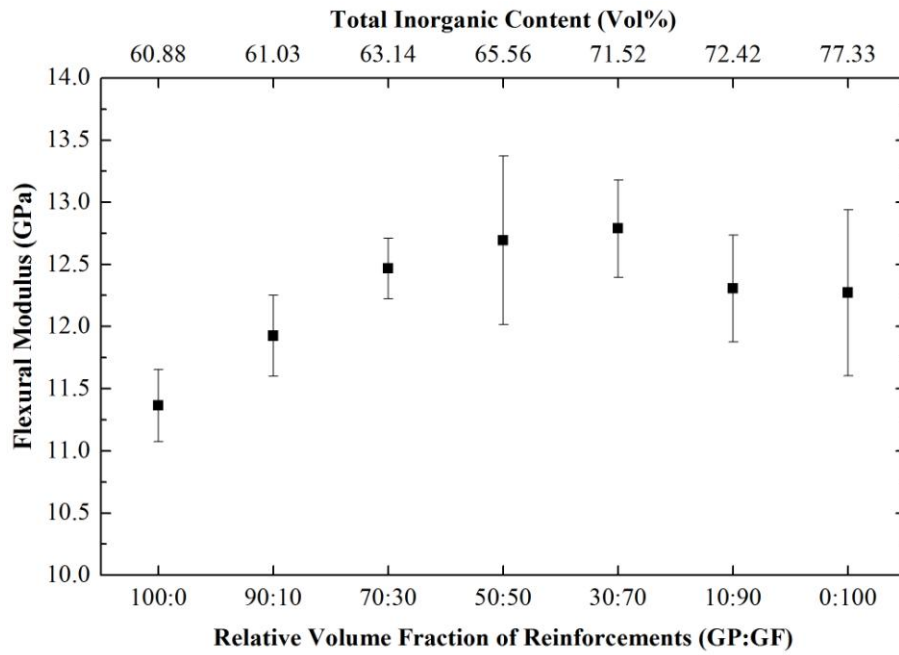
Figure 4.39 Variation in flexural modulus as a function of relative volume fractions of glass platelets and flakes for composites HASC processed under the applied pressures of (a) 50 MPa and (b) 100 MPa

107
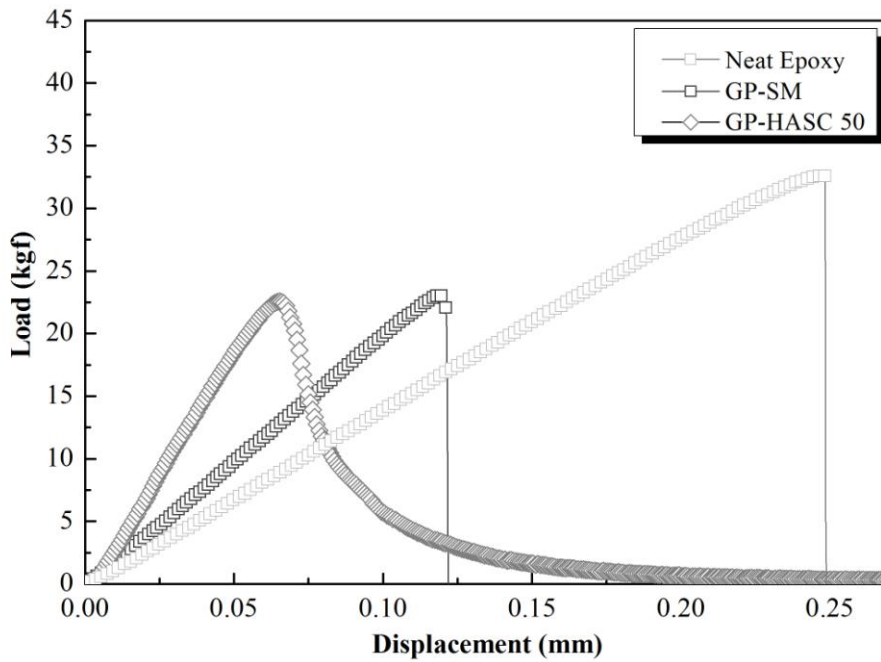
Figure 4.40 Load-displacement curves of SENB specimens of simple mixed and HASC processed composites reinforced by as-received platelets along with the load-displacement curve of the neat epoxy.

Load-displacement curves of simple mixed and HASC processed composites reinforced by surface functionalized platelets is shown in Figure 4.41 together with the load-displacement curves of composites reinforced by as-received platelets for comparison. Average WOF values of simple mixed and HASC processed composites reinforced by silane treated platelets are 135 J/m^2 and 149 J/m^2, respectively. Although reinforcing the epoxy matrix with silane treated glass platelets has led to ~18% and ~49% enhancement in WOF values of simple mixed and HASC processed, respectively, with respect to the composites reinforced by as-received platelets, WOF values are still lower than the WOF value of the neat epoxy.

When Figure 4.22 and Figure 4.41 are compared it can be deduced that although fracture behaviors seem to be similar, composite reinforced by surface functionalized glass platelets exhibit a tail behavior after ~50% sudden decrease in load, while surface functionalized alumina platelet reinforced composite reveals a tail behavior right after the maximum load has been achieved.
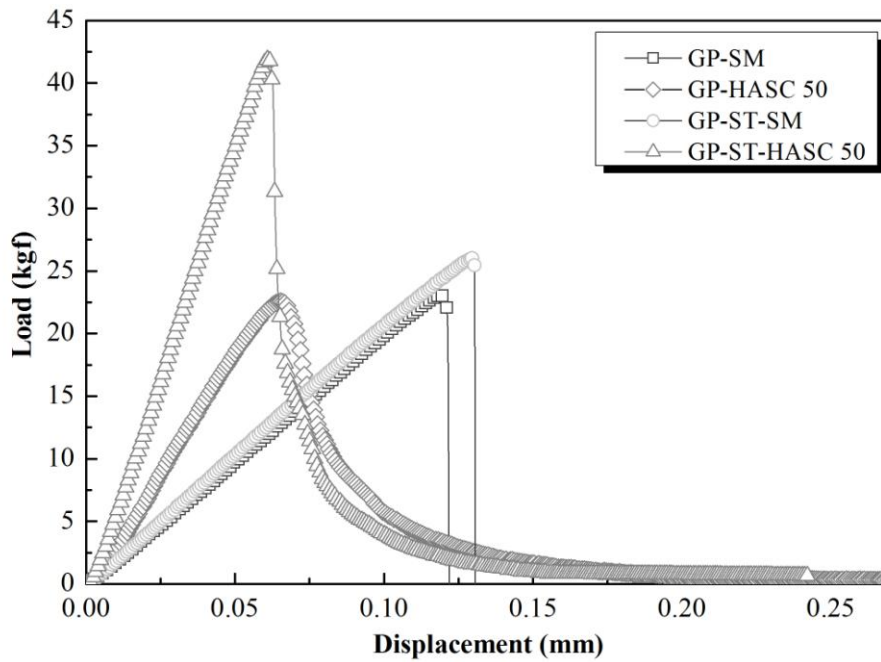
Figure 4.41 Load-displacement curves of SENB specimens of simple mixed and HASC processed composites reinforced by as-received and silane treated glass platelets.

Furthermore, WOF values are higher in the case of composites reinforced by either silane treated or as-received alumina platelet reinforced composites as compared to glass platelet reinforced composites. Higher WOF values in the case of alumina platelet reinforced composites can be attributed to higher aspect ratio of alumina platelets as compared to glass platelets which leads to an increase in the crack deflection path and hence increase in the resulting energy absorption.

Figure 4.42 shows the load-displacement curves of composites reinforced by either as-received or silane treated high aspect ratio glass flakes along with the load-displacement curve of the neat epoxy for comparison. Composite reinforced by well-aligned as-received glass flake exhibits considerably higher WOF value, which was determined as 221 J/m^2, as compared to composites reinforced by lower aspect ratio glass and alumina platelets. The tail behavior following the maximum in load-displacement curve explicitly illustrates the fact that the crack growth is stable for hierarchically arranged GF-HASC 50 composite. It also clear from this figure that surface treatment applied on the glass flakes further improves both the strength and the WOF value (~31% higher than the WOF value of composite reinforced by as-received flakes) still revealing stable crack growth evident by the tail behavior.
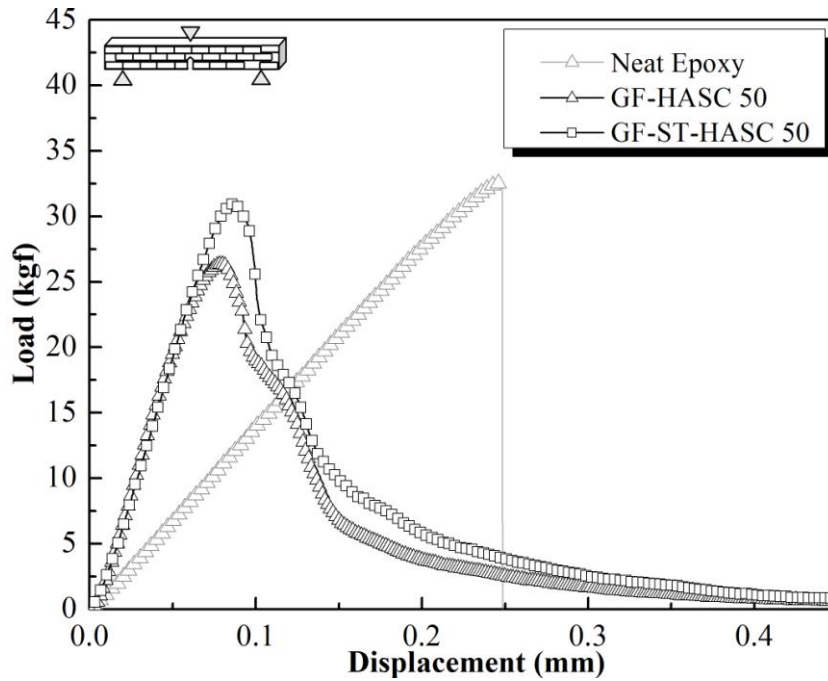
Figure 4.42 Load-displacement curves of SENB specimens of HASC processed composites reinforced by as-received and silane treated glass flakes along with the load-displacement curve of neat epoxy for comparison.

Fractographs of GF-HASC 50 WOF specimen (Figure 4.43) clearly demonstrates that crack propagates through the weak interface between the flakes and the matrix continuously deflecting around the well-aligned high aspect ratio flake edges leaving the flake surfaces smooth and clean. The zigzag pattern of the crack leads to an increase in the crack path, and hence energy absorption, until fracture. The path of a secondary crack is shown in Figure 4.43.a, revealing the extensive crack deflection exceeding 200 μm. Therefore, it can be deduced that flake debonding and crack deflection along with the flake pull-out lead to a tortuous crack path resulting in high work of fracture values for composites reinforced by high aspect ratio glass flakes.

Figure 4.44 shows the load vs. displacement curves of HASC processed composites reinforced by mixed surface functionalized glass reinforcements under the applied pressure of 50 MPa with SENB specimen geometry. It is clear from this figure that although the maximum load decreases with the increase in the volume fraction of glass flakes, tail behavior becomes more pronounced which is an indication of stable crack growth. This situation is also reflected in the resulting WOF values (Figure 4.45) such that the energy absorbed until fracture increases with the increase in the volume fraction of glass flakes due to the increase in the crack deflection path as mentioned previously.

110

(a)

100 μm

(b)

10 μm
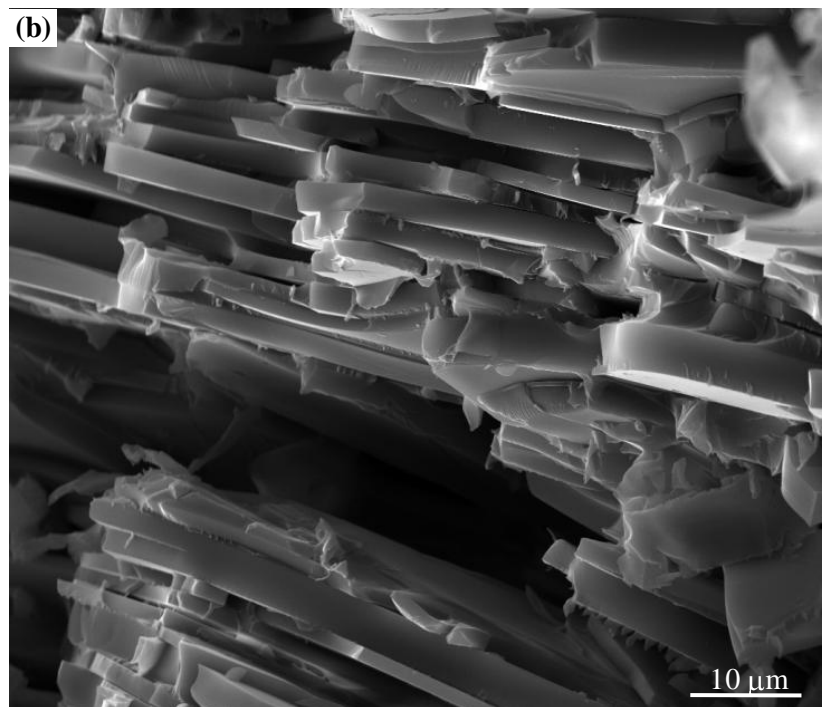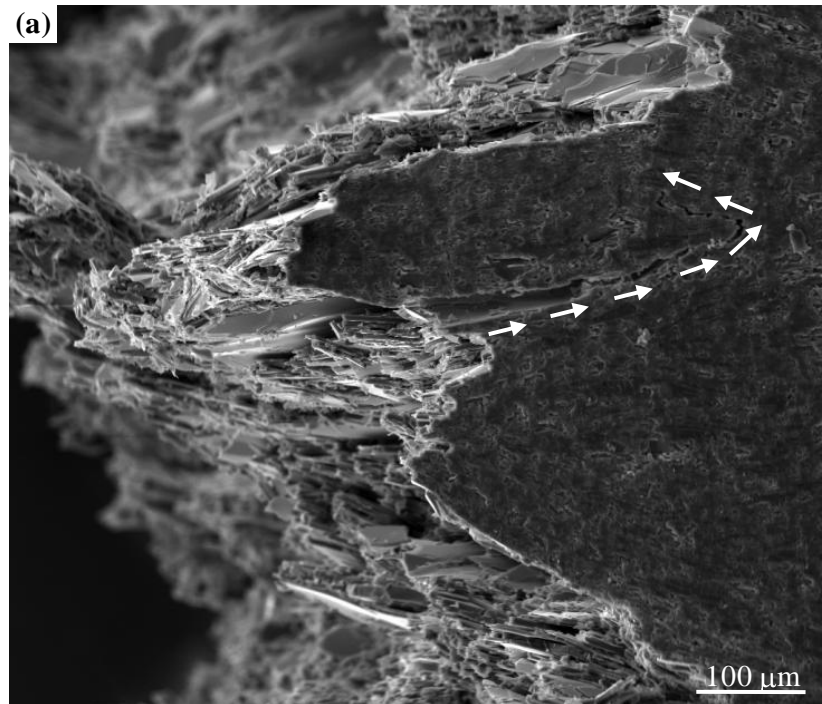
Figure 4.43 Fracture surface of WOF specimen GF-HASC 50.
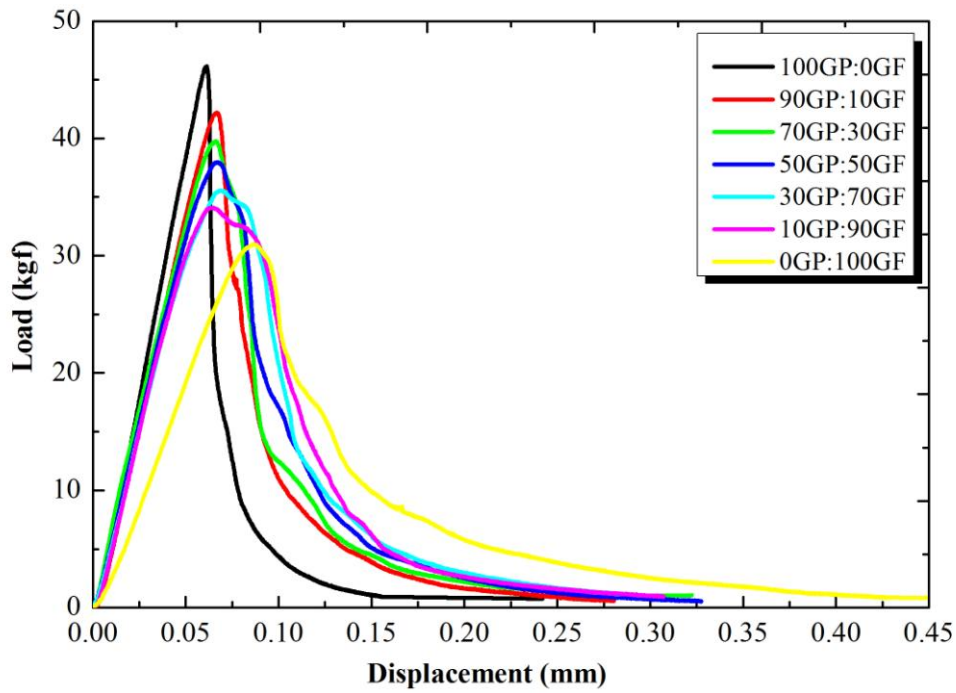
Figure 4.44 Load-displacement curves of SENB specimens of HASC processed composites reinforced by surface functionalized mixed glass reinforcements.
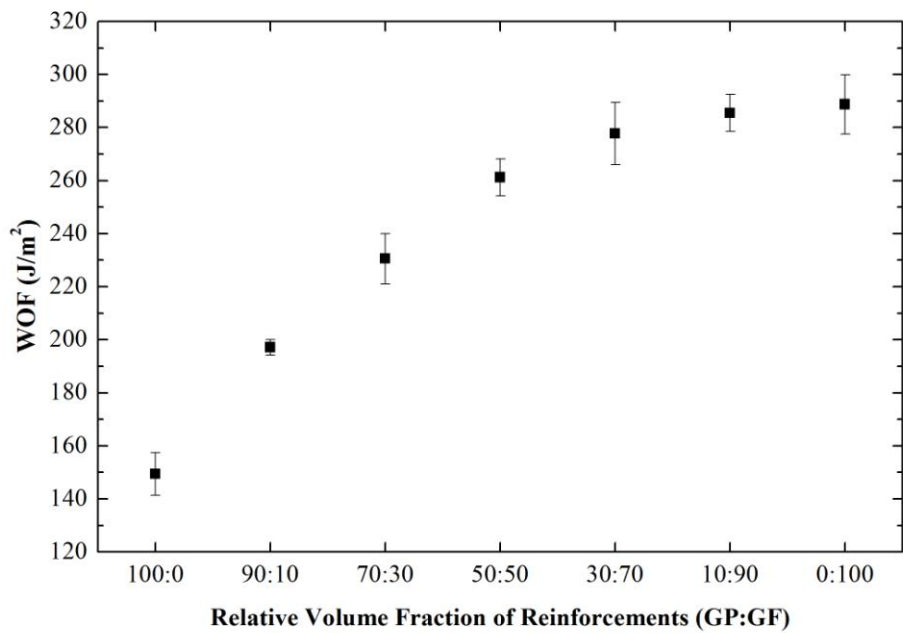
Figure 4.45 Variation in WOF values as a function of relative volume fraction of surface functionalized glass reinforcements.

4.2.4 Glass Flake-Epoxy Matrix Composites Fabricated by HASC at Low Processing Pressures

As mentioned in Section 4.2.1, high aspect ratio glass flake-epoxy matrix HASC processed composites exhibit microstructural features such as flake clusters, voids, and fractured flakes combined effect of which leads to significant reduction in flexural strength values as compared to neat epoxy either due to stress concentration sites or decreasing the effective stress transfer from the matrix to the flakes. These microstructural features are thought to be from the high inorganic content of the initial reinforcement-resin mixture which results in an increase in the viscosity and makes the elimination of entrapped air voids difficult during HASC processing, as well as from the high processing pressures and resulting high inorganic content. On this account, in order to determine the optimum inorganic content high aspect ratio glass flake reinforced epoxy matrix composites were fabricated by HASC processing under the application of six different pressures ranging between 0.5-10 MPa. Furthermore, in order to decrease the viscosity of the initial inorganic-organic mixture the starting glass flake content was kept lower than 20 vol%.

Figure 4.46 demonstrates the inorganic content of the composites, determined by thermogravimetric analysis (TGA), as a function of applied low hot-pressing pressures. It is explicit that volume fraction of the glass flakes increases with the increase in the applied hot-pressing pressures ranging between 41-71 vol%.
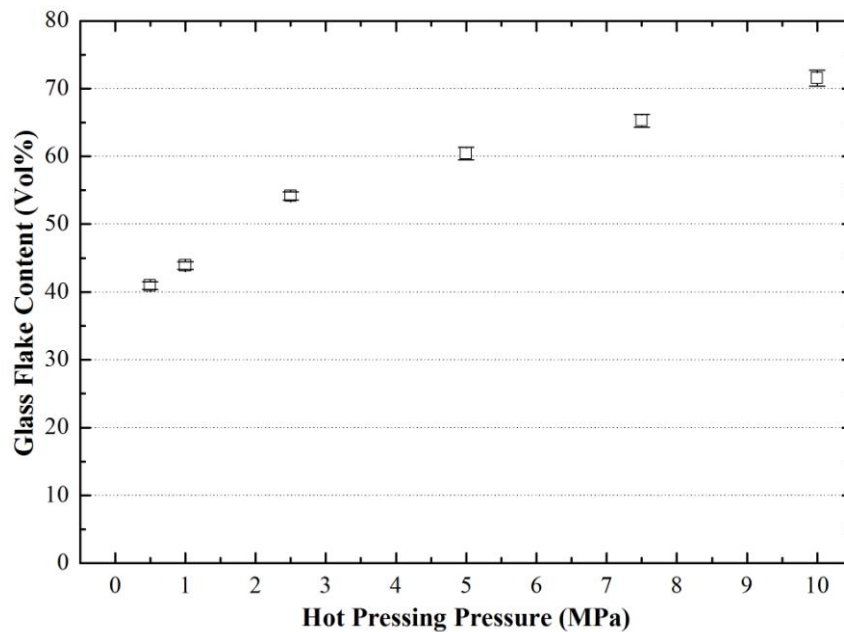
Figure 4.46 Glass flake content of the composites fabricated under the action of low HASC processing pressures.

Figure 4.47.a shows the flexural stress versus strain curves obtained from 3PB tests for the fabricated composites reinforced by as-received glass flakes. Incorporation of well aligned high aspect ratio glass flakes leads to an increase in flexural strength value of neat epoxy up to an inorganic content of ~65 vol% (Figure 4.48). This enhancement is ranging between ~23-50% with a maximum achieved for composite reinforced by 44 vol% glass flakes (Figure 4.47.b). Further increase in the glass flake content up to ~65 vol% leads to a decrease in flexural strength values being still at least ~23% higher than that of the neat epoxy. An impressive point here is that obtained flexural strength values are more outstanding than those of both alumina and glass platelet reinforced epoxy matrix composites indicating the effectiveness of the high aspect ratio reinforcements in carrying higher loads. Furthermore, HASC processing proves its efficiency in fabricating hierarchically arranged high aspect ratio inorganic-organic composites leading to a microstructural architecture resembling to "brick-and-mortar" structure (Figure 4.48).

However, the case for the composite reinforced by ~71 vol% inorganic flakes is completely different such that the incorporation of such amount of high aspect ratio glass flakes leads to ~34% reduction in the strength of the neat epoxy. This considerable reduction in the flexural strength value can be attributed to changes in microstructural features such as enlargement of flake clusters and fracture of flakes along with the lack of bonding between the flakes and the epoxy matrix (Figure 4.48.e), which either leads to formation of stress concentration sites or decreases the effective stress transfer from the matrix to the flakes, as in the case of glass flake reinforced composites HASC processed under the applied pressures of 50 MPa and 100 MPa.

Reinforcing the epoxy matrix with well aligned high aspect ratio glass flakes also imparts ~6.5-8 fold extra stiffness to neat epoxy (Figure 4.47.b). The enhancement in stiffness increases with the increase in the glass flake content up to ~54 vol%. However, further increase in the glass flake content leads to slight decrease in the flexural modulus values, which is thought to be caused either by the increase in the size of the flake clusters or fracture of the flakes leading to a decrease in effective reinforcement aspect ratio. The enhancement achieved in flexural modulus values are higher as compared with the lower aspect ratio glass platelet reinforced composites demonstrating the impact of reinforcement aspect ratio on the stiffness of a composite as mentioned in Section 4.2.1. It is explicit that incorporated high aspect ratio rigid reinforcements effectively constrict the deformation of the epoxy matrix especially in the vicinity of the inorganic flakes.

114
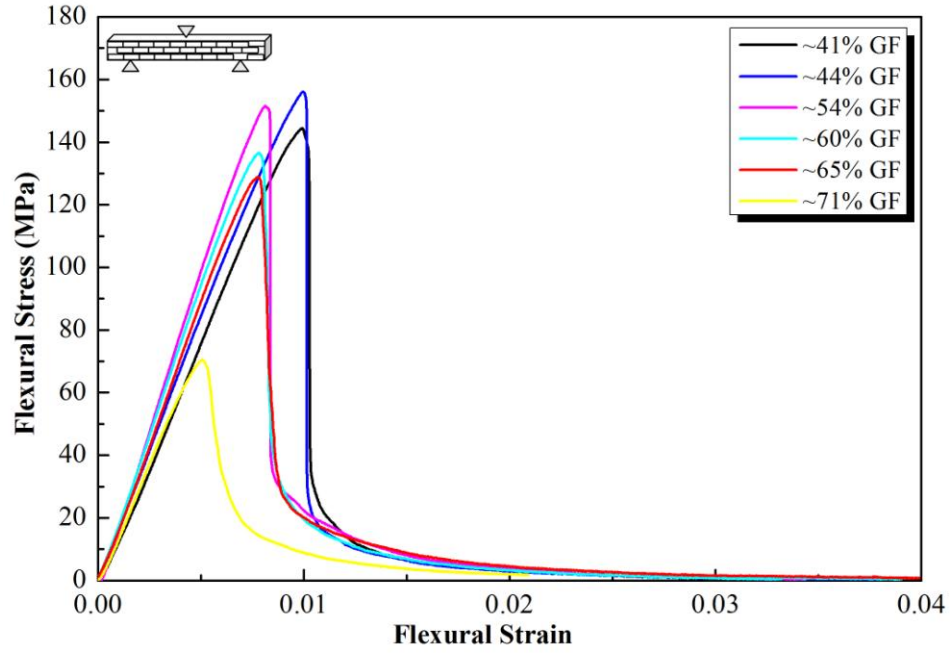
(a)
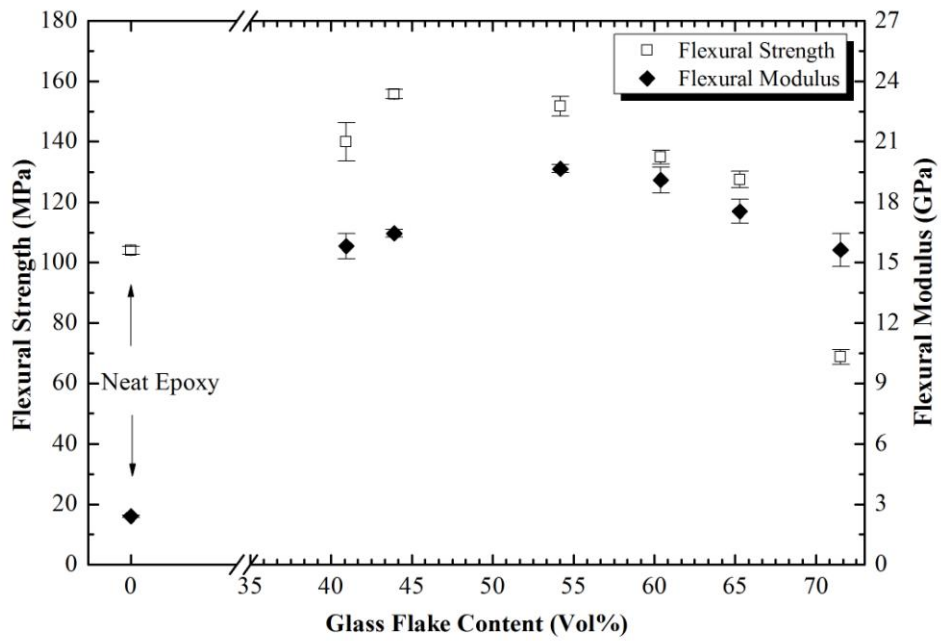
(b)

Figure 4.47 (a) Flexural stress-strain curves and (b) Variation in flexural strength and modulus as a function of glass flake content.
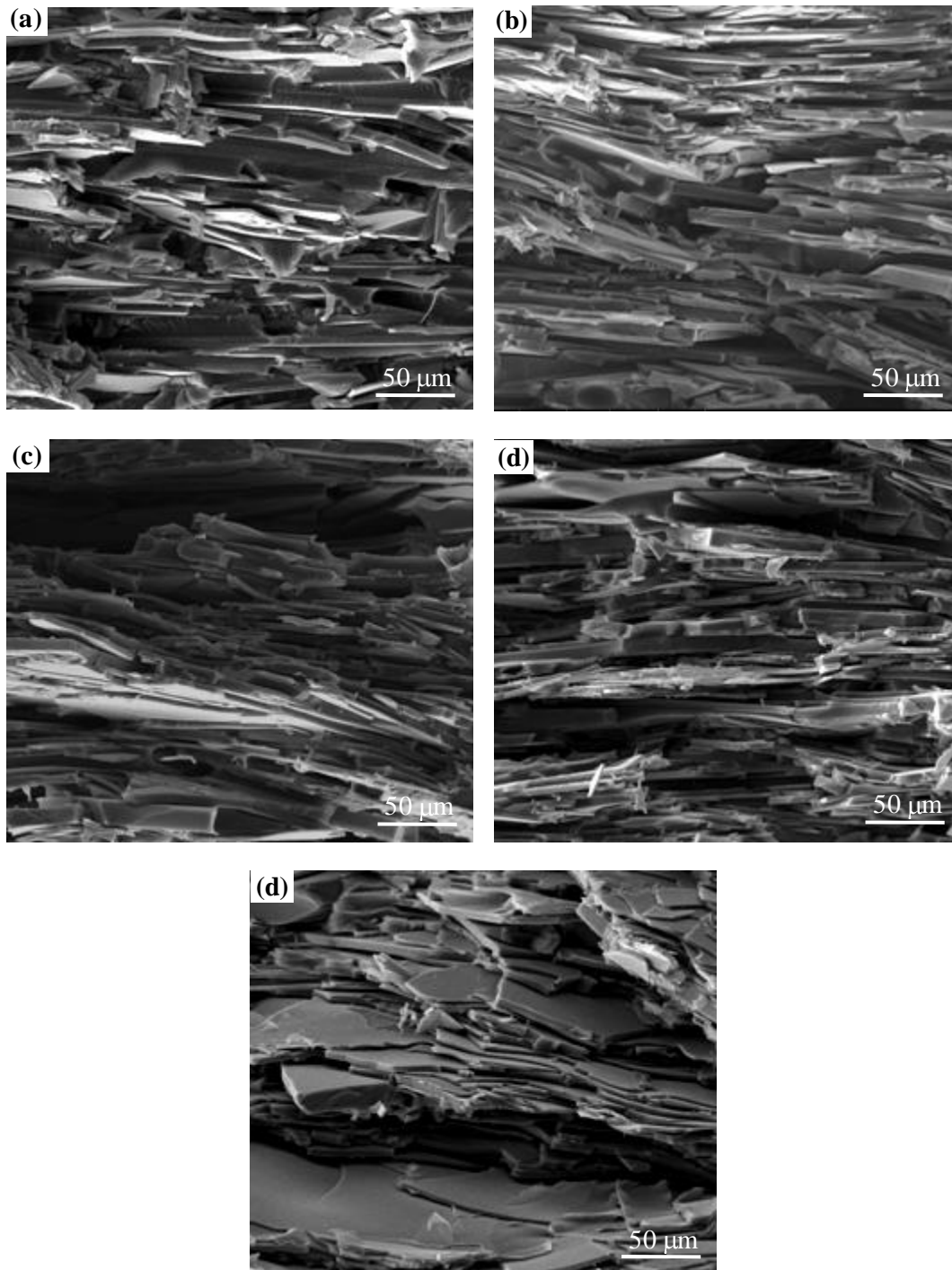
Figure 4.48 Fracture surfaces of epoxy matrix composites reinforced by (a) ~44 vol%, (b) ~54 vol%, (c) ~60 vol%, (d) ~65 vol%, (e) ~71 vol% surface functionalized glass flakes.

In order to reveal the effect of surface treatment on mechanical properties of composites reinforced by high aspect ratio glass flakes, composites with an inorganic content of 44 vol%, 54 vol%, 65 vol% and 71 vol% were fabricated using APS treated glass flakes (GF-ST). Figure 4.49 illustrates flexural stress-strain curves for composites reinforced by surface functionalized glass flakes. Reinforcing the epoxy by surface functionalized glass flakes leads to ~6-31% and ~4-22% enhancement in flexural strength and flexural modulus values with respect to their counterparts reinforced by as-received flakes (Figure 4.50). The enhancements in flexural strength and modulus values increase with the increase in glass flake contents revealing the fact that the effect of coupling at the reinforcement-matrix interface becomes more pronounced with the increase in the available total interfacial area.
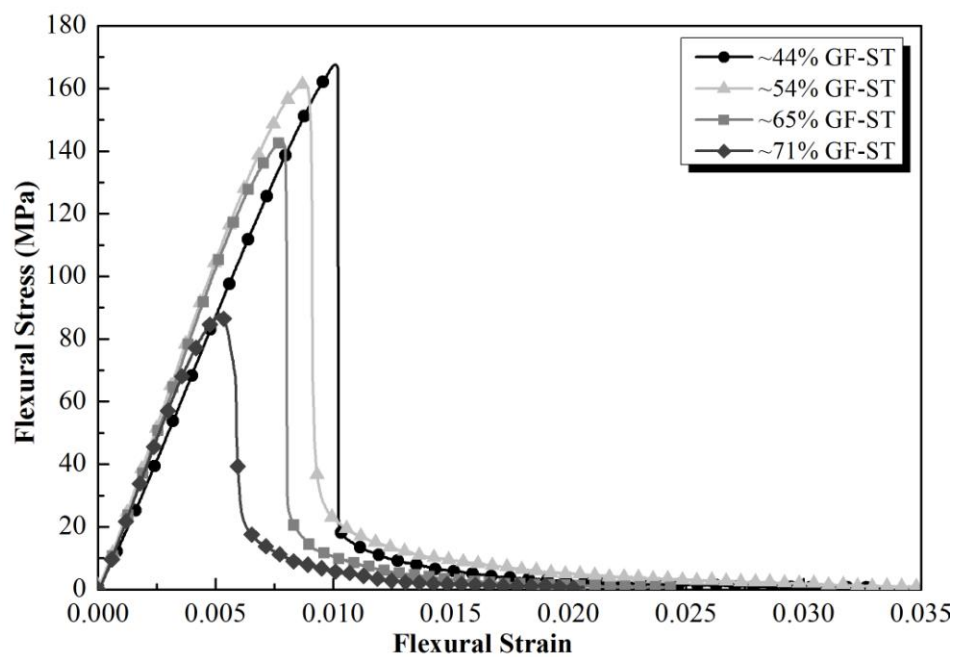
Figure 4.49 Flexural stress-strain curves of composites reinforced by surface functionalized glass flakes.

117
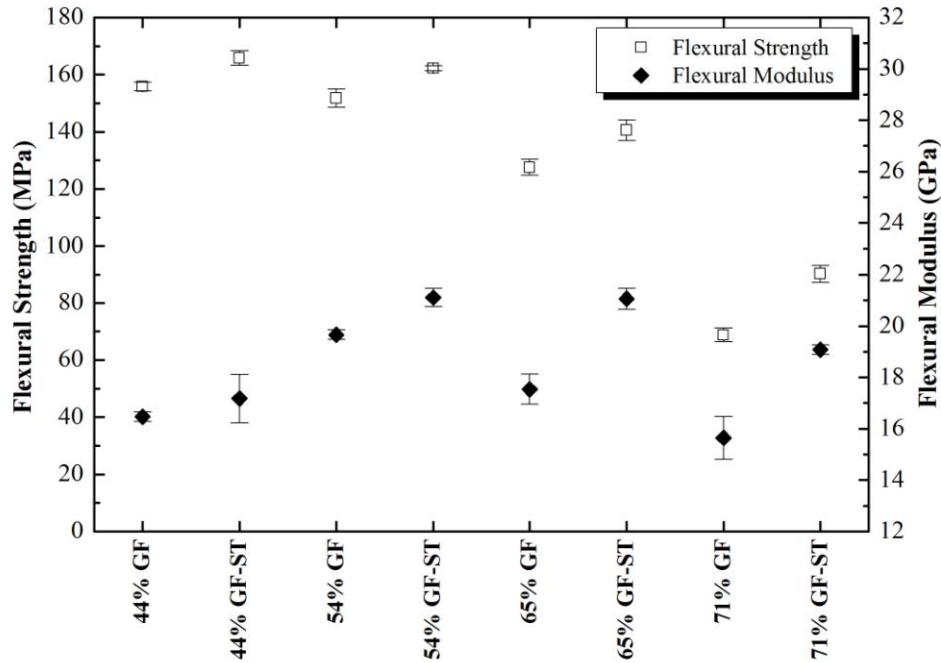
Figure 4.50 Effect of glass flake surface functionalization on flexural strength and modulus of composites HASC processed at low processing pressures.

Along with the mechanical strength data, fracture surface of composites reinforced by as-received and APS treated glass flakes (Figure 4.51) emphasize the effect of surface functionalization on interfacial adhesion. In these fractographs, rough platelet surfaces indicate the adhesion of the epoxy to glass flake surfaces, and hence presence of an effective interfacial chemical bonding between the flakes and the matrix. It is again clear that for these composites main fracture mechanism is not platelet-matrix debonding, yet rather it is via propagation of crack through the matrix deflecting near the flakes edges leaving the surfaces of flakes covered with epoxy.

118
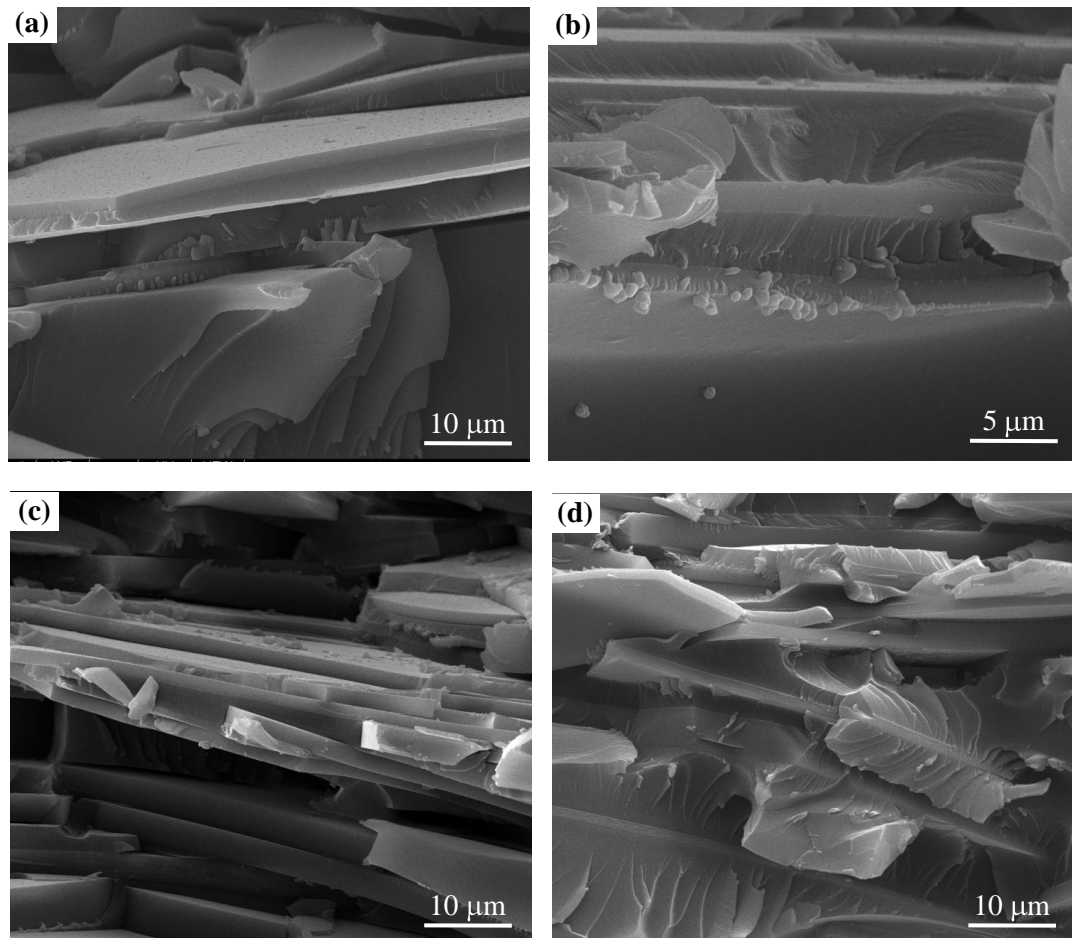
Figure 4.51 Fracture surfaces of composites reinforced by (a) 44 vol% GF, (b) 44 vol% GF-ST, (c) 71 vol% GF and (d) 71 vol% GF-ST.

In order to evaluate the effect of interfacial strength on the energy absorbed until fracture, WOF tests were conducted for the composite reinforced by the glass flake content of 44 vol% for which the flexural strength value is maximum (Figure 4.50). Figure 4.52 shows the load vs. displacement curves of the SENB composite samples reinforced by glass flakes either in as-received condition or surface treated with APS. Average WOF value of the composite reinforced by as-received flakes was calculated as 620 J/m^2 which is ~77% higher than the WOF value of the neat epoxy. Surface functionalization of the glass flakes has led to only ~1.6% improvement in the WOF value with respect to composites reinforced by as-received flakes.

The fracture surface of the WOF specimen reinforced by as-received platelets (Figure 4.53.a) indicates that the crack meanders around the high aspect ratio glass flakes deflecting near the edges. Extensive crack deflection along with flake pull-out leads to highly torturous crack path (Figure 4.53.b) leading to high energy absorption until fracture.
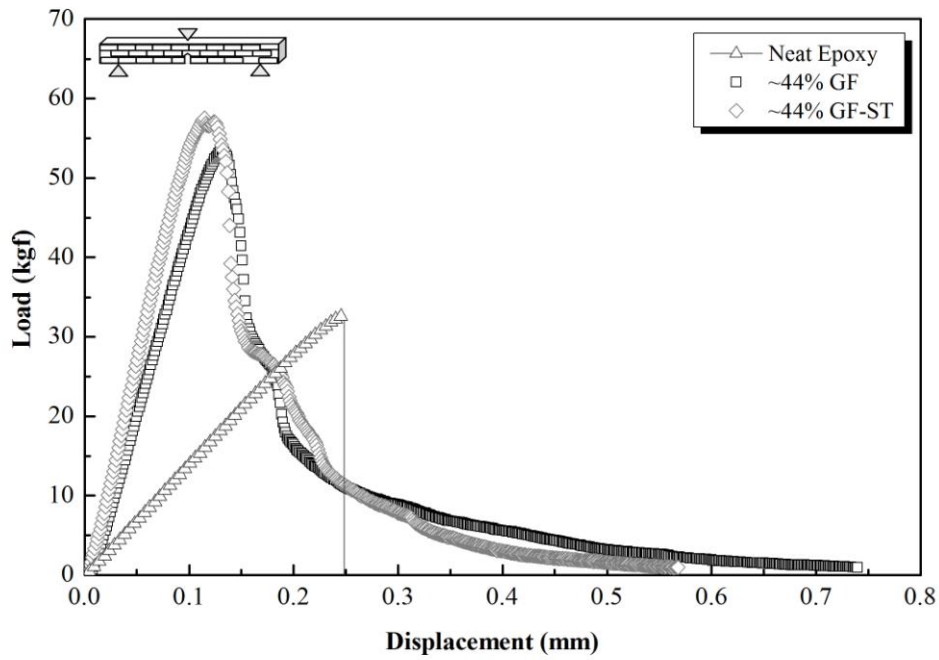
Figure 4.52 Load-displacement curves for composites reinforced either with 44 vol% GF or GF-ST along with the load vs. displacement curve of neat epoxy for comparison.
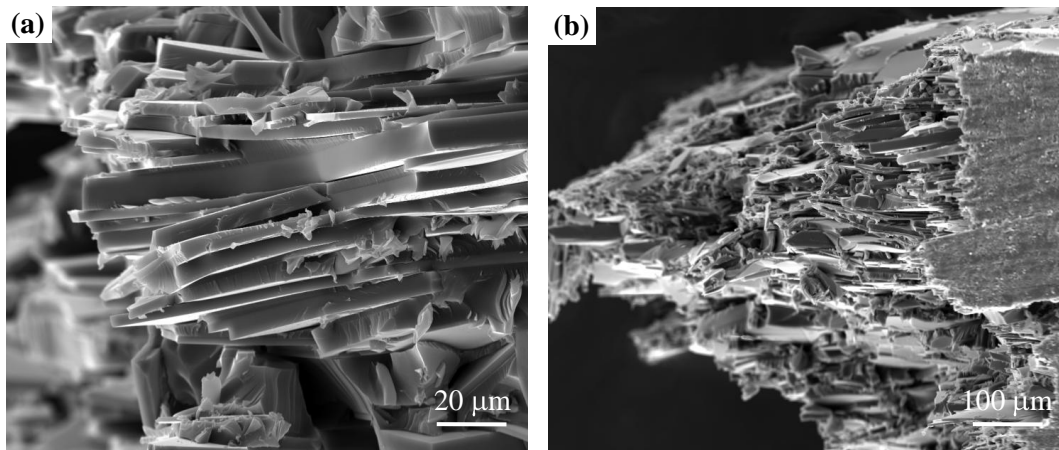
Figure 4.53 Fracture surface of WOF specimen from the composite 44 vol% GF HASC processed at low processing pressure.

When mechanical performances of composites reinforced by alumina platelets, glass platelets and glass flakes are compared, it is clear that reinforcing the epoxy with optimum fraction of high aspect ratio flakes is more effective in terms of improving both the flexural strength and the energy absorbed values until fracture. Actually, the increase in the reinforcing efficiency with increasing aspect ratio is an expected result due to the fact that, as aforementioned, stress transferred from the matrix to the reinforcements increases with the increase in shear stress transfer length leading to higher flexural strength values [15, 84, 85]. Furthermore, unlike composites reinforced by either alumina or glass platelets, for which after maximum stress failure occurs suddenly, 3PB test results indicated that composites reinforced by high aspect ratio glass flakes show a tail behavior indicating the fact that high aspect ratio glass flakes continue to carry load until their embedded parts are completely pulled-out off the matrix.

In terms of the energy absorbed values of a notched specimen until fracture, glass flakes are more effective than either alumina or glass platelets as indicated by the higher WOF values. For all composites fabricated by HASC processing, as a result of the well-alignment of the high strength inorganic reinforcements with an aspect ratio lower than the critical value, crack have propagated either through the weak interface or matrix, depending on the interfacial strength, deflecting near the edges of reinforcements leading to a fracture mode based on platelet pull-out. On the other hand, for composites reinforced by high aspect ratio flakes, during the growth of the stable crack, crack had to meander around the high aspect ratio reinforcements which have led to a highly tortuous path, and hence increase in the energy absorbed values.

4.3 Comparison of HASC Processed Brick-and Mortar Structured Bulk Composites with Other Nacre-Mimetic Bulk Composites

As mentioned in Sub-Section 2.2.2, various processing strategies have been suggested to replicate the hierarchical "brick-and-mortar" structure of nacre and its resulting mechanical properties such as ice templating [11, 44, 123, 124], "gel casting and hot-pressing" [46, 47], flake powder metallurgy routes [48-50], magnetic alignment [51] etc. Although, all these methodologies are effective for the production of nacre-like brick-and-mortar structured composites, most of these methods are multi-step and time-consuming processes. Therefore, there is still a need for a single step, time and power efficient, easily scalable processing pathway that enables the fabrication of bulk composites reinforced by well-aligned inorganic reinforcements. In this study, a newly proposed novel processing pathway called "Hot-press Assisted Slip Casting (HASC)" has been successfully applied to fabricate bulk nacre-mimetic epoxy matrix composites reinforced by alumina platelets, glass platelets or glass flakes of high volume fraction. Beside its effectiveness in fabricating polymer matrix composites reinforced by well-aligned inorganic reinforcements, HASC processing pathway also offers various advantages over other suggested methodologies as it is an easy, single step, time (total processing time takes less than one hour) and manpower efficient methodology.

Through HASC processing, epoxy matrix composites reinforced by well-aligned alumina platelets with a content as high as 68 vol% were successfully fabricated. As a result of high inorganic content and preferential alignment of 2D reinforcements, fabricated composites have exhibited enhanced mechanical performance with respect to both simple mixed composite and neat epoxy. The maximum enhancement in flexural strength and modulus values were achieved at an alumina platelet content of ~59 vol% being ~2 and ~13-fold, respectively, as compared to neat epoxy. These improvements in mechanical performance are either on the same order or higher as compared to the reported values for brick-and-mortar structured alumina reinforcement-polymer matrix composites fabricated either by magnetic alignment [51] or "gel casting and hot-pressing" [46]. Magnetically aligned alumina-polyurethane matrix composite with an inorganic content of 20 vol% exhibited ~1.5-fold increase in tensile strength with respect to its neat polymer counterpart [51]. In addition to this, in the case of brick-and-mortar structured 10 vol% alumina platelet-epoxy matrix composite achieved enhancement in flexural modulus with respect to neat epoxy was reported as ~2.5 fold [51]. Nacre-mimetic alumina-polypropylene composite with an inorganic content of 40 vol% fabricated by an another suggested processing pathway, combined gel casting and hot-pressing, has exhibited ~1.8 and ~13-fold higher tensile strength and stiffness values, respectively, as compared to neat polypropylene [46].

In a study of Munch et al. [11], layered and brick-and-mortar structured nacre-mimetic alumina-PMMA composites with an inorganic content of 80 vol% were fabricated through freeze casting. Despite its high inorganic content and interfacial features such as surface roughness of the inorganic reinforcement and ceramic bridges between the adjacent alumina lamellas as in the case of natural nacre, reported improvements in flexural strength are lower than those achieved in this study. However, treatment of the inorganic surfaces with γ-(trimethoxysilyl)propyl methacrylate has led to ~90% enhancement in the flexural strength value of the brick-and-mortar structured composite, which is higher than the enhancement achieved in this study through the applied silane treatment.

As in the case of alumina reinforced composites, for composites reinforced by high aspect ratio as-received glass flakes, HASC processing has also led to considerable improvement in flexural strength and flexural modulus values with respect to neat epoxy up to an inorganic content of 65 vol%. Achieved flexural strength values are comparable with those reported in a study of Kakisawa et al. [49] that focused on the fabrication of nacre-like bulk composites using nickel coated glass flakes through powder metallurgy route. Although achieved flexural strengths are in the same order, reported WOF value of the composite fabricated by powder metallurgy route with an inorganic content of 80 vol% is much lower than the WOF value of the HASC processed composite of the current study with an inorganic content of 44 vol%.

CHAPTER 5

CONCLUSION

Throughout this study, Hot-press Assisted Slip Casting (HASC) process was used in order to fabricate organic matrix bulk composites reinforced by preferentially oriented 2D inorganic reinforcements such as platelets or flakes. As mentioned previously, HASC process is a newly proposed technique combining two relatively easy and conventional material processing methods; hot-pressing and slip casting. This one-step, easy, fast and scalable processing pathway enables the fabrication of polymer matrix composites reinforced by high volume fraction of well-aligned inorganic reinforcements, in less than one hour, by draining the liquid resin and favoring platelet or flake orientation during processing. Therefore, with the use of this method, it is possible to fabricate organic matrix bulk composites exhibiting even complex shapes with a lamellar microstructural architecture resembling to brick-and-mortar structure of natural nacre.

Although, versatility of HASC processing allows fabrication of composites with wide variety of organic matrix-high strength inorganic reinforcement combinations, in the scope of this study, epoxy matrix composites were reinforced by either 2D alumina or glass reinforcements. As glass reinforcements, glass platelets and glass flakes with two different aspect ratios were used to investigate the effect of aspect ratio on the final properties. In order to reveal the effect of interfacial adhesion on the mechanical properties of the fabricated composites, surfaces of the reinforcements were treated with organofunctional silanes having epoxy- (GPS) and amino- (APS) functional groups in the case of alumina platelets and amino-functional group in the case of glass platelets and flakes.

The crucial points of the experimental investigations can be summarized as follows:

- Being an easy, fast and scalable process, HASC processing has proved its efficiency in fabricating composites with an architecture of "brick-and-mortar" by providing well alignment of the 2D inorganic reinforcements, especially platelets and flakes having high aspect ratios, even at low processing pressures leading to improved mechanical properties compared to the neat matrix and the composite with irregular inorganic distribution.

- The increase in the applied processing pressures both leads to an increase in the amount of inorganic content and enhances the alignment of 2D inorganic reinforcements. Nevertheless, the incorporation of inorganic reinforcement higher than an optimum value leads to an increase in the fraction of voids and in the size

123

of the platelet cluster which deteriorate the mechanical performance of the composite.

For alumina platelet reinforced epoxy matrix composites;

- Incorporation of alumina platelets with an aspect ratio of >30 into epoxy matrix led to an increase in the flexural strength, flexural modulus and hardness even in the case of simple mixed composite. Increase in the platelet content and enhancement in platelet orientation through HASC processing resulted in substantial improvement in the mechanical performance with respect to both neat epoxy and simple mixed composites.

- XPS characterization studies have proven the adsorption of GPS and APS silanes on the surfaces of alumina platelets.

- For APS treatment, deconvolution of N1s core levels indicated that 81% of the adsorbed silane molecules interacted with the alumina platelet surfaces via free amine group while 19% of them via protonated amino groups, in the case of silane treatment in ethanol-water mixture. These percentages were 54% and 46%, respectively, in the case of alumina platelets treated in water. On the other hand, the interaction between amino silane and platelet surface occurred merely through silanol groups for APS treated platelets in toluene.

- Functionalization of platelet surfaces with epoxy-functional silane in ethanol-water mixture improved the compatibility and interfacial bonding between the platelets and the matrix leading to enhancement of the mechanical properties of composite having nacre-like lamellar architecture. However, treatment of alumina platelet surfaces with epoxy-functional silane in water has led to decrease in flexural strength and strain values with respect to composites reinforced by as-received platelets.

- For APS treated alumina platelets, independent of the solvent used in the surface treatment procedure, surface functionalization resulted in significant improvement in flexural strength, strain and modulus. This improvement was most pronounced in the case of composites reinforced by alumina platelets treated in toluene, and least in the case of composites reinforced by alumina platelets treated in water. This indicates that interaction of silane molecule with the surface and the orientation of silane molecules on the surface of the inorganic platelets has a strong influence on the effectiveness of the silane treatment.

For glass platelet and glass flake reinforced epoxy matrix composites;

- For both glass flakes and platelets, applied high processing pressures resulted in fracture of 2D reinforcements during processing.

- Incorporation of glass platelets with an aspect ratio ~15-20 led to a decrease in the flexural strength and strain, yet an increase in the flexural modulus and hardness values for both simple mixed and HASC processed composites. This decrease could be attributed to lack of coupling at the interface along with the lower stress transfer lengths which led to a decrease in the reinforcing efficiency for these low aspect ratio platelets.

- For composites reinforced by glass flakes with an aspect ratio of ~150, HASC processing at low processing pressures led to best result. Incorporation of ~41-65 vol% glass flakes resulted in an improvement, however, further increase in the inorganic content led to a dramatic decrease in the mechanical performance of neat epoxy as these flakes had more tendencies to form large flake clusters and to fracture during processing.

- XPS characterization studies proved the adsorption of APS silane on the surfaces of glass platelets and flakes. Deconvolution of N1s core levels indicated that interaction between amino silane and glass surfaces occurred merely through silanol groups.

- Surface functionalization of the glass platelets and flakes with APS led to a considerable enhancement in both flexural strength and strain with respect to those of neat epoxy and composites reinforced by as-received platelets.

Furthermore, for composites reinforced by either 2D alumina or glass reinforcements;

- Three-point bending (3PB) tests indicated that unlike to alumina and glass platelet reinforced composites, for which after maximum stress failure occurs suddenly, for glass flake reinforced composites following an increase up to the maximum, stress decreased abruptly to some extent and then begun to decrease gradually. The distinction between mechanical behaviors can be attributed to the higher aspect ratio of the glass flakes such that flakes continued carrying load until their embedded parts were completely pulled-out of the matrix leading to a slowly descending curve called tail behavior.

- 3PB load-displacement curves of the simple mixed composites demonstrated that crack propagation was unstable leading to catastrophic failure. However, for HASC processed composites with a microstructural architecture resembling to brick-and-mortar structure, crack propagation was stable as indicated by the tail behavior following the maximum in load-displacement curve.

- For all HASC processed composites reinforced by either as-received or silane treated platelets/flakes, fracture was mainly governed by platelet pull-out mechanism indicating that the aspect ratio of the platelets and flakes, used in this study, were lower than the critical aspect ratio.

- For HASC processed composites reinforced by as-received reinforcements, crack propagates through the weak reinforcement-matrix interface, whereas for composites reinforced by surface functionalized platelets or flakes, crack propagated through the matrix deflecting near the reinforcement edges leaving the surfaces of platelets or flakes covered with epoxy.

- Results of the mechanical characterization studies indicated implicitly the impact of interfacial adhesion on the performance of composites.

- The effect of coupling at the reinforcement-matrix interface was more pronounced for HASC processed composites with high inorganic content as the available interfacial area increases with the increase in the inorganic content.

- When work of fracture (WOF) values of composites reinforced by alumina platelets, glass platelets and glass flakes were compared, it was clear that reinforcing the epoxy by high aspect ratio flakes was more effective in terms of the energy absorbed until fracture. This result can be attributed to the extensive crack deflection leading to a highly tortuous crack path in the case of composites reinforced by high aspect ratio reinforcements.

- Among all 2D reinforcements used in this study, glass flakes with an aspect ratio of ~150 was more effective in reinforcing the epoxy matrix.

CHAPTER 6

RECOMMENDATIONS FOR FUTURE WORK

In this study, the main task was to fabricate polymer matrix composites with microstructural architectures inspired by one of the most intriguing natural materials, nacre, using a newly proposed processing pathway "Hot-press Assisted Slip Casting." Although organic matrix bulk composites reinforced by preferentially oriented 2D fillers leading to a lamellar architecture mimicking brick-and-mortar structure of natural nacre were successfully fabricated through HASC processing, achieved inorganic contents were lower than that of the natural nacre which is as high as 95vol% [14, 15].

Although achieved enhancements in terms of flexural strength and modulus with respect to neat polymer counterpart are either comparable or even higher as compared with those of other studies reported in literature, as mentioned in Section 4.3, they are still lower than the reported flexural strength and modulus values of the natural nacre. Maximum flexural strength and flexural modulus values attained in this study are ranging between ~147-150 MPa and ~23-26 GPa, respectively, for composites reinforced by 59 vol% surface functionalized alumina platelets and ~166 MPa and ~17 GPa, respectively, for composites reinforced by 44 vol% surface functionalized high aspect ratio glass flakes. However, reported flexural strength and modulus values are 223 MPa and 69 GPa, respectively, for abalone nacre [17].

Furthermore, the work of fracture value (WOF) of wet nacre has been determined as 1240 J/m^2 [15]. The maximum WOF values are ranging between ~174-178 J/m^2 for composites reinforced by 59vol% alumina platelets surface functionalized either with GPS or APS. These WOF values are much lower than those of the neat epoxy and natural nacre. In the case of composites reinforced by 44 vol% surface functionalized glass flakes, the attained WOF value was ~630 J/m^2 which is ~80% higher than the WOF value of neat epoxy, although it is still ~50% lower than that of the natural nacre.

It is clear that despite its structurally weaker constituents, nacre exhibits superior mechanical performance with respect to HASC processed brick-and-mortar structured composites fabricated in the scope of this study. This discrepancy can be attributed to two facts. Firstly, nacre consists of 95 vol% perfectly aligned aragonite platelets, each of which was wrapped with a very thin layer of soft organic phase. In this study, maximum attained inorganic content was ~68vol% in the case of composites reinforced by alumina platelets, while it was ~63 vol% and ~78 vol% in the case of composites reinforced by either glass platelets or flakes, respectively. All of the achieved inorganic contents are lower than the

inorganic content of the natural nacre. Furthermore, results of the mechanical characterization studies indicated that incorporation of inorganic reinforcements above an optimum amount has led to degradation in the mechanical performance of the fabricated composites due to the fact that excessive drainage of the epoxy resin has also led to an increase in the fraction of platelet clusters and voids, both of which deteriorates the mechanical performance by either leading to decrease in the effective stress transfer or by acting as potential sites for stress concentration. Therefore, in addition to reinforcing the composite with high inorganic content, attaining a uniform and homogeneous structure, as in the case of natural nacre, is a crucial task otherwise of which stress transfer becomes a real challenge.

Second reason can be the fact that beside its fascinating brick-and-mortar architecture, nacre also exhibits intriguing interfacial features, such as surface waviness of aragonite platelets, platelet interlocks as well as mineral bridges and nanoasperities, each of which has been suggested to undertake a critical task and contribute to the high mechanical performance of the nacre [16-22, 56]. For instance, platelet sliding induced large inelastic deformation resulting from the strain hardening phenomena has been proposed as the prominent toughening mechanism and the main reason for the robustness of nacre [17, 22, 59, 79], while micro-scale dovetail like surface waviness of the aragonite platelets has been suggested as the origin of strain hardening phenomena found in nacre [22]. However, in the scope of this study, low cost commercial 2D reinforcements with smooth surfaces were used. These reinforcements are being widely used in industrial applications for various purposes which do not include their usage as composite material reinforcements or fillers.

To sum up, nacre is a complex material consisting of multi-scale intriguing hierarchical arrangements. In Section 2.1, the structure-property relationship found in nacre was discussed in a detailed manner. Although, the crucial points deduced from the observed structure-property relationships guide the bio-inspiration studies, artificial replication of the multi-scale hierarchical structures and key structural features is a difficult task using the current technology [13]. Consequently, previous bio-inspiration studies and also this particular study have mainly focused on replicating the hierarchical "brick-and-mortar" architecture of nacre. In Section 2.2.1, the design principle underlying the micro-scale hierarchical architecture of nacre was summarized. In this context, new engineering approaches can be developed to wholly apply the design guidelines mentioned in Section 2.2.1 to achieve bio-inspired structural composites with higher strength, stiffness and toughness.

REFERENCES

[1]   M.A. Meyers, A.Y.M. Lin, Y. Seki, P.Y. Chen, B.K. Kad, S. Bodde, Structural Biological Composites: An Overview, JOM 58 (2006) 35-41.

[2]   P.-Y. Chen, A.Y.M. Lin, A.G. Stokes, Y. Seki, S.G. Bodde, J. McKittrick, M.A. Meyers, Structural Biological Materials: Overview of Current Research, JOM 60 (2008) 23-32.

[3]   A. Nova, S. Keten, N.M. Pugno, A. Redaelli, M.J. Buehler, Molecular and Nanostructural Mechanisms of Deformation, Strength and Toughness of Spider Silk Fibrils, Nano Letters 10 (2010) 2626-2634.

[4]   F. Barthelat, Biomimetics for Next Generation Materials, Philosophical Transactions 365 (2007) 2907-2919.

[5]   K. Liu, L. Jiang, Bio-Inspired Design of Multiscale Structures for Function Integration, Nano Today 6 (2011) 155-175.

[6]   K. Liu, L. Jiang, Multifunctional Integration: From Biological to Bio-Inspired Materials, ACS Nano 5 (2011) 6786–6790.

[7]   V.C. Sundar, A. D.Yablon, J.L. Grazul, M. Ian, J. Aizenberg, Fibre-Optical Features of a Glass Sponge, Nature 424 (2003) 899-900.

[8]   M. Johnson, S.L. Walter, B.D. Flinn, G. Mayer, Influence of Moisture on the Mechanical Behavior of a Natural Composite, Acta Biomaterialia 6 (2010) 2181-2188.

[9]   A.R. Studart, Towards High-Performance Bioinspired Composites, Advanced Materials 24 (2012) 5024-5044.

[10]   C. Ortiz, M.C. Boyce, Bioinspired Structural Materials, Science 319 (2008) 1053-1054.

[11]   E. Munch, M.E. Launey, D.H. Alsem, E. Saiz, A.P. Tomsia, R.O. Ritchie, Tough, Bio-Inspired Hybrid Materials, Science 322 (2008) 1516-1520.

[12]   L.J. Bonderer, A.R. Studart, L.J. Gauckler, Bioinspired Design and Assembly of Platelet Reinforced Polymer Films, Science 319 (2008) 1069-1071.

[13]   F. Barthelat, Nacre from Mollusk Shells: A Model for High-performance Structural Materials, Bioinspiration & Biomimetics 5 (2010) 1-8.

[14]   D.K. Dubey, V. Tomar, Role of Molecular Level Interfacial Forces in Hard Biomaterial Mechanics: A Review, Annals of Biomedical Engineering 38 (2010) 2040-2055.

[15] A.P. Jackson, J.V.F. Vincent, R.M. Turner, The Mechanical Design of Nacre, Proceedings of Royal Society B 234 (1988) 415-441.

[16] A.G. Evans, Z. Suo, R.Z. Wang, I.A. Aksay, M.Y. He, J.W. Hutchinson, Model for the Robust Mechanical Behavior of Nacre, Journal of Materials Research 16 (2001) 2475-2485.

[17] R.Z. Wang, Z. Suo, A.G. Evans, N. Yao, I.A. Aksay, Deformation Mechanisms in Nacre, Journal of Materials Research 16 (2001) 2485-2493.

[18] T.E. Schaffer, C. Ionescu-Zanetti, R. Proksch, M. Fritz, D.A. Walters, N. Almqvist, C.M. Zaremba, A.M. Belcher, B.L. Smith, G.D. Stucky, D.E. Morse, P.K. Hansma, Does Abalone Nacre Form by Heteroepitaxial Nucleation or by Growth through Mineral Bridges?, Chemistry of Materials 9 (1977) 1731-1740.

[19] F. Song, X.H. Zhang, Y.L. Bai, Microstructure and Characteristics in the Organic Matrix Layers of Nacre, Journal of Materials Research 17 (2002) 1567-1570.

[20] F. Song, A.K. Soh, Y.L. Bai, Structural and Mechanical Properties of the Organic Matrix Layers of Nacre, Biomaterials 24 (2003) 3623-3631.

[21] M.A. Meyers, A.Y.M. Lin, P.Y. Chen, J. Muyco, Mechanical Strength of Abalone Nacre: Role of the Soft Organic Layer, Journal of the Mechanical Behavior of Biomedical Materials I (2008) 76-85.

[22] F. Barthelat, H. Tang, P.D. Zavattieri, C.M. Li, H.D. Espinosa, On the Mechanics of Mother-of-Pearl: A Key Feature in the Material Hierarchical Structure, Journal of the Mechanics and Physics of Solids 55 (2007) 306–337.

[23] G.M. Luz, J.F. Mano, Mineralized Structures in Nature: Examples and Inspirations for The Design of New Composite Materials and Biomaterials, Composites Science and Technology 70 (2010) 1777-1788.

[24] J. Sun, B. Bhushan, Hierarchical Structure and Mechanical Properties of Nacre: A Review, RSC Advances 2 (2012) 7617-7632.

[25] V. Vertlib, M. Dietiker, M. Plötze, L. Yezek, R. Spolenak, A.M. Puzrin, Fast Assembly of Bio-inspired Nanocomposite Films, Journal of Materials Research 23 (2008) 1026-1035.

[26] L.J. Bonderer, A.R. Studart, J. Woltersdorf, E. Pippel, L.J. Gauckler, Strong and Ductile Platelet-Reinforced Polymer Films Inspired by Nature: Microstructure and Mechanical Properties, Journal of Material Research 24 (2009) 2741-2754.

[27] H.B. Yao, H.Y. Fang, Z.H. Tan, L.H. Wu, S.H. Yu, Biologically Inspired, Strong, Transparent and Functional Layered Organic–Inorganic Hybrid Films, Angewandte Chemie 122 (2010) 2186 –2191.

[28] W. Zhang, G. Xu, R. Ding, K. Duan, J. Qiao, Nacre Biomimetic Design—A Possible Approach to Prepare Low Infrared Emissivity Composite Coatings, Materials Science and Engineering C 33 (2013) 99-102.

[29] J. Wang, Q. Cheng, Z. Tang, Layered Nanocomposites Inspired by the Structure and Mechanical Properties of Nacre, Chemical Society Reviews 41 (2012) 1111-1129.

[30]   P. Podsiadlo, A.K. Kaushik, E.M. Arruda, A.M. Waas, B.S. Shim, J. Xu, H. Nandivada, B.G. Pumplin, J. Lahann, A. Ramamoorthy, N.A. Kotov, Ultrastrong and Stiff Layered Polymer Nanocomposites, Science 318 (2007) 80-83.

[31]   Y. Xu, W. Hong, H. Bai, C. Li, G. Shi, Strong and Ductile Poly(vinyl alcohol)/Graphene Oxide Composite Films with a Layered Structure, Carbon 47 (2009) 3538-3543.

[32]   X. Wang, H. Bai, Z. Yao, A. Liu, G. Shi, Electrically Conductive and Mechanically Strong Biomimetic Chitosan/Reduced Graphene Oxide Composite Films, Journal of Materials Chemistry 20 (2010) 9032-9036.

[33]   J.M. Malho, P. Laaksonen, A. Walther, O. Ikkala, M.B. Linder, Facile Method for Stiff, Tough, and Strong Nanocomposites by Direct Exfoliation of Multilayered Graphene into Native Nanocellulose Matrix, Biomacromolecules 13 (2012) 1093−1099.

[34]   K. Shikinaka, K. Aizawa, N. Fujii, Y. Osada, M. Tokita, J. Watanabe, K. Shigehara, Flexible, Transparent Nanocomposite Film with a Large Clay Component and Ordered Structure Obtained by a Simple Solution-Casting Method, Langmuir 26 (2010) 12493-12495.

[35]   W. Zhu, C.H. Lu, F.C. Chang, S.W. Kuo, Supramolecular Ionic Strength-Modulating Microstructures and Properties of Nacre-like Biomimetic Nanocomposites Containing High Loading Clay, RSC Advances 2 (2012) 6295-6305.

[36]   C. Aulin, G. Salazar-Alvarez, T. Lindstrom, High Strength, Flexible and Transparent Nanofibrillated Cellulose–Nanoclay Biohybrid Films with Tunable Oxygen and Water Vapor Permeability, Nanoscale 4 (2012) 6622-6628.

[37]   S. Korkut, J.D. Roy-Mayhew, D.M. Dabbs, D.L. Milius, I.A. Aksay, High Surface Area Tapes Produced with Functionalized Graphene, ACS Nano 5 (2011) 5214-5222.

[38]   R. Libanori, F.H.L. Münch, D.M. Montenegro, A.R. Studart, Hierarchical Reinforcement of Polyurethane-Based Composites with Inorganic Micro- and Nanoplatelets, Composites Science and Technology 72 (2012) 435–445.

[39]   D.A. Kunz, J. Schmid, P. Feicht, J. Erath, A. Fery, J. Breu, Clay-Based Nanocomposite Coating for Flexible Optoelectronics Applying Commercial Polymers, ACS Nano 7 (2013) 4275–4280.

[40]   T.H. Lin, W.H. Huang, I.K. Jun, P. Jiang, Electrophoretic Co-deposition of Biomimetic Nanoplatelet–Polyelectrolyte Composites, Electrochemistry Communications 11 (2009) 14-17.

[41]   Y.P. Guo, Y. Zhou, Nacre Coatings Deposited by Electrophoresis on Ti6Al4V Substrates, Surface & Coatings Technology 201 (2007) 7505-7512.

[42]   J.L. He, W.Z. Li, H.D. Li, J.Wang, L.D. Wang, Simulation of Nacre with TiC/Teflon Multilayers and a Study of Their Properties, Surface and Coatings Technology 103-104 (1998) 109-112.

[43]   R. Chen, C. Wang, Y. Huang, H. Le, An Efficient Biomimetic Process for Fabrication of Artificial Nacre with Ordered Structure, Materials Science and Engineering C 28 (2008) 218-222.

[44]   M.E. Launey, E. Munch, D.H. Alsem, H.B. Barth, E. Saiz, A.P. Tomsia, R.O. Ritchie, Designing Highly Toughened Hybrid Composites Through Nature-Inspired Hierarchical Complexity, Acta Materialia 57 (2009) 2919-2932.

[45]   A. Dutta, S.A. Tekalur, Synthetic Staggered Architecture Composites, Materials and Design 46 (2013) 802-808.

[46]   L.J. Bonderer, K. Feldman, L.J. Gauckler, Platelet-Reinforced Polymer Matrix Composites by Combined Gel-Casting and Hot-Pressing. Part I: Polypropylene matrix composites, Composites Science and Technology 70 (2010) 1958-1965.

[47]   L.J. Bonderer, K. Feldman, L.J. Gauckler, Platelet-Reinforced Polymer Matrix Composites by Combined Gel-Casting and Hot-Pressing. Part II: Thermoplastic polyurethane matrix composites, Composites Science and Technology 70 (2010) 1966-1972.

[48]   H. Kakisawa, K. Minagawa, S. Takamori, Y. Osawa, Fabrication of Nano-Laminar Composite from Glass Flake, Journal of the Ceramic Society of Japan 113 (2005) 808-811.

[49]   H. Kakisawa, T. Sumitomo, R. Inoue, Y. Kagawa, Fabrication of Nature-Inspired Bulk Laminar Composites by a Powder Processing, Composites Science and Technology 70 (2010) 161-166.

[50]   Z.Q. Li, L. Jiang, G.L. Fan, D.Zhang, Bio-mimetic Metal Matrix Nanocomposites Fabricated by Flake Powder Metallurgy, 18th International Conference on Composite Materials (ICCM-18), Jeju, South Korea, 2011.

[51]   R.M. Erb, R. Libanori, N. Rothfuchs, A.R. Studart, Composites Reinforced in Three Dimensions by Using Low Magnetic Fields, Science 335 (2012) 199-204.

[52]   K.K. Chawla, Composite Materials, Springer-Verlag Inc, New York, 2001.

[53]   D.D.L. Chung, Composite Materials Science and Applications, Springer-Verlag London Limited, Manchaster, 2010.

[54]   H. Wei, N. Ma, F. Shi, Z. Wang, X. Zhang, Artificial Nacre by Alternating Preperation of Layer-by-Layer Polymer Films and $CaCO_3$ Strata, Chem. Mater. 19 (2007) 1974-1978.

[55]   K.S. Katti, D.R. Katti, Why is Nacre so Tough and Strong?, Materials Science and Engineering C 26 (2006) 1317 – 1324.

[56]   A.Y.M. Lin, P.Y. Chen, M.A. Meyers, The Growth of Nacre in the Abalone Shell Acta Biomaterialia 4 (2008) 131-138

[57]   N. Yao, A. Epstein, A. Akey, Crystal Growth via Spiral Motion in Abalone Shell Nacre, Journal of Material Research 21 (2006) 1939-1944.

[58]   X. Li, Nanoscale Structural and Mechanical Characterization of Natural Nanocomposites: Seashells, Journal of Materials 59 (2007) 71-74.

132

[59]   H.D. Espinosa, J.E. Rim, F. Barthelat, M.J. Buehler, Merger of Structure and Material in Nacre and Bone, Progress in Materials Science 54 (2009) 1059–1100.

[60]   K.S. Katti, D.R. Katti, S.M. Pradhan, A. Bhosle, Platelet Interlocks are the Key to Toughness and Strength in Nacre, Journal of Material Research 20 (2005) 1097-1100.

[61]   X. Li, W.-C. Chang, Y.J. Chao, R. Wang, M. Chang, Nanoscale Structural and Mechanical Characterization of a Natural Nanocomposite Material: The Shell of Red Abalone, Nano Letters 4 (2004) 613-617.

[62]   M.A. Meyers, C.T. Lim, A. Li, B.R.H. Nizam, E.P.S. Tan, Y. Seki, J. McKittrick, The Role of Organic Intertile Layer in Abalone Nacre, Materials Science and Engineering C 29 (2009) 2398–2410.

[63]   G.M. Luz, J.F. Mano, Biomimetic Design of Materials and Biomaterials Inspired by The Structure of Nacre, Philosophical Transactions of The Royal Society A 367 (2009) 1587–1605.

[64]   H.J. Qi, B.J.F. Bruet, J.S. Palmer, C. Ortiz, M.C. Boyce, Micromechanics and Macromechanics of the Tensile Deformation of Nacre, in: A.G. Holzapfel, W.R. Ogden (Eds.), Mechanics of Biological Tissue Springer, Berlin, 2006, pp. 189-203.

[65]   M. Launspacha, K. Rückmanna, M. Gummicha, H. Rademakera, H. Doschkeb, M. Radmacherb, M. Fritz, Immobilisation and Characterisation of the Demineralised, Fully Hydrated Organic Matrix of Nacre – An Atomic Force Microscopy Study, Micron 43 (2012) 1351–1363.

[66]   M. Rousseau, E. Lopez, P. Stempflé, M. Brendlé, L. Franke, A. Guette, R. Naslain, X. Bourrat, Multiscale Structure of Sheet Nacre, Biomaterials 26 (2005) 6254-6262.

[67]   M.I. Lopez, P.Y. Chen, J. McKittrick, M.A. Meyers, Growth of Nacre in Abalone: Seasonal and Feeding Effects, Materials Science and Engineering C 31 (2011) 238-245.

[68]   J.D. Currey, Mechanical Properties of Mother of Pearl in Tension, Proceedings of the Royal Society of London. Series B, Biological Sciences 196 (1977) 443-463.

[69]   M. Sarıkaya, K.E. Gunnison, M. Yasrebi, I.A. Aksay, Mechanical Property-Microstructural Relationships in Abolone Shell, Material Research Society Symposium Proceedings 174 (1990) 109-116.

[70]   R.Z. Wang, H.B. Wen, F.Z. Cui, H.B. Zhang, H.D. Li, Observations of Damage Morphologies in Nacre during Deformation and Fracture, Journal of Materials Science 30 (1995) 2299–2304.

[71]   Q.L. Feng, F.Z. Cui, G. Pu, R.Z. Wang, H.D. Li, Crystal Orientation, Toughening Mechanisms and a Mimic of Nacre, Materials Science and Engineering C 11 (2000) 19-25.

[72]   B. Mohanty, K.S. Katti, D.R. Katti, Experimental Investigation of Nanomechanics of the Mineral-Protein Interface in Nacre Mechanics Research Communications 35 (2007) 17-23.

[73] R. Wang, H.S. Gupta, Deformation and Fracture Mechanisms of Bone and Nacre, Annual Reviews of Materials Research 41 (2011) 41-73.

[74] F. Song, Y. Bai, Mineral Bridges of Nacre and Its Effects, Acta Mechanica Sinica 17 (2001) 251-257.

[75] G. Mayer, M. Sarikaya, Rigid Biological Composite Materials: Structural Examples for Biomimetic Design, Experimental Mechanics 42 (2002) 395-403.

[76] Q. Chen, N.M. Pugno, Bio-mimetic Mechanisms of Natural Hierarchical Materials: A Review, Journal of the Mechanical Behavior of Biomedical Materials 19 (2013) 3-33.

[77] H. Kakisawa, T. Sumitomo, The Toughening Mechanism of Nacre and Structural Materials Inspired by Nacre, Science and Technology of Advanced Materials 12 (2011) 1-14.

[78] A. Lin, M.A. Meyers, Growth and Structure in Abalone Shell, Materials Science and Engineering A 390 (2005) 27–41.

[79] F. Barthelat, R. Rabiei, Toughness Amplification in Natural Composites, Journal of the Mechanics and Physics of Solids 59 (2011) 829-840.

[80] F. Barthelat, H.D. Espinosa, An Experimental Investigation of Deformation and Fracture of Nacre–Mother of Pearl, Experimental Mechanics 47 (2007) 311-324.

[81] B.L. Smith, T. E.Schaeffer, M. Viani, J.B. Thompson, N.A. Frederick, J. Kindt, Molecular Mechanistic Origin of the Toughness of Natural Adhesives, Fibres and Composites, Nature 399 (1999) 761-763.

[82] R. Rabiei, S. Bekah, F. Barthelat, Failure Mode Transition in Nacre and Bone-Like Materials, Acta Biomaterialia 6 (2010) 4081–4089.

[83] X. Li, Z.-H. Xu, R. Wang, In Situ Observation of Nanograin Rotation and Deformation in Nacre, Nano Letters 6 (2006) 2301-2304.

[84] J. Rexer, E. Anderson, Composites with Planar Reinforcements (Flakes, Ribbons) - A Review, Polymer Engineering and Science 19 (1979) 1-11.

[85] M. Xanthos, Modification of Polymer Properties with Functional Fillers, in: M. Xanthos (Ed.), Functional Fillers for Plastics, WILEY-VCH Verlag GmbH & Co. KGaA, Weinheim, 2010, pp. 19-42.

[86] J. Han, Y. Dou, D. Yan, J. Ma, M. Wei, D.G. Evans, X. Duan, Biomimetic Design and Assembly of Organic–Inorganic Composite Films with Simultaneously Enhanced Strength and Toughness, Chemical Commununications 47 (2011) 5274-5276.

[87] S. Bekah, R. Rabiei, F. Barthelat, Structure, Scaling, and Performance of Natural Micro- and Nanocomposites, BioNanoScience 1 (2011) 53–61.

[88] H. Gao, B. Ji, I.L. Jager, E. Arz, P. Fratzl, Materials Become Insensitive to Flaws at Nanoscale:Lessons from Nature, Applied Physical Sciences 100 (2003) 5597-5600.

[89] G.E. Padawer, N. Beecher, On the Strength and Stiffness of Planar Reinforced Plastic Resins, Polymer Engineering and Science 70 (1970) 185-192.

[90] J. Lusis, R.T. Woodhams, M. Xanthos, The Effect of Flake Aspect Ratio on the Flexural Properties of Mica Reinforced Plastics, Polymer Engineering and Science 13 (1973) 139-145.

[91] J. Tsai, C.T. Sun, Effect of Platelet Dispersion on the Load Transfer Efficiency in Nanoclay Composites, Journal of Composite Materials 38 (2004) 567-579.

[92] A. Yasmin, I.M. Daniel, Mechanical and Thermal Properties of Graphite Platelet/Epoxy Composites, Polymer 45 (2004) 8211-8219.

[93] X. Li, H. Gao, W.A. Scrivens, D. Fei, V. Thakur, M.A. Sutton, A.P. Reynolds, M.L. Myrick, Structural and Mechanical Characterization of Nanoclay-Reinforced Agarose Nanocomposites, Nanotechnology 16 (2005) 2020-2029.

[94] B. Pajarito, M. Kubouchi, S. Aoki, T. Sakai, Effect of Flake Orientation Anisotropy on Aging and Durability of Glass/Epoxy Composites, 18th International Conference on Composite Materials (ICCM-18), Jeju, South Korea, 2011.

[95] P. Fratzl, A Composite Matter of Alignment, Science 335 (2012) 177-178.

[96] G. Decher, Fuzzy Nanoassemblies: Toward Layered Polymeric Multicomposites, Science 277 (1997) 1232-1237.

[97] P. Lavalle, J.C. Voegel, D. Vautier, B. Senger, P. Schaaf, V. Ball, Dynamic Aspects of Films Prepared by a Sequential Deposition of Species: Perspectives for Smart and Responsive Materials, Advanced Materials 23 (2011) 1191-1221.

[98] S.M. Waraich, B. Hering, Z. Burghard, J. Bill, P. Behrens, H. Menzel, Fabrication and Characterization of Biocompatible Nacre-Like Structures from α-Zirconium Hydrogen Phosphate Hydrate and Chitosan, Journal of Colloid and Interface Science 367 (2012) 74-82.

[99] Y. Zhang, J.R.G. Evans, Approaches to the Manufacture of Layered Nanocomposites, Applied Surface Science 258 (2012) 2098- 2102.

[100] K. Ariga, J.P. Hill, Q. Ji, Layer-by-Layer Assembly as a Versatile Bottom-up Nanofabrication Technique for Exploratory Research and Realistic Application, Physical Chemistry Chemical Physics 9 (2007) 2319-2340.

[101] J. Wang, L. Lin, Q. Cheng, L. Jiang, A Strong Bio-Inspired Layered PNIPAM–Clay Nanocomposite Hydrogel, Angewandte Chemie 124 (2012) 4754 -4758.

[102] C.N. Wu, T. Saito, S. Fujisawa, H. Fukuzumi, A. Isogai, Ultrastrong and High Gas-Barrier Nanocellulose/Clay-Layered Composites, Biomacromolecules 13 (2012) 1927−1932.

[103] L. Huang, C. Li, W. Yuan, G. Shi, Strong Composite Films with Layered Structures Prepared by Casting Silk Fibroin–Graphene Oxide Hydrogels, Nanoscale 5 (2013) 3780-3785.

[104] Y.Q. Li, T. Yu, T.Y. Yang, L.X. Zheng, K. Liao, Bio-Inspired Nacre-like Composite Films Based on Graphene with Superior Mechanical, Electrical, and Biocompatible Properties, Advanced Materials 24 (2012) 3426-3431.

[105] P. Das, S. Schipmann, J.M. Malho, B. Zhu, U. Klemradt, A. Walther, Facile Access to Large-Scale, Self-Assembled, Nacre-Inspired, High-Performance Materials with Tunable Nanoscale Periodicities, ACS Applied Materials and Interfaces 5 (2013) 3738−3747.

[106] H.B. Yao, Z.H. Tan, H.Y. Fang, S.H. Yu, Artificial Nacre-like Bionanocomposite Films from the Self-Assembly of Chitosan–Montmorillonite Hybrid Building Blocks, Angewandte Chemie International Edition 49 (2010) 10127 -10131.

[107] A. Walther, I. Bjurhager, J.M. Malho, J. Pere, J. Ruokolainen, L.A. Berglund, O. Ikkala, Large-Area, Lightweight and Thick Biomimetic Composites with Superior Material Properties via Fast, Economic, and Green Pathways, Nano Letters 10 (2010) 2742-2748.

[108] A. Walther, I. Bjurhager, J.M. Malho, J. Ruokolainen, L. Berglund, O. Ikkala, Supramolecular Control of Stiffness and Strength in Lightweight High-Performance Nacre-Mimetic Paper with Fire-Shielding Properties, Angewandte Chemie International Edition 49 (2010) 6448 -6453.

[109] Y. Zhang, J.R.G. Evans, Alignment of Layered Double Hydroxide Platelets, Colloids and Surfaces A: Physicochemical and Engineering Aspects 408 (2012) 71-78.

[110] F. Bennadji-Gridi, A. Smith, J.P. Bonnet, Montmorillonite Based Artificial Nacre Prepared via a Drying Process, Materials Science and Engineering B 130 (2006) 132-136.

[111] H.J. Nam, T. Ebina, F. Mizukami, Formability and Properties of Self-standing Clay Film by Montmorillonite with Different Interlayer Cations, Colloids and Surfaces A: Physicochemical and Engineering Aspects 346 (2009) 158-163.

[112] P. Walley, Y. Zhang, J.R.G. Evans, Self-Assembly of Montmorillonite Platelets during Drying, Bioinspiration and Biomimetics 7 (2012) 1-8.

[113] D.A. Dikin, S. Stankovich, E.J. Zimney, R.D. Piner, G.H.B. Dommett, G. Evmenenko, S.T. Nguyen, R.S. Ruoff, Preparation and Characterization of Graphene Oxide Paper, Nature 448 (2007) 457-460.

[114] Q. Cheng, M. Wu, M. Li, L. Jiang, Z. Tang, Ultratough Artificial Nacre Based on Conjugated Cross-linked Graphene Oxide, Angewandte Chemie International Edition 52 (2013) 3750 -3755.

[115] Z. Tang, N.A. Kotov, S. Magonov, B. Öztürk, Nanostructured Artificial Nacre, Nature 2 (2003) 413-418.

[116] P. Podsiadlo, A.K. Kaushik, B.S. Shim, A. Agarwal, Z. Tang, A.M. Waas, E.M. Arruda, N.A. Kotov, Can Nature's Design be Improved Upon High Strength, Transparent Nacre-Like Nanocomposites with Double Network of Sacrificial Cross Links, Journal of Physical Chemistry B 112 (2008) 14359-14363.

[117] T.U. Patro, H.D. Wagner, Layer-by-Layer Assembled PVA/Laponite Multilayer Free-Standing Films and Their Mechanical and Thermal Properties, Nanotechnology 22 (2011) 455706 455701-455712.

[118] Y. Shu, P. Yin, B. Liang, S. Wang, L. Gao, H. Wang, L. Guo, Layer by Layer Assembly of Heparin/Layered Double Hydroxide Completely Renewable Ultrathin Films with Enhanced Strength and Blood Compatibility, Journal of Materials Chemistry 22 (2012) 21667-21672.

[119] S. Zhang, J. Zhang, Z. Zhang, H. Dang, W. Lua, Q. Xue, Preparation and Characterization of Self-Assembled Organic–Inorganic Nacre-Like Nanocomposite Thin Films, Materials Letters 58 (2004) 2266– 2269.

[120] X. Zhang, C. Liu, W. Wu, J. Wang, Evaporation-Induced Self-Assembly of Organic–Inorganic Ordered Nanocomposite Thin Films that Mimic Nacre, Materials Letters 60 (2006) 2086-2089.

[121] Z. Burghard, L. Zini, V. Srot, P. Bellina, P.A.v. Aken, J. Bill, Toughening Through Nature-Adapted Nanoscale Design, Nano Letters 9 (2009) 4103-4108.

[122] I. Zlotnikov, I. Gotman, Z. Burghard, J. Bill, E.Y. Gutmanas, Synthesis and Mechanical Behavior of Bioinspired ZrO2–Organic Nacre-Like Laminar Nanocomposites, Colloids and Surfaces A: Physicochemical and Engineering Aspects 361 (2010) 138-142.

[123] S. Deville, E. Saiz, R.K. Nalla, A.P. Tomsia, Freezing as a Path to Build Complex Composites, Science 311 (2006) 515-518.

[124] M.E. Launey, E. Munch, D.H. Alsem, E. Saiz, A.P. Tomsia, R.O. Ritchie, A Novel Biomimetic Approach to the Design of High-Performance Ceramic-Metal Composites, Journal of Royal Society Interface 7 (2010) 741-753.

[125] T.S. Suzuki, T. Uchikoshi, Y. Sakka, Control of Texture in Alumina by Colloidal Processing in a Strong Magnetic Field, Science and Technology of Advanced Materials 7 (2006) 356-364.

[126] Y. Sakka, Fabrication of Highly Microstructure Controlled Ceramics by Novel Colloidal Processing, Journal of the Ceramic Society of Japan 114 (2006) 371-376.

[127] W. Chen, Y. Kinemuchi, T. Tamura, K. Miwa, K. Watari, Fabrication of Textured Ferroelectric Ceramics by Magnetic Alignment via Gel Casting, Journal of the European Ceramic Society 27 (2007) 655–661.

[128] X. Zhu, T.S. Suzuki, T. Uchikoshi, Y. Sakka, Highly Texturing β-Sialon via Strong Magnetic Field Alignment, Journal of American Ceramic Society 91 (2008) 620-623.

[129] H. Koerner, E. Hampton, D. Dean, Z. Turgut, L. Drummy, P. Mirau, R. Vaia, Generating Triaxial Reinforced Epoxy/Montmorillonite Nanocomposites with Uniaxial Magnetic Fields, Chemistry of Materials 17 (2005) 1990-1996.

[130] L. Sun, K. Keshoju, H. Xing, Magnetic Field Mediated Nanowire Alignment in Liquids for Nanocomposite Synthesis, Nanotechnology 19 (2008) 1-6.

[131] T. Kimura, H. Ago, M. Tobita, S. Ohshima, M. Kyotani, M. Yumura, Polymer Composites of Carbon Nanotubes Aligned by a Magnetic Field, Advanced Materials 14 (2002) 1380-1383.

[132] E.S. Choi, J.S. Brooks, D.L. Eaton, M.S. Al-Haik, M.Y. Hussaini, H. Garmestani, D. Li, K. Dahmen, Enhancement of Thermal and Electrical Properties of Carbon Nanotube Polymer Composites by Magnetic Field Processing, Journal of Applied Physics 94 (2003) 6034-6039.

[133] G. Chen, W. Zhao, H. Tang, H. Wang, Preparation and Surface Characterization of Highly Ordered Polymer/Graphite Nanosheet Composites, Materials and Manufacturing Processes 22 (2007) 733-736.

[134] M.S. Mauter, M. Elimelech, C.O. Osuji, Nanocomposites of Vertically Aligned Single-Walled Carbon Nanotubes by Magnetic Alignment and Polymerization of a Lyotropic Precursor, ACS Nano 4 (2010) 6651–6658.

[135] I.I.T. Kim, A. Tannenbaum, R. Tannenbaum, Anisotropic Conductivity of Magnetic Carbon Nanotubes Embedded in Epoxy Matrices, Carbon 49 (2011) 54-61.

[136] O. Malkina, H. Mahfuz, K. Sorge, A. Rondinone, J. Chen, Magnetic Alignment of SWCNTs Decorated with Fe3O4 to Enhance Mechanical Properties of SC-15 Epoxy, AIP Advances 3 (2013) 1-11.

[137] D. Shi, P. He, J. Lian, X. Chaud, S.L. Bud'ko, E. Beaugnon, L.M. Wang, R.C. Ewing, R. Tournier, Magnetic Alignment of Carbon Nanofibers in Polymer Composites and Anisotropy of Mechanical Properties, Journal of Applied Physics 97 (2005) 1-5.

[138] D. Shi, P. He, P. Zhao, F.F. Guo, F. Wang, C. Huth, X. Chaud, S.L. Bud'ko, J. Lian, Magnetic Alignment of Ni/Co-Coated Carbon Nanotubes in Polystyrene Composites, Composites Part B: Engineering 42 (2011) 1532-1538.

[139] J.G. Marsden, L.P. Ziemianski, Organofunctional Silanes - Functions, Applications and Advantages, British Polymer Journal 11 (1979) 199-205.

[140] S. Goyal, Silanes: Chemistry and applications, The Journal of Indian Prosthodontic Society 6 (2006) 14-18.

[141] V. Smits, P. Chevalier, D. Deheunynck, S. Miller, A New Filler Dispersion Technology, Reinforced Plastics 52 (2008) 37-43.

[142] B. Borup, K. Weissenbach, Silane Coupling Agents, in: M. Xanthos (Ed.), Functional Fillers for Plastics, WILEY-VCH Verlag GmbH & Co. KGaA, Weinheim, 2010, pp. 63-90.

[143] G.L. Witucki, A Silane Primer: Chemistry and Applications of AIkoxy Silanes, Journal of Coatings Technology 65 (1993) 57-60.

[144] F. Ishida, Controlled Interphases in Glass Fiber and Particulate Reinforced Polymers: Structure of Silane Coupling Agents in Solutions and on Substrates in: G. Akovali (Ed.), The Interfacial Interactions in Polymeric Composites, Kluwer Academic Publishers, Netherlands, 1993, pp. 169-199.

[145] D.I. Tee, M. Mariatti, A. Azizan, C.H. See, K.F. Chong, Effect of Silane-Based Coupling Agent on the Properties of Silver Nanoparticles Filled Epoxy Composites, Composites Science and Technology 67 (2007) 2584-2591.

[146] Y. Xie, C.A.S. Hill, Z. Xiao, H. Militz, C. Mai, Silane Coupling Agents used for Natural Fiber/Polymer Composites: A review, Composites: Part A 41 (2010) 806-819.

[147] D.K. Shukla, S.V. Kasisomayajula, V. Parameswaran, Epoxy Composites using Functionalized Alumina Platelets as Reinforcements, Composites Science and Technology 68 (2008) 3055-3063.

[148] A. Rattana, J.D. Hermes, M.L. Abel, J.F. Watts, The Interaction of a Commercial Dry Film Adhesive with Aluminium and Organosilane Treated Aluminium Surfaces: A Study by XPS and ToF-SIMS, International Journal of Adhesion & Adhesives 22 (2002) 205-218.

[149] J.D. Miller, K. Hoh, H. Ishida, Studies of the Simulation of Silane Coupling Agent Structures on Particulate Fillers; The pH Effect, Polymer Composites 5 (1984) 18-28.

[150] P. Walker, Silane and Other Adhesion Promoters in Adhesive Technology, in: A. Pizzi, K.L. Mittal (Eds.), Handbook of Adhesive Technology, Taylor & Francis Group, New York, 2003.

[151] P. Eaton, P. Holmes, J. Yarwood, In Situ and Ex Situ FTIR–ATR and Raman Microscopic Studies of Organosilane Hydrolysis and the Effect of Hydrolysis on Silane Diffusion through a Polymeric Film, Journal of Applied Polymer Science 82 (2001) 2016-2026.

[152] A. Simon, T. Cohen-Bouhacina, M.C. Porte, J.P. Aime, C. Baquey, Study of Two Grafting Methods for Obtaining a 3-Aminopropyltriethoxysilane Monolayer on Silica Surface, Journal of Colloid and Interface Science 251 (2002) 278-283.

[153] M.C.B. Salon, M.N. Belgacem, Competition between Hydrolysis and Condensation Reactions of Trialkoxysilanes, as a Function of the Amount of Water and the Nature of the Organic Group, Colloids and Surfaces A: Physicochemical Engineering Aspects 366 (2010) 147-154.

[154] S. Shokoohi, A. Arefazar, R. Khosrokhavar, Silane Coupling Agents in Polymer-based Reinforced Composites: A Review, Journal of Reinforced Plastics and Composites 27 (2008) 473-485.

[155] H. Ishida, A Review of Recent Progress in the Studies of Molecular and Microstructure of Coupling Agents and Their Functions in Composites, Coatings and Adhesive Joints, Polymer Composites 5 (1984) 101-123.

[156] W.J.v. Ooij, D. Zhu, M. Stacy, A. Seth, T. Mugada, J. Gandhi, P.Puomi, Corrosion Protection Properties of Organosilanes-An Overview, Tsinghua Science and Technology 10 (2005) 639-664.

[157] H. Ishida, S. Naviroj, S.K. Tripathy, J.J. Fitzgerald, J.L. Koenig, The Structure of an Aminosilane Coupling Agent in Aqueous Solutions and Partially Cured Solids, Journal of Polymer Science 20 (1982) 701-718.

[158] M.L. Abel, A. Rattana, J.F. Watts, The Interaction of γ-Glycidoxypropyltrimethoxysilane with Oxidised Aluminium Substrates: The Effect of Drying Temperature, Journal of Adhesion 73 (2000) 313-340.

[159] J.L. Koenig, H. Emadipour, Mechanical Characterization of the Interfacial Strength of Glass-Reinforced Composites, Polymer Composites 6 (1985) 142-150.

[160] A.T. DiBenedetto, Tailoring of Interfaces in Glass Fiber Reinforced Polymer Composites: A Review, Materials Science and Engineering A 302 (2001) 74-82.

[161] M.S. Soto, P. Pages, T. Lacorte, K. Briceno, F. Carrasco, Curing FTIR Study and Mechanical Characterization of Glass Bead Filled Trifunctional Epoxy Composites, Composites Science and Technology 67 (2007) 1974-1985.

[162] D.G. Kurth, T. Bein, Thin Films of (3-Aminopropyl)triethoxysilane on Aluminum Oxide and Gold Substrates, Langmuir 11 (1995) 3061-3067.

[163] C.M. Bertelsen, F.J. Boerio, Linking Mechanical Properties of Silanes to Their Chemical Structure: An Analytical Study of γ-GPS Solutions and Films, Progress in Organic Coatings 41 (2001) 239-246.

[164] M.L. Abel, R. Joannic, M. Fayos, E. Lafontaine, S.J. Shaw, J.F. Watts, Effect of Solvent Nature on the Interaction of γ- Glycidoxypropyl trimethoxy Silane on Oxidised Aluminium Surface: A Study by Solution Chemistry and Surface Analysis, International Journal of Adhesion & Adhesives 26 (2006) 16-27.

[165] J.S. Quinton, P.C. Dastoor, Conformational Dynamics of γ-APS on the Iron Oxide Surface: An Adsorption Kinetic Study using XPS and ToF-SIMS, Surface and Interface Analysis 30 (2000) 21-24.

[166] D. Kowalczyk, S. Slomkowski, M.M. Chehimi, M. Delamar, Adsorption of Aminopropyltriethoxy Silane on Quartz: an XPS and Contact Angle Measurements Study, International Journal of Adhesion and Adhesives 16 (1996) 227-232.

[167] J.A. Howarter, J.P. Youngblood, Optimization of Silica Silanization by 3-Aminopropyltriethoxysilane, Langmuir 22 (2006) 11142-11147.

[168] J. Gu, Q. Zhang, J. Dang, J. Zhang, S. Chen, Preparation and Mechanical Properties Researches of Silane Coupling Reagent Modified β-Silicon Carbide Filled Epoxy Composites, Polymer Bulletin 62 (2009) 689-697.

[169] A.M. Shanmugharaj, J.H. Bae, K.Y. Lee, W.H. Noh, S.H. Lee, S.H. Ryu, Physical and Chemical Characteristics of Multiwalled Carbon Nanotubes Functionalized with Aminosilane and Its Influence on the Properties of Natural Rubber Composites, Composites Science and Technology 67 (2007) 1813-1822.

[170] B.B. Johnsen, K. Olafsen, A. Stori, Reflection-Absorption FT-IR Studies of the Specific Interaction of Amines and an Epoxy Adhesive with GPS Treated Aluminium Surfaces, International Journal of Adhesion & Adhesives 23 (2003) 155-163.

[171] A. Ahagon, A.N. Gent, Effect of Interfacial Bonding on the Strength of Adhesion, Journal of Polymer Science 13 (1976) 1285-1300.

[172] G.B. Hoflund, Spectroscopic Techniques: X-ray Photoelectron Spectrosopy, Auger Electron Spectroscopy, and Ion Scattering Spectroscopy, in: J.C. Riviere, S. Myhra (Eds.), Handbook of Surface and Interface Analysis, Marcel Dekker Inc., New York, 1998.

[173] F. Awaja, M. Gilbert, G. Kelly, B. Fox, P.J. Pigram, Adhesion of Polymers, Progress in Polymer Science 34 (2009) 948-968.

[174] P.E.J. Flewitt, R.K. Wild, Physical Methods for Materials Characterisation, Institute of Physics Publishing Ltd., London, 1994.

[175] M. Xanthos, Polymers and Polymer Composites, in: M. Xanthos (Ed.), Functional Fillers for Plastics, WILEY-VCH Verlag GmbH & Co. KGaA, Weinheim, 2010, pp. 3-18.

[176] E. Vassileva, K. Friedrich, Epoxy/Alumina Nanoparticle Composites. I. Dynamic Mechanical Behavior, Journal of Applied Polymer Science 89 (2003) 3774-3785.

[177] K. Shimizu, M.L. Abel, J.F. Watts, Evaluation of the Interaction and Adsorption of γ-Glycidoxy propyl trimethoxy silane with Grit-Blasted Aluminium: A ToFSIMS and XPS Study, The Journal of Adhesion 84 (2008) 725-741.

[178] L.M. Matuana, J.J. Balatinecz, Effect of Surface Properties on the Adhesion between PVC and Wood Veneer Laminates, Polymer Engineering and Science 38 (1998) 765-773.

[179] A.S.M. Chong, X.S. Zhao, Functionalization of SBA-15 with APTES and Characterization of Functionalized Materials, Journal of Physical Chemistry B 107 (2003) 12650-12657.

[180] M.R. Horner, F.J. Boerio, H.M. Clearfield, An XPS Investigation of the Adsorption of Aminosilanes onto Metal Substrates, Journal of Adhesion Science and Technology 6 (1992) 1-22.

[181] C. Perruchot, M.M. Chehimi, M. Delamar, E. Cabet-Deliry, B. Miksa, S. Slomkowski, M.A. Khan, S.P. Armes, Chemical Deposition and Characterization of Thin Polypyrrole Films on Glass Plates: Role of Organosilane Treatment, Colloid Polymer Science 278 (2000) 1139-1154.

[182] X. Liu, J.L. Thomason, F.R. Jones, XPS and AFM Study of Interaction of Organosilane and Sizing with E-Glass Fibre Surface, The Journal of Adhesion 84 (2008) 322-338.

APPENDIX A

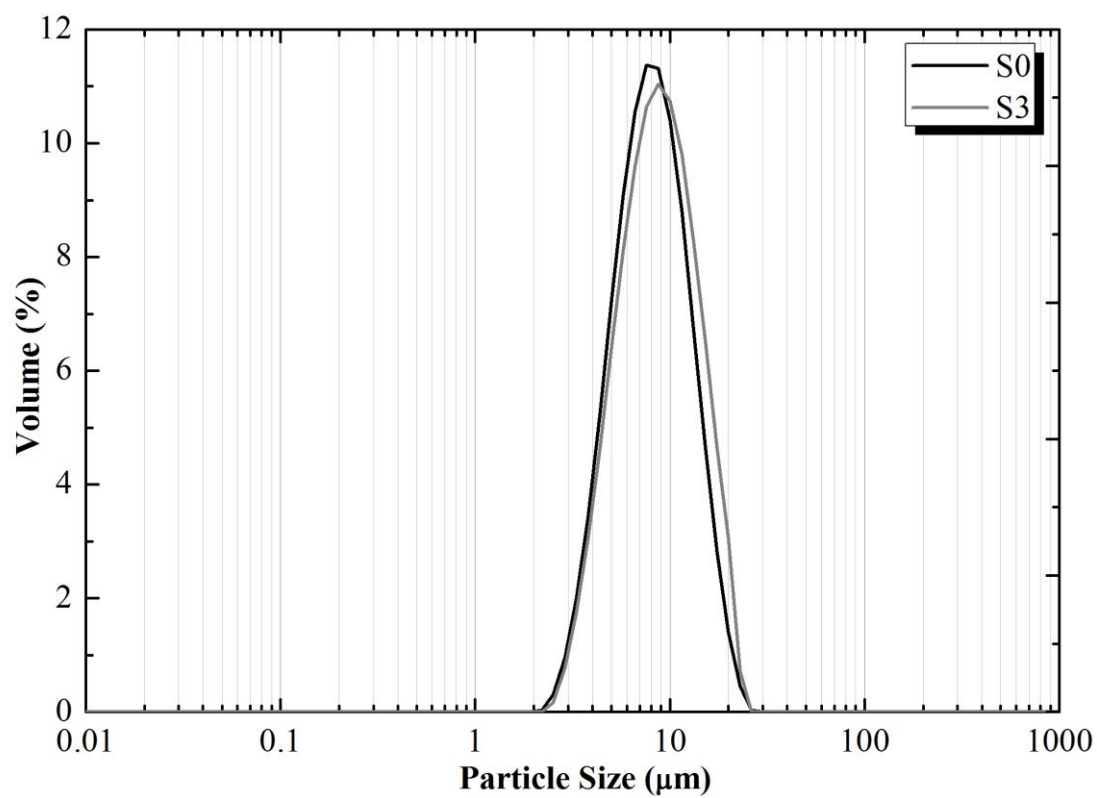## PARTICLE SIZE DISTRIBUTION CURVES

Figure A.1 Particle size distribution of alumina platelets treated with APS in toluene (S3) along with the particle size distribution of as-received platelets (S0).
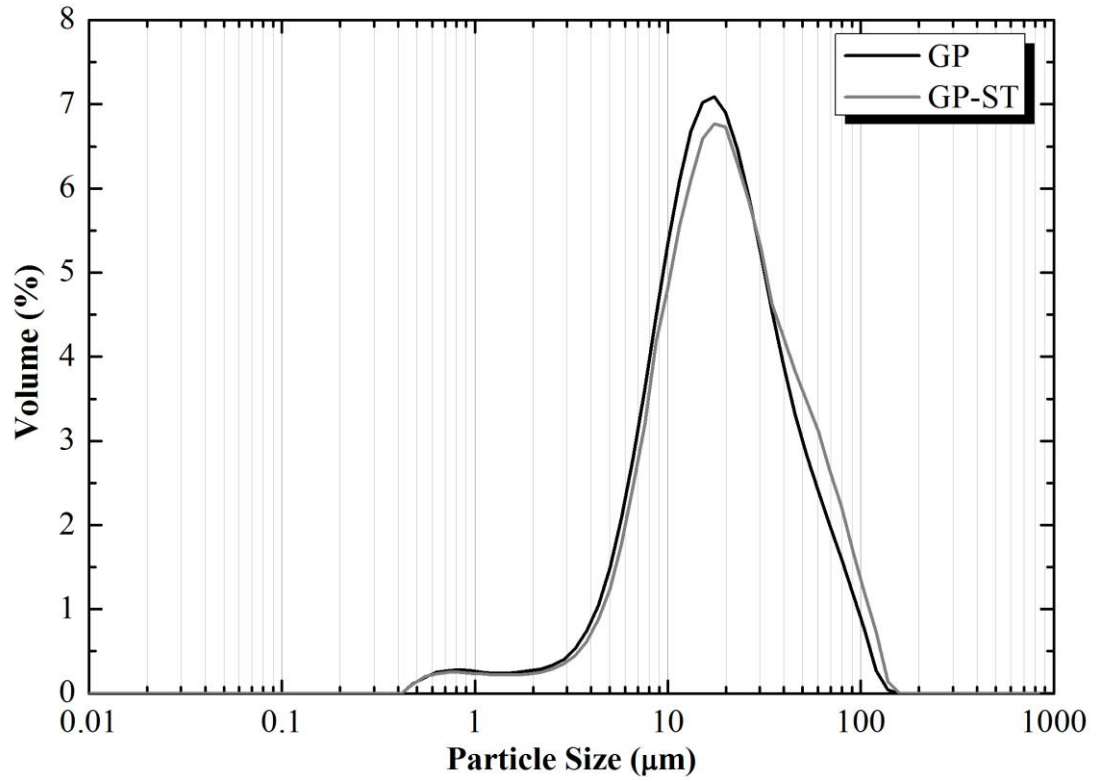
Figure A.2 Particle size distribution of glass platelets treated with APS (GP-ST) along with the particle size distribution of as-received platelets (GP).
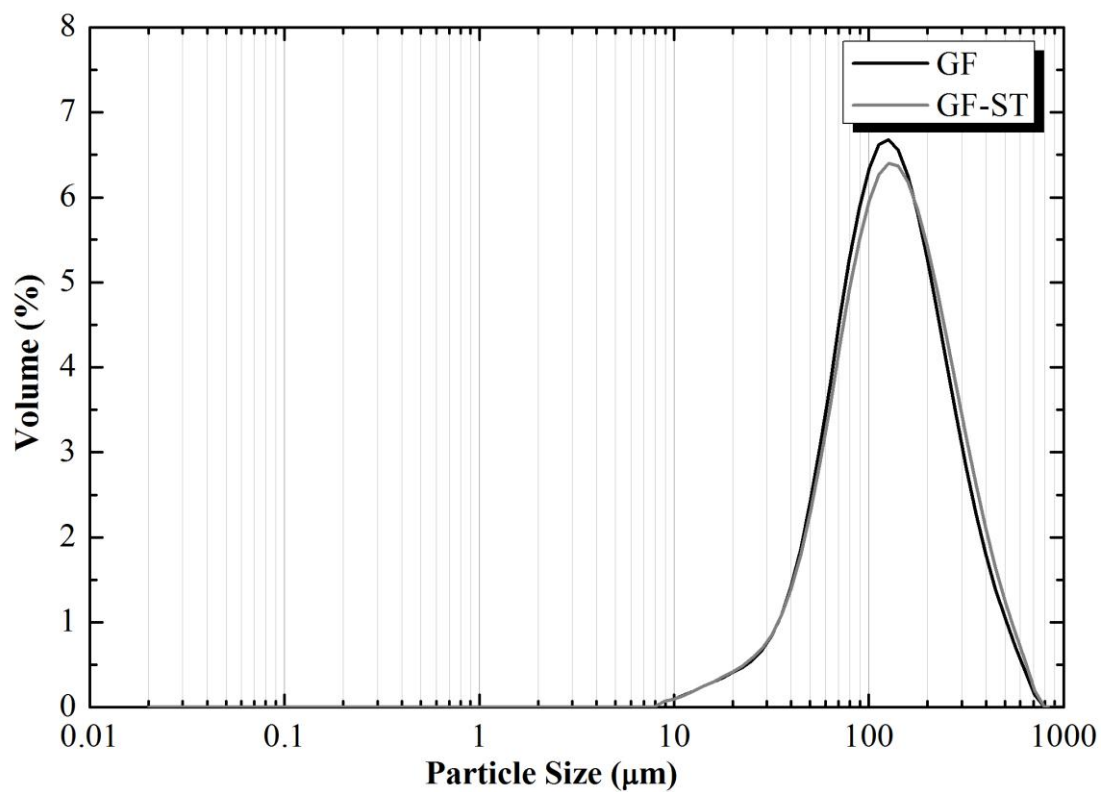
Figure A.3 Particle size distribution of glass flakes treated with APS (GF-ST) along with the particle size distribution of as-received flakes (GF).

CURRICULUM VITAE

PERSONAL INFORMATION

Surname, Name: GÜRBÜZ, Selen Nimet
Nationality: Turkish (TC)
Date and Place of Birth: 22 February 1979, Gebze
Marital Status: Married
Phone: +90 312 217 5671
Fax: -
Email: gurbuzselen@hotmail.com.tr

EDUCATION

Degree	Institution	Year of Graduation
MS	METU, Metallurgical and Materials Engineering	2004
BS	METU, Metallurgical and Materials Engineering	2001
High School	Gazi Anatolian High School, Ankara	1996

WORK EXPERIENCE

Year	Place	Enrollment
2008-Present	TAEK-Sarayköy Nuclear Research and Training Center	Researcher
2001-2008	METU, Dept. of Metallurgical and Materials Engineering	Teaching Assistant
2000 August	Rutaş Die Casting Co. Ltd.	Intern Engineering Student
1999 July	Mitaş Energy and Metal Construction Inc.	Intern Engineering Student

FOREIGN LANGUAGES

Advanced English

PUBLICATIONS

Journal Publications:

S. N. Gurbuz, A. F. Dericioglu, "Effect of reinforcement surface functionalization on the mechanical properties of nacre-like bulk lamellar composites processed by a hybrid conventional method", Materials Science and Engineering C, 33, 2011–2019, 2013.

Zdeněk Chlup, Ivo Dlouhý, Selen Gürbüz, Arcan F. Dericioglu, Vladislav Kozák, "Interfacial characterization in transparent spinel matrix reinforced by SiC fiber", Key Engineering Materials, 413, 252-259, 2009.

Conference Presentations:

S. N. Gürbüz, A. F. Dericioglu, "Processing and characterization of inorganic-organic bio-inspired bulk laminar composites", European Conference on Biological Materials Science, Euro Bio-inspired Materials, Potsdam, Germany, 2012.

S. N. Gürbüz, A. Günes, A. F. Dericioglu, "Fabrication and characterization of bio-inspired nacre-like bulk lamellar composites by HASC", International Metallurgy and Materials Congress (IMMC), Istanbul, TURKEY, 2012.

Selen N. Gürbüz, M. Vedat Akdeniz, Amdulla O. Mekhrabov, "Synthesis and characterization of Fe-B based bulk amorphous alloy systems", International Metallurgy and Materials Congress (IMMC), Istanbul, TURKEY, 2005.

Selen N. Gürbüz, Amdulla O. Mekhrabov, M. Vedat Akdeniz, "Modeling of glass forming ability of Fe-B based alloy systems", International Metallurgy and Materials Congress (IMMC), Istanbul, TURKEY, 2005.

HOBBIES

Walking, swimming, reading, movies